Department Chemie
der Technischen Universität München

NMR structural characterization of beta-amyloid peptides and their inhibitors

Zhongjing Chen

Vollständiger Abdruck der von der Fakultät für Chemie der Technischen Universität München zur Erlangung des akademischen Grades eines

Doktors der Naturwissenschaften

genehmigten Dissertation.

Vorsitzender: Univ.-Prof. Dr. St. J. Glaser

Prüfer der Dissertation:
1. Univ.-Prof. Dr. H. Kessler
2. Univ.-Prof. Dr. B. Reif
   Humboldt Universität Berlin
3. Univ.-Prof. Dr. S. Weinkauf

Die Dissertation wurde am 21.10.2004 bei der Technischen Universität München eingereicht und durch die Fakultät für Chemie am 24.11.2004 angenommen.

dedicated to my family

Acknowledgement

First of all I would like to thank Prof. Dr. Bernd Reif for giving me the opportunity to finish my PhD work in his group. His scientific insights, supports and his numerous discussions on these projects and my thesis writing are especially valuable for the implement of this work. His always-ready-to-help attitude facilitated my work very much. I thank him for his continuous interest in my work, for his constant assistance of my scientific work.

I am very grateful to Prof. Dr. Horst Kessler for providing a wonderful work atmosphere and supervision of my project in TUM. From October 2000 to March 2003, part of work for this PhD thesis has been carried out in the working group of Prof. Dr. Horst Kessler at the "Institut für Organische Chemie und Biochemie der Technischen Universität München", under subgroup of Prof. Dr. Bernd Reif. There I started my first peptide synthesis and purification, and also had the possibility to use the high field NMR (specially 900 MHz) spectrometers. I very much enjoyed the great scientific freedom, excellent working conditions, and the inspiring, and amicable atmosphere at the institute. I would like to thank all my colleagues in the working group of Professor Kessler, especially:

- Martin Sukopp, for introducing peptide synthesis and helping me resolve many synthetic problems,
- Georgette Thumshirn, for helping me with HPLC problems,
- Angelika Kühlewein for introducing me the Circular Dichroism experiments,
- Mona Wolff, for ordering the chemicals,
- Dr. Rainer Haeßner for his support of NMR, hardware and software problems,
- Dr. Gerd Gemmecker for providing me ample NMR measurement time,
- Burghard Cordes and Dr. W. Spahl for recording MS-spectra,
- Evelyn Bruckmaier and Marianne Machule for secretarial assistance,
- the "NCE" members, Michael John, Melina Haupt, Markus Heller, Dr. Murray Coles, Vincent Truffault,
- And all mentioned and unmentioned co-workers.

I would like also to thank Prof. Dr. Weinkauf in TUM for her kind helping to make Electron Microscopy experiments.

From March 2003 to October 2004, the rest of work for this thesis has been carried out in the working group of Prof. Dr. Bernd Reif at the Forschungsinstitut für Molekulare Pharmakologie. I would like to thank the colleagues in FMP:

- Prof. Dr. H. Oschkinat for the NMR-facilities at FMP-Berlin,
- Dr. Peter Schmiedt for NMR measurement time arrangement,
- Dr. Krause for Molecular Dynamics,
- Dr. Ronald for introducing the CNSsolve program,
- Dr. Beyermann for his kindness of allowing me using the wonderful peptide chemistry lab,
- Dr. Lorenz and Martina Ringling for performing the EM experiments,
- Frau Lerch for performing ESI Mass spectra.

Many thanks to Saravanakumar Narayanan for numerous discussions about my projects, to Veniamin Chevelkov and Maggy Hologne for helping me with solid-state NMR experiments.

I also would like to thank Dr. Johannes Winkler for his insightful comments on this manuscript.

All this contributed to the success of this work.

I would like to thank all my friends in München, Hannover and Berlin for their support and friendship.

Special thanks to my parents who give me endlessly love and encouragement. Many thanks to my sisters: Shuhua, thank you for helping me solve many problems in the life, especially after I came to Germany; to Zhongzhou, who always cheers me up throughout the time and shares me with her happiness. Also, I would like to thank my husband, Ling Zhou, for his love, supports and understanding throughout the years. Their love has been the best support for me to finish my doctoral study in Germany.

Parts of this thesis have been or will be published in due course:

1. **Zhongjing chen** and Bernd Reif (2004), Measurements of residual dipolar couplings in peptide inhibitors weakly aligned by transient binding to peptide amyloid fibrils. *Journal of Biomolecular NMR*, **29** (4): 525-530.

2. Veniamin Chevelkov, **Zhongjing Chen**, Wolfgang Bermel, Bernd Reif (2004), Resolution enhancement in MAS solid-state NMR by application of ^{13}C homonuclear scalar decoupling during acquisition. *Journal of Magnetic Resonance.* (In press)

3. **Zhongjing Chen**, Gerd Krause and Bernd Reif, Structural studies of peptide inhibitors bound to β-Amyloid fibrils. (Manuscript prepared for the Submission to Journal of Molecular Biology)

Abstract

Polymerization of the soluble β–amyloid peptide into highly ordered fibrils is hypothesized to be a causative event in the development of Alzheimer's Disease. Structural information of β–amyloid fibril formation is fundamental for the development of diagnostics and therapeutic approaches, and in addition might be valuable for elucidating fundamental mechanisms of protein folding and assembly. Study of interactions of Aβ with inhibitors can provide important indirect information of the amyloid fibril structure.

In this work, the structure of peptide inhibitors to Aβ fibril formation is studied with the aid of synthetic peptides and NMR spectroscopy, as well as Electron Microscopy and Circular Dichroism Spectroscopy. The short fragment of the β-amyloid peptide $A\beta^{14-23}$ and its peptide inhibitors iAβ5 (LPFFD) and $iA\beta5^{inv}$ (DPFFL) are synthesized manually with and without ^{19}F-, ^{13}C- and ^{15}N-labelling using standard Fmoc peptide synthesis protocols. Distance restraints for peptide inhibitors in the bound state are obtained on the basis of trNOE intensities and are used for structural calculations using the CNSsolve program. The orientation of the peptide inhibitors relative to Aβ is further investigated using trRDC techniques. In a final step, NOE-derived NMR structures of iAβ5 and $iA\beta5^{inv}$ are docked manually to the published structural models of fibrillar $A\beta^{14-23}$ and $A\beta^{1-40}$, respectively, and the models of the complex are refined with experimental trRDC data. The model provides a structural basis for understanding the inhibitory effect of iAβ5 or $iA\beta5^{inv}$ during fibril formation and gives hints to better understand the fibril disassembly process. Our findings provide a basis for further *in vitro* modeling of amyloid fibril assembly, structure, and possibly also disruption of such assemblies. We believe our structural data will contribute to an improved understanding of the mechanisms of amyloid formation and to the development of therapeutic agents for amyloid diseases.

Moreover, structure of amyloid fibrils formed from *de novo* designed amyloid peptides is investigated by solid-state NMR. With the aid of isotopic labelling, complete ^{13}C and ^{15}N assignments for STVIIE fibrils are obtained from by 2D ^{13}C-^{13}C and ^{13}C-^{15}N correlation experiments. PDSD experiments provide information about peptide packing in the fibrils. Primary assignments of the 1D ^{13}C spectra for STVIIT and STVIYE fibrils are obtained. The comparison of the chemical shifts shows that the one amino acid substitution causes the larger ^{13}C chemical shift changes on the neighbouring residues which could explain the different morphology observed for these fibrils.

Zusammenfassung

Nach heutigem Stand der Wissenschaft ist die Polymerisierung des löslichen β–Amyloid-Peptids in hoch geordnete Fibrillen ein ursächliches Ereignis bei der Entstehung von Alzheimerischen Krankheit. Für die Entwicklung von diagnostischen und therapeutischen Methoden ist die Kenntnis der Strukturen der β–Amyloid-Peptidfibrillen essenziell und kann potenziell auch zu neuen Grundlagenkenntnissen auf dem Gebiet der Proteinfaltung und Assemblierung von Protein Komplexen führen. Untersuchungen struktureller Wechselwirkungen zwischen Aβ und Inhibitoren der Fibrillenbildung können indirekt wichtige Erkenntnisse zu den Bildungsmechanismen von Amyloidfibrillen liefern.

In der vorliegenden Arbeit wurde die Struktur von Peptidinhibitoren der Aβ-Fibrillenbildung mit Hilfe von synthetischen Peptiden und NMR-Spektroskopie, Elektronenmikroskopie und CD-Spektroskopie untersucht. Ein kurzes Fragment des β–Amyloid-Peptids $A\beta^{14-23}$ und die Peptidinhibitoren iAβ5 (LPFFD) und $iA\beta5^{inv}$ (DPFFL) wurden sowohl mit als auch ohne ^{19}F-, ^{13}C- and ^{15}N-Markierung auf Grundlage von Standard-Fmoc-Protokollen manuell synthetisiert. Entfernungs-Restraints wurden auf der Grundlage der NOE-Intensitäten berechnet und für strukturelle Berechnungen mit Hilfe des Programms CNSsolve verwendet. Die räumliche Orientierung der Peptidinhibitoren relativ zur Aβ–Fibrille wurde mittels trRDC-Methoden genauer untersucht. In einem letzten Schritt wurden die NOE-berechneten NMR-Strukturmodelle von iAβ5 und $iA\beta5^{inv}$ manuell an bekannte Strukturmodelle der $A\beta^{14-23}$- und $A\beta^{1-40}$-Fibrillen angelagert, und die Modelle dieses Komplexes wurden mit experimentellen trRDC-Daten verfeinert. Aus den Dockingmodellen dieses Komplexes wurden die Bindungsstellen von iAβ5 und $iA\beta5^{inv}$ ermittelt. Aus den vorliegenden Ergebnissen schlussfolgern wir, dass iAβ5 und $iA\beta5^{inv}$ Aβ-Fibrillen durch Bindung an die für die Fibrillenbildung essenziellen Bereiche auflösen kann. Die Inhibitoren können somit zur Disaggregation von Fibrillen führen. Unsere Ergebnisse bilden eine Grundlage für weitergehende *in vitro* Modellierungen der Amyloidfibrillenbildung, der Amyloidstruktur und möglicherweise der Auflösung dieser Fibrillen. Unsere Strukturdaten können zu einem besseren Verständnis der Mechanismen der Amyloidfibrillenbildung und zur Entwicklung von Therapien für Amyloiderkrankungen beitragen.

Darüber hinaus wurde mittels Solid-State-NMR die Strukturen von Amyloidfibrillen untersucht, die von *de novo*-entworfenen Amyloidpeptiden gebildet werden. Mit Hilfe von Isotopenmarkierung wurden ^{13}C- und ^{15}N-Zuordnungen für STVIIE-gebildete Fibrillen durch 2D ^{13}C-^{13}C und ^{13}C-^{15}N Korrelationsexperimente ermittelt. PDSD Experimente liefern

Informationen über die Packung der Amyloid-Peptide relativ zueinander. Weiterhin konnten eine vorläufige Zuordnung der ^{13}C chemischen Verschiebungen von STVIIT und STVIYE erhalten werden. Ein Vergleich der chemischen Verschiebungen in Bezug auf STVIIE zeigt, dass Substitution einer Aminsäure zu großen Änderungen führt, die die unterschiedliche Morphologien dieser Fibrillen erklären kann.

Contents

1.0	**Introduction**	**1**
1.1	Alzheimer's Disease	2
1.2	Structural studies on Aβ	5
1.2.1	The structure of Aβ in solution	6
1.2.2	The structure of β-amyloid fibrils	10
1.3	Inhibition and reversion of Aβ amyloidogenesis as a therapeutic amyloid-related target for AD	14
1.4	Peptides synthesis	17
1.5	Structural studies by Electron Microscopy	22
1.6	Structural studies by Circular Dichroism	24
1.7	Structural studies by Liquid State NMR Spectroscopy	25
1.7.1	Theory of NMR spectroscopy	26
1.7.2	Structural studies on proteins by solution NMR	30
1.8	Structural Studies by Solid-state NMR Spectroscopy	33
1.8.1	Theory of solid-state NMR spectroscopy	33
1.8.2	Basic solid-state NMR techniques	36
1.9	Overview of this thesis	41
	References	42
2.0	**Materials and Methods**	**51**
2.1	Instruments	51
2.2	Materials	52
2.2.1	Chemicals	52
2.2.2	Labelled Fmoc Amino Acids	52
2.3	peptide synthesis	53
2.4	Fibrillization of β-amyloid	64
2.5	Electron Microscopy	65
2.6	Circular Dichroism	65
2.7	Thioflavine T Fluorescence Assay	66
2.8	Solution NMR	66
2.9	Solid-state NMR	72
2.10	Structure calculation	73
2.11	Determination of peptide alignment tensor	74
2.12	Molecular Modeling	75
	References	76
3.0	**Results and Discussion**	**77**
3.1	Peptide synthesis and purification	77
3.2	$A\beta^{14-23}$ forms similar fibrils as $A\beta^{1-40}$ as observed by Electron Microscopy	78
3.3	Effect of peptide inhibitor iAβ5/$iA\beta5^{inv}$ on Aβ fibril formation as observed by EM	79
3.4	Aβ secondary structure studies by CD Spectroscopy	82
3.5	The influence of LPFFD on the ThT binding of $A\beta^{14-23}$	85
3.6	The assignment of iAβ5/$iA\beta5^{inv}$ in the NMR spectra	86

3.7	Binding of iAβ/iAβ5^{inv} to Aβ peptides studied by solution NMR	92
3.8	Structural studies by trNOE experiments	93
3.9	Structural calculation of iAβ5 bound to Aβ$^{14-23}$	98
3.10	Measurement of residual dipolar couplings in peptide inhibitors bound to Aβ fibrils	99
3.10.1	Alignment of amyloid fibrils	100
3.10.2	Measurement of RDCs for iAβ5^{inv} bound to Aβ fibrils using amyloid fibrils as orienting medium	102
3.10.3	Measurement of RDCs for KLVFFKK bound to Aβ fibrils using amyloid fibrils as orienting medium	107
3.11	Order tensor determination for iAβ5^{inv} bound to Aβ fibrils	109
3.12	Validation of NOE-derived structures for iAβ5^{inv} by RDCs	115
3.13	The docking model of iAβ5/ iAβ5^{inv} bound to Aβ fibrils	116
3.14	Structural studies of Aβ$^{14-23}$ by ^{19}F NMR	120
3.15	Structural studies of *de novo* designed peptide-based amyloid fibrils by solid state NMR	124
	References	130
4.0	**Summary**	**135**
5.0	**Appendix**	**137**

Abbreviations

Abbreviations for amino acids follow the rules of the IUPAC-IUB Commission of Biochemical Nomenclature in *J. Biol. Chem.* (1972) 247, 977-983. Additional abbreviations:

Aβ	β–Amyloid
AβPP	β–Amyloid Precursor Protein
ACN	Acetonitrile
AD	Alzheimer's Diesease
BSE	Bovine Spongiform Encephalopathy
CD	Circular Dichroism
COSY	Correlation Spectroscopy
CR	Congo Red
DCM	Dichloromethane
DIPEA	Diisopropylethylamine
DMF	Dimethylformamide
EM	Electron Microscopy
Fmoc	9-Fluorenylmethoxycarbonyl
Fmoc-ONSu	(*N*-Fluorenylmethoxycarbonyloxy)-*N*-succinimid
HFIP	Hexafluoroisopropanol
HOBt	1-Hydroxybenzotriazole
HSQC	Heteronuclear Single Quantum Coherence
MeOH	Methanol
mg	Milligram
MS	Mass Spectrometry
MW	Molecular weight
MHz	Megahertz
µM	Micromolar
µmol	Micromol
nm	Nanometer
nM	Nanomolar
NMP	*N*-Methylpyrrolidinone
NMR	Nuclear Magnetic Resonance
NOE	Nuclear Overhauser Enhancement
NOESY	Nuclear Overhauser Enhancement Spectroscopy
ppm	parts per million

ROESY	Rotating frame Overhauser Enhancement Spectroscopy
RP-HPLC	Reversed-Phase High Performance Liquid Chromatography
RMSD	root mean square deviation
sAβ	Soluble β-amyloid
SPPS	Solid Phase Peptide Synthesis
TFA	Trifluoroacetic acid
TBTU	*O*-(1*H*-Benzotriazol-1-yl)-*N*,*N*,*N*′,*N*′,-tetramethyluronium Hexafluorophosphate
TCP	Tritylchlorid-Polystyrol-resin
THF	Tetrahydrofuran
TIPS	Triisopropylsilane
TOCSY	Total Correlation Spectroscopy
UV	Ultraviolet

1 Introduction

Amyloidoses are protein deposition diseases, of which the more well known are Alzheimer's disease, Huntington's disease, Bovine Spongiform Encephalopathy (BSE), familial amyloid polyneuropathy (FAP) and Parkinson's disease (*1-7*). Extensive studies from three diverse disciplines, neuropathology, genetics, and biophysics show that all of these amyloid diseases are characterized by insoluble assemblies, amyloid deposits, containing extremely insoluble protein fibrils that share similar morphological features (80- to 150-Å fibrils) but comprise many different proteins with no obvious sequence similarity (see Table 1-1) (*8-20*). However, the pathogenesis of these neurodegenerative diseases remains unclear, and effective therapies are currently unavailable. Theoretical and experimental data from many laboratories worldwide support the amyloid hypothesis which suggests that the process of amyloid fibril formation as the cause of well over a hundred distinct amyloid diseases, maladies associated with the aberrant self-assembly of any one of twenty non-homologous human proteins/peptides (*6, 21-26*). Additional interest in amyloid deposits comes from another discipline: structural biology. Despite large differences in the size, native structure and function, many proteins or peptides form amyloid fibrils of remarkably similar morphology and properties (*6, 17, 27-31*), including some *de novo*-designed peptides (*28, 32-35*). One of the defining features of all amyloid deposits is their ability to display positive apple green birefringence under polarized light after binding amyloidophilic dyes such as Congo red (*19, 36-39*). Electron Microscopic examination of amyloid fibrils revealed fibrils are 5-10 nm in width and of indefinite length (*31, 40-42*). X-ray diffraction analysis revealed a so called cross-b diffraction pattern (*43-48*), showing that the fibrils ordered in the beta pleated sheet conformation, with the direction of the polypeptide backbone perpendicular to the fibrils' axis. The similar characteristic structures of amyloid suggest that the key elements of the fibril formation process may be common to all proteins involved. It follows that inhibition of fibril formation could be a viable therapeutic strategy for all amyloidosis. However, the underlying processes that lead to the polymerization of normally soluble proteins and peptides into aggregation in these diseases are poorly understood (*17, 49*), which complicates the right therapeutic targets for treating amyloid diseases. Therefore, it is critical to understand the mechanisms of these process at a molecular level. A proper system could offer insights into the molecular details of amyloid fibril formation in an easy way. Amyloidogenic peptide fragments of the Alzheimer's amyloid peptide βA4 are an excellent model system for such research for several reasons (*50*): The aggregating species, Aβ, are readily available (*51*); both

in vitro and *in vivo* model systems for toxicity of the aggregates have been developed (*52, 53*); considerable structural data have been collected on this system (*41, 46, 49, 54-65*). These features render Aβ an excellent test system for evaluating general strategies for altering protein aggregation.

Table 1-1 List of some amyloidogenesis and their related proteins

Diseases	Involved proteins
Alzheimer's Disease	Amyloid β-protein
Parkinson's disease	α-Synuclein
Creutzfeldt–Jakob disease	Prion protein
Huntington's disease	Huntingtin
Familial Amyloid Polyneuropathy	Transthyretin
Diabetes type 2	Amylin
Amyotrophic lateral sclerosis (ALS)	Superoxide dismutase (SOD)
Haemodialysis-related amyloidosis	β2-Microglobulin
Reactive amyloidosis	Amyloid-A
Cystic fibrosis	CFTR protein
Sickle cell anemia	Hemoglobin

1.1 Alzheimer'S Disease (AD)

ALZHEIMER'S DISEASE (AD) is a progressive, neurodegenerative disease characterized by loss of function and death of nerve cells in several areas of the brain, leading to loss of mental functions such as memory and learning (*25, 66-75*). It is the most common cause of dementia among people age 65 and older (*10*). AD has two abnormal structures in the brain as its main characteristics: amyloid plaques and neurofibrillary tangles (*9, 76, 77*). Plaques are dense, largely insoluble deposits of protein and cellular material outside and around the brain's neurons. Tangles are insoluble twisted fibrils that build up inside neurons (*42*). In normal aging, nerve cells in the brain are not lost in large numbers. In contrast, AD destroys neurons in parts of the brain that control memory, especially the hippocampus and related structures (*66, 70*). As nerve cells in the hippocampus stop functioning properly, short-term memory fails, and often, a person's ability to perform easy and familiar tasks begins to decline. AD also attacks the cerebral cortex, particularly the areas responsible for language and reasoning. Here, AD begins to take away language skills and change a person's ability to make judgments. Personality changes also may occur. Emotional outbursts and disturbing behaviour, such as wandering and agitation, begin to happen and become more and more frequent as the disease runs its course. Eventually, many other areas of the brain are involved, all these brain regions shrink, and the AD patient becomes bedridden, incontinent, totally helpless, and unresponsive to the outside world. AD presents a major health problem because of its enormous impact on individuals, families, the health care system, and society as a

whole. As more and more people live longer, the number of people affected by diseases of aging, including AD, will continue to grow, which makes the disease an urgent research priority.

Research into the basic biology of the aging nervous system is critical to understanding what goes wrong in the brain of a person with AD. Understanding its underlying mechanisms will provide the basis for advances in all other areas of research, including diagnosis, treatment, prevention, and care.

AD was long considered among the most obscure and intractable of human maladies. However, in the past decade, knowledge about factors that may contribute to the onset of Alzheimer's Disease has grown considerably (*11, 66-69, 75, 77-82*). For example, mutations in three genes (APP, PS-1, and PS-2) cause familial Alzheimer's disease by alteration of the rate of generation of the amyloid peptide or the length of this peptide (*83*); the "plaque-associated" proteins, like apolipoprotein E4 (*84, 85*), transthyretin (*86*), serum amyloid A (*82, 87*) , promote the formation of toxic fibrillar aggregates or the chronic inflammatory responses. Based on the emerging findings, there is an increasing belief that the amyloid fibrils formed in the brain in Alzheimer's disease play an important causative link in the pathology (*2, 21, 67, 71, 88*). The amyloid cascade hypothesis proposes Aβ as the central trigger of the pathological changes observed in the brains of AD patients, such as synapse loss, activation of inflammatory processes, the induction of neurofibrillary changes leading to the formation of paired helical filaments and, ultimately, neuronal death (Fig. 1-1) (*10, 21, 67*). It has formed the basis for numerous research activities, which have significantly contributed to our understanding of AD.

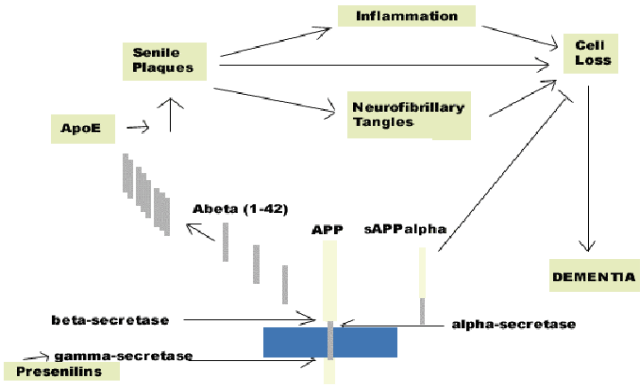

Fig. 1-1. The amyloid cascade hypothesis of Alzheimer's Disease.

Biochemical analysis of the amyloid isolated from Alzheimer's disease brain tissue indicates that amyloid plaques are composed of a family of polypeptides named β–amyloid peptide (Aβ), a 39-42 residue fragment with 28 extracellular and 11-15 transmembrane amino acid long regions (*89*), which is encoded by a gene on chromosome 21 as part of a larger protein, named amyloid precursor protein (APP) (see Fig.1-2) (*90-94*). APP is one of many proteins that are associated with cell membranes (*95*). Proteolytic cleavage of APP occurs in two distinct manners via either the α-secretase pathway or the β-secretase pathway (*93, 96*). The former pathway involves neuronal secretion of $sAPP_{\alpha}$ by a putative α-secretase enzyme which precludes the formation of full-length Aβ, as cleavage occurs between residues corresponding to Aβ residues 16 and 17. Traditionally the α-secretase pathway has been called the nonamyloidogenic pathway since full-length Aβ is not formed. Full-length Aβ is generated by the β-secretase or amyloidogenic pathway, where N-terminus of APP was sequentially cleaved by a β-secretase and γ-secretase, leaving the amyloidogenic Aβ in the extracellular space. APP metabolism by the β-secretase pathway was initially proposed to be an abnormal proteolytic processing event specific to, and with a causative role in, AD. However, proteolysis of APP via the β-secretase pathway has been found to be a normal process which occurs ubiquitously in both AD and non-demented individuals (*97*).

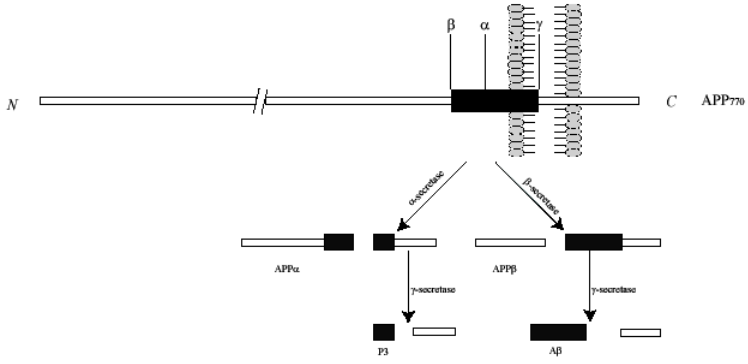

Fig. 1-2. Schematic prepresentation of APP processing.

The location of the γ-secretase cleavage site is variable which causes the *C*-terminus of Aβ to vary between amino acids 39 and 43. This heterogeneous cleavage pattern can be explained by γ-secretase actually being multiple enzymes, or by Aβ generation occuring in different cellular sites where conditions affect enzymic specificity (*95*). Two variants, $A\beta^{1-40}$ and $A\beta^{1-42}$, which differ by truncation at the carboxyl terminus (Fig. 1-2), are the predominant β-amyloid peptides (*93, 98*). $A\beta^{1-40}$, a shorter β-amyloid, is more soluble and aggregates slowly, and $A\beta^{1-42}$, slightly longer, is a "sticky" β-amyloid peptide that rapidly forms insoluble

clumps (*93*). It was found that more amyloidogenic $A\beta^{1-42}$ is the principal specie associated with senile plaque amyloid (*99*).

An ever-increasing body of genetic, physiologic, and biochemical data supports the hypothesis that fibrillogenesis of the β-amyloid protein is an important event in Alzheimer's disease. However, there are still many questions remaining unclear regarding the relationship of Aβ and AD (*74*). The most difficult one to answer concerns the nature of the neurotoxic effect of the peptide itself in the brain. More recently, Aβ oligomeric intermediates, rather than fully formed fibrils, are considered to be the predominant toxic species, based on the *in vitro* and *in vivo* observations that small, soluble, and diffusible oligomeric Aβ species are also capable of initiating pathogenic events (*52, 100-104*). However, the debate about precisely which species of Aβ injures neurons and their processes in vivo will continue for some time. All these uncertainties complicate identifying therapeutic targets for AD and underline the need for a clear understanding of the molecular mechanism of Aβ fibrillogenesis.

1.2 Structural studies on Aβ

Therapeutic strategies based on the rational design of aggregation inhibitors require knowledge of the molecular structure of amyloid fibrils. The problem of determining and understanding the molecular structures of amyloid fibrils has attracted considerable attention and effort over the past decade. Although complete, high-resolution structures have not yet been obtained, key features of structural conformations and supramolecular organization within amyloid fibrils formed in vitro from variant synthetic Aβ peptides have been elucidated using a variety of novel experimental methods, including electron microscopy, circular dichroism spectroscopy, magnetic resonance spectroscopy, X-ray fibre diffraction (*43*), Fourier transform infrared spectroscopy (FTIR), and other biochemical techniques (*64*) (see Table 1-2).

The field of structural studies of Aβ amyloid is extremely complex and encompasses the structure of the soluble Aβ peptide, its polymerization into intermediates and from intermediates to amyloid fibrils, to the fibrils themselves and finally to amyloid deposition in vivo. Structural studies of soluble Aβ have concentrated on using NMR, CD and FTIR methods to look at the structure of different regions of Aβ in various solvents. Atomic force

microscopy (AFM) has proved a valuable tool to investigate the nature of the intermediates in the amyloid pathway. Transmission EM and fibre diffraction have been used to examine the structure of the amyloid fibrils, as well as methods of solid-state NMR and FTIR.

Table 1-2. Structural studies on variant Aβ peptides.

	Structure/conformation	Experimental conditions	Methods	Reference
$A\beta^{1-28}$	Random coil	Water (pH1-4)	CD	(61)
$A\beta^{1-28}$	α-helix; increased temperature leads to decrease in helix, 13-20 remain most stable helix	TFE (4-7)	NMR	(61, 105)
$A\beta^{1-28}$	β-sheet	Water (pH4-7)	CD	(105)
$A\beta^{1-28}$	Not α-helical, extended strand	Water (pH5.6)	NMR	(106)
$A\beta^{1-28}$	α-helix, bend at 12	Membrane mimic, SDS and TFE	NMR	(55)
$A\beta^{1-28}$	C-terminal α-helix, N-terminal turn (flexible)	DMSO	NMR	(107)
$A\beta^{1-28}$	Fibrillar, cross-β	aqeous	EM, FD	(51)
$A\beta^{1-39}$	Random coil and β-sheet	Aqueous (pH 7.3)	CD	(61)
	α-helix	TFE (30%) (pH 1-4, 7-10)	CD	(61)
	β-sheet (60%)	Aqueous (pH 7.4)	CD	(108)
$A\beta^{12-28}$	α-helix 16-24	SDS (pH2.6)	NMR	(109)
$A\beta^{10-23}$	β-sheet (antiparallel)	Solid state	FTIR	(110)
$A\beta^{10-35}$	β-sheet (parallel), in register	Dried from water (pH 7.4)	ssNMR	(111-113)
$A\beta^{10-35}$	β-sheet (parallel), in register	PH 3.7 or pH 7.4	STEM, ssNMR	(54)
$A\beta^{10-43}$	80% β-sheet	Water	CD	(110)
	28% α-helix	HFIP	CD	(110)
$A\beta^{16-22}$	β-sheets (antiparallel)	1.0 mM phosphate buffer, pH 7.0	EM, ssNMR	(114)
$A\beta^{25-35}$	β-sheet > random coil (decreased concentration)	Aqueous (pH4, 5)	CD	(115)
	β-sheet	PH5.5, pH 7.4		
$A\beta^{29-42}$	β-sheet (antiparallel)	Solid state	FTIR	(110)
	β-sheet	Aqueous (pH 7.4)	CD	(110)
$A\beta^{34-42}$	β-sheet (antiparallel)	aqueous	FTIR, ssNMR	(116)
$A\beta^{1-40}$	α-helix 15-36, kink 25-27	SDS (pH 5.1)	NMR	(117)
	α-helix 15-23, 31-35	TFE (40%) (pH 2.8)	NMR	(118)
	Cross-β	water	FD	(46)
	β-sheet (parallel, in-register)	Aqueous (pH 7.4)	ssNMR	(119)
	β-sheet (parallel, in-register), residuce 1-9 without structure	PBS (140 mM NaCl, 3 mM KCl, 10 mM phosphate, pH 7.4)	ssNMR	(120)
	1-10, disordered; 12-24 and 30-40, β-strand; 25-29, a bend	Aqueous, pH 7.4	x-ray, EM, ssNMR	(60)
	α-helix 10-24 and 28-42	SDS (pH 7.2)	NMR	(65)
$A\beta^{1-42}$	β-sheet	water	CD	(61)
	β-sheet, in-register parallel	Aqueous, pH 7.4	EM, STEM, ssNMR	(54)
	α-helix 10-24 and 28-42	SDS (pH 7.2)	NMR	(65)

1.2.1 The structure of Aβ in solution.

The sequence of $A\beta^{1-42}$ is as follows (*121, 122*):

NH_2-DEAFRHDSGY^{10}EVHHQKLVFF^{20}AEDVGSNKGA^{30}IIGLMVGGVV^{40}IA-COOH

The $A\beta^{1-40}$ sequence is divided into two regions: residues 1-28 make up a relatively hydrophilic domain with a high proportion of charged residues (46%). In the amyloid precursor protein, this domain is extracellular. The carboxyl-terminal residues 28-40 make up a richly hydrophobic domain that is associated with the cell membrane in the amyloid precursor protein (*46*). Amino acid sequence analyses of the Aβ peptide by the Chou-Fasman and Garnier-Osguthorpe-Robson methods indicate that the probability of finding a β-strand conformation in Aβ is high within the C-terminal region after residue 28. The region between amino acids 10 and 24 presents a high and similar probability to display either an α-helix or β-strand conformation (*56*). There are also probably two β-turns between residues 6 and 8 and between residues 24 and 29. Using synthetic peptides and spectroscopic techniques, the secondary structure assignments obtained by predictive methods have been confirmed (*61, 105*).

Detailed secondary structural analysis by CD spectroscopy indicated that $A\beta^{1-42}$ formed approximately 90% β-sheet in aqueous buffer at pH 7.3 and the *C*-terminal $A\beta^{29–42}$ peptide fragment adopts approximately 100% β–sheet structure under these conditions. The addition of 25% (v/v) TFE, which promotes intra-chain hydrogen bonding, thereby stabilizing α-helical structures, induced α-helical structure for $A\beta^{1-42}$, $A\beta^{1-39}$ and $A\beta^{1-28}$, but $A\beta^{29-42}$ remained in a β-sheet conformation. The N-terminal domain exists as a soluble monomeric α-helical structure at pH 1-4 and pH greater than 7. However, at pH 4-7 it rapidly precipitates into an oligomeric β-sheet structure. Conformation studies on Aβ peptides in aqueous solution are complicated by their tendency to aggregate. To structurally characterize the nonaggregated state of the β-amyloid peptide, tri-dimensional structures of Aβ have been obtained using smaller fragments in aqueous solution or full-length peptides in nonphysiological conditions (pH, presence of strong organic solvents or detergents) to avoid protein aggregation (*55, 65*). The N-terminal 28-amino-acid fragment of β-amyloid was studied in detail by ^{1}H-NMR in water–trifluoroethanol (TFE) solutions and was found to have a predominantly α-helical structure (*55*). However, in another study undertaken by Eker et.al., $A\beta^{1-28}$ adopts a predominantly polyproline II conformation in D2O at acidic pD (*123*). Recently, NMR structures of $A\beta^{1-40}$ and $A\beta^{1-42}$ have been determined in aqueous trifluoroethanol (*118*), in SDS micelles (*65, 117*) and in aqueous solutions of fluorinated alcohols (*62*). All these NMR data hint to the presence of two helical regions encompassing residues 8–25 and 28–38, connected through a flexible kink or a regular type I β-turn. Thus,

Aβ generally forms α-helical conformation in organic solvents whereas in aqueous buffer or in water it is predominantly β-sheet, although this can be affected by pH, concentration and incubation time.

Studies of the Aβ peptide in various "membrane mimicking" solvents had suggested an α-helical conformation for the soluble Aβ peptide, while peptide aggregation and precipitation was observed to occur following β-sheet formation by $A\beta^{1-39}$ and $A\beta^{1-42}$ in a time dependent manner indicating that formation of β-sheet structure is directly related to peptide aggregation (*61, 124-127*). Therefore, it is suggested that the Aβ peptide undergoes a conformation transition from α-helical to β-sheet structure during amyloidogenesis. Indeed, Zagorski and Barrow (*105*) obtained NMR evidence for an α-helix to β-strand conformational switch in β-amyloid (residues 1–28) with increasing temperature to 35°C or increasing pH from acidic to neutral range, and upon forming a β-sheet structure, the peptide became insoluble. A similar loss of solubility, associated with a conformational switch from an α-helical state, is observed for a β-amyloid fragment comprising amino acids 12–28, in the presence of micelles of the zwitterionic lipid dodecylphosphocholine. Moreover, a detailed ^{1}H-NMR structure of $A\beta^{1-28}$ in DMSO indicated a degree of conformational flexibility in the peptide, but confirmed that under some conditions it assumed an extended structure consistent with a β-strand (*107*). β-Sheet formation by Aβ was observed to be strongly dependent on environmental conditions, and such factors inducing the protein structural changes were identified over the last few years (*128, 129*). For example, it was found that β-Sheet formation and peptide aggregation exhibited pH dependence and were most rapid at pH 5.5, as evidenced by changes in the CD spectra corresponding to complete β-sheet formation. The observation that β-sheet formation by Aβ was promoted at low pH is, particularly, of interest as the pH in AD brain has been found to be slightly lower than in normal brain, and this acidolysis may result in enhanced Aβ deposition. Regions of the Aβ peptide responsible for conformational switching and fibrillogenesis have been examined using solvents at various pH to look at the effect of ionization on side chains, amino acid substitutions and truncation of Aβ from either the N- or C-terminus. Previous data show that the hydrophilic *N*-terminal of Aβ can form α-helix, random coil and β-sheet structures, strongly depending on solution conditions, while $A\beta^{29-42}$ remained in a β-sheet conformation, regardless of TFE content, pH or temperature (*61*). These results suggest that the hydrophobic segment in the C-terminal domain of Aβ is largely responsible for the propensity to form β-sheet exhibited by Aβ , while Aβ conformation is

more dependent on the secondary structure adopted by the N-terminal domain. This was also supported by the following observations: the single mutation of valine 18 (an amino acid forming β-sheets) to alanine (an amino acid forming α-helices) induced a significant increment of the α-helical content of $A\beta^{1-40}$ and dramatically diminished fibrillogenesis; the substitution of glutamine for glutamic acid at position 22 (the so-called "Dutch" peptide) decreased the propensity of the Aβ N-terminal domain to adopt an α-helical structure, with a concomitant increase in amyloid formation (*126*).

Given the growing evidence for a causative role of Aβ amyloid formation in Alzheimer's disease, it is becoming increasingly important to describe the mechanism of amyloid formation. The aggregation and assembly of Aβ peptides is a dynamic process, which is thought to proceed via a nucleation-dependent mechanism with a number of factors affecting the rate and equilibrium of fibril assembly. Numerous studies have been undertaken to help understand this mechanism, using a range of biophysical techniques including Fourier transform infrared spectroscopy, electron microscopy, Thioflavin T fluorescence, X-ray fibre diffraction, atomic force microscopy, surface plasmon resonance, cryoelectron microscopy and NMR spectroscopy (*129-147*). Key parameters promoting the assembly of amyloid fibrils and sedimentable aggregates include high peptide concentration (above 0.75 mg/ml), long incubation times, low pH (pH 5-6), and mechanical agitation (*59, 148*). The length of the carboxyl terminus is also critical in determining the assembly dynamics. The longer $A\beta^{1-42}$ isoform aggregates more rapidly at pH 7.4. Moreover, many reports have identified either specific residues or segments of Aβ that affect the solubility or toxicity of the peptide. For example, the replacement of hydrophobic for hydrophilic residues in the βA4 sequence impairs the formation of fibrils (*110*). Hilbich and co-workers (*110, 149*) reported that substitution of two or more hydrophobic amino acid residues between positions 17 and 20 in Aβ results in dramatically increased peptide solubility and reduced β-sheet content in Circular Dichroism (CD) spectra. Replacement of single residues in this region of Aβ with proline residues also decreased the aggregation propensity of the peptide (*150*). The work of Tjernberg and co-workers (*151*) and Hughes and colleagues (*152*) demonstrates that short Aβ peptide fragments with substitutions in the central hydrophobic cluster (LVFF) can alter the assembly of full-length Aβ. Substitution of residues Lys16 in $A\beta^{1-28}$ (*51*) or Phe19 or 20 for Ala in 10-23 (*110*) results in peptides unable to form amyloid-like fibrils in vitro. All these data suggest that the insolubility of Aβ is mainly due to its hydrophobic residues. Since this

region of Aβ is important for both intra- and intermolecular interactions (*45*), point substitutions in this part of the primary sequence may have important effects on the solution conformation of the peptide and consequently on the rate of plaque growth.

It may not necessarily be true that there is a distinct and reliable correlation between *in vitro* solution structure and Aβ deposition, however it is possible that particular conformational features in soluble Aβ may contribute to a better understanding of Aβ deposition in AD. Studies on Aβ peptides in solution have revealed a common theme in which the soluble full-length or fragments of the peptide have been converted from a α-helical structure or random coil structure to a β-structure upon aggregation. Inhibition of the process is therefore an appropriate target for therapeutic intervention to delay or prevent the progression of the disease.

1.2.2 Structure of β-amyloid fibrils.

Amyloid fibrils in AD are insoluble, ordered aggregates of normally soluble proteins. High-resolution structural studies of Aβ fibrils have proved very difficult because of the insolubility of the peptide at the concentrations required for NMR studies and the formation of noncrystalline aggregates unsuitable for X-ray diffraction (*56, 130*). So far, experimental studies on the structures of amyloid fibrils have been limited mainly to electron microscopy, low-angle X-ray fibril diffraction and solid-state NMR (see Table 1-2) (*27, 46, 49, 54, 114, 119, 120, 153-157*).

Electron microscopy of amyloids, including those made from variant Aβ peptides, often show ordered twisting, paired fibrils of 70-120 Å in diameter and of indeterminate length (*100, 158, 159*). An electron micrograph of $A\beta^{1-40}$ amyloid fibrils formed in vitro is shown in Fig. 1-3. (Fig. 1-3). $A\beta^{1-40}$ fibrils have a diameter of approximately 70 Å, whereas the predicted length of a 40-residue peptide in the β-strand conformation, with no turns, would be considerably longer, suggesting either the existence of a turn in the fibrils under the conditions of EM studies or a low-resolution picture demonstrating some type of “average” dimension in a molecule with two unequal axes (*47*). The morphological development of the Aβ polymerization process in detail from pseudo-spherical structures and protofibrils to mature thioflavin-T-positive/Congo red-positive amyloid fibrils under different experimental conditions was described using transmission electron microscopy. Moreover, the various polymorphic fibrillar assemblies were structurally characterized (*160*). These results provide

the framework for future investigations into how target compounds may interfere with the polymerization process.

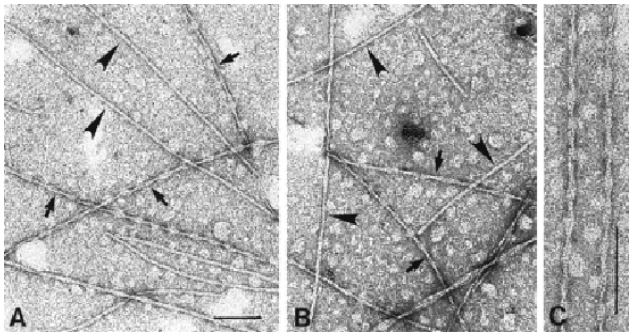

Fig. 1-3. Electron micrographs of $A\beta^{1-40}$.

In spite of differences among amyloid proteins, the apparent generalizability of amyloid structure lends support to the model peptide approach: generalizability implies reducibility. Systematically selected Aβ-fragments containing the $A\beta^{16–20}$ sequence, previously shown to be essential for Aβ·Aβ binding, were incubated in a physiological buffer. $A\beta^{14–23}$ was identified to be the shortest fibril-forming sequence as observed by EM. Substitutions in this decapeptide impaired fibril formation and deletion of the decapeptide from $A\beta^{1-42}$ inhibited fibril formation completely. Thus, it could serve as an invaluable preamble to the study of the native proteins.

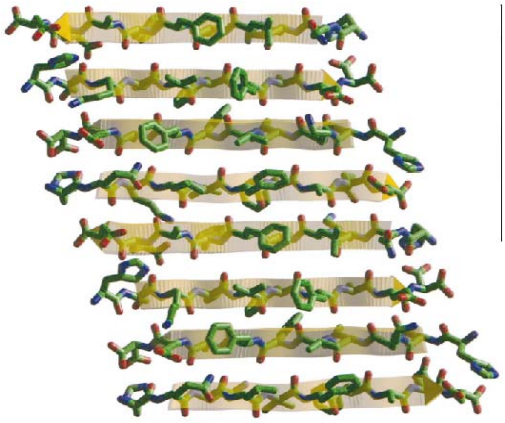

Fig. 1-4. Molecular modeling of A $\beta^{14–23}$. Two strands of the fibrilforming decamer $A\beta^{14–23}$ were aligned as an antiparallel b-sheet and subjected to energy minimization schemes. Note that His and Asp form ion pairs at both ends of the dimer. Two dimers were aligned. The resulting tetramer was energy minimized, and two ion pairs, Lys (*blue*) and Glu (*red*), were formed between the dimers. Two tetramers were aligned to form an octamer and were energy minimized. The fibril axis is in the plane of the paper and perpendicular to the peptide chains, and the Lys/Glu pairs are alternatively above and below the plane.

Molecular modelling of $A\beta^{14–23}$ oligomers in an antiparallel β-sheet conformation displayed favourable hydrophobic interactions stabilized by salt bridges between all charged residues (Fig. 1-4). The $A\beta^{14–23}$ fibril polymerisation was suggested to proceed via the formation of dimers, then tetramers and finally oligomers, in which the charged residues form ion pairs and

the hydrophobic residues forma hydrophobic core. This same pathway for fibrillogenesis of $A\beta^{14–23}$ is supported by results from other groups for $A\beta^{1-40}$ and $A\beta^{1-42}$ (*161-163*).

Fibre diffraction studies have shown that the Aβ in its fibril form is a predominantly β-pleated sheet conformation and exhibits the characteristic X-ray diffraction pattern first described for cross-β silk as indicated in Fig. 1-5 (*43, 48, 64*). Strong meridional diffraction pattern corresponding to a characteristic spacing of 4.7 Å is usually observed for kinds of amyloid fibrils, and is assigned to the distance between adjacent peptide chains in the β-sheets that comprise a corss-β structure. Strong equatorial diffraction signals corresponding to 8 ~ 11 Å range are also observed in most amyloid fibrils, and are commonly assigned to be the distance

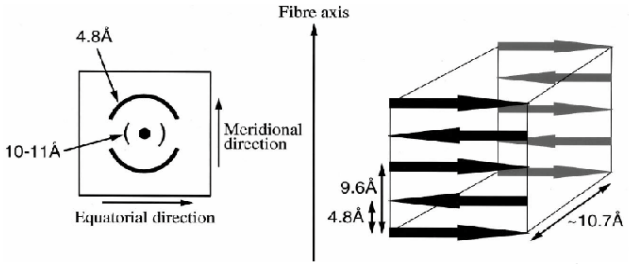

Fig. 1-5. The characteristic cross-β spacings from X-ray fibre diffreaction from amyloid fibrils. A strong 4.8 Å reflection on the meridian correspoinds to the hydrogen bonding distance between β-strands (shown right), and a more diffuse 10-11 Å reflection on the equator shows the intersheet distance of about 10.7 Å.

between β-sheet layers in a laminated structure which depends on the size of side chain groups. Thus, it is generally agreed that the β-strands are arranged perpendicular to the fibre axis and hydrogen bonds between adjacent peptide chains are going parallel to fibril axis. Fibre diffraction images from magnetically aligned fragments of the Aβ peptide have been obtained, leading to a model of β-sheet crystallites arranged in a pentagonal or hexagonal array (*45*). However, the packing arrangement of the β-sheets within the protofilament has yet to be resolved.

Fibre diffraction and solid-state NMR have revealed much about how the β-sheets are arranged within the amyloid fibril protofilament. Fibre diffraction data show only the repeating structure within a molecule. Solid-state NMR is capable of measuring interactions over relatively short ranges (~6 Å), and therefore contributes information about the local interactions within the β-sheets.

A structural model for amyloid fibrils formed by $A\beta^{1-40}$, based on a set of experimental constraints from solid-state NMR spectroscopy was presented by Tycko and co-workers (*27,*

60): Approximately the first 10 residues of $A\beta^{1-40}$ are structurally disordered in the fibrils. Residues 12-24 and 30-40 adopt β-strand conformations and form parallel β-sheets through intermolecular hydrogen bonding. Residues 25-29 contain a bend of the peptide backbone that brings the two β-sheets in contact through sidechain-sidechain interactions. A single cross-β unit is then a double-layered β-sheet structure with a hydrophobic core and one hydrophobic face. The only charged sidechains in the core are those of D23 and K28, which form salt bridges (Fig. 1-6).

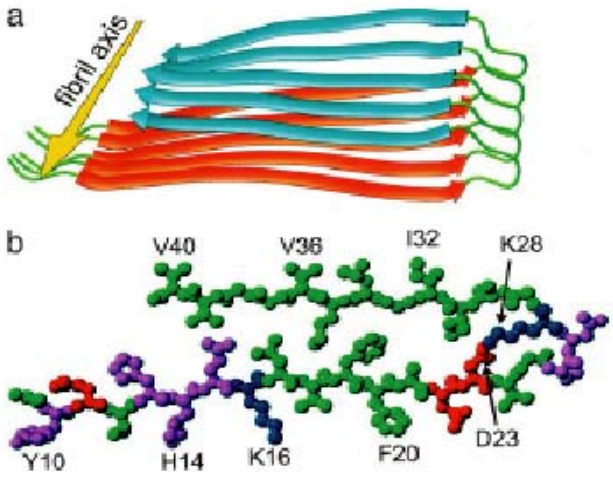

Fig. 1-6. Structural model for $A\beta^{1-40}$ protofilaments, derived by energy minimization with constraints based on solid-state NMR data (*60*). The model is also consistent with overall dimensions and MPL from EM and STEM and with the characteristic spacings in X-ray fiber diffraction patterns. (a) Ribbon representation of residues 9-40, viewed down the long axis of the protofilament. Each molecule contains two β-strands (red and blue) that form separate parallel β-sheets in a double-layered cross-β motif. Two such cross-β units comprise the protofilament, which is then a four-layered structure. (b) Atomic representation of residues 1-40.

There is essentially no amino acid sequence homology between Aβ and other amyloidogenic proteins, nor among any of the other amyloidogenic proteins. Nevertheless, quite remarkably, all amyloid proteins form linear fibrils of similar overall structure: that of a rod shaped fibril of β-sheet secondary structure. This pattern may well be related to many of the physical properties of amyloids: all amyloids have in common the ability to bind Congo red and thioflavin dyes; all are protease resistant in their fibrillar form and remain insoluble even in the presence of strong detergents like SDS, and they all give characteristic reflections of 5 and 10 Å in X-ray diffraction of powders (*48*). For these reasons, it seems likely that structural insights into Aβ fibrils will have a more general applicability to all or many amyloids. Thus, an approach towards resolving the structure of the Aβ fibril is a clinically relevant first step in our understanding of the more general phenomenon of amyloid deposition. It is, furthermore, a paradigm for understanding the wider biophysical problems of protein self-assembly and quaternary structure, as well as the pathways of protein folding.

To summarize, experimental data are beginning to shed light on issues such as the nature of the intermolecular interactions that stabilize amyloid structures, the molecular structural basis for polymorphism in amyloid fibrils, the universality of amyloid structures, and the balance between structural order and disorder within amyloid fibrils. Future structural data will contribute to an improved understanding of the mechanisms of amyloid formation and the mechanism of amyloid fibrils interacting with inhibitors, leading to the development of therapeutic agents for amyloid diseases.

1.3 Inhibition and reversion of Aβ amyloidogenesis as a therapeutic amyloid-related target for AD

Aβ amyloid formation and deposition is an early event in AD and perhaps a causative factor in AD as mentioned afore. Inhibiting Aβ fibrillogenesis is thus an important strategy for AD therapy. There are several possible targets to lower the cerebral amyloid burden in AD, like reduction of APP gene expression, alteration of APP processing, inhibition and reversion of Aβ misfolding and aggregation, enhancing the clearance of amyloid plaques and prevention of amyloid neurotoxicity (*76, 164, 165*). However, progress in developing therapies for AD is slow due to many unclear issues about AD. APP gene expression could be diminished by using modern techniques of gene therapy such as antisense oligonucleotides or genetically engineered ribozymes. But, until the biological function of APP is established, it remains possible that lowering APP production might produce undesirable side effects. As mentioned above, Aβ is generated from APP by two proteolytic cleavage events that involve the activity of at least two enzymes, named β- and γ-secretase. Inhibition of these enzymes or activation of nonamyloidogenic APP processing will probably reduce the brain concentration of sAβ and hence slow the formation of amyloid. However, it is likely that both β- and γ-secretase cleave many other proteins, which could be essential for proper functioning of the cell. Therefore, inhibitors of these enzymes may have profound toxic effects. Amyloid removal may be problematic due to their high insolubility, the attachment of a number of amyloid-binding proteins and the presence of various degenerating cell types, including dystrophic neurites, astrocytes, and microglial cells (*130*). Prevention of amyloid neurotoxicity requires fully understanding the diverse aspects of amyloidogenesis in AD, which are unfortunately unclear. Also, the uncertainties about the molecular mechanism of in vitro Aβ neurotoxicity complicate the use of this target as a therapy for AD. The available evidence indicates that Aβ misfolding and oligomerization are probably the first pathological processes in AD. This fact

and the abundant knowledge accumulated about the molecular mechanism of amyloid formation make the inhibition of Aβ amyloidogenesis an attractive therapeutic target for AD (*166*). Therefore, instead of focusing on inhibiting the production of Aβ in the brain or removing existing plaques (*23, 88, 164*), an alternative strategy is to identify small molecules capable of binding Aβ (*50, 167*), thus disrupting the formation of aggregates and altering aggregate structure, or by inhibiting interactions of Aβ with other receptors. Recent studies showed that full assembly of Aβ into mature fibres similar to those found in plaques is not necessary for toxicity. Smaller aggregates with molecular weights corresponding to dimers (*100, 101*), trimers, and tetramers (*52*) exhibit toxicity in cell culture as well. These findings support and highlight the necessity that Aβ assembly intermediates be included as targets in AD drug development.

Based on the conformation/oligomerization hypothesis (*26*), engineering compounds with the ability to stabilize the sAβ conformation, to destabilize the altered amyloidogenic conformer, and to prevent the required conformational transition could be effective inhibitors of amyloid plaque formation and very potent drug candidates for AD treatment. The intrinsic affinity of Aβ for itself suggested that Aβ-specific interactions could be adapted to the development of compounds that would bind to Aβ and prevent it from polymerizing (*53, 168, 169*). Currently, small negatively charged molecules are being investigated regarding their ability to block polymerization of Aβ or to disassemble preformed amyloid fibrils (*76, 148, 170*).

Soto and co-workers proposed that fibrillogenesis can be inhibited by short synthetic peptides partially homologous to Aβ which contain residues acting as β-sheet breaker peptides (*148, 171, 172*). In their studies, a β-sheet breaker peptide iAβ5 (LPFFD) was designed from the central hydrophobic region in the N-terminal domain of Aβ, amino acids 17-20 (LVFF) in order to specifically bind to the Aβ region implicated in β-sheet formation. A proline residue was added into the sequence to disrupt β-sheet formation, as incorporation of this amino acid within a β-pleated structure is highly unfavourable (*150*); a charged residue was added at the end of the peptide to increase solubility. It was demonstrated that iAβ5 inhibits amyloid β-protein fibrillogenesis, disassembles preformed fibrils *in vitro* and prevents neuronal death induced by fibrils in cell culture (Fig. 1-7). In addition, the β-sheet breaker peptide significantly reduced amyloid β-protein deposition *in vivo* and completely blockers the formation of amyloid fibrils in a rat brain model of amyloidosis. They hypothesized that two

main molecular events occur during the processing: first, binding between β-sheet breaker peptides and Aβ and second, conformational destabilization of β-sheet structures. Binding may be triggered via specific interaction recognition mechanisms dependent on the similarity of the sequence of the peptide with the self-recognition motif of Aβ. The interaction seems to be dependent on and stabilized by hydrophobic interactions. Previous data showed that the replacement of hydrophobic with hydrophilic residues in the internal Aβ region (amino acids 17–21: LVFFA) impairs fibrils formation (*149*), suggesting that Aβ assembly is partially driven by hydrophobic interactions. Therefore β-sheet breaker peptides, partially homologous to this hydrophobic region, may bind to Aβ by similar intermolecular interactions resulting in a competitive replacement of Aβ molecules by some β-sheet breaker peptides. A proline residue, introduced in the structure of the β-sheet breaker peptide, acts as β-sheet blocker because of its constraint to fold in a β-sheet structure. A key characteristic of proline residues is the ability to interconvert between cis and trans conformations. It is possible that this feature of proline might be important to destabilize intermolecular β-sheets. Recently it was shown that the pharmacological profile of β-sheet breaker peptides can be improved to produce compounds with drug-like properties that might offer a new promise in the treatment of Alzheimer's disease (*88*). However, the detailed mechanism of iAβ5 interacting with Aβ fibrils awaits further study, as its understanding will require the elucidation of the tri-dimensional structure of the complex protein/peptide (Aβ/β-sheet breaker).

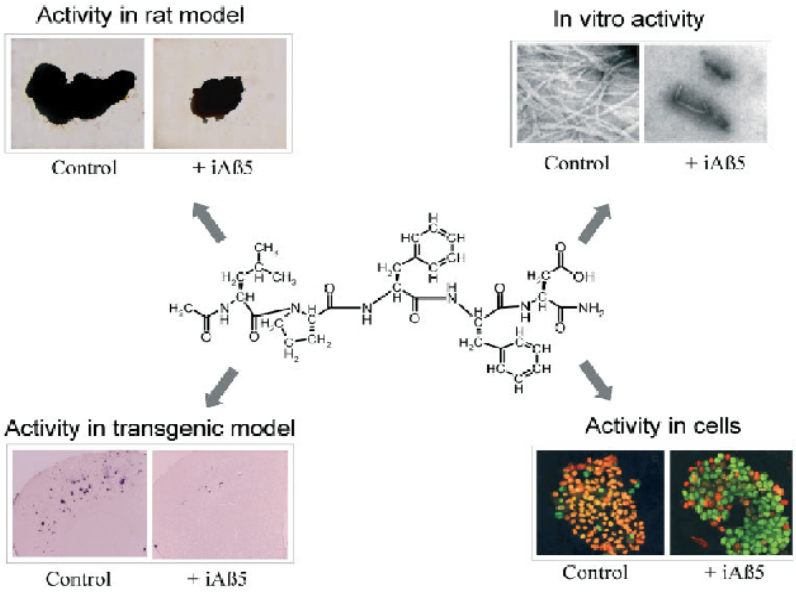

Fig. 1-7. β-sheet breaker peptides as a promising approach for the treatment of AD. A 5 residue-peptide (chemical structure in center panel) has been shown to be active in everal in vitro, cellular, and in vivo models (*76*).

Given the hypothesis that aggregation intermediates are responsible for Aβ toxicity, one approach to this problem is to identify compounds that bind Aβ, because these might interfere with its aggregation and toxicity (*50*). These binding candidate compounds could theoretically prevent all aggregation, or alternatively cause further association of toxic oligomers into larger nontoxic aggregates. The latter was proofed by Murphy and co-workers. The inhibitors were designed as containing a ‘‘recognition domain’’, a short peptide sequence homologous to a fragment of full-length Aβ (KLVFF, 16– 20), and a ‘‘disrupting domain’’, a polypeptide chain with the ability to interfere with Aβ aggregation (*53, 173, 174*). It was shown that the inhibitors that protected PC-12 cells from Aβ toxicity actually increased the rate of Aβ aggregation and these peptides designed to interfere with Aβ aggregation also inhibited Aβ-associated toxicity (*173*). Among these peptides, $KLVFFK_6$ was the most potent at preventing Aβ-associated toxicity to PC-12 cells and caused the largest change in Aβ aggregation kinetics and aggregate morphology (*53*). A detailed mathematical model of the specific step(s) in the aggregation pathway affected by $KLVFFK_6$ was suggested based on their experimental data: (1) the inhibitor does not change the distribution of Aβ between amyloid and nonamyloid paths; (2) it affects most strongly the rate of lateral aggregation of Aβ filaments into fibrils; (3) it interacts with aggregated, not monomeric, Aβ, to enhance hydrophobically driven association (*175*).

Structural information regarding the interaction with the target molecule is of major interest to suggest new design strategies in the search for better inhibitors of Aβ toxicity and to transform them into peptide mimetics. Meanwhile, such a study of interactions of Aβ with inhibitors can contribute in valuable mechanistic understanding of the amyloid, such as the arrangements of the constituent peptides and how these peptides pack together in the fibril. It could be the fundamental event in the development of therapies for those diseases, and also for elucidating fundamental mechanisms of protein folding and assembly.

1.4 Peptide synthesis

Examination of the events by which monomeric Aβ associates into oligomers and fibrils is of central importance to elucidate the molecular mechanisms underlying AD pathogenesis. Synthetic Aβ peptides were shown to be a powerful tool in the structural research of Aβ. The fact that fibrils formed from synthetic peptides *in vitro* are identical to those in vivo as

determined by EM and x-ray diffraction, and are toxic to neuron, underlines the validity of in vitro synthetic Aβ aggregation studies (*51, 89, 176, 177*).

Aβ peptides have been successfully prepared by both Boc-SPPS and Fmoc-SPPS for use in a range of structural and biological studies (*178*). Automated Boc- SPPS was used for the preparation of $A\beta^{1-42}$, $A\beta^{1-39}$, $A\beta^{1-28}$ and $A\beta^{29-42}$ in the studies by Barrow *et al*. . Recently, Liu *et al*., He and Barrow have reported the successful use of an *in situ* neutralization Boc-SPPS methodology for the preparation of $A\beta^{1-28}$, $A\beta^{1-40}$ and analogues thereof.

Solid phase peptide synthesis (SPPS) is a quick and easy approach to synthesizing peptides and small proteins (*179*). It is used extensively in the field of bioorganic chemistry. The general scheme for solid-phase peptide synthesis is outlined in Fig. 1-8.

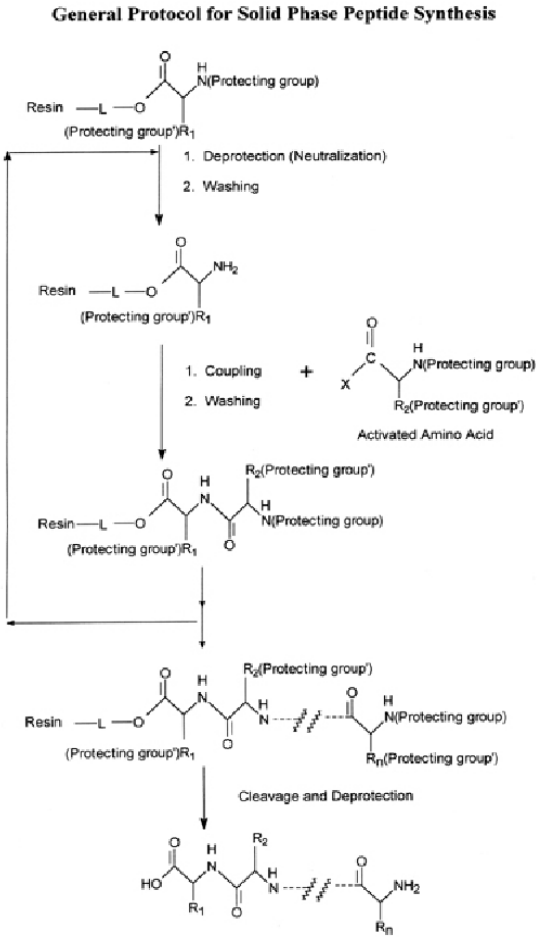

Fig. 1-8. General scheme for solid-phase peptide synthesis.

The C-terminal amino acid with N-α-derivatizing is attached to an insoluble support via a linker. The N-α-blocking group is then deprotected and the amino acid-linker-support is thoroughly washed with solvent. The next amino acid (which is N-α-derivatized) is then

coupled to the amino acid-linker-support as either a preactivated species or directly in the presence of an activator. After this reaction is complete, the N-α-dipeptide-linker-support is washed with solvent. The deprotection/coupling cycle is repeated until the desired sequence of amino acids is generated. The peptide-linker-support is cleaved to obtain the peptide as a free acid or amide, depending on the chemical nature of the linker. Ideally, the cleavage reagent also removes the amino acid side chain protecting groups, which are stable to the deprotection reagent.

The solid support is a synthetic polymer that bears reactive groups such as -OH, -Cl. These groups are made so that they can react easily with the carboxyl group of an N-α-protected amino acid, thereby covalently binding it to the polymer. The amino acid may be attached directly to the linker-support or first attached to the linker, with subsequent attachment of the amino acid-linker to the support. There are lots of different linkers utilized in Fmoc SPPS, such as p-alkoxybenzyl alcohol/p-hydroxymethylphenoxy (HMP) and 2-chlorotrityl-chloride resin (TCP). The great variety of available peptide-to-resin linkers permits eventual cleavage of synthesized polypeptides as free acids, side-chain protected peptide acid fragments, amides, and hydrazides, as well as a number of less common carboxyl derivatives.

The loading of the first amino acid to the linker-resin often requires ester bond formation, which is efficiently catalysed by base. Initial Fmoc SPPS loaded the first amino acid with DCC/DMAP (N, N-dicyclohexylcarbodiimide/4-dimethylaminopyridine). It was subsequently reported that Fmoc amino acid was loaded very efficiently in the presence of 1 equiv. of N, N-diisopropylethylamine (DIPEA) in dichloromethane (DCM).

Now the extensively explored α-amino blocking group is the base labile 9-fluorenylmethoxycarbonyl (Fmoc) group which can be removed under non-acidic conditions.

The structure of the Fmoc protecting group is as follows:

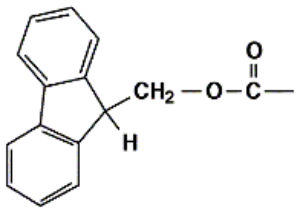

Fluorenylmethyl succinimidyl carbonate (Fmoc-ONSu) was shown to be the optimum reagent for preparation of Fmoc amino acids because it can efficiently attach to the amino acid in

aqueous dioxane, aqueous acetone, aqueous DMF, or aqueous acetonitrile in the presence of $NaHCO_3$ or Na_2CO_3 (*179*).

Dichloromethane (DCM), dimethylformamide (DMF) or N-methylpyrrolidone (NMP) is the primary solvent for deprotection, coupling, and washing.

To begin each coupling, the Fmoc group on the resin bound amino acid/peptide must be removed. The electron withdrawing fluorine ring system of the Fmoc group renders the lone hydrogen on the α-carbon very acidic, and therefore susceptible to removal by weak bases. The Fmoc group is most often deprotected in SPPS by 20-50% piperidine /DMF or 30% piperidine /35% toluene /35% DMF.

Generally, an amino acid consists of a side chain group which defines the different structures of the amino acids. Certain side chains contain functional groups that can interfere with the formation of the amide bond. Therefore, it is important to mask the functional groups of the amino acid side chains. *t*Bu side chain protection group is traditionally used in Fmoc SPPS in that it is base stable and TFA labile. Asp, Glu, Ser, Thr, Tyr, Cys, can be side chain protected by it. *Tert*-butyloxycarbonyl (Boc) is another often used side chain protection group. It can be used for His, Arg, Lys. Trityl (Trt) can be used for Gln, His, Cys, Arg. The mild base deprotection of Fmoc SPPS permits some amino acids to be incorporated without side chain protection, such as Met, Trp.

To ensure homogeneous peptide products, Fmoc amino acid acylation reactions must be maximally efficient. Benzotriazolyl N-oxytrisdimethylaminophosphonium hexafluorophosphate (BOP) and 2-(1H-benzotriazol-1-yl)-1, 1, 3, 3-tetramethyl uranium hexafluorophosphate (HBTU) are two of the more popular activating agents now used. Other additives such as HOBT (1-hydroxybenzotriazole) or imidazole are used in order to suppress racemization during coupling and achieve rapid coupling.

Once the peptide is complete, it is ready to be cleaved from the resin. Since non-acidic conditions are utilized for N-α-amino group deprotection, weak acids such as dilute TFA can be used for cleavage and side chain deprotection. Strong acid such as hydrofluoric acid (HF) cleavage is also compatible with Fmoc amino acid side chain protecting groups. Alternate cleavage conditions, such as alkali, photolysis, fluoride ions, or hydrogenation, are used primarily for peptide isolation with intact side chain protecting groups or to produce a unique peptide carboxyl terminus.

SPPS has been demonstrated to provide a facile means for the preparation of a wide range of peptide sequences. However, despite the substantial optimization and development the method has undergone since its introduction, a subset of sequences still prove problematic to prepare. These so-called "difficult" sequences, of which Aβ is a prime example, are poorly solvated while bound to the solid phase, which results in reduced Nα-amino acid acylation and deprotection yields (*10*).

The synthesis of $A\beta^{1-28}$, $A\beta^{1-30}$, $A\beta^{1-33}$, $A\beta^{1-36}$, $A\beta^{1-39}$, $A\beta^{1-42}$, $A\beta^{1-47}$ and $A\beta^{1-52}$ by Fmoc-SPPS was undertaken by Burdick *et al*. as part of a systematic analysis of the role of the hydrophobic *C*-terminal region of Aβ (*177*). In this study, the assembly and purification of all of the peptides up to $A\beta^{1-42}$ was found to proceed relatively smoothly, with adequate peptide yield and purity being obtained throughout. However, $A\beta^{1-42}$ proved problematic to purify and adequate characterizations of the $A\beta^{1-47}$ and $A\beta^{1-52}$ samples prepared were not achieved. More recently, the stepwise Fmoc-SPPS of $A\beta^{1-39}$ and $A\beta^{1-40}$ have been performed and the identities of the substantial amounts of side products formed during these syntheses investigated (*180, 181*). Further optimization of the Fmoc-SPPS of 'difficult' sequences by the use of HATU activation for regions of the target sequence known to be prone to aggregation has also been reported to enable preparation of Aβ and other aggregating sequences with a high yield and better than 90% initial purity (*182*). The synthesis of $A\beta^{1-42}$ and $A\beta^{1-43}$ has also been achieved by the segment condensation of fully-protected peptide fragments previously prepared by Boc-SPPS in organic solution (*183*). $A\beta^{1(3)-9}$, $A\beta^{10-19}$, $A\beta^{20-25}$, $A\beta^{26-29}$, $A\beta^{30-33}$ and $A\beta^{34-42(43)}$ were ligated in a stepwise manner using a mixture of chloroform and phenol to solubilize these weakly soluble fragments. The preparation of $A\beta^{1-43}$ and $A\beta^{25-35}$ has also been successfully performed using Fmoc-SPPS together with Hmb backbone amide protection (*184-186*). $A\beta^{1-43}$ was initially prepared using Hmb protection of Gly38, Gly33, Gly29, Gly25 and Phe20 (*185*). Hmb groups were incorporated using *N*, *O*bisFmoc-Hmb amino acid Pfp esters, and their acylation was performed using *N*-carboxy anhydrides in DCM. The positioning of the Hmb amino acids was largely dictated by the previously noted ability of these protecting groups to abolish peptide aggregation for five or six residues after their incorporation during 'difficult' sequence assembly (*187*).

The SPPS method is a practical method to synthesize isotope-labelled analogues that are required for structural studies. ^{13}C- and ^{15}N-labelled Aβ peptides were well studied by solid-state NMR, where isotopic substitution provides the source points for measuring distances in

aggregated Aβ (*111-114, 119*). In some cases, modified functional groups could be easily incorporated into peptide sequences for investigation of structures, such as that employed by Gordon (*188*). In this study, amide bonds in $A\beta^{16-20}$ were replaced with ester bonds to investigate the effect of backbone hydrogen bonding in amyloid fibrils. The experimental data demonstrate that this ester peptide is predominantly monomeric under solution conditions, inhibits the aggregation of the $A\beta^{1-40}$ peptide and disassembles preformed $A\beta^{1-40}$ fibrils. These results suggest that backbone hydrogen bonding is critical for the assembly of amyloid fibrils.

SPPS could also be used to obtain peptide by substituting certain residues in the sequence with specified amino acids for structural studies (*149, 189, 190*). For example, an $A\beta^{10-35}$-NH2 analogue with a single point substitution (F19T) in this region was synthesized and examined (*189*). Unlike $A\beta^{10-35}$-NH2, the F19T analogue was plaque growth incompetent, and NMR analysis indicated that the mutant peptide was significantly less folded than wild-type Aβ, suggesting that the plaque competence of Aβ correlates to peptide folding.

1.5 Structural studies by Electron Microscopy

Electron Microscopy was used in the studies on structures of amyloid fibrils. Electron Microscopy can yield information about the surface features of an object or "how it looks", its texture; direct relation between these features and materials properties (hardness, reflectivity, etc.); the shape and size of the particles making up the object; direct relation between these structures and materials properties (ductility, strength, reactivity, etc.); the elements and compounds that the object is composed of and the relative amounts of them; direct relationship between composition and materials properties (melting point, reactivity, hardness, etc.); how the atoms are arranged in the object; direct relation between these arrangements and materials properties (conductivity, electrical properties, strength, etc.).

Electron Microscopes (EM) function as follows: a stream of electrons is formed and accelerated toward the specimen using a positive electrical potential. With metal apertures and magnetic lenses this stream is confined and focused into a thin, focused, monochromatic beam. Then this beam is focused onto the sample using a magnetic lens. Interactions thus occur inside the irradiated sample, affecting the electron beam. These interactions and effects are detected and transformed into an image.

Specimen interaction is what makes Electron Microscopy possible. The energetic electrons in the microscope strike the sample and various reactions can occur as shown below. The reactions noted on the top side of the diagram are utilized when examining thick or bulk specimens (SEM) while the reactions on the bottom side are those examined in thin or foil specimens (TEM).

Electron microscopy and image processing is one of the most powerful tools in the structural investigation of large biological complexes. Insights into the structural organization of the complexes can be gained without the necessity of crystallizing the complex. This provides the means for observing structural changes during function of complexes unhindered by crystal contacts.

Electron microscopy has been used to examine the morphology of fibrils formed from different sequence peptides in different defined conditions (*42, 47, 160, 177, 191*). The morphology and molecular architecture of amyloid fibrils are apparently very similar, although they are formed from proteins with widely different native structures, sizes, and localization. In these EM images, fibrils contained both twisted, paired fibrils with a maximum width of about 16 nm, with a superhelical repeat distance of ~110 nm, and monomeric fibrils of ~8 nm diameter. Also, it has been reported that fibril morphology of Aβ is dependent on pH value as shown by EM (*54*).

Electron microscopy has been used to study the factors that either promote or inhibit Aβ fibril formation and aggregation and the driving forces that are involved in the fibrillogenesis (*41, 167*). Identification of these factors and understanding of the driving forces behind these interactions as well as identification of the structural motifs necessary for these interactions will help to elucidate potential sites on Aβ that may be targeted to prevent amyloid formation and its associated toxicity. EM has also been used to assay the influence of identified candidate compounds on the assembly of Aβ fibrils (*167*). Fraser and co-workers found out that inositol could stabilize small aggregates of $A\beta^{1-42}$ that do not proceed to form fibrils as demonstrated by Electron microscopy, thus representing a potential candidate for inhibiting nucleation (*41*).

Electron microscopy has been used to study the assembly process of β-amyloid (*160*). The time course of Aβ fibril formation was characterized using a variety of assays and various experimental conditions. The detailed morphological development of the Aβ polymerization

process was described from pseudo-spherical structures and protofibrils to mature thioflavin-T-positive/Congo red-positive amyloid fibrils. Moreover, the various polymorphic fibrillar assemblies were structurally characterized using transmission electron microscopy and their mass was determined using scanning transmission electron microscopy. These results provide the framework for future investigations into how target compounds may interfere with the polymerization process.

1.6 Structural studies by Circular Dichroism

Circular Dichroism spectroscopy, which is a form of light absorption spectroscopy that measures the difference in absorbance of right- and left-circularly polarized light (rather than the commonly used absorbance of isotropic light) by a substance, has been extensively applied to the structural characterization of peptides in solution (*192*). The phenomenon of circular dichroism is very sensitive to the secondary structures of polypeptides and proteins: alpha helix, parallel and antiparallel beta sheet, turn. Therefore the analysis of CD spectra can yield valuable information about secondary structure of biological macromolecules (*192*) and can be used to monitor relative structural changes of proteins due to environmental influences on the sample (pH, denaturants, temperature etc.). Considering all CD spectra as a combination of those secondary structures, it is possible to estimate the amount of these secondary structures in a given protein using curve fitting algorithms. This approach converged CD spectroscopy not only a qualitative, but a semi-quantitative method determining the secondary structural propensity of proteins and peptides in solution.

The application of CD for conformational studies in peptides (like proteins) can be largely grouped into 1.) monitoring conformational changes (e.g., monomer-oligomer, substrate binding, denaturation, etc.) and 2.) estimation of secondary structural content. As already mentioned, CD is particularly well-suited to determine structural changes in both proteins and peptides.

The secondary structures of the synthetic, naturally occurring, β–amyloid peptides in solution have been studied by Barrow *et al* using CD spectroscopy (*61, 124*). In their work, several factors on the β-sheet formation have been monitored, like pH, peptide concentration, time dependence and solvent effect. It was found that in aqueous trifluoroethanol solution, the $A\beta^{1-28}$, $A\beta^{1-39}$, and $A\beta^{1-42}$ peptides adopt monomeric α-helical structures at both low and high pH, whereas at intermediate pH (4 to 7), an oligomeric β structure predominates. The hydrophobic

carboxyl-terminal segment, $A\beta^{29-42}$, exists exclusively as an oligomeric β-sheet in solution, regardless of differences in solvent, pH, or temperature. A pH-dependent transition of $A\beta^{10-35}$ from coil to β-structure was most obvious in the circular dichroic spectra (*47*). CD spectroscopy was also used to assess whether the selected peptides could prevent Aβ from adopting a β-sheet conformation (*175, 193*). It was found that the presence of 10 μM D-KLVFFA during the L-Aβ incubation prevented this random coil to β-sheet-rich secondary structure transition, maintaining Aβ close to its original conformation. The secondary structure was followed as a function of time and concentration by CD (*169*).

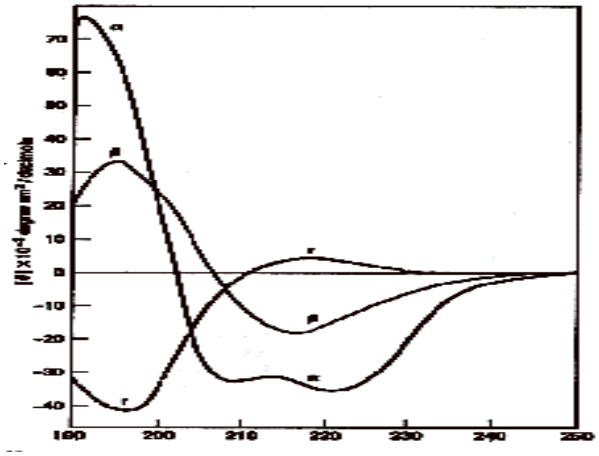

Fig. 1-9. Circular dichroism spectra of poly (Lys) in the α-helical (α), β -sheet (β), and random coil (r) conformations (From "Proteins: Structures and Molecular Properties, by T.E. Creighton).

The structural studies by CD spectroscopy allow qualitative studies of the structure of peptides in solution.

1.7 Structural studies by solution NMR spectroscopy

A detailed understanding of the function of a biological macromolecule requires knowledge of its three-dimensional structure. Nuclear magnetic resonance (NMR) spectroscopy is currently the most powerful technique capable of determining high-resolution structures of biological macromolecules such as proteins and nucleic acids at atomic resolution. The basic phenomenon of NMR was discovered in 1945: the energy levels of atomic nuclei are split up by a magnetic field. Transitions between these energy levels can be induced by exciting the sample with radiation whose frequency is equivalent to the energy difference between the two levels. The nuclei of greatest interest for organic chemistry and biochemistry, H, C, N, and P, all have isotopes with spin ½ having a magnetic moment, though for C and N the natural abundance of these isotopes (^{13}C, ^{15}N) is very small. However, these isotopes can be

incorporated into biomolecules through isotope labelling. Since 1960, the field of NMR has seen an explosive growth which started with the development of pulsed Fourier-transform NMR and multidimensional NMR spectroscopy. The first NMR-derived three-dimensional solution structure of a small protein was determined in 1985, since then major improvements in NMR hardware (magnetic field strength, cryoprobes) and NMR methodology, combined with the availability of molecular biology and biochemical methods for preparation and isotope labeling of recombinant proteins have dramatically increased the use of NMR for the characterization of structure and dynamics of biological molecules in solution. These improvements are ongoing and are designed to overcome the two main problems with NMR of biomacromolecules, namely signal-to-noise and spectral overlap. Importantly, biomolecular NMR spectroscopy can provide information about conformational dynamics and exchange processes of biomolecules at timescales ranging from picoseconds to seconds, and is very efficient in determining ligand binding and mapping interaction surfaces of protein-ligand complexes.

In the following, the basic principles of NMR are described and the applications of biomolecular NMR in structural biology are introduced.

1.7.1 Theory of NMR spectroscopy

In an external magnetic field B_0, nuclei with spin ½ are aligned either in a parallel or antiparallel orientation with respect to the magnetic field. The parallel α state is lower in energy than the antiparallel β state. The energy of these levels is given by the classical formula for a magnetic dipole in a homogenous magnetic field of the strength B_0:

$$E = - \mu_z * B_0 = - m * \gamma * h/(2\pi) * B_0 ,$$

where, h, the Planck's constant; γ, the gyromagnetic ratio; m, the magnetic quantum number, an integer number between $-I$ and $+I$.

Therefore, the population of the α state is greater than that of the β state (Boltzmann distribution), and a macroscopic magnetization along the B_0 field exists due to this population difference. The magnetic moment of each nucleus precesses around B_0. The frequency of this precession is the larmor frequency (ω_0) which is equivalent to the energy difference between the two levels. In order to measure the precession frequencies, the system is disturbed and brought into a non-equilibrium state which allows monitoring the transverse (x or y)

magnetization. This can be done by applying an oscillatory magnetic field B_1 that rotates the magnetization away from the z-axis toward the x, y plane. Being composed of individual nuclear *spins*, a *transverse* (in the *x*, *y* plane) macroscopic magnetization Mx,y (*coherence*) starts precessing about the *z* axis with the Larmor frequency (in the lab coordinate system) under the influence of the static B_0 field, thus inducing a current in the receiver coil, which is then recorded and called the free induction decay (FID). The FID obtained from a FT NMR experiment is a superposition of the frequencies of all spins in the molecule as a function of time, F(t). In order to obtain the corresponding spectrum F(ω) (intensity as a function of frequency) a Fourier transformation is performed. Fourier transformation is a simple mathematical operation which translates a function in the time domain into the frequency domain.

Relaxation and NMR linewidths After a 90° pulse has been applied to the equilibrium *z*-magnetization, a transverse magnetization is created in which the phases of the individual spin precession frequencies are correlated. Such a non-random superposition of states is called coherence. However, the population difference between the α and β-states (which corresponds to the *z*-magnetization) has disappeared. Thus, the system is in a non-equilibrium state and will therefore relax back into the equilibrium state. This is described by two relaxation processes. The loss of phase-coherence in the transverse plane due to spin-spin interactions defines the T_2 or transverse relaxation time. In addition, the population difference along *z* is restored by interactions with the surroundings. This spin-lattice relaxation is described by the T_1 or longitudinal relaxation time. The linewidth of an NMR signal is described by the exponential decay of the FID, and reciprocal to the transverse relaxation time T_2. It scales with the molecular tumbling rate in solution and therefore increases with higher molecular weight. This is the main reason for the molecular weight limitation of NMR.

Chemical Shifts The static magnetic field B_0 is shielded by the electrons in the local environment of a spin. Therefore, the individual resonance frequencies are slightly different reflecting the different chemical surroundings. The resonance frequencies are called chemical shifts and are measured in *parts per million (ppm)* in order to have chemical shift values independent of the static magnetic field strength. For example, backbone amide protons H^N in a protein resonate around 8 ppm, while H^α spins have resonance frequencies between 3.5-5.5 ppm.

J-coupling Scalar or J-couplings are mediated through *chemical bonds* connecting two spins. The energy levels of each spin are slightly altered depending on the spin state of a scalar coupled spin (α or β). This gives rise to a splitting of the resonance lines. Typical coupling constants are: ^{1}J (H^N, N) ~ 92 Hz, $^{3}J(H^N,H^\alpha)$ ~ 2-10 Hz, $^{>3}J < 1$. ^{3}J-couplings are well-correlated with the central dihedral angle by an empirical correlation, the Karplus curve. For example, ^{3}J (H^N,H^α) defines the backbone angle ϕ in proteins. Scalar couplings are used in multidimensional (2D, 3D, 4D) correlation experiments to transfer magnetization from one spin to another in order to identify spin systems, e.g. spins which are connected by not more than three chemical bonds. For example, the amino acid ^{1}H spin system of Alanine consists of H^N, H^α and H^β.

Nuclear Overhauser Effect (NOE) The nuclear Overhauser effect is a result of cross relaxation between *dipolar coupled* spins as a result of spin/spin interactions *through space*. Dipolar couplings are usually in the kHz range, and depend on the distance between the two spins and the orientation of the internuclear vector with respect to the static magnetic field B_0. Fortunately, due to the fast overall tumbling of molecules in solution, the dipolar couplings are averaged to zero. Nevertheless, the dipolar couplings give rise to spin/spin and spin/lattice relaxation. The NOE is a result of cross-relaxation between spins and is defined by the transition rates W_0 and W_2 which involve spin flips of both spins. The NOE allows to transfer magnetization from one spin to another *through space*, and scales with the distance r between the two spins (NOE ~ $1/r_6$), e.g. two protons in a protein. Therefore the NOE is related to the three-dimensional structure of a molecule. For interproton distances > 5 Å, the NOE is too small and not observable.

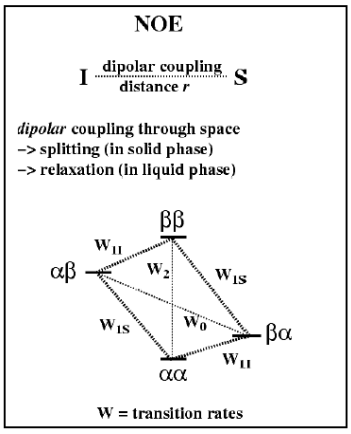

Residual Dipolar couplings For two directly coupled nuclei A and B, the direct dipolar coupling interaction is quantified by (*194*)

$$D^{AB} = \frac{-\mu_0 h \gamma_A \gamma_B}{8\pi^3} \left\langle r_{AB}^{-3} \right\rangle \left\langle \frac{3\cos^2\theta - 1}{2} \right\rangle \qquad [1\text{-}1]$$

where μ_0 is the permeability of free space, γ_A and γ_B are the magnetogyric ratios of the coupled nuclei, and $<r^{-3}_{AB}>$ is the motionally-averaged inverse cube of the internuclear distance, θ is the time-dependent angle between a unit vector in the internuclear direction and a unit vector parallel to B_0, and the brackets signify the time average of the quantity. Normally, the random, isotropic sampling of angles by a molecule tumbling in solution reduces the RDC to zero. This isotropic sampling may be made anisotropic by a magnetically induced alignment or with the aid of various types of media. This anisotropic sampling will result in a measurable RDC that is indicative of the average orientation of an inter-nuclear vector.

Since the introduction of two–dimensional methods, NMR spectroscopy has developed into the most important method for the investigation of the structure, dynamics, and reactions of molecules. The basic 2D NMR experiment consists of exciting the nuclei with two pulses or groups of pulses then receiving the free induction decay (FID). The acquisition is carried out many times, incrementing the delay (evolution time - t_1) between the two pulse groups. Any two-dimensional NMR experiment is composed of four separate segments: preparation period, evolution period, mixing period, detection. A pulse sequence for a typical 2D experiment is shown in Fig. 1-10.

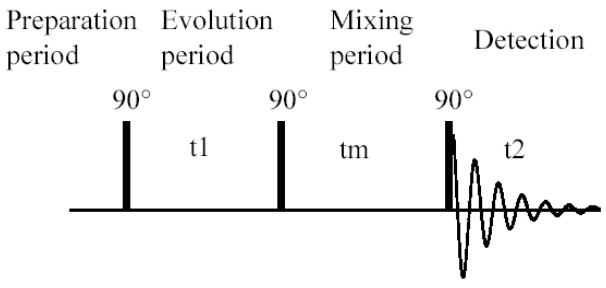

Fig. 1-10. The Pulse Sequence for 2D NOESY Experiment.

The preparation period can be as simple as a delay and a pulse or a very complicated series of pulses. The evolution period is the variable time, t1, in which the first chemical shifts are allowed to evolve. The mixing period is the “heart” of a 2D experiment. The type of correlation observed is a result of the type of mixing. For example, NOESY mixing allows for

cross relaxation between nuclei close in space and can measure internuclear distances. TOSCY or COSY mixing periods allows for magnetization to be transferred between scalar coupled nuclei, giving rise to correlations between nuclei with couplings. The detection period is the recording of the FID.

1.7.2 Structural studies on proteins by solution NMR

NMR does not directly produce an image of a protein. Rather, it is able to yield a wealth of indirect structural information from which the three-dimensional structure can only be revealed by extensive data analysis and computer calculations. The principle of a NMR structure determination can be summarized as follows: preparation of the protein solution, the NMR measurements, the assignment of NMR signals to individual atoms in the molecule, identification of conformational constrains (e.g. distances between hydrogen atoms), the calculation of the 3D structure on the basis of the experimental constraints.

In principle, each spin in one molecule should be characterized by a unique NMR line, so that the NMR spectrum of a protein will show NMR signals of each spin with slightly different frequencies. In the initial stage of investigation by NMR spectroscopy, each resonance observed in an NMR spectrum must be assigned to a specific nucleus in the investigated molecule. Experiments such as 2D COSY and TOCSY are employed for the identification of amino acid spin systems. Normally, each spin system will contain all the atoms of one amino acid residue. The first step in sequential assignment is the identification of certain amino acids by using the marker tool. Once a spin system is found, and noted with one or several markers, the same process is repeated till all the spin systems are assigned. Once the NMR signals are assigned, experimental parameters which define the three-dimensional structure are measured.

Structural information from NMR experiments comes primarily from magnetization transfer between pairs of protons through bond (scalar or *J coupling*) or through space (the Nuclear Overhauser Effect *NOE*). J-coupling constants, which are mediated through chemical bonds provide information about dihedral angles, and thus can define the peptide backbone and side chain conformations. The intensity of a NOE is proportional to the inverse of the sixth power of the distance separating the two nuclei.

NOE is a sensitive probe of short internuclear distances, based on the nuclear Overhauser effect (NOE), which is a result of cross-talk between different spins (normally protons) and

depends on the *through-space* distance between these spins. NOEs are typically only observed between protons which are separated by less than 5-6 Å. Transferred NOE Experiments are a special kind of NOE experiments which are applicable to macromolecule-ligand complexes in medium or fast exchange (see Fig. 1-11). Whenever the dissociation rate constant of the complex is fast compared to the T1-relaxation time-scale of the experiment, the observed NOE effects represent the bound state of the ligand molecule and are called trNOEs. One- and two-dimensional transferred nuclear Overhauser spectroscopy (trNOESY) are unique techniques used to determine the conformation of a small ligand molecule bound to a macromolecule or molecular assembly in solution (*195-197*). *tr*NOE and trNOESY have been used to study structures of substrates, inhibitors, and coenzymes bound to numerous enzymes, peptides bound to membranes, peptides bound to proteins, and an antigen bound to antibody (*198-202*). *tr*NOE and trNOESY methods have been shown to be very powerful in determining conformations of nucleotides bound to enzymes . The NOE cross-peaks for each proton pair of a nucleotide can be easily identified and inter-proton distances of the enzyme-bound nucleotide can thus be determined by their relative NOE intensities. A molecular model of the enzyme-bound nucleotide can then be constructed using an energy minimization molecular modelling program with the NOE determined inter-proton distance constraints.

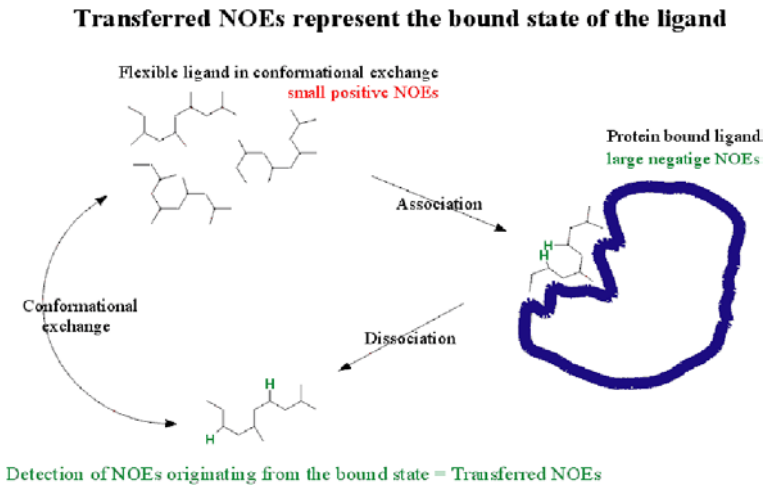

Fig. 1-11. Principle of the trNOE experiment. The NOE is only operative when the ligand is bound, since the ligand experiences a long correlation time (τc) only in the bound state. The relaxation is transferred and measured on the resonances of the ligand in the free state. The relaxation thus contains exclusively information on the geometry (projection angles and distances) of the ligand in the bound state.

Recently, new NMR parameters, such as residual dipolar couplings (RDCs) and cross-correlated relaxation effects (CCRs) (*203*) have been shown to provide distance independent projection angles for bond vectors, e.g. N–H and C^{α}-H^{α} bonds in proteins (*201, 204-206*). Especially, RDCs are extremely useful for defining the relative orientation of two domains of

a protein (NOEs between separate domains are often not observed due to the 5 Å upper distance limit for observation of an NOE). Recently, it was found, that it is possible to measure residual dipolar couplings in solution by weakly aligning a molecule in the solution (*194, 207, 208*). If only a fraction of 1 out of 1000 molecules is aligned, the dipolar couplings, which in the solid state are in the kHz range, are scaled down to a few Hz. The weakly alignment could be introduced by anisotropic solution, e.g. bicelle type lyotropic liquid crystals (*209*), phage particles (*210, 211*), purple membrane fragments (*212, 213*) or strained polyacrylamide gels (*214-216*) (for an overview see (*217*)). This allows to utilize the distance and the angle dependence of dipolar couplings in order to obtain orientational restraints, while still obtaining high-resolution NMR spectra. As shown by equation (1-1), if angles are available from structure, RDCs will provide useful distance restraints for structure refinement (*218*); if the internuclear distance is fixed, as in one-bond spins, N-H, C-H, RDCs will provide useful angular restraints for refining or directly determine the structure of proteins (*219*), nucleic acids (*220*) or carbohydrates (*221*). Residual dipolar couplings provide not only additional structural information, but are crucial to define *long range* interactions, e.g. the relative orientation of two protein domains (*222, 223*). For most studies unspecific interactions between the alignment medium and the solute are used to obtain structural information. However, similar to transferred NOE (*202, 224*), transferred cross correlated relaxation (*225-227*), specific interactions in the limit of weak binding can be also exploited to obtain information about transiently bound peptides and proteins (*228, 229*).

In studies of molecular complexes, binding strength is of central importance for the selection of appropriate NMR experiments. Strongly bound complexes with an affinity that exceeds the micromolar range can often be considered as a single entity and the weight limit for high-resolution NMR applies to the overall complex. Within this weight limit the structure of the entire complex is accessible. Isotope labelling of only one interaction partner allows reduction of spectral complexity and application of elaborate spectral editing schemes. Deuterium labelling might be advantageous to reduce dipolar relaxation and thus spectral linewidth. Weakly bound complexes (affinity smaller than 10 mM) offer an opportunity to obtain at least some structural data of molecular assemblies that exceed the weight limit of high-resolution NMR. Of practical importance is the case where the interacting molecules have very different size. The smaller molecule in the complex is usually termed the "ligand". Fast exchange between free and bound ligand is crucial for a class of experiments that allow determination of the bound ligand structure. Cross-relaxation is much more efficient in the macromolecule-

bound ligand compared to the free state. Dipolar couplings are zero in case of an isotropically tumbling free ligand but can be very large if the ligand is bound to an aligned macromolecule. Nuclear Overhauser enhancements (NOEs) and residual dipolar couplings (RDCs) detected with standard high-resolution NMR on the free form of a rapidly exchanging ligand are therefore dominated by contributions originating in the bound state and can be used to characterize of the bound ligand. This approach was recently used to determine the high-resolution structure and orientation of a fragment of the G-protein transducin bound to the membrane receptor rhodopsin in its natural environment, a disk membrane vesicle prepared from rod cells of bovine retinas (*230*).

1.8 Structural studies by solid-state NMR spectroscopy

Over the past two decades, solid-state NMR has emerged as a powerful method for structural studies of soft solid biomolecules, such as membrane proteins and amyloid systems. In contrast to that in solution, fast molecular tumbling in most solids is absent and signals in the spectrum is extremely broad (≈ 150 ppm) and generally uninterpretable due to three major anisotropic interactions: chemical shift anisotropy (CSA), homonuclear dipolar interactions and heteronuclear dipolar couplings of spin ½ nuclei. To overcome this problem, the magic-angle spinning (MAS) technique has been developed to obtain high resolution spectra, where the spectral resolution is highly improved by mechanically rotating the sample at the “magic” angle, that is around an axis tilted of 54.7° relative to the external magnetic field. The rotation about this axis removes the broadening and leads to a considerable sharpening of the lines in spectrum.

MAS introduced NMR spectra provides sufficiently resolved peaks and allows us to extract the information about the structure or dynamics of the molecule. This has important advantages for structural investigations by solid-sate MAS NMR. First, well-established strategies for resonance assignment known from solution NMR can be implemented in solid-state MAS NMR, and chemical shift databases compiled from solution NMR studies can be accessed to identify amino-acids by means of their characteristic side-chain correlation patterns.

1.8.1 Theory of solid-state NMR spectroscopy

For a spin in the external magnetic field, the Hamiltonian could be written as

$$H = H_Z + H_{CS} + H_D + H_J + H_Q. \qquad [1\text{-}2]$$

H_z is the Zeeman Hamiltonian, describing the interaction of the spin (I) with the external magnetic field and has the form

$$H_z = -\gamma\, I\, B_0, \qquad [1\text{-}3]$$

where γ is the gyromagnetic ratio of the spin I and B_0 is the external magnetic field.

H_{CS} describes the effect of B_0 on the surrounding electrons and could be written as

$$H_{CS} = \gamma\, \sigma\, I\, B_0, \qquad [1\text{-}4]$$

where σ is the shielding tensor and has orientation dependence. Considering the anisotropy of the chemical shift, one could divide the chemical shift Hamiltonian into an isotropic term and an anisotropic term as

$$H_{CS} = \gamma I_Z B_0 \left\{ \sigma_{iso} + \frac{1}{2}\sigma_{CSA}\left[\left(3\cos^2\theta - 1\right) + \eta_{CSA}\sin^2\theta\cos 2\phi\right]\right\}, \qquad [1\text{-}5]$$

where, σ_{iso} is the isotropic chemical shielding factor ($\sigma_{iso} = 1/3\,(\sigma_{11} + \sigma_{22} + \sigma_{33})$), σ_{CSA} is the anisotropy of the chemical shifts and η_{CSA} is the asymmetry of the chemical shift shielding tensor. The two angles θ and ϕ describe the orientation of the chemical shielding tensor with respect to the B_0 field.

H_D is the dipolar Hamiltonian which describes the through-space coupling between two nuclear spins I and S. For the homonuclear dipolar coupling it has the form as

$$H_D = -\frac{\mu_0}{4\pi}\frac{\gamma_I\gamma_K\hbar}{r_{IS}^3}\frac{\left(3\cos^2\theta - 1\right)}{2}\left[2I_ZS_Z - \frac{1}{2}(IS)\right], \qquad [1\text{-}6]$$

and for heteronuclear dipolar coupling it has the form as

$$H_D = -\frac{\mu_0}{4\pi}\frac{\gamma_I\gamma_K\hbar}{r_{IS}^3}\frac{\left(3\cos^2\theta - 1\right)}{2}2I_ZS_Z, \qquad [1\text{-}7]$$

where, μ_0 is the permeability of free space, γ_I and γ_S are gyromagnetic ratios of the I and S spins, respectively, r_{IS} is the internucelar distance and I_Z and S_Z are the components of the nuclear spin angular momentum operators I and S, respectively. The angle θ describes the

orientation of the internuclear vector with respect to the orientation of the external magnetic field.

H_J is the *J*-coupling Haniltonian which describes the coupling between two nuclei that is mediated through the electrons and has the form as

$$H_J = 2\pi J_{IS} IS\,, \qquad [1\text{-}8]$$

where J_{IS} is a second-rank tensor whose size depends on the orientation of the molecule relative to the static magnetic field.

Usually H_Q is the quadrupolar coupling for a spin whose spin-quantum number is larger than ½ and has the form as

$$H_Q = \frac{e^2 qQ}{2I(2I-1)}\frac{1}{2}\left[\left(3\cos^2\theta - 1\right) + \eta_k \sin^2\theta \cos 2\alpha a\right]\left(3I_Z^2 - I(I+1)\right). \qquad [1\text{-}9]$$

It is clear from these equations that H_{CS}, H_D, H_J and H_Q all have the analogous angular terms and are of orientation dependence. In liquid state, molecules usually are tumbling very fast due to Brownian motion, and such a fast tumbling leads to a time averaging of all orientation-dependent properties. Therefore, the spin Hamiltonian in liquids appears to be purely isotropic and only the isotropic average of any anisotropic parts of the Hamiltonian could be observed. However, in solids, there is much less mobility in the molecule, therefore, these anisotropic terms remain invariant over time and result in line broadening as shown in Fig. 1-12.

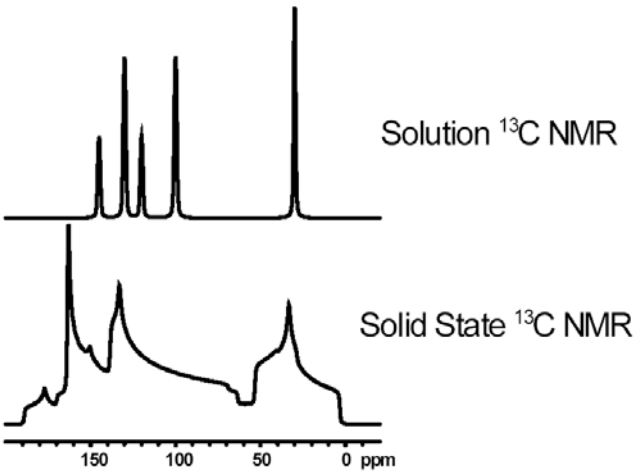

Fig. 1-12. Comparison of solution ^{13}C spectrum and solid-state ^{13}C spectrum.

1.8.2 Basic solid-state NMR techniques

Magic Angle Spinning

One approach to eliminate the interactions to give narrower lines is magic angle sample spinning (*231, 232*). This is done because the value of $(3\cos^2\theta - 1)$ term is zero when the vector between two nuclei makes an angle $\theta = 54.74°$ (the magic angle) with the static magnetic field as shown in Fig. 1-13. Therefore, chemical shift anisotropy, dipolar couplings and quadrupolar interactions can be averaged to zero. *J* coupling is on the order of 10^2 Hz, is much smaller to be observable in solid-state NMR.

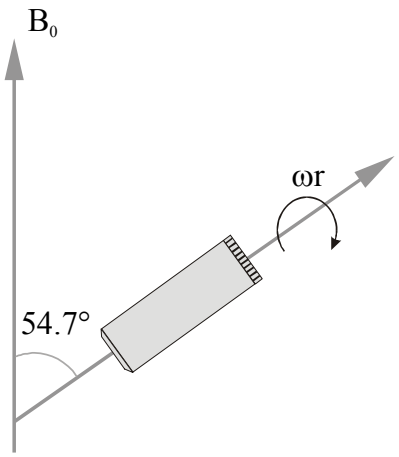

Fig. 1-13. Magic Angle Spinning of a rotor with a spinning frequency of ω_r.

To date the effect of MAS on different Hamiltonians, homogeneous and inhomogeneous Hamiltonians would be introduced here. Anisotropic interactions can be divided into inhomogeneous interactions including the chemical shift, the first-order quadrupolar interaction and heteronuclear dipolar coupling and homogeneous one referring to homonuclear dipolar interactions. In the inhomogeneous case, for example, in a ^{13}C spectrum, where the CSA interaction overrides the homonuclear dipolar interaction, the broad line splits up into many narrow lines which are spaced by the spinning frequency under MAS at a low spinning frequencies . If we increase the spinning frequency, the spacing of the lines gets larger and finally we end up with a single line at the isotropic chemical shift (seen in Fig. 1-14). The same effect of MAS is presented on a spectrum where the heteronuclear dipolar coupling interaction is the dominant interaction experienced by the spin. Although these sidebands are often a nuisance (they can be minimized by spinning at a frequency greater than the width of the CSA pattern), in some instances their presence provides additional information about a sample (*233*).

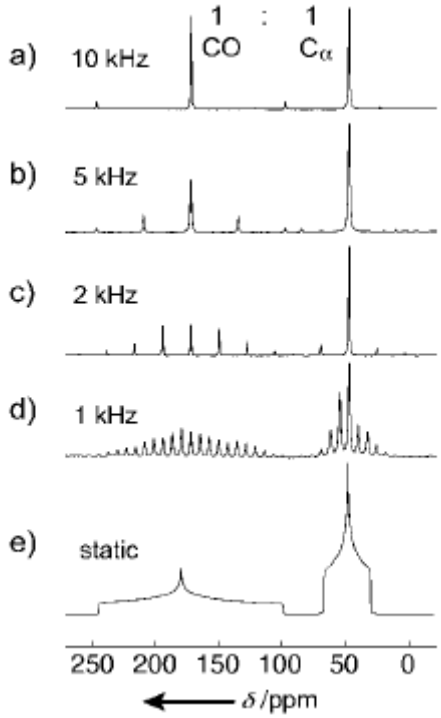

Fig. 1-14. Solid-state ^{13}C NMR spectra (125 MHz) of a uniformly ^{13}C-labeled (10%) glycine powder sample. The spectra (a-d) were acquired under CW ^{1}H decouping and MAS at the given spinning speeds. Spectrum e represents a powder spectrum reconstructed from the CSA parameters obtained by fitting the sideband intensities in spectra a-d.

For the homogeneous case, the same pattern of spinning sidebands could be obtained for a single homonuclear dipolar coupling interaction. However, for a network of multiple homonuclear dipolar couplings, the pattern changes. One would observe no changes of the spectrum if the spinning frequency of MAS much slower than the line-width.

Cross Polarization

Using a given magnetic field strength and assuming that the quality factor of the detection coil and the receiver system is frequency independent, the signal of a nucleus with given gyromagnetic ratio γ_I is given by $S \propto I\,(I+1)\,N\,\gamma^3$. Here, I is the spin-quantum number of the spin, and N is the number of nuclei in the sample. The noise can often be assumed to depend on $\gamma^{1/2}$, thus a signal-to-noise ratio has the form: $\frac{S}{N} \propto I(I+1)N\gamma^{\frac{5}{2}}$. Therefore, the direct excitation and detection of spins such as ^{13}C and ^{15}N with a low gyromagnetic ratio is plagued by their low sensitivity.

To enhance the signals from rare nuclei, many solid-state NMR experiments today routinely involve the transfer of polarization from abundant nuclei (usually ^{1}H nuclei) by using a technique called cross polarization (CP) (*234*). The process of CP occurs through the

tendency of the magnetization to flow from highly polarized nuclei to nuclei with lower polarizations when the two are brought into contact, similar to heat flow from a hot object to a cold object when the two are in thermal contact. For homonuclear spins, the magnetization can be exchanged through mutual energy conserving spin flips. For heteronuclear pairs such as ^{1}H and ^{13}C, these spin flips are not energy-conserving at high magnetic fields. Therefore, the exchange of magnetization must be driven externally by the application of RF fields. Among the techniques for establishing a dipolar contact between two different spin systems I and S, a particularly effective approach is that of Hartmann and Hahn. The Hartmann-Hahn method requires the simultaneous application of two continuous RF fields, one at the resonance frequency of the I spin and one at the resonance frequency of the S spin. The effect of any RF field is to rotate the magnetization about the axis of the applied field. The rotation rate depends on the frequency and amplitude of the RF field. An RF field that oscillates at the I-spin frequency, for example, 500 MHz, would have essentially no effect on S spins with a frequency of 125 MHz and vice versa. By applying two RF fields, one tuned to the I spins and the other to the S spins, both the I and S spins can be rotated independently around a particular axis at rates determined by the amplitudes of the two applied fields. When the rotation frequencies of the I and S spins are equal, an energy conserving dipolar contact between the two spin systems is created. The differences in energy are supplied by the RF fields. It is through this dipolar contact that the polarization is transferred between the I and S spins. One way to describe how this connection is established is by using a reference frame rotating at both the I and the S spin rotation frequencies. In the doubly rotating frame, the spacing between the spin-up and spin-down energy levels is equal for the I and S spins .

The experimental implementation of this concept to obtain high-resolution NMR spectra of rare or dilute S spins is shown in Fig. 1-15. First, the proton magnetization is brought into the xy plane by a $\pi/2$ pulse. RF fields are then applied to the I and S spins for a period τ_{CP}, causing the magnetization to be exchanged between the I spins and the S spins in their respective rotating frame. Finally, the S spins are detected while the I spins are decoupled. This sequence forms the basis of proton-enhanced NMR spectroscopy which, through the combination of CP and MAS, opened the way to routine high-sensitivity, high-resolution, solid-state ^{13}C NMR spectroscopy. The increase in the S-spin magnetization during the CP

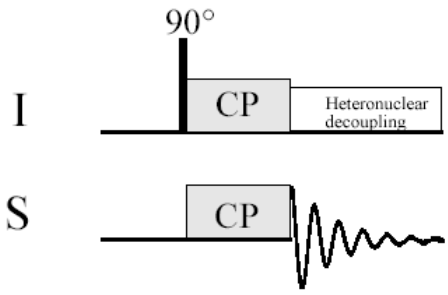

Fig. 1-15. Pulse sequence for CP of ^{13}C (S) nuclei by protons (I) with detection of the ^{13}C magnetization.

mixing period τ_{CP} depends on the strength of the I ± S dipolar coupling. The polarization buildup in the unprotonated carbonyl carbon atom requires a longer CP time than for the α carbon atom, which is quickly polarized by its bonded protons. Typical mixing times range from 100 μs to 10 ms. The polarization buildup curve starts to decay beyond a certain mixing time as a result of relaxation and magnetization-transport phenomena.

The maximum enhancement for a CP contact period under the Hartmann-Hahn conditions $\omega_I = \omega_S$ ($\gamma_I B_I = \gamma_S B_S$) is γ_I/γ_S (γ_I and γ_S are gyromagnetic ratios of spins I and S, respectively; B_I and B_S are nutation rates imposed by the RF fields). Apart from gaining a factor of by using the CP, the relaxation properties of high-abundance nuclei would also be useful. In most NMR experiments, the acquisition or sampling rate is dictated by the relaxation time (T_1) of the detected nuclei. Under CP conditions, the sampling rate depends on the relaxation time of the nuclei from which the magnetization is transferred. As the protons in the solid state typically relax more rapidly than most other spin ½ nuclei, many more scans can be acquired in a given amount of time in such an experiment than in a simple single-pulse experiment that detects the rare ^{13}C nucleus directly.

Heteronuclear dipolar decoupling

In principle, MAS is sufficient to average out all anisotropic second-rank tensor contributions to the Hamiltonian. Experimentally we find that even at spinning frequencies as high as 50 kHz the ^{13}C spectrum of a protonated sample is still quite broad if we do not apply proton decoupling. As have been known, a proton whose spin is parallel to the external field (spin-up) produces a shift in the resonance frequency of a ^{13}C nucleus that is opposite to the shift produced by a proton whose spin is antiparallel to the external field (spin-down). By constantly applying radio-frequency (RF) pulses that rotate the proton nuclear spins between their spin-up and spin-down states, the average orientation of the ^{1}H magnetic moments tends

to zero, and the dipolar coupling is essentially averaged away (this also applies to the *J* coupling) (*235, 236*). This continuous wave (CW) spin decoupling is widely used to eliminate heteronuclear couplings in solid-state NMR spectroscopy.

Recently, multipulse decouplings have been successfully employed for heteronuclear decoupling. The two-pulse phase modulation (TPPM) was shown to produce results superior to simple CW decouping, particularly under MAS (*237*). As shown in Fig. 1-16 the TPPM sequence breaks the CW irradiation into a series of discrete time periods τ (in the order of 3 ± 20 μs) during which the phase of the irradiation alternates between $\phi/2$ and $\phi/2$. Typically, the values of τ and ϕ must be optimized for a particular sample in order to produce the smallest possible line widths. A typical ϕ value is about 50°, and τ is often adjusted to give a flip angle of approximately 150°.

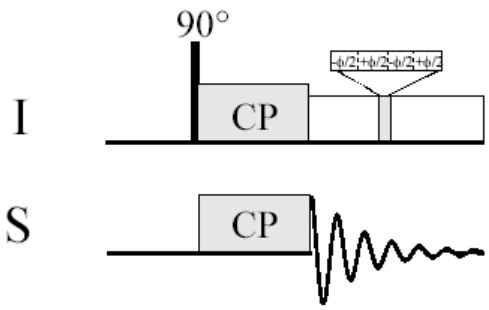

Fig. 1-16. TPPM heteronuclear dipolar decoupling sequence. RF irradiation is applied continuously, with an alternating phase shift of $+\phi/2$ and $-\phi/2$, for every time period τ.

Homonuclear dipolar decoupling

For low-γ nuclei such as ^{13}C and ^{15}N, the homonuclear dipolar coupling can often be removed by MAS, as even for directly bonded ^{13}C nuclei, the dipolar coupling constant *d* does not exceed 5 kHz. The homonuclear dipolar interaction has perhaps the largest impact on ^{1}H solid-state NMR spectroscopy, as the strength of the homonuclear dipolar coupling between two proton spins can routinely approach 100 kHz because of their large gyromagnetic ratio. The problem of strong ^{1}H-^{1}H dipolar coupling is exacerbated by the high abundance of protons in most organic systems, which results in a network of strongly coupled spins that are very difficult to decouple from each other. As a result, solid-state ^{1}H MAS NMR spectra typically consist of a single broad peak, with a line width in the order of 50 kHz. In contrast to the success for heteronuclear decoupling, CW has no effect on the homonuclear decoupling since the magnetization of the two nuclei cannot be manipulated independently. Other

multipulse sequences like WAHUHA (*238*), MREV-8 (*239*), BR-24 (*240*) and MSHOT (*241*) have been much more successful in many applications. These techniques would be talked in detail here since they are not so often used in this work.

The elegant techniques outlined here are powerful and often sufficient tools for many applications in basic chemical analysis and characterization of solid samples. A combination of high-power CW decoupling, cross-polarization, high-speed MAS and advanced multipulse and multidimensional techniques, can rapidly yield one-dimensional solid-state spectra of compounds containing spin 1/2 nuclei of low natural abundance such as ^{13}C, ^{15}N, and ^{29}Si, with sufficient spectral sensitivity and resolution.

1.9 Overview of this thesis

Knowledge of the Aβ fibril structure is essential for understanding the abnormal assembly and deposition of these fibrils and could lead to the rational design of therapeutic agents for the prevention or even disaggregation of the fibrils. Moreover, elucidation of the structure of Aβ fibrils would be an important step towards understanding the propagating structure of other fibrillar proteins involved in amyloidosis.

We reasoned that compounds which bind Aβ would be likely to alter its aggregation pathways and thereby prevent its toxic effects. Compounds with these characteristics serve as useful probes for the molecular mechanisms underlying amyloid formation and pathology and as leads for the design of therapeutic agents. We were especially interested in investigating the interactions between Aβ and several inhibitors which are known to prevent fibril formation. Working with full length Aβ peptides requires special precautions and preconditioning of the samples. In this thesis, $A\beta^{14-23}$ was initially selected as a model peptide for inhibition studies. The selection of $A\beta^{14-23}$ was based on the following considerations: (1) Model peptide studies have demonstrated that truncated peptides form fibrils morphologically similar to those of the full-length peptide (*59, 121, 129, 176*); the short fragment $A\beta^{14-23}$ of the $A\beta^{1-40}$ peptide was reported to be the shortest fibril-forming peptide (*59*); substitutions in this decapeptide impaired fibril formation and deletion of the decapeptide from $A\beta^{1-42}$ inhibited fibril formation completely. (2) $A\beta^{14-23}$ incorporates the core region, point mutations of which significantly obstruct fibril formation; in some cases, such modifications have been used to generate inhibitors of fibrillogenesis (*59, 148, 149, 151, 172, 189, 190*). (3) The use of $A\beta^{14-23}$

allowed the reproducible and controlled formation of fibrils from aqueous solutions, under defined conditions of pH, ionic strength, and peptide concentration, and thus yielded the required homogeneous fibrils.

The central hydrophobic region in the N-terminal domain of Aβ, amino acids 17-20 (LVFF), served as a template for designing the β–sheet breaker peptide iAβ5 (LPFFD) and KLVFFKK, which are known to prevent neurotoxicity in cell essays (*53, 148, 173*).

The aim of this work was to determine the bound-state structure of peptide inhibitor to Aβ fibrils. In this work, $A\beta^{14-23}$ and its inhibitors (iAβ5, $iA\beta5^{inv}$ and KLVFFKK) with and without spin-labelling were first synthesized via the Fmoc-SPPS protocol. The solution structure of these peptide inhibitors in the presence of $A\beta^{1-40}$ or $A\beta^{14-23}$ fibrils were investigated by multidimensional solution NMR spectroscopy. Furthermore, the model of inhibitors bound to Aβ fibrils were determined by molecular docking. The structure information is potentially of interest to design peptide mimetics with a higher bioavailability, is supposed to be valuable structural information for amyloid fibril proteins/peptides.

Furthermore, the structure of fibrils formed from *de novo* peptides was studied by solid-state NMR. The idea behind it is that the such a simplified system could be more easily handled and offer additional insights into the molecular details of amyloid fibril formation which may be common to all fibril formation process of amyloidogenic proteins or peptides.

References

1. Koo, E., Lansbury, P. J., and Kelly, J. (1999) *Proc. Natl. Acad. Sci. 96*, 9989-9990.
2. Hardy, J. (1997) *Proc. Natl. Acad. Sci. 94*, 2095-2097.
3. Ironside, J., and Head, M. (2004) *Curr. Top. Microbiol. Immunol. 284*, 133-159.
4. Jeffrey, M., and Gonzalez, L. (2004) *Curr. Top. Microbiol. Immunol. 284*, 65-97.
5. Kelly, J. W. (2000) *Nat. struct. biol. 7*, 824-826.
6. Kelly, J. W. (2002) *Nat. Struct. biol. 9*, 323-325.
7. Meredith, L. (2004) *Methods Mol. Med. 92*, 183-202.
8. Bellotti, V., Mangione, P., and Merlini, G. (2000) *J. Struct. Biol. 130*, 280-289.
9. Braak, H., and Tredici, K. D. (2004) *Neurobiol. Aging 25*, 713–718.
10. Clippingdale, A. B., Wade, J. D., and Barrow, C. J. (2001) *J. Peptide Sci. 7*, 227-249.
11. Chiti, F., Calamai, M., Taddei, N., Stefan, M., Rampon, G., and Dobson, C. (2002) *Proc. Natl. Acad. Sci. 9*, 16419-16426.
12. Damas, A. M., and Saraiva, M. J. (2000) *J. Struct. Biol. 130*, 290-299.
13. El-Agnaf, O. M. A., and Irvine, G. B. (2000) *J. Struct. Biol. 130*, 300-309.
14. Goldsbury, C., Goldie, K., Pellaud, J., Seelig, J., Frey, P., Mueller, S. A., Kistler, J., Cooper, G. J. S., and Aebi, U. (2000) *J. Struct. Biol. 130*, 352-362.

15. Jaroniec, C., MacPhee, C., Astrof, N., Dobson, C., and Griffin, R. (2002) *Proc. Natl. Acad. Sci. 99*, 16748-16753.
16. Kessler, J. C., Rochet, J.-C., and Peter T. Lansbury, J. (2003) *Biochemistry 42*, 672-678.
17. Kisilevsky, R. (2000) *J. Struct. Biol. 130*, 99-108.
18. McParland, V., Kalverda, A., Homans, S., and Radford, S. (2002) *Nat. Struct. Biol. 9*, 326-331.
19. Sipe, J. D., and Cohen, A. S. (2000) *J. Struct. Biol. 130*, 89-98.
20. Soto, C. (1999) *J. Mol. Med. 77*, 412-418.
21. Hardy, J., and Selkoe, D. (2002) *Science 297*, 353-356.
22. Lansbury, P. J. (1999) *Proc. Natl. Acad. Sci. 96*, 3342-3344.
23. Masliah, E., Hansen, L. A., Rockenstein, E., and Hashimoto, M. (2002) *Drug Dev. Res. 56*, 282-292.
24. Morozova-Roche, L. A., Zurdo, J. s., Spencer, A., Noppe, W., Receveur, V., Archer, D. B., Joniau, M., and Dobson, C. M. (2000) *J. Struct. Biol. 130*, 339–351.
25. Selkoe, D. (2002) *J. Clin. Invest. 110*, 1375-1381.
26. Soto, C. (2001) *FEBS Letters 498*, 204-207.
27. Tycko, R. (2003) *Biochemistry 42*, 3151-3159.
28. Paz, M. L. p. d. l., and Serrano, L. (2004) *Proc. Natl. Acad. Sci. 101*, 87-92.
29. Hoshino, M., Katou, H., Hagihara, Y., Hasegawa, K., Naiki, H., and Goto, Y. (2002) *Nat. Struct. Biol. 9*, 332-336.
30. Miranker, A. D. (2004) *Proc. Natl. Acad. Sci. 101*, 4335–4336.
31. Zurdo, J. s., Guijarro, J. I. a., and Dobson, C. M. (2001) *J. Am. Chem. Soc. 123*, 8141-8142.
32. Kammerer, R. A., Kostrewa, D., Zurdo, J. s., Detken, A., Garcý´a-Echeverrý´a, C., Green, J. D., ller, S. A. M., Meier, B. H., Winkler, F. K., Dobson, C. M., and Steinmetz, M. O. (2004) *Proc. Natl. Acad. Sci. 101*, 4435–4440.
33. Paz, M. L. p. d. l., Goldie, K., Zurdo, J., Lacroix, E., Dobson, C. M., Hoenger, A., and Serrano, L. (2002) *Proc. Natl. Acad. Sci. 99*, 16052–16057.
34. Lim, A., Makhov, A. M., Bond, J., Inouye, H., Connors, L. H., Griffith, J. D., Erickson, B. W., Kirschner, D. A., and Costello, C. E. (2000) *J. Struct. Biol. 130*, 363–370.
35. Fezoui, Y., Hartley, D., Walsh, D., Selkoe, D., Osterhout, J., and Teplow, D. (2000) *Nat. Struct. Biol. 7*, 1095-1099.
36. Kim, Y.-S., Randolph, T. W., Manning, M. C., Stevens, F. J., and Carpenter, J. F. (2003) *J. Biol. Chem. 278*, 10842-10850.
37. Ashburn, T., Han, H., McGuinness, B., and Lansbury, P. J. (1996) *Chem. Biol. 3*, 351-358.
38. Turnell, W., and Finch, J. (1992) *J. Mol. Biol. 227*, 1205-1223.
39. Lorenzo, A., and Yankner, B. A. (1994) *Proc. Natl. Acad. Sci. 91*, 12243-12247.
40. Lashuel, H. A., LaBrenz, S. R., Woo, L., Serpell, L. C., and Kelly, J. W. (2000) *J. Am. Chem. Soc. 122*, 5262-5277.
41. McLaurin, J., Yang, D.-S., Yip, C. M., and Fraser, P. E. (2000) *J. Struct. Biol. 130*, 259-270.
42. Crowther, R. A., and Goedert, M. (2000) *J. Struct. Biol. 130*, 271-279.
43. Blake, C., and Serpell, L. (1996) *Structure. 4*, 989-998.
44. Kirschner, D., Abraham, C., and Selkoe, D. (1986) *Proc. Natl. Acad. Sci. 82*, 503-507.
45. Inouye, H., Fraser, P. E., and Kirschner, D. A. (1993) *Biophys. J. 64*, 502-519.
46. Malinchik, S. B., Inouye, H., Szumowski, K. E., and Kirschner, D. A. (1998) *Biophys. J. 74*, 537–545.
47. Lynn, D. G., and Meredithb, S. C. (2000) *J. Struct. Biol. 130*, 153-173.

48. Sunde, M., Serpell, L., Bartlam, M., Fraser, P., Pepys, M., and Blake, C. (1997) *J. Mol. Biol. 273*, 729-739.
49. Tycko, R. (2004) *Curr. Opin. Struct. Biol. 14*, 96-103.
50. Cairo, C. W., Strzelec, A., Murphy, R. M., and Kiessling, L. L. (2002) *Biochemistry 41*, 8620-8629.
51. Kirschner, D., Inouye, H., Duffy, L., Sinclair, A., Lind, M., and Selkoe, D. (1987) *Proc. Natl. Acad. Sci. 84*, 6953-6957.
52. Lambert, M., Barlow, A., Chromy, B., Edwards, C., Freed, R., Liosatos, M., Morgan, T., Rozovsky, I., Trommer, B., Viola, K., Wals, P., Zhang, C., Finch, C., Krafft, G., and Klein, W. (1998) *Proc. Natl. Acad. Sci. 95*, 6448-6453.
53. Pallitto, M. M., Ghanta, J., Heinzelman, P., Kiessling, L. L., and Murphy, R. M. (1999) *Biochemistry 38*, 3570-3578.
54. Antzutkin, O. N., Leapman, R. D., Balbach, J. J., and Tycko, R. (2002) *Biochemistry 41*, 15436-15450.
55. Talafous, J., Marcinowski, K., Klopman, G., and Zagorski, M. (1994) *Biochemistry 33*, 7788-7796.
56. Soto, C., Branes, M., Alvarez, J., and Inestrosa, N. (1994) *J. Neurochem. 63*, 1191-1198.
57. Chaney, M., Webster, S., Kuo, Y., and Roher, A. (1998) *Protein Eng. 11*, 761-767.
58. Li, L., Darden, T., Bartolotti, L., Kominos, D., and Pedersen, L. (1999) *Biophys. J. 76*, 2871-2878.
59. Tjernberg, L. O., Callaway, D. J. E., Tjernberg, A., Hahne, S., Lilliehöök, C., Terenius, L., Thyberg, J., and Nordstedt, C. (1999) *J. Biol. Chem. 274*, 12619–12625.
60. Petkova, A. T., Ishii, Y., Balbach, J. J., Antzutkin, O. N., Leapman, R. D., Delaglio, F., and Tycko, R. (2002) *Proc. Natl. Acad. Sci. 99*, 16742–16747.
61. Barrow, C., and Zagorski, M. (1991) *Science 253*, 179-182.
62. Crescenzi, O., Tomaselli, S., Guerrini, R., Salvadori, S., D'Ursi, A. M., Temussi, P. A., and Picone, D. (2002) *Eur. J. Biochem. 269*, 5642–5648.
63. Serpell, L., Blake, C., and Fraser, P. (2000) *Biochemistry 39*, 13269-13275.
64. Serpell, L. (2000) *Biochim. Biophys. Acta. 1502*, 16-30.
65. Shao, H., Jao, S.-c., Ma, K., and Zagorski, M. G. (1999) *J. Mol. Biol. 285*, 755-773.
66. Selkoe, D. (2001) *Physiol. Rev. 81*, 741-766.
67. Sommer, B. (2002) *Curr. Opin. Pharmacol. 2*, 87-92.
68. Glenner, G. G., and Wong, C. (1984) *Biochem. Biophys. Res. Commun. 120*, 885-890.
69. Selkoe, D. (1991) *Neuron. 6*, 487-498.
70. Selkoe, D. (1996) *J. Biol. Chem. 271*, 18295-18298.
71. Selkoe, D. (1997) *Science 275*, 630-631.
72. Selkoe, D. (2002) *Science 298*, 789-791.
73. Selkoe, D., Physicians, A. C. o., and Society, A. P. (2004) *Ann. Intern. Med. 140*, 627-638.
74. Selkoe, D., and Schenk, D. (2003) *Annu. Rev. Pharmacol. Toxicol. 43*, 545-584.
75. Selkoe, D. J. (1991) *Nature 354*, 432-433.
76. Adessi, C., and Soto, C. (2002) *Drug Dev. Res. 56*, 184-193.
77. Mehta, P. D., and Pirttilä, T. (2002) *Drug Dev. Res. 56*, 74-84.
78. Fassbender, K., Masters, C., and Beyreuther, K. (2001) *Naturwissenschaften. 88*, 261-267.
79. Fine, R. E. (1999) *Alzheimer Disease and Associated Disorders 13*, S82-S87.
80. Butterfield, D. A., and Bush, A. I. (2004) *Neurobiol. Aging 25*, 563–568.
81. Cherny, R. A., Barnham, K. J., Lynch, T., Volitakis, I., Li, Q.-X., McLean, C. A., Multhaup, G., Beyreuther, K., Tanzi, R. E., Masters, C. L., and Bush, A. I. (2000) *J. Struct. Biol. 130*, 209-216.

82. Chung, T., Sipe, J., McKee, A., Fine, R., Schreiber, B., Liang, J., and Johnson, R. (2000) *Amyloid 7*, 105-110.
83. Hutton, M., and Hardy, J. (1997) *Hum. Mol. Genet. 6*, 1639-1646.
84. Golabek, A., Soto, C., Vogel, T., and Wisniewski, T. (1996) *J. Biol. Chem. 271*, 10602-10606.
85. Evans, K., Berger, E., Cho, C., Weisgraber, K., and Lansbury, P. J. (1995) *Proc. Natl. Acad. Sci. 92*, 763-767.
86. Liu, K., Cho, H. S., Lashuel, H. A., Kelly, J. W., and Wemmer, D. E. (2000) *Nat. Struct. biol. 7*, 754-757.
87. Liang, J., Sloane, J., Wells, J., Abraham, C., Fine, R., and Sipe, J. (1997) *Neurosci. Lett. 225*, 73-76.
88. Adessi, C., Frossard, M.-J., Boissard, C., Fraga, S., Bieler, S., Ruckle, T., Vilbois, F., Robinson, S. M., Mutter, M., Banks, W. A., and Soto, C. (2003) *J. Biol. Chem. 278*, 13905-13911.
89. Mori, H., Takio, K., Ogawara, M., and Selkoe, D. (1992) *J. Biol. Chem. 267*, 17082-17086.
90. Palmert, M., Podlisny, M., Witker, D., Oltersdorf, T., Younkin, L., Selkoe, D., and Younkin, S. (1989) *Proc. Natl. Acad. Sci. 86*, 6338-6342.
91. Tamaoka, A., Kalaria, R., Lieberburg, I., and Selkoe, D. (1992) *Proc. Natl. Acad. Sci. 89*, 1345-1349.
92. Näslund, J., Schierhorn, A., Hellman, U., Lannfelt, L., Roses, A. D., Tjernberg, L. O., Silberring, J., Gandy, S. E., Winblad, B., Greengard, P., Nordstedt, C., and Terenius, L. (1994) *Proc. Natl. Acad. Sci. 91*, 8378-8382.
93. Citron, M., Diehl, T., Gordon, G., Biere, A., Seubert, P., and Selkoe, D. (1996) *Proc. Natl. Acad. Sci. 93*, 13170-13175.
94. Näslund, J., Karlström, A. R., Tjernberg, L. O., Schierhorn, A., Terenius, L., and Nordstedt, C. (1996) *J. Neurochem. 67*, 294-301.
95. Mattson, M. (1997) *Physiol. Rev. 77*, 1081-1132.
96. Esler, W. P., and Wolfe, M. S. (2001) *Science 293*, 1449-1454.
97. Haass, C., Schlossmacher, M., Hung, A., Vigo-Pelfrey, C., Mellon, A., Ostaszewski, B., Lieberburg, I., Koo, E., Schenk, D., Teplow, D., and al., e. (1992) *Nature 359*, 322-325.
98. Kuo, Y.-M., Emmerling, M. R., Vigo-Pelfrey, C., Kasunici, T. C., Kirkpatrick, J. B., Murdoch, G. H., Ball, M. J., and Roher, A. E. (1996) *J. Biol. Chem. 271*, 4077-4081.
99. Roher, A. E., Lowenson, J. D., Clarke, S., Woods, A. S., Cotter, R. J., Gowing, E., and Ball, M. J. (1993) *Proc. Natl. Acad. Sci. 90*, 10836-10840.
100. Roher, A. E., Chaney, M. O., Kuo, Y.-M., Webster, S. D., Stinei, W. B., Haverkamp, L. J., Woods, A. S., Cotter, R. J., Tuohy, J. M., Krafft, G. A., Bonnell, B. S., and Emmerling, M. R. (1996) *J. Biol. Chem. 271*, 20631–20635.
101. Walsh, D., Klyubin, I., Fadeeva, J., Cullen, W., Anwyl, R., Wolfe, M., Rowan, M., and Selkoe, D. (2002) *Nature 416*, 535-539.
102. Caughey, B., and Lansbury, P. J. (2003) *Annu. Rev. Neurosci. 26*, 267-298.
103. Klein, W. L., Jr., W. B. S., and Teplow, D. B. (2004) *Neurobiol. Aging 25*, 569–580.
104. Walsh, D., Klyubin, I., Fadeeva, J., Rowan, M., and Selkoe, D. (2002) *Biochem. Soc. Trans. 30*, 552-557.
105. Zagorski, M., and Barrow , C. (1992) *Biochemistry 31*, 5621-5631.
106. Lee, J., Stimson, E., Ghilardi, J., Mantyh, P., Lu, Y.-A., Felix, A., Llanos, W., Behbin, A., Cummings, M., Criekinge, M. V., Timms, W., and Maggio, J. (1995) *Biochemistry 34*, 5191-5200.
107. Sorimachi, K., and Craik, D. (1994) *Eur. J. Biochem. 219*, 237-251.
108. Shen, C.-L., and Murphy, R. M. (1995) *Biophys. J. 69*, 640-651.

109. Fletcher, T. G., and Keire, D. A. (1997) *Protein Sci. 6*, 666-675.
110. Hilbich, C., Kisters-Woike, B., Reed, J., Masters, C., and Beyreuther, K. (1991) *J. Mol. Biol. 218*, 149-163.
111. Benzinger, T., Gregory, D., Burkoth, T., Miller-Auer, H., Lynn, D., Botto, R., and Meredith, S. (1998) *Proc. Natl. Acad. Sci. 95*, 13407-13412.
112. Benzinger, T., Gregory, D., Burkoth, T., Miller-Auer, H., Lynn, D., Botto, R., and Meredith, S. (2000) *Biochemistry 39*, 3491-3499.
113. Burkoth, T. S., Benzinger, T. L. S., Urban, V., Morgan, D. M., Gregory, D. M., Thiyagarajan, P., Botto, R. E., Meredith, S. C., and Lynn, D. G. (2000) *J. Am. Chem. Soc. 122*, 7883-7889.
114. Balbach, J. J., Ishii, Y., Antzutkin, O. N., Leapman, R. D., Rizzo, N. W., Dyda, F., Reed, J., and Tycko, R. (2000) *Biochemistry 39*, 13748-13759.
115. Terzi, E., Holzemann, G., and Seelig, J. (1994) *Biochemistry 33*, 7434-7441.
116. Lansbury, P. J., Costa, P., Griffiths, J., Simon, E., Auger, M., Halverson, K., Kocisko, D., Hendsch, Z., Ashburn, T., Spencer, R., and al., e. (1995) *Nat. Struct. Biol. 2*, 990-998.
117. Coles, M., Bicknell, W., Watson, A., Fairlie, D., and Craik, D. (1998) *Biochemistry 37*, 11064-11077.
118. Sticht, H., Bayer, P., Willbold, D., Dames, S., Hilbich, C., Beyreuther, K., Frank, R., and Rosch, P. (1995) *Eur. J. Biochem. 233*, 293-298.
119. Antzutkin, O. N., Balbach, J. J., Leapman, R. D., Rizzo, N. W., Reed, J., and Tycko, R. (2000) *Proc. Natl. Acad. Sci. 97*, 13045-13050.
120. Balbach, J., Petkova, A., Oyler, N., Antzutkin, O., Gordon, D., Meredith, S., and Tycko, R. (2002) *Biophys. J. 83*, 1205-1216.
121. Fraser, P., Duffy, L., O'Malley, M., Nguyen, J., Inouye, H., and Kirschner, D. (1991) *J. Neurosci. Res. 28*, 474-485.
122. Kang, J., Lemaire, H., Unterbeck, A., Salbaum, J., Masters, C., Grzeschik, K., Multhaup, G., Beyreuther, K., and Muller-Hill, B. (1987) *Nature 325*, 733-736.
123. Eker, F., Griebenow, K., and Schweitzer-Stenne, R. (2004) *Biochemistry 43*, 6893-6898.
124. Barrow, C., Yasuda, A., Kenny, P., and Zagorski, M. (1992) *J. Mol. Biol. 225*, 1075-1093.
125. Soto, C., and Castano, E. (1996) *Biochem. J. 314*, 701-707.
126. Soto, C., Castano, E., Frangione, B., and Inestrosa, N. (1995) *J. Biol. Chem. 270*, 3063-3067.
127. Soto, C., Castano, E., Kumar, R., Beavis, R., and Frangione, B. (1995) *Neurosci. Lett. 200*, 105-108.
128. Zagorski, M., J, Y., Shao, H., Ma, K., Zeng, H., and Hong, A. (1999) *Methods Enzymol. 309*, 189-204.
129. Fraser, P., Nguyen, J., Surewicz, W., and Kirschner, D. (1991) *Biophys. J. 60*, 1190-1201.
130. Teplow, D. B. (1998) *Amyloid: Int. J. Exp. Cloin. Invest. 5*, 121-142.
131. Murphy, R. M., and Pallitto, M. M. (2000) *J. Struct. Biol. 130*, 109-122.
132. Wood, S. J., Maleeff, B., Hart, T., and Wetzel, R. (1996) *J. Mol. Biol. 256*, 870-877.
133. Cannon, M., Williams, A., Wetzel, R., and Myszka, D. (2004) *Anal. Biochem. 328*, 67-75.
134. Ban, T., Hamada, D., Hasegawa, K., Naiki, H., and Goto, Y. (2003) *J. Biol. Chem. 278*, 16462-16465.
135. Esler, W. P., Stimson, E. R., Jennings, J. M., Vinters, H. V., Ghilardi, J. R., Lee, J. P., Mantyh, P. W., and Maggio, J. E. (2000) *Biochemistry 39*, 6288-6295.

136. Harper, J., Wong, S., Lieber, C., and Lansbury, P. J. (1999) *Biochemistry 38*, 8972-8980.
137. Harper, J. D. (1997) *Annu. Rev. Biochem. 66*, 385–407.
138. Hasegawa, K., Ono, K., Yamada, M., and Naiki, H. (2002) *Biochemistry 41*, 13489-13498.
139. Huang, T., Yang, D., Fraser, P., and Chakrabartty, A. (2000) *J. Biol. Chem. 275*, 36436-36440.
140. Inouye, H., and Kirschner, D. (2000) *J. Struct. Biol. 130*, 123-129.
141. Jarvet, J., Damberg, P., Bodell, K., Eriksson, L. E. G., and Gräslund, A. (2000) *J. Am. Chem. Soc. 122*, 4261-4268.
142. Lakdawala, A. S., Morgan, D. M., Liotta, D. C., Lynn, D. G., and Snyder, J. P. (2002) *J. Am. Chem. Soc. 124*, 15150-15151.
143. LEVINE-III, H. (1993) *Protein Sci. 2*, 404-410.
144. Ma, B., and Nussinov, R. (2002) *Proc. Natl. Acad. Sci. 99*, 14126-14131.
145. Ma, K., Clancy, E. L., Zhang, Y., Ray, D. G., Wollenberg, K., and Zagorski, M. G. (1999) *J. Am. Chem. Soc. 121*, 8698-8706.
146. Stine, W. B. J., Dahlgren, K. N., Krafft, G., and LaDu, M. J. (2003) *J. Biol. Chem. 278*, 11612-11622.
147. Fezoui, Y., and Teplow, D. (2002) *J Biol Chem. 277*, 36948-54.
148. Soto, C., Sigurdsson, E., Morelli, L., Kumar, R., Castano, E., and Frangione, B. (1998) *Nat. Med. 4*, 822-826.
149. Hilbich, C., Kisters-Woike, B., Reed, J., Masters, C., and Beyreuther, K. (1992) *J. Mol. Biol. 228*, 460-473.
150. Wood, S., Wetzel, R., Martin, J., and Hurle, M. (1995) *Biochemistry 34*, 724-730.
151. Tjernberg, L. O., Näslund, J., Lindqvist, F., Johansson, J., Karlström, A. R., Thyberg, J., Terenius, L., and Nordstedt, C. (1996) *J. Biol. Chem. 271*, 8545-8548.
152. Hughes, S. R., Goyal, S., Sun, J. E., Gonzalez-DeWhitt, P., Fortes, M. A., Ried, N. G., and Sahasrabudhe, S. R. (1996) *Proc. Natl. Acad. Sci. 93*, 2065-2070.
153. Makin, O., and Serpell, L. (2002) *Biochem. Soc. Trans. 30*, 521-525.
154. Mikros, E., Benaki, D., Humpfer, E., Spraul, M., Loukas, S., Stassinopoulou, C., and Pelecanou, M. (2001) *Angew. Chem. Int. Ed. Engl. 40*, 3603-3605.
155. Petkova, A. T., Buntkowsky, G., Dyda, F., Leapman, R. D., Yau, W. M., and Tycko, R. (2004) *J. Mol. Biol. 335*, 247-260.
156. Tycko, R. (2000) *Curr. Opin. Chem. Biol. 4*, 500-506.
157. Tycko, R., and Ishii, Y. (2003) *J. Am. Chem. Soc. 125*, 6606-6607.
158. Serpell, L., and Smith, J. (2000) *J. Mol. Biol. 299*, 225-231.
159. Serpell, L., Sunde, M., Benson, M., Tennent, G., Pepys , M., and Fraser, P. (2000) *J. Mol. Biol. 300*, 1033-1039.
160. Goldsbury, C. S., Wirtz, S., Müller, S. A., Sunderji, S., Wicki, P., Aebi, U., and Frey, P. (2000) *J. Struct. Biol. 130*, 217–231.
161. Walsh, D., Hartley, D., Kusumoto, Y., Fezoui, Y., Condron , M., Lomakin, A., Benedek, G., Selkoe, D., and Teplow, D. (1999) *J. Biol. Chem. 274*, 25945-25952.
162. Walsh, D., Lomakin, A., Benedek, G., Condron, M., and Teplow, D. (1997) *J. Biol. Chem. 272*, 22364-22372.
163. Harper, J., Wong, S., Lieber, C., and Lansbury, P. (1997) *Chem. Biol. 4*, 119-125.
164. Lahiri, D. K., Farlow, M. R., Greig, N. H., and Sambamurti, K. (2002) *Drug Dev. Res. 56*, 267-281.
165. Lansbury, P. T. J. (2001) *Nat. Biotechnol. 19*, 112-113.
166. D'Andrea, M. R., Lee, D. H. S., Wang, H.-Y., and Nagele, R. G. (2002) *Drug Dev. Res. 56*, 194-200.

167. Bohrmann, B., Adrian, M., Dubochet, J., Kuner, P., ller, F. M., Huber, W., Nordstedt, C., and Döbeli, H. (2000) *J. Struct. Biol. 130*, 232-246.
168. Matsunagaa, Y., Fujiib, A., Awasthia, A., Yokotanib, J., Takakurab, T., and Yamadaa, T. (2004) *Regulatory Peptides 120*, 227– 236.
169. Tjernberg, L. O., Tjernberg, A., Bark, N., Shi, Y., Ruzsicska, B. P., Bu, Z., Thyberg, J., and Callaway, D. J. E. (2002) *Biochem. J. 366*, 343-351.
170. Findeis, M. A., Musso, G. M., Arico-Muendel, C. C., Benjamin, H. W., Hundal, A. M., Lee, J.-J., Chin, J., Kelley, M., Wakefield, J., Hayward, N. J., and Molineaux, S. M. (1999) *Biochemistry 38*, 6791-6800.
171. Permanne, B., Adessi, C. l., Saborio, G. P., Fraga, S., Frossard, M.-J., Dorpe, J. V., Dewachter, I., Banks, W. A., Leuven, F. V., and Soto, C. (2002) *FASEB J. 16*, 860-862.
172. Soto, C., Kindy, M. S., Baumann, M., and Frangione, B. (1996) *Biochemical and Biophysical Research Communications 226*, 672–680.
173. Lowe, T. L., Strzelec, A., Kiessling, L. L., and Murphy, R. M. (2001) *Biochemistry 40*, 7882-7889.
174. Ghanta, J., Shen, C.-L., Kiessling, L. L., and Murphy, R. M. (1996) *J. Biol. Chem. 271*, 29525-29528.
175. Kim, J., and Murphy, R. (2004) *Biophys. J. 86*, 3194-3203.
176. Fraser, P., Nguyen, J., Inouye, H., Surewicz, W., Selkoe, D., Podlisny, M., and Kirschner, D. A. (1992) *Biochemistry 31*, 10716-10723.
177. Burdick, D., Soreghan, B., Kwon, M., Kosmoski, J., Knauer, M., Henschen, A., Yates, J., Cotman, C., and Glabe, C. (1992) *J. Biol. Chem. 267*, 546-554.
178. Fülöp, L. V., Penke, B., and NDI, M. R. Z. (2001) *J. Peptide Sci. 7*, 397–401.
179. Fields, G. B., and Noble, R. L. (1990) *Int. J. Peptide Protein Res. 35*, 161-214.
180. Hamdan, M., Masin, B., and Rovatti, L. (1996) *Rapid Commun. Mass Spec. 10*, 1739-1742.
181. Vyas, S., and Duffy, L. (1997) *Protein Pepteide Lett. 4*, 99-106.
182. El-Agnaf, O., Goodwin, H., Sheridan, J., Frears, E., and Austen, B. (2000) *Peptide protein Lett. 7*, 1-8.
183. Inui, T., Nishio, H., Bodi, J., Nishiuchi, Y., and Kimura, T.
184. Quibell, M., Turnell, W., and Johnson, T. (1995) *J. Chem. Soc. Perkin 1*, 2019–2024.
185. Quibell, M., Turnell, W., and Johnson, T. (1994) *J. Org. Chem. 59*, 1745–1750.
186. El-Agnaf, O., Harriott, P., Guthrie, D., Irvine, B., and Walker, B. (1994) *Lett. Peptide Sci. 1*, 135–141.
187. Johnson, T., Quibell, M., Owen, D., and Sheppard, R. (1993) *J.Chem. Soc. Chem. Commun.*, 369–372.
188. Gordon, D., and Meredith, S. (2003) *Biochemistry 42*, 475-485.
189. Esler, W., Stimson, E., Ghilardi, J., Lu, Y., Felix, A., Vinters, H., Mantyh, P., Lee, J., and Maggio, J. (1996) *Biochemistry 35*, 13914-13921.
190. Fraser, P., McLachlan, D., Surewicz, W., Mizzen, C., Snow, A., Nguyen, J., and Kirschner, D. (1994) *J. Mol. Biol. 244*, 64-73.
191. Wille, H., Prusiner, S. B., and Cohen, F. E. (2000) *J. Struct. Biol. 130*, 323-338.
192. Alder, A. J., Greenfield, N. J., and Fasman, G. D. (1973) *Meth. Enzymology 27*, 675.
193. Chalifour, R. J., McLaughlin, R. W., Lavoie, L., Morissette, C., Tremblay, N., Boulé, M., Sarazin, P., Stéa, D., Lacombe, D., Tremblay, P., and Gervais, F. (2003) *J. Biol. Chem. 278*, 34874-34881.
194. Bryce, D., and Bax, A. (2004) *J. Biomol. NMR 28*, 273-287.
195. Koide, S., Yokoyama, S., Matsuzawa, H., Miyazawa, T., and Ohta, T. (1989) *J. Biol. Chem. 264*, 8676-8679.

196. Seelig, G., Prosise, W., Hawkins, J., and Senior, M. (1995) *J. Biol. Chem. 270*, 9241-9249.
197. Eisenmesser, E. Z., Zabell, A. P. R., and Post, C. B. (2000) *J. Biomol. NMR 17*, 17–32.
198. Arimoto, R., Kisselev, O., Makara, G., and Marshall, G. (2001) *Biophys. J. 81*, 3285-3293.
199. Zhou, C., Swaney, S., Shinabarge, r. D., and Stockman, B. (2002) *Antimicrob Agents Chemother 46*, 625-629.
200. Carlomagno, T., Felli, I. C., Czech, M., Fischer, R., Sprinzl, M., and Griesinger, C. (1999) *J. Am. Chem. Soc. 121*, 1945-1948.
201. Blommers, M. J. J., Stark, W., Jones, C. E., Head, D., Owen, C. E., and Jahnke, W. (1999) *J. Am. Chem. Soc. 121*, 1949-1953.
202. Casset, F., Hamelryck, T., Loris, R., Brisson, J.-R., Tellier, C., Dao-Thi, M.-H., Wyns, L., Poortmans, F., rez, S. P., and Imberty, A. (1995) *J. Biol. Chem. 270*, 25619–25628.
203. Carlomagno, T., Blommers, M. J. J., Meiler, J., Cuenoud, B., and Griesinger, C. (2001) *J. Am. Chem. Soc. 123*, 7364-7370.
204. Carlomagno, T., Maurer, M., Hennig, M., and Griesinger, C. (2000) *J. Am. Chem. Soc. 122*, 5105-5113.
205. Blommers, M. J. J., and Jahnke, W. (1998) *Angew. Chem. Int. Ed. 37*, 456-458.
206. Boisbouvier, J., and Bax, A. (2002) *J. Am. Chem. Soc. 124*, 11038-11045.
207. Bax, A. (2003) *Protein Sci. 12*, 1-16.
208. Bax, A., Kontaxis, G., and Tjandra, N. (2001) *Meth. Enzymol. 339*, 127-174.
209. Sanders, C. R., and Schwonek, J. P. (1992) *Biochemistry 31*, 8898-8905.
210. Clore, G. M., Starich, M. R., and Gronenborn, A. M. (1998) *J. Am. Chem. Soc. 120*, 10571-10572.
211. Hansen, M. R., Mueller, L., and Pardi, A. (1998) *Nature Struct. Biol. 5*, 1065-1074.
212. Sass, J., Cordier, F., Hoffmann, A., Rogowski, M., Cousin, A., Omichinski, J. G., Löwen, H., and Grzesiek, S. (1999) *J. Am. Chem. Soc. 121*, 2047-2055.
213. Koenig, B. W., Hu, J.-S., Ottiger, M., Bose, S., Hendler, R. W., and Bax, A. (1999) *J. Am. Chem. Soc. 121*, 1385-1386.
214. Sass, H. J., Musco, G., Stahl, S. J., Wingfield, P. T., and Grzesiek, S. (2000) *J. Biomol. NMR 18*, 303-309.
215. Ishii, Y., Markus, M. A., and Tycko, R. (2001) *J. Biomol. NMR 21*, 141-151.
216. Meier, S., Haussinger, D., and Grzesiek, S. (2001) *J. Biomol. NMR 24*, 351-356.
217. Prestegard, J. H., and Kishore, A. I. (2001) *Curr. Opin. Chem. Biol. 5*, 584-590.
218. Hansen, M. R., Rance, M., and Pardi, A. (1998) *J. Am. Chem. Soc. 120*, 11210-11211.
219. Umemoto, K., Leffler, H., Venot, A., Valafar, H., and Prestegard, J. (2003) *Biochemistry 42*, 3688-3695.
220. Boisbouvier, J. r. m., Delaglio, F., and Bax, A. (2003) *Proc. Natl. Acad. Sci. 100*, 11333–11338.
221. Tian, F., Al-Hashimi, H., Craighead, J., and Prestegard, J. (2001) *J. Am. Chem. Soc. 123*, 485-492.
222. Jain, N., Noble, S., and Prestegard, J. (2003) *J. Mol. Biol. 328*, 451-462.
223. Fischer, M., Losonczi, J., Weaver, J., and Prestegard, J. (1999) *Biochemistry 38*, 9013-9022.
224. Ni, F. (1994) *Prog. NMR Spectr. 26*, 517-606.
225. Felli, I. C., Richter, C., Griesinger, C., and Schwalbe, H. (1999) *J. Am. Chem. Soc. 121*, 1956-1957.
226. Carlomagno, T., Felli, I. C., Czech, M., Fischer, R., Sprinzl, M., and Griesinger, C. (1999) *J. Am. Chem. Soc. 121*, 1943-1948.

227. Blommers, M. J. J., Stark, W., Jones, C. E., Head, D., Owen, C. E., and Jahnke, W. (1999) *J. Am. Chem. Soc. 121*, 1949-1953.
228. Bolon, P. J., Al-Hashimi, H. M., and Prestegard, J. H. (1999) *J. Mol. Biol. 293*, 107-115.
229. Koenig, B. W., Mitchell, D. C., König, S., Grzesiek, S., Litman, B. J., and Bax, A. (2000) *J. Biomol. NMR 16*, 121–125.
230. Koenig, B. W., Kontaxis, G., Mitchell, D. C., Louis, J. M., Litman, B. J., and Bax, A. (2002) *J. Mol. Biol. 322*, 441-461.
231. Andrew, E. R., Bradbury, A., and Eades, R. G. (1958) *Nature 182*, 1659.
232. Lowe, I. J. (1959) *Phys. Rev. Lett. 2*, 285-287.
233. Herzfeld, J., and Berger, A. (1980) *J. Chem. Phys. 73*, 6021-6030.
234. Mehring, M. (1983) *High Resolution NMR in Solids*, Springer, New York.
235. Bloch, F. (1956) *Phys. Rev. 102*, 104-135.
236. Bloch, F. (1958) *Phys. Rev. 111*, 841-853.
237. Bennett, A. E., Rienstra, C. M., Auger, M., Lakshmi, K. V., and Griffin, R. G. (1995) *J. Chem. Phys. 103*, 6951-6958.
238. Waugh, J. S., Huber, L. M., and Haeberlen, U. (1968) *Phys. Rev. Lett. 20*, 180-182.
239. Mansfield, P. (1971) *J. Phys. C. 4*, 1444-1452.
240. Burum, D. P., and Rhim, W. K. (1979) *J. Chem. Phys. 71*, 944-956.
241. Hohwy, M., Bower, P. V., Jakobser, H. J., and Nielsen, N. C. (1997) *Chem. Phys. Lett. 273*, 297-303.

2 Materials and Methods

2.1 Instruments

HPLC: RP-HPLC analysis and semiscale preparations were carried out on a Waters (high pressure pump 510, multi-wavelength detector 490 E, chromatography workstation Maxima 820), a Beckman (high pressure pump 110B, gradient mixer, controller 420, UV detector Uvicord from Knauer), or an Amersham Pharmacia Biotech (Äkta Basic 10/100, autosampler A-900) facility. RP-HPLC preparative separations were carried out on a Beckman System Gold (high pressure pump module 126, UV detector 166). A C-18 column (YMC-Pack ODS/A column) was used. As solvents, solvent A: H2O + 0.1% CF3COOH, and B: CH3CN + 0.1% CF3COOH with UV detection at 220 and 254 nm, were used.

HPLC-ESI Mass spectrometer: HPLC-ESI mass spectra were recorded on a Finnigan LCQ-ESI with HPLC conjunction LCQ (HPLCsystem Hewlett Packard HP 1100, Nucleosil 100 $5C_{18}$).

CD: Jasco spectropolarimeter 715 with a PTC-343 temperature controller (cells with optical paths of 1 mm).

EM: EM 902A (Carl Zeiss, Oberkochen, Germany) equipped with MegaView III camera and analySIS® software (soft imaging system, Münster, Germany).

NMR : AVANCE DRX 600 /750/ 800/ 900 MHz solution NMR Spectrometer and 400 MHz/600 MHz solid-state NMR spectrometer (Bruker, Karlstruhe, Germany).

Centrifuge : A14 LabTop Microcentrifuge (Jouan, Unterhaching, Germany), Servall Superspeed RC-2B and RC5B Plus with rotors GS3, GSA and SS34

Centrifuge with rotor S4180 and F2402 (Beckman, Fullerton, USA)

Lyophilizer : CHRIST ALPHA 1-4 (Osterode am Harz, Germany)

pH Meter : E512 Metrohm AG CH-9100 (Herisau, Switzerland)

Shaker : Lab Shaker and Certomat MO (B.Braun, Melsungen, Germany)

Ultrasonicator : Sonifier B-12 (Branson SONIC Power Company, USA)

UV spectrometer: LKB Ultrospec II, M 4050 UV/VIS spectrophotometer (Biochrom, Cambridge, GB)

Fluorescence spectrophotometer: FluoroMax I (Spex, Edison, USA) thermostatted quartz cells.

2.2 Materials

2.2.1 Chemicals

Solvents for moisture sensitive reactions were distilled and dried according to standard procedures. All other solvents were distilled before use. NMP was purchased from BASF, and wasn't distilled later. Pd/C was donated by Degussa, Frankfurt/M., Germany. For solid-phase synthesis TCP resin (0.9 mmol/g, tritylchloropolystyrene-resin) from *PepChem Goldammer & Clausen* or TCP resin(1.3 mmol/g) from *Novabiochem*; Fmoc protected amino acids, were purchased *from NovaBiochem, Alexis, Merck, Bachem, Neosystem, Aldrich, Advanced Chemtech, Synthetech* and *MultisynTech.* All other reagents were from *Aldrich, Fluka, perSeptive Macrocyclics* and *Merck* unless otherwise noted.

2.2.2 Labelled Fmoc Amino Acids

Isotopically labelled FMOC-protected amino acids were obtained from Cambridge Isotopes Laboratories.

FMOC-Phe(4-F)-OH was obtained from *Sigma-Aldrich Chemie GmbH.*

FMOC protected, ^{15}N- and 10%-^{13}C- labelled amino acids were purchased from Senn Chemicals, Switzerland.

Synthetic $A\beta^{1-40}$ was purchased from *BioSource*, USA.

2.3 peptide synthesis

Peptides were synthesized manually by solid-phase peptide synthesis procedures appropriate for monomers equipped with fluorenylmethoxycarbonyl protecting groups (Fmoc).

2.3.1 General procedure for Fmoc protection of amino acids

A solution of certain amino acid in Acetone/H2O (1:1, 40 ml/g) with 1.05 equiv Fmoc-ONSu and 1.20 equiv $NaHCO_3$ was stirred till achieving clear solution. 1.5 N HCl was added to this solution to pH 2. Acetone was removed under reduced pressure. The residue was suspended in ethyl acetate and the aqueous phase was extracted with AcOEt (3 ×). The combined organic phases were washed with HCl prepared at pH2 (2 x), H2O (2 x), then dried (by $MgSO_4$) and concentrated under reduced pressure. The crude product was dissolved in chloroform, slowly heating when necessary. *n*-Hexan was added for crystallisation. Crystals were filtered and dried afterwards. Samples of the product were characterized by HPLC and NMR respectively.

2.3.2 General procedure for anchoring of the first Fmoc-protected amino acid on TCP resin

The unloaded dry TCP resin in a syringe (exact known weight), completed with a filter, was swollen in NMP/DMF (30 min). The resin was filtered off, and a solution (~ 0.125 M) of Fmoc-protected amino acid (with respect of the theoretical capacity of the TCP resin: for natural abundance Fmoc amino acids, using 1.2 equiv; for Fmoc-^{13}C,^{15}N-AA, using 1.0 equiv) and DIPEA (with respect to the quantity of Fmoc-protected amino acid used: for natural abundance Fmoc amino acids, using 2.5 equiv; for Fmoc-^{13}C,^{15}N-AA, using 2.08 equiv) in DCM (abs.) was added. After shaking for 1 h at rt the capping solution (10% DIPEA in MeOH) was added. After 15 min the resin was filtered off, and the resin was washed with DCM (3 × 3 min), NMP (3 × 3 min), and MeOH (3 × 3 min), and dried

overnight under vacuum. Subsequently the exact weight of the dried resin was determined, and the loading of the resin was calculated:

$$C\left[mol/g\right] = \left(m_{total} - m_{resin}\right) / \left\{\left(\mathrm{MG}_{\mathrm{Xaa}} - M_{HCl}\right) m_{total}\right\}$$

C loading rate
m_{resin} mass of resin before loading
m_{total} mass of loaded resin
MG_{Xaa} molar weight of the Fmoc-protected amino acid (Xaa)

The loading of the resin could also be measured by UV spectrometer. An indication of loading of a compound on a resin can be ascertained by obtaining an Fmoc number. The piperidine adduct produced on Fmoc removal absorbs UV at 301 nm. Given that prior art shows (a) the cleavage is quantitative and reproduceable and (b) the reaction between the fluorene based Michael acceptor and piperidine is quantitative, then the UV absorption of the piperidine adduct may be used as a measure of the loading of the resin. This is achieved through and adaption of the Beer-Lambert Law: $C\left[mog/g\right] = \Delta E / A \bullet C'$

A constant of the UV spectrometer (for the spectrometer used: A=6000)
C' concentration of test solution

After removing of the capping solvent, resin was washing the with NMP/DMF, then certain amount of 20% piperidine/DMF solution was added to syringe to remove the FMOC protecting group, the deprotection reaction solution was collected and measured by UV spectrometer.

2.3.3 General procedure of coupling for solid-phase peptide synthesis

The Fmoc-protecting group of the amino acid attached to the resin was removed by treating the resin with a 20% piperidine solution in NMP/DMF (2 ×10 min). The resin was filtered off and washed with NMP/DMF (5 × 3 min), before a solution of the next Fmoc protected amino acid (3 equiv Fmoc-AA-OH, but 1.7 equiv Fmoc-^{13}C,^{15}N-AA), TBTU/ HOBt (3 equiv for natural abundance Fmoc amino acids, 1.7 equiv for Fmoc-^{13}C,^{15}N-AA) and

DIPEA (8.3 equiv for natural abundance Fmoc amino acids, 4.7 equiv for Fmoc-^{13}C,^{15}N-AA) in NMP was added. After 1-3 h reaction was complete (monitoring by ESI-HPLC-MS). The resin was washed with NMP/DMF (5 × 3 min), prior to the subsequent Fmoc-deprotection and coupling steps.

When the next coupling could not be done in the same day, usually after finishing the coupling, the resin was washed five times with NMP/DMF, stayed in NMP overnight with Fmoc protected group.

For the preloaded resin, it was first swelled for 30 min in NMP. Then the Fmoc-protecting group of the amino acid attached to the resin was removed by treating the resin with a 20% piperidine solution in NMP/DMF (3 ×10 min). The resin was filtered off and washed with NMP/DMF (5 × 3 min), and ready for the coupling of the next Fmoc-protected amino acid.

2.3.4 General procedure of cleavage for solid-phase peptide synthesis

After coupling of the last amino acid, the resin was washed with NMP/DMF (3 × 3 min), CH2Cl2 (1 × 3 min), and dried overnight under vacuum. The peptides were cleaved from the dry resin using a mixture of TFA:TIPS:H_2O (10:1:1) (3 × 3.6 ml) within 10 minutes.

If the cleavage is done right after the coupling, then to dry the resin is not necessary. After washing resin with NMP (3 x), DCM (3 x), a small amount (~1 ml) of TIPS+DCM (1:1) was added to the resin, then using the normal cleavage solution. The cleavage solution stayed 1 hour before removing TFA under reduced pressure (for peptide STVIIE, the cleavage solution must stay more than 2 hours). The solution of products with trace of TFA was precipitated in 20 times excess diethylether. The solid in the solvent was centrifuged and washed by diethylether (2 x), centrifuged, and dried under low pressure.

The dry crude peptides were purified via RP-HPLC performing on C-18 column (YMC-Pack ODS/A) with water and ACN with 0.1 % TFA as eluents. The purity and identity for

the peptides were assessed by ESI-MS and RP-HPLC-ESI-MS analyses performing on a Finnigan LCQ-ESI Spectrometer coupled to a Hewlett Packard HP1100 HPLC-System.

2.3.5 Synthesis of Fmoc-4-^{19}F-Phe

0.5 g 4-fluro-phenylalanine with 0.966 g Fmoc-ONSu (1.05 equiv) and 0.275 g $NaHCO_3$ (1.20 equiv) in 20 ml Acetone/H2O (1:1) was stirred till achieving clear solution. 1.5 N HCl was added to this solution to reach pH 2. Acetone was removed under reduced pressure. The residue was suspended in ethyl acetate and the aqueous phase was extracted with AcOEt (3 x). The combined organic phase was washed with HCl prepared at pH 2 (2 x), H2O (2 x), then dried (by $MgSO_4$) and concentrated under reduced pressure. The crude product was dissolved in chloroform, slowly heating when necessary. *n*-Hexan was added for crystallisation. Crystals were filtered and dried afterwards. The final product (1.02 g) was characterized by HPLC-MS: 1658.9 [4M+K]+; 1238.2 [2M+Na]+; 849.3 [2M+K]+; 833.3 [2M+Na]+; 811.1 [2M+H]+; 428.3 [M+Na]+; 406.0 [M+H]+; *t*R=24.38 min (Anal. HPLC, 10-90% B in 30 min); Yield: 93%.

2.3.6 Synthesis of iAβ5 (LPFFD)

In a syringe (10 ml), completed with a filter, TCP resin (0.5 g, ~0.9 mmol·g^{-1}) was swelled in NMP (30 min). After filtering off the resin, a solution of Fmoc-Asp(OtBu)-OH (0.222 g, 0.54 mmol, 1.2 equiv) and DIPEA (192 µl, 3.75 mmol, 8.3 equiv) in CH2Cl2 (4 ml) was added. After 1h, 1 ml MeOH was added into the syringe, 10 minutes later, the resin was filtered off, washed with CH_2Cl_2 (3×3 min), DMF (3×3 min) and MeOH (3×3 min), before dried under reduced pressure overnight. The resin's loading was 0.64 mmol g^{-1}, according to gravimetric measurements. In a syringe (10 ml) the Fmoc-Asp (OtBu)-OH loaded resin (0.66 g, 0.64 mmol·g^{-1}, 0.42 mmol) was swelled for 30 min in NMP. According to general procedure Fmoc-Phe-OH (0.490 g, 1.27 mmol, 3 equiv), Fmoc- Phe-OH (0.490 g, 1.27 mmol, 3 equiv), Fmoc-Pro-OH (0.428 g, 1.27 mmol, 3 equiv) and Fmoc-Leu-OH (0.448 g,

1.27 mmol, 3 equiv) were coupled subsequently. The following Fmoc-deprotection and cleavage steps yielded the product, iAβ5, characterized by HPLC-MS: 1313.4 [2M+K]+; 1297.4 [2M+Na]+; 1275.4 [2M+H]+; 660.4 [M+Na]+; 638.4 [M+H]+; *t*R =12.23 min (HPLC-MS, 10-90%B in 15 min); *t*R =23.24 min (Anal. HPLC, 5-50% B in 30 min). Purification by RP-HPLC (36-50 % B in 30 min) produced 177.6 mg iAβ5**,** yield: 66 %.

2.3.7 Synthesis of iAβ5^{inv} (DPFFL)

In a syringe (5 ml), completed with a filter, TCP resin (0.1 g, ~1.3 mmol·g^{-1}) was swelled in DMF (30 min). After filtering off the resin, a solution of Fmoc-Leu-OH (0.092 g, 0.26 mmol, 2.0 equiv) and DIPEA (89 µl, 0.52 mmol, 4.0 equiv) in CH_2Cl_2 (1 ml) was added. After 1 h, 1 ml DIPEA/MeOH (1:9) was added into the syringe, 10 minutes later the resin was filtered off, washed with CH_2Cl_2 (3×3 min), DMF (3×3 min). The loading ratio checked by UV spectrometer was 1.25 mmol·g^{-1}. According to general procedure Fmoc-Phe-OH (0.145 g, 0.375 mmol, 3 equiv), Fmoc-Phe-OH (0.145 g, 0.375 mmol, 3 equiv), Fmoc-Pro-OH (0.126 g, 0.375 mmol, 3 equiv) and Fmoc-Asp (OtBu)-OH (0.154 g, 0.375 mmol, 3 equiv) were coupled subsequently. Here, HBTU was used as activating agent. The following Fmoc-deprotection and cleavage steps yielded the product, iAβ5^{inv}, characterized by MS: 676.14 [M+K]+; 660.17 [M+Na]+; 638.20 [M+H]+; *t*R=37.27 min (anal. HPLC, 5-60%B in 80 min). Purification by RP-HPLC (*t*R =55.42 min, 10-60 % B in 70 min) yielded iAβ5^{inv} (55.7 mg, 70 %).

2.3.8 Synthesis of ^{19}F-iAβ5

This peptide was ^{19}F labelled in the para-position of the aromatic ring of Phe3. Synthesis procedure was the same as that for iAβ5, except for the coupling of Fmoc- Phe (4-F)-OH. In a syringe (10 ml) with a filter, TCP resin (0.5 g, ~0.9 mmol·g^{-1}) was used. After loading, the resin was dried under reduced pressure overnight and the resin's loading was 0.54 mmol·g^{-1}, according to gravimetric measurements. When Fmoc- Phe (4-F)-OH was coupled, 1.7 equiv

was taken for TBTU, HOBt and Fmoc-AA, 4.7 equiv for DIPEA. And the coupling time was 2 h instead of 1 h for normal coupling. After this coupling, according to general procedure, Fmoc-Pro-OH (0.344 g, 1.02 mmol, 3 equiv) and Fmoc-Leu-OH (0.360 g, 1.02 mmol, 3 equiv) were coupled subsequently. The following Fmoc-deprotection and cleavage steps yielded the product, ^{19}F-iAβ5, characterized by MS: 1349.4 [2M+K]+; 1333.2 [2M+Na]+; 1311.3 [2M+H]+; 694.2 [M+K]+; 678.4 [M+Na]+; 656.3 [M+H]+; *t*R=23.93 min (Anal. HPLC, 5-50%B in 30 min). Purification by RP-HPLC (*t*R =15 min, 15-60 % B in 30 min) yielded ^{19}F-iAβ5 (140 mg, 63 %).

2.3.9 Synthesis of U-^{13}C, ^{15}N-iAβ5

This peptide has been fully labelled in ^{15}N, ^{13}C. In a syringe (5 ml), completed with a filter, TCP resin (0.333 g, ~0.9 mmol·g^{-1}) was swelled in NMP (30 min). After filtering off the resin, a solution of ^{15}N-Fmoc-L-Aspartic acid (OBt)-$^{13}C_4$ (0.125 g, 0.3 mmol, 1.0 equiv) and DIPEA (107 µl, 0.625 mmol, 2.08 equiv) in CH2Cl2 (~2 ml) was added. After 1 h, a small amount of DIPEA was added into the reaction solution to reach pH 9. After another 1 h, 1 ml DIPEA/MeOH (1:9) was added into the syringe, 10 minutes later the resin was filtered off, washed with CH2Cl2 (3×3 min), DMF (3×3 min) and dried under reduced pressure overnight. The resin's loading was 0.616 mmol·g^{-1}, according to gravimetric measurements. 0.3 g loaded resin was taken for the following synthesis. According to general procedure ^{15}N-Fmoc-L-Phenylalanine-U-$^{13}C_9$ (0.125 g, 0.31 mmol, 1.7 equiv), ^{15}N-Fmoc-L-Phenylalanine-U-$^{13}C_9$ (0.125 g, 0.31 mmol, 1.7 equiv), ^{15}N-Fmoc-L-Proline-U-$^{13}C_5$ (0.110 g, 0.32 mmol, 1.73 equiv) and ^{15}N-Fmoc-L-Leucine-$^{13}C_6$ (0.114 g, 0.316 mmol, 1.7 equiv) were coupled subsequently, and the coupling time for each amino acid was 2 h. The following Fmoc-deprotection and cleavage steps yielded the product, U-^{13}C, ^{15}N-iAβ5, characterized by MS: 1351.5 [2M+H]+; 676.5 [M+H]+; *t*R =15.46 min (Anal. HPLC: 15-65% B in 30min). Purification by RP-HPLC (*t*R =23 min, 15-48 % B in 25 min) yielded u-^{13}C, ^{15}N-iAβ5 (85.8 mg, 69 %).

2.3.10 Synthesis of ^{15}N, 10%^{13}C-iAβ5^{inv}

This peptide has 100% enriched in ^{15}N and 10 % randomly enriched in ^{13}C. The synthesis procedure was done as that for U-^{13}C, ^{15}N-iAβ5. In a syringe (5 ml) with a filter, TCP resin (0.555 g, ~0.9 mmol·g^{-1}) was swelled in NMP (30 min). After filtering off the resin, a solution of Fmoc-Leu-OH (0.208 g, 0.59 mmol, 1.17 equiv) and DIPEA (178 µL, 1.04 mmol, 1.8 equiv) in CH2Cl2 (1 ml) was added. After 1 h, a small amount of DIPEA was added into the reaction solution to reach pH 9. After another 1 h, 1 ml DIPEA/MeOH (1:9) was added into the syringe, 10 minutes later the resin was filtered off, washed with CH2Cl2 (3×3 min), DMF (3×3 min) and dried under reduced pressure overnight. The resin's loading was 0.57 mmol·g^{-1}, according to gravimetric measurements. According to general procedure Fmoc-Phe-OH (0.135 g, 0.35 mmol, 1.7 equiv), Fmoc- Phe-OH (0.135 g, 0.35 mmol, 1.7 equiv), Fmoc-Pro-OH (0.116 g, 0.34 mmol, 1.7 equiv) and Fmoc-Asp (OtBu)-OH (0.122 g, 0.30 mmol, 1.5 equiv) were coupled subsequently, and the coupling time for each amino acid was 2 h. The following Fmoc-deprotection and cleavage steps yielded the product, ^{15}N, 10%^{13}C-iAβ5^{inv}, characterized by MS: 1296.3, 1295.2, 1294.3, 1292.2 [2M+H]+; 649.3, 648.3, 647.3, 646.3 [M+H]+; *t*R =18.46 min (Anal. HPLC, 5-75 %B in 30 min). Purification by RP-HPLC (*t*R =23.7 min, 5-75 % B in 30 min) yielded ^{15}N, 10%^{13}C-iAβ5^{inv} (52.6 mg, 41 %).

2.3.11 Synthesis of Aβ$^{14–23}$ (HQKLVFFAED)

In a syringe (10 ml), completed with a filter, TCP resin (0.5 g, ~0.9 mmol·g^{-1}) was swelled in NMP (30 min). After filtering off the resin, a solution of Fmoc-Asp (OtBu)-OH (0.222 g, 0.54 mmol, 1.20 equiv) and DIPEA (192.6 µl, 1.125 mmol, 2.5 equiv) in CH2Cl2 (4 ml) was added. After 1 h, 1 ml DIPEA/MeOH (1:9) was added into the syringe, 10 minutes later the resin was filtered off, washed with CH2Cl2 (3×3 min), DMF (3×3 min) and dried under reduced pressure overnight. The resin's loading was 0.65 mmol·g^{-1}, according to gravimetric measurements. According to general procedure Fmoc-Glu (OtBu)-OH (0.41 g,

0.974 mmol, 3 equiv), Fmoc- Ala-OH (0.303 g, 0.974 mmol, 3 equiv), Fmoc-Phe-OH (0.377 g, 0.974 mmol, 3 equiv), Fmoc-Phe-OH (0.377 g, 0.974 mmol, 3 equiv), Fmoc-Val-OH (0.33 g, 0.974 mmol, 3 equiv), Fmoc-Leu-OH (0.344 g, 0.974 mmol, 3 equiv), Fmoc-Lys (Boc)-OH (0.455 g, 0.974 mmol, 3 equiv), Fmoc-Gln (Trt)-OH (0.594 g, 0.974 mmol, 3 equiv) and Fmoc-His (Trt)-OH (0.602 g, 0.974 mmol, 3 equiv), were coupled subsequently. The following Fmoc-deprotection and cleavage steps yielded the product, $A\beta^{14–23}$, characterized by MS: 1272.1 [M+K]+; 1256.1 [M+Na]+; 1234.1 [M+H]+; *t*R =10.51 min (HPLC-MS: 10-90%B in 15 min). Purification via RP-HPLC (*t*R =24.5 min, 10-60 % B in 30 min) yielded $A\beta^{14–23}$ as a white fluffy powder after lyophilization: (148.1 mg, 37 %).

2.3.12 Synthesis of ^{19}F-Aβ^{14-23} (HQKLVF*FAED)

This peptide was ^{19}F labelled in the para-position of the aromatic ring of Phe19. Synthesis procedure was the same as that for $A\beta^{14–23}$, except for the coupling of Fmoc- Phe (4-F)-OH. In a syringe (10 ml) with a filter, TCP resin (0.5 g, ~0.9 mmol·g^{-1}) was used. After loading, the resin was dried under reduced pressure overnight. The resin's loading was 0.58 mmol·g^{-1}, according to gravimetric measurements. According to general procedure Fmoc-Glu (OtBu)-OH, Fmoc- Ala-OH and Fmoc-Phe-OH were coupled continuously. Then Fmoc-Phe-OH (0.353 g, 0.87 mmol, 2.3 equiv) was used for the coupling. Then Fmoc-Val-OH (0.33 g, 0.974 mmol, 3 equiv), Fmoc-Leu-OH (0.344 g, 0.974 mmol, 3 equiv), Fmoc-Lys (Boc)-OH (0.455 g, 0.974 mmol, 3 equiv), Fmoc-Gln (Trt)-OH (0.594 g, 0.974 mmol, 3 equiv) and Fmoc-His (Trt)-OH (0.602 g, 0.974 mmol, 3 equiv), were coupled subsequently. The following Fmoc-deprotection and cleavage steps yielded the product, $A\beta^{14–23}$, characterized by MS: 1295.4 [M-H+2Na]+; 1289.4 [M+K]+; 1273.4 [M+Na]+; 1252.4 [M_{C13}+H]+; 1251.5 [M+H]+; *t*R =16.07 min (Anal. HPLC: 10-60%B in 30 min). Purification by RP-HPLC (*t*R =23.7 min, 10-60 % B in 30 min) yielded ^{19}F-$A\beta^{14–23}$ (162.8 mg, 35 %).

2.3.13 Synthesis of KLVFFKK

In a syringe (10 ml), completed with a filter, TCP resin (0.25 g, ~1.3 mmol·g^{-1}) was swelled in DMF (30 min). After filtering off the resin, a solution of Fmoc-Lys (Boc)-OH (0.25 g, 0.54 mmol, 2.0 equiv) and DIPEA (222 µl, 1.08 mmol, 4.0 equiv) in CH2Cl2 (2 ml) was added. After 1 h, 1 ml DIPEA/MeOH (1:9) was added into the syringe, 10 minutes later the resin was filtered off, washed with CH2Cl2 (3×3 min), DMF (3×3 min). The loading ratio checked by UV spectrometer was 1.26 mmol·g^{-1}. According to general procedure Fmoc-Lys (Boc)-OH (0.35 g, 0.945 mmol, 3 equiv), Fmoc-Phe-OH (0.366 g, 0.945 mmol, 3 equiv), Fmoc-Phe-OH (0.366 g, 0.945 mmol, 3 equiv), Fmoc-Val-OH (0.321 g, 0.945 mmol, 3 equiv), Fmoc-Leu-OH (0.334 g, 0.945 mmol, 3 equiv), Fmoc-Lys (Boc)-OH (0.35 g, 0.945 mmol, 3 equiv), were coupled subsequently. The following Fmoc-deprotection and cleavage steps yielded the product, KLVFFKK, characterized by MS: 909.53 [M+H]+; 455.27 [M/2+H]+; 303.85 [M/3+H]+; *t*R =2.8 min (Anal. HPLC: 5-90%B in 40 min). Purification via RP-HPLC (*t*R =8.5 min, 1-60 % B in 70 min) yielded KLVFFKK as a white fluffy powder after lyophilization: (115.1 mg, 47 %).

2.3.14 Synthesis of STVIIE

In a syringe (5 ml), completed with a filter, TCP resin (0.30 g, ~1.14 mmol·g^{-1}) was swelled in DMF (30 min). After filtering off the resin, a solution of Fmoc-^{13}C,^{15}N-Glu(OtBu)-OH (0.148 g, 0.34 mmol, 1.0 equiv) and DIPEA (117 µl, 0.68 mmol, 2.0 equiv) in CH_2Cl_2 (2 ml) was added. After 1 h, a few drops of DIPEA was added into reaction solution to reach pH 9. Two hours after the reaction, 1 ml DIPEA/MeOH (1:9) was added into the syringe, 10 minutes later the resin was filtered off, washed with CH_2Cl_2 (3×3 min), DMF (3×3 min). The loading ratio checked by UV spectrometer was 0.768 mmol·g^{-1}. According to general procedure Fmoc-^{13}C,^{15}N-Ile-OH (0.141 g, 0.392 mmol, 1.7 equiv), Fmoc-^{13}C,^{15}N-Ile-OH (0.141 g, 0.392 mmol, 1.7 equiv), Fmoc-^{13}C,^{15}N-Val-OH (0.135 mg, 0.392 mmol, 1.7 equiv), Fmoc-^{13}C,^{15}N-Thr-OH (0.136 mg, 0.392 mmol, 1.7 equiv) and Fmoc-^{13}C,^{15}N-

Ser(OtBu)-OH (0.152 g, 0.392 mmol, 1.7 equiv) were coupled subsequently. Here, Fmoc-Threonine was used with the side chain protection. It was confirmed by the successful synthesis of STVIIE at natural abundance using Fmoc-Thr-OH with non side chain protection group. This The following Fmoc-deprotection and cleavage steps yielded the product, STVIIE, characterized by MS: 611.34 [M+H]+; *t*R=6.68 min (anal. HPLC, 5-95%B in 40 min). Purification by RP-HPLC (*t*R =7.52 min, 1-50 % B in 70 min) yielded STVIIE (135.45 mg, 63 %).

2.3.15 Synthesis of u-^{13}C,^{15}N-STVIIE

In a syringe (5 ml), completed with a filter, TCP resin (0.30 g, ~1.14 mmol·g^{-1}) was swelled in DMF (30 min). After filtering off the resin, a solution of Fmoc-^{13}C,^{15}N-Glu(OtBu)-OH (0.148 g, 0.34 mmol, 1.0 equiv) and DIPEA (117 µl, 0.68 mmol, 2.0 equiv) in CH_2Cl_2 (2 ml) was added. After 1 h, a few drops of DIPEA was added into reaction solution to reach pH 9. Two hours after the reaction, 1 ml DIPEA/MeOH (1:9) was added into the syringe, 10 minutes later the resin was filtered off, washed with CH_2Cl_2 (3×3 min), DMF (3×3 min). The loading ratio checked by UV spectrometer was 0.768 mmol·g^{-1}. According to general procedure Fmoc-^{13}C,^{15}N-Ile-OH (0.141 g, 0.392 mmol, 1.7 equiv), Fmoc-^{13}C,^{15}N-Ile-OH (0.141 g, 0.392 mmol, 1.7 equiv), Fmoc-^{13}C,^{15}N-Val-OH (0.135 mg, 0.392 mmol, 1.7 equiv), Fmoc-^{13}C,^{15}N-Thr-OH (0.136 mg, 0.392 mmol, 1.7 equiv) and Fmoc-^{13}C,^{15}N-Ser(OtBu)-OH (0.152 g, 0.392 mmol, 1.7 equiv) were coupled subsequently. Here, Fmoc-Threonine was used with the side chain protection. It was confirmed by the successful synthesis of STVIIE at natural abundance using Fmoc-Thr-OH with non side chain protection group. This can be done because Threonine coupling was involved in the second to the last step. The following Fmoc-deprotection and cleavage steps yielded the product, ^{13}C,^{15}N-STVIIE, characterized by MS: 696.37 [M+H]+; *t*R=6.68 min (anal. HPLC, 5-95%B in 40 min). Purification by RP-HPLC (*t*R =7.62 min, 1-50 % B in 70 min) yielded STVIIE (90.45 mg, 38 %).

2.3.16 Synthesis of STVIIT

In a syringe (5 ml), completed with a filter, TCP resin (0.25 g, ~1.3 mmol·g^{-1}) was swelled in DMF (30 min). After filtering off the resin, a solution of Fmoc-Thr(OtBu)-OH (0.258 g, 0.65 mmol, 2.0 equiv) and DIPEA (222 µl, 1.3 mmol, 4.0 equiv) in CH_2Cl_2 (2 ml) was added. After 1 h, 1 ml DIPEA/MeOH (1:9) was added into the syringe, 10 minutes later the resin was filtered off, washed with CH_2Cl_2 (3×3 min), DMF (3×3 min). The loading ratio checked by UV spectrometer was 1.21 mmol·g^{-1}. According to general procedure Fmoc-Ile-OH (0.318 g, 0.90 mmol, 3 equiv), Fmoc-Ile-OH (0.318 g, 0.90 mmol, 3 equiv), Fmoc-Val-OH (0.305 mg, 0.9 mmol, 3 equiv), Fmoc-Thr(OtBu)-OH (0.358 mg, 0.9 mmol, 3 equiv) and Fmoc-Ser(OtBu)-OH (0.345 g, 0.9 mmol, 3 equiv) were coupled subsequently. HBTU was used as a activating agent. The following Fmoc-deprotection and cleavage steps yielded the product, STVIIT, characterized by MS: 633.34 [M+H]+; *t*R=6.15 min (anal. HPLC, 5-95%B in 40 min). Purification by RP-HPLC (*t*R =9.47 min, 1-30 % B in 70 min) yielded STVIIT (145.45 mg, 71 %).

2.3.17 Synthesis of STVIYE

In a syringe (5 ml), completed with a filter, TCP resin (0.25 g, ~1.3 mmol·g^{-1}) was swelled in DMF (30 min). After filtering off the resin, a solution of Fmoc-Glu(OtBu)-OH (0.267 g, 0.65 mmol, 2.0 equiv) and DIPEA (222 µl, 1.3 mmol, 4.0 equiv) in CH_2Cl_2 (2 ml) was added. After 1 h, 1 ml DIPEA/MeOH (1:9) was added into the syringe, 10 minutes later the resin was filtered off, washed with CH_2Cl_2 (3×3 min), DMF (3×3 min). The loading ratio checked by UV spectrometer was 1.26 mmol·g^{-1}. According to general procedure Fmoc-Tyr(OtBu)-OH (0.434 g, 0.945 mmol, 3 equiv), Fmoc-Ile-OH (0.334 g, 0.945 mmol, 3 equiv), Fmoc-Val-OH (0.321 mg, 0.945 mmol, 3 equiv), Fmoc-Thr(OtBu)-OH (0.376 mg, 0.945 mmol, 3 equiv) and Fmoc-Ser(OtBu)-OH (0.362 g, 0.945 mmol, 3 equiv) were coupled subsequently. HBTU was used as a activating agent. The following Fmoc-deprotection and cleavage steps yielded the product, STVIIT, characterized by MS: 711.34

[M+H]+; *t*R=6.98 min (anal. HPLC, 5-95%B in 40 min). Purification by RP-HPLC (*t*R =9.344 min, 1-20 % B in 70 min) yielded STVIIT (131.64 mg, 57 %).

2.4 Fibrillization

Aβ fibrils The buffer has been adjusted to pH 4.0, 10 mM PO_4^{3-}, in order to allow for optimal formation of fibrils (*1*). Fibrillar peptides were prepared following the protocol described by Zagorski and co-workers (*2*). In this protocol (Fig. 2-1), lyophilized $A\beta^{14-23}$ was solubilized first in TFA (Trifluoro-acetic acid). The solutions were kept at room temperature for 1 or 2 hours, until the peptides completely dissolved. After removal of the solvent with dry nitrogen gas, $A\beta^{14-23}$ was re-solubilized in HFIP (Hexafluoro-isopropanol). A small amount of the concentrated stock solution (0.37 mg / 50 µl) was transferred to the aqueous buffer to yield a certain concentration. The samples were kept in the room temperature without disturb.

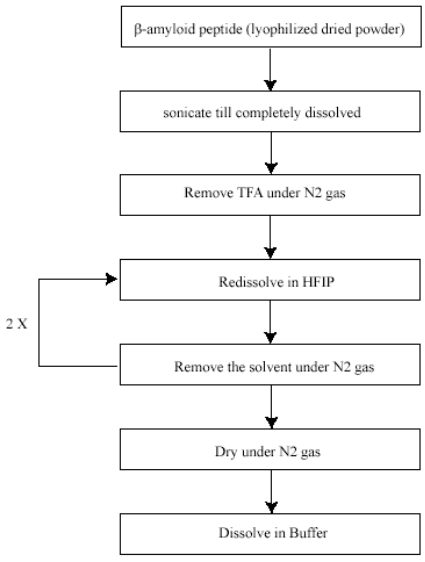

Fig. 2-1. Fibril preparation protocol for Aβ peptides.

Fibrils formed from de novo peptides Fibrils were prepared using a procedure described by Paz et al. (*3*). Briefly, stock peptide solutions were prepared by dissolving a weighed amount of peptide into buffered solution (20 mM glycine/HCl) whose pH had been adjusted

previously to 2.6. Samples were immediately sonicated (10 min) to dissemble preformed nuclei and centrifuged (5 min at 16,100 x g) to deposit insoluble material. Solutions at concentration of ~1.5 mM were prepared by diluting a known volume of stock solution into buffer. Then, peptide solutions were incubated at room temperature. Mature fibrils were formed after 7 days incubation and the solutions were ultracentrifuged (24 hours at 250,000 x g). The pellets were packed to rotors for solid-state NMR experiments.

2.5 Electron Microscopy

For Aβ peptides alone, lyophilized peptide powder was treated by the methods described above, and incubated for 7 days before the EM measurements. For the mixture samples, Aβ fibrils was grown alone 7 days before the addition of peptide inhibitors. EM measurements were performed 7 days after the co-incubation. The incubated samples (5 μl) were placed on grids covered by a carbon-stabilized formvar film. Excess fluid was withdrawn after 30 s, and the grids were negatively stained with 3% uranyl acetate in water. Excess fluid was blotted off and grids were allowed to dry in air. The stained grids were then examined and photographed in EM 902A (Carl Zeiss, Oberkochen, Germany) equipped with MegaView III camera (soft imaging system, Münster, Germany). Images were acquired and processed by means of the analySIS® Digital Micrograph program (soft imaging system, Münster, Germany).

2.6 Circular Dichroism spectroscopy

All CD measurements were made on a Jasco J-720 spectropolarimeter. Samples were prepared following the protocol described by Zagorski and co-workers: lyophilized Aβ was solublized first in TFA (Trifluoro-acetic acid). The solutions were kept at room temperature for 1 or 2 hours, until the peptides completely dissolved. After removal of the solvent with dry nitrogen gas, Aβ was re-solubilized in HFIP (Hexafluoro-isopropanol). A small amount of the concentrated stock solution (0.37 mg / 50 μl) is transferred to the aqueous buffer to

yield a certain concentration. CD studies were performed using a 1 mm quartz cell in the wavelength range of 190- 240 nm at 30°C. Data points were collected in 0.2 nm intervals at a rate of 500 nm/min with 0.25 sec response time and an average of 6 scans was used to generate the data. The final CD spectrum for a given sample was determined by subtracting the buffer-blank spectrum from that acquired for the sample. The far-UV CD spectra were smoothed by using the noise reducing option in the software supplied by the vendor (JASCO). The direct CD measurements (θ, in mdeg) were converted to molar ellipticity, using $[\theta] = \theta/(10 \cdot C \cdot l)$, where C is the molar concentration (mol/l) and l the path length. The molar ellipticity [θ] is in units deg cm^2 $dmol^{-1}$.

2.7 Thioflavine T Fluorescence Assay

The incubated samples were vortex mixed and 40 µl aliquots were withdrawn and mixed with 960 µl of thioflavine T (ThT) in 50 mM phosphate buffer, pH 7.0. Analyses were performed in a FluoroMax I (Spex, Edison, USA) fluorescence spectrophotometer and thermostated quartz cells. During the measurements, both the excitation and emission wavelength were set to 446 nm and 490 nm respectively with a spectral bandwidth of 5 nm. The final concentration of the amyloid like intermediates has been set to 5 µM and that of Thioflavin T has been set to 50 µM to make 1:10 of peptide: Thioflavin T. The emission spectra have been obtained by scanning from 460 nm to 540 nm.

2.8 Solution NMR

All NMR spectra were recorded on Bruker Avance 600 MHz and 750 MHz NMR spectrometers using a 5-mm triple-resonance probe with 3-axis gradients at a temperature of 30 °C. Spectra were calibrated with respect to internal TMS (0 ppm). Other spectrometer characteristics as well as calibrated spectral widths used are reported in appendix 5.1. Modified pulse programs and experimental parameters are summarized in appendix 5.2. WATERGATE (*4*) was applied for suppression of the water resonance in ^1H NMR

experiments. All NMR spectra were processed and analyzed with Xwinnmr [‘XWINNMR V3.0’, Bruker, Karlsruhe].

TOCSY experiments

TOCSY is the abbreviation for TOtal Correlation SpectroscopY. It is also called HOHAHA (HOmonuclear HArtmann HAhn). The TOCSY experiment provides through bond correlations between all the atoms in a single spin-system e.g. all the protons in a single amino acid. Thus each amino acid has a characteristic pattern of signals from which the amino acid can be identified. However, some amino acids have identical spin systems and therefore identical signal patterns. They are: cysteine, aspartic acid, phenylalanine, histidine, asparagine, tryptophane and tyrosine ('AMX systems') on the one hand and glutamic acid, glutamine and methionine ('AM(PT)X systems') on the other hand. More or less, TOCSY constitutes a very efficient transfer element for the assignment of proteins, nucleic acids, and oligosaccharides.

The TOCSY sequence works by applying a strong RF field, called a "spin-lock", along one axis (Fig. 2-2). Under the influence of this field magnetization is transferred from on spin to another through the scalar coupling interactions. The efficiency of the magnetization transfer depends on the J-coupling constant, i.e. Magnetization is transferred more efficiently through large couplings. In this work, TOCSY with DIPSI-2 (*5*) mixing sequence was used.

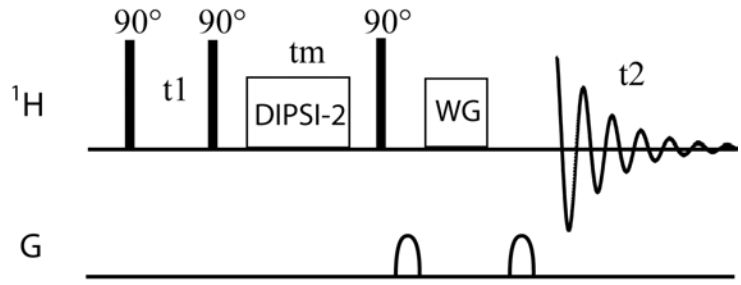

Fig. 2-2. Pulse sequence for the TOCSY experiments used in this work. Isotropic mixing sequence DIPSI-2 was used for desirable magnetization transfer and WATERGATE (WG) technique was used for water suppression.

The length of the DIPSI-2 mixing sequence is governed by the equation $\tau_m = \left(\frac{\pi}{2}\right) \times 115.112n$, where *n* is the number of times which the supercycle is repeated and $\pi/2$ is the appropriate pulse length. An isotropic mixing sequence must possess complete supercycles, otherwise the properties induced by a composite pulse sequence are nullified, n = 18 was used in the TOCSY experiments in this work and the mixing time τ_m was approximately 50 ms.

The rf pulse power level used during the isotropic mixing sequence was set to achieve the pulse length of ~25 μs corresponding to 10 kHz.

TOCSY spectra were recorded at 30 °C, using a 48 ms mixing time. Data matrices with 200× 512 complex points were acquired using acquisition times of 26 ms (F1) and 68 ms (F2). Quadrature detection in F1 was accomplished with the States-TPPI method (*6*). Sine-bell window functions, phase-shifted by 838 and 728, were used for processing in the F1 and F2 dimensions, respectively. Data matrices were zero-filled to 1024×2048 points.

NOESY experiments

NOESY stands for **N**uclear **O**verhauser **E**nhancement **S**pectroscop**Y**. The NOESY experiment is crucial for the determination of protein structure. It uses the dipolar interaction of spins (the nuclear Overhauser effect, NOE) for correlation of protons. The intensity of the NOE is proportional to $1/r^6$, with r being the distance between the protons: The correlation between two protons depends on the distance between them, but normally a signal is only observed if their distance is smaller than 5 Å. The NOESY experiment correlates all protons which are close enough. It also correlates protons which are distant in the amino acid sequence but close in space due to tertiary structure. This is the most important information for the determination of protein structures.

NOESY pulse sequence scheme is shown previously in Fig. 1-11. The pulse sequence starts as usual with a 90° pulse followed by an evolution time t1. This delay is varied systematically as usual to provide chemical shift information in the F1 domain. Then another 90° pulse transmit some of the magnetization to the Z axis and during the following mixing period, the non-equilibria Z components will exchange magnetization through Nuclear Overhauser Effect (NOE). After some time (shorter than the relaxation time T1), the transverse magnetization is restored by the third pulse and detected. If relaxation exchange (or chemical exchange) have taken place during the mixing time, cross peaks will be observed in the spectra.

In this work, NOESY spectra were recorded at 30 °C. The mixing time for peptide in the bound state was varied from 10 to 500 ms. Typical two-dimensional data sets consisted of a data matrix of 1,024 by 128 complex points, with 64 scans collected for each increment. The sweep width in both dimensions was 8,012 Hz. The indirect dimension was zero filled during processing.

HSQC experiments

Heteronuclear **S**ingle **Q**uantum **C**oorelation (HSQC) experiments (*7*) correlate protons with their directly attached heteronuclei. Proton magnetization is detected (during t2 - detection time) while the low-gamma nuclei evolves during the evolution time - t1. Because of the detection of the high frequency nuclei, this sequence is very sensitive. The enhancement in sensitivity this experiment permits is much greater than the enhancement obtainable by simple NOE (Nuclear Overhauser Effect).

The pulse sequence for HSQC experiments is shown in Fig. 2-3. The HSQC experiment starts with proton magnetization. Therefore the recycle time is based on proton relaxation time (1.26 * T_1). The first INEPT step is used to create proton antiphase magnetization (2 τ delay) which is then transferred to the directly attached heteronuclei (carbon or nitrogen).

This X nuclei magnetization is left to evolve with its chemical shift (during t1 - evolution time). Usually, the effect of proton coupling and chemical shift is removed by the use of a 180° proton pulse applied at mid evolution time. However, it can be taken out in order to obtain the couplings between the directly coupled spins, as employed below. The double 90° pulse applied to both nuclei (in the beginning of the last INEPT step) transfers the magnetization back to proton as an anti-phased magnetization, which is then refocus during the last (2 τ delay). The proton in-phase magnetization can then be detected in the presence of the X-nuclei decoupler.

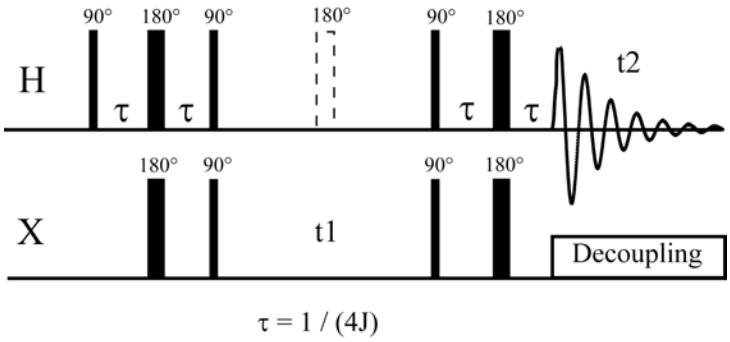

Fig. 2-3. Pulse sequence scheme for HSQC experiments. The open 180° pulse can be employed for regular HSQC experiments or be taken out for certain desired information.

In this work, for measurement of trRDCs, 2D $^{1}H,^{15}N$ and $^{1}H,^{13}C$ correlation spectra are recorded on iAβ5^{inv} performed on a Bruker 750 MHz solution state NMR spectrometer, without ^{1}H decoupling in the indirect dimension. Two sets of experiments were carried out for coupling measurements on iAβ5^{inv}. In the first set, data were collected for a sample of 5 mM iAβ5^{inv} alone in 10 mM $PO4^{3-}$ of pH 4 at 30°C in a isotropic state and in the second set, data were collected for a sample of same amount of iAβ5^{inv} with 0.5 mM Aβ$^{14-23}$ or 0.1 mM Aβ$^{1-40}$ in the same buffer and experimental conditions corresponding to the aligned state. Aβ fibrils were incubated alone about two days before addition of peptide inhibitors.

Proton-coupled ^{1}H-^{15}N HSQC spectra were recorded on ^{15}N-labelled iAβ5^{inv} in absence and presence of Aβ$^{14-23}$, and the data matrix size was 256 × 4096 complex points, resulting in acquisition times of 140 ms and 273 ms in F1 and F2, respectively. Eight transients per FID

were acquired, and quadrature in the F1 dimension was achieved in the Echo-antiecho manner. Data matrices were zero-filled to 2048 × 16384 points.

Proton-coupled ^{1}H-$^{13}C^{\alpha}$ HSQC spectra were recorded on natural abundance iA$\beta5^{inv}$ in absence and presence of $A\beta^{1-40}$ at carry ^{13}C frequency of 10.75 KHz without ^{1}H decoupling in F1 dimension, and the data matrix size was 256 × 1318 complex points, resulting in acquisition times of 27 ms and 80 ms in F1 and F2, respectively. 64 transients per FID were acquired, and quadrature in the F1 dimension was achieved in the Echo-antiecho manner. Data matrices were zero-filled to 16384 × 32768 points.

Proton-coupled ^{1}H-$^{13}C^{\beta}$ HSQC spectra were recorded on natural abundance iA$\beta5^{inv}$ at carry ^{13}C frequency of 5846.6 Hz with the decoupler turned off during acquisition (pulse sequence in Fig. 2-4), and the data matrix size was 256 × 4096 complex points, resulting in acquisition times of 17 ms and 248 ms in F1 and F2, respectively. 128 transients per FID were acquired, and quadrature in the F1 dimension was achieved in the Echo-antiecho manner. Data matrices were zero-filled to 16384 × 16384 points.

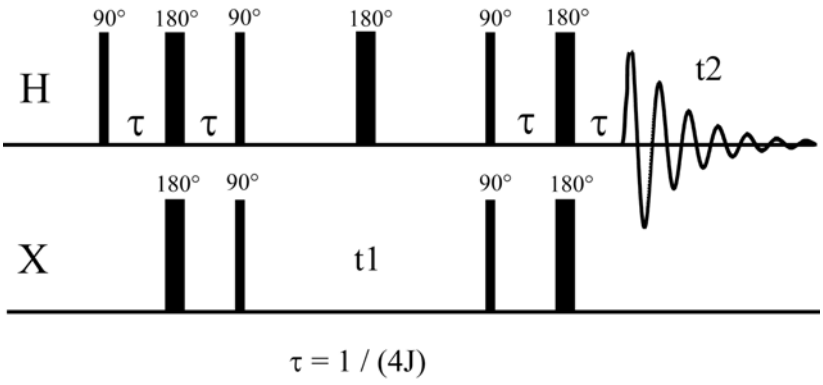

Fig. 2-4. Modified HSQC employed for obtaining ^{1}H-^{13}C couplings for side chain groups.

Proton-coupled ^{1}H-^{13}C HSQC spectra on resonance of aromatic rings were recorded on natural abundance iA$\beta5^{inv}$ at carry ^{13}C frequency of 24611 Hz with the decoupler turned off during acquisition, and the data matrix size was 256 × 4096 complex points, resulting in acquisition times of 85 ms and 248 ms in F1 and F2, respectively. 160 transients per FID

were acquired, and quadrature in the F1 dimension was achieved in the Echo-antiecho manner. Data matrices were zero-filled to 16384 × 32768 points.

Diffusion Ordered Spectroscopy (DOSY)

Pulsed-field gradient (PFG) experiments with water-suppressed longitudinal encoding decoding (water-sLED) pulse (*8*) was performed to determine the molecular size of peptide inhibitors without Aβ fibrils using internal standard methods (*9*). In the experiment, the duration of the gradients was set to 2.0 ms; 30.0 ms was used as delay to allow for diffusion between the dephasing and rephasing gradient, and 32 points have been recorded in the indirect dimension. Sine shaped gradients and a gradient ramp with a maximum gradient strength of 35 G/cm have been used. Gradient strengths are always given in $\%^2$ with respect to maximum gradient strength (100% = 35 G/cm). Internal standard method has been used in order to compensate for the viscosity effects. Tetramethylsilane (M_r = 83 Da) was used as an internal reference to calculate the molecular mass of the possible oligomers.

2.9 Solid-state NMR

1D MAS ^{13}C NMR spectra were obtained with a Bruker AVANCE 400/500 (DRX) spectrometer. A 4-mm HR-MAS probe was used together with a rotor containing an inner spacer in order to improve B_0 homogeneity and spinning stability as well as to improve the suppression of solvent signals. 1D ^{13}C spectra were acquired at a carbon NMR frequency of 100 MHz and magic-angle spinning (MAS) frequencies of 9 kHz using a frequency selective ^{1}H-^{13}C cross-polarization technique with mixing periods of 1 ms. All measurements were performed at 7°C.

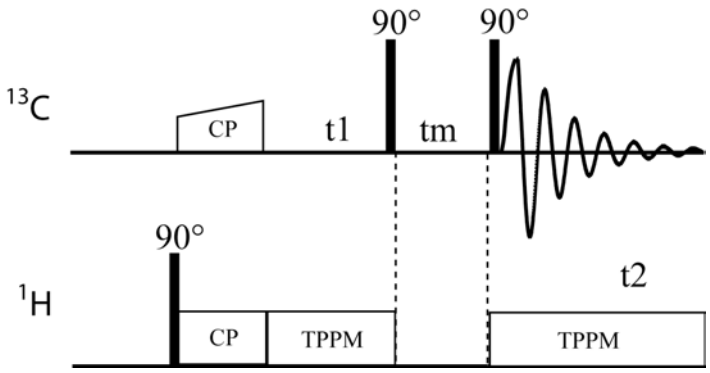

Fig. 2-5. Pulse program of a standard 2D homonuclear PDSD dipolar correlation experiment, applicable in the case of ^{13}C-^{13}C correlation spectra. Following 1H excitation, a ramped cross-polarization between ^{1}H and ^{13}C creates the initial ^{13}C magnetization. During the following evolution period, proton decoupling is applied, using the two-pulse phase modulation technique (TPPM). Following the carbon evolution, a 90º pulse on the low-γ nucleus brings back the magnetization along the z-axis. During the mixing time t_{mix}, proton decoupling is switched off and the polarization transfer between 13C spins occur in the presence of ^{1}H-^{1}H and ^{1}H-^{13}C dipolar couplings. In the following detection period, magnetization of ^{13}C is detected while proton decoupling is applied using TPPM.

2D MAS ^{13}C-^{13}C NMR spectra were recorded on a Bruker 600 MHz spectrometer. A triple resonance probe was equipped with a 4-mm-diameter rotor. MAS frequency was set to 11 kHz and TPPM of 90 kHz was used for heteronuclear decoupling in both dimensions. Acquisition time t_1^{max} = 10 ms and t_2^{max} = 30 ms were used with TPPI for phase sensitive detection. About 10 mg peptides (*de novo* peptides) were used for each experiment. Total experimental time was 12 hours. All measurements were performed at ~0°C.

1D ^{19}F MAS NMR spectrum was recorded on a Bruker 400 MHz spectrometer. 2D ^{19}F, ^{19}F-C7 experiments were carried out on a Bruker 600 MHz spectrometer in Karlsruhe, Germany.

2.10 Structure calculation

Structure calculation are on the basis of simulated annealing protocols implemented with a program CNSsolve. Transferred-NOESY data (750 MHz) were used for the extraction of distance restraints for use in quantitative structure calculations. Each resolved cross peaks were integrated using XWINNMR. The cross peak intensities were calibrated against the

cross peak intensity of phenyl-ring protons, because the distance (2.56 Å) is fixed and well known. Distances were derived from the intensities after calibration according to

$$r_{ij} = r_{ref}\left(\frac{V_{ref}}{V_{ij}}\right)^{\frac{1}{6}}$$

Where, V is the intensity of cross peak, and r is the internuclear distance. NOE-derived distance restraints were used as upper bounds. The resulting distance restraints are listed in Appendix 5.2.5-5.2.7.

All structure calculations, minimizations and simulated annealing procedures were carried out using CNSsolve version 1.0 (*10*). Molecular structures were visualized and manipulated using Sybyl (version 6.9.2; Tripos Inc., St. Louis, MO) or MOLMOL (*11*). Initial embedded structures were generated from sequence structures using the sequence annealing protocol. Default values were used for all force constants and molecular parameters that were involved. High-temperature Cartesian molecular dynamics of with a 0.015 ps time step at 50000 K (1000 steps) were conducted. Cooling was then achieved by 1000 steps with a 0.015 ps time step. The 200 generated structures were then minimized with 1000 steps of **van der Waals** energy minimization. A final minimization of 10 cycles of 200 steps with an NOE scale factor of 75 kcal·mol^{-1} and a dihedral scale factor of 400 kcal·mol^{-1} was run.

2.11 Determination of peptide alignment tensor

Dipolar couplings were calculated as the difference between the oriented coupling ($^1J_{CH}$ + $^1D_{CH}$ or $^1J_{NH}$ + $^1D_{NH}$) and the isotropic couplings ($^1J_{CH}$ or $^1J_{NH}$). In each case, 2D HSQC spectra was transformed and phased with the same parameters. Single FID slices across the resonance under investigation were analyzed independently. Order tensors were determined using the calculated bound-state dipolar couplings and associated NOE-derived structures by inputting into a singular value decomposition program for determination of order tensor elements implemented in PALES (*12*). For the order tensor determination of iAβ5^{inv} bound

to $A\beta^{14-23}$, a total of 8 RDC values were used; for that of $iA\beta5^{inv}$ bound to $A\beta^{1-40}$, a total of 10 RDCs were used. These values correspond to residues for which assignments are available and there was no significant overlap of resonances or change in chemical shift positions between the free and bound state. Errors in dipolar couplings were set to estimated experimental precision.

2.12 Molecular Modeling

For selection of suitable structural templates for the oligomerized amyloid peptides, we adopted the structural model of the anti parallel β-strand orientation for $A\beta^{14-23}$ peptide provided by Callaway (*13*) and the suggested structural model of the parallel β-strand orientation for the $A\beta^{1-40}$ peptide based on solid-state NMR data (*14*).

The amyloid bound NMR-structures of the peptide inhibitors (iAβ5 and $iA\beta5^{inv}$) were docked to the structural model of $A\beta^{14-23}$ and $A\beta^{1-40}$ by three approaches. For automatic docking, the docking module FlexX of the Sybyl 6.91 program package from *Tripos Inc.* was used. For manual docking and docking by constrained molecular dynamic simulations, functional data, complementary side chain properties and the RDC data (for $iA\beta5^{inv}$) constraining the relative orientation of ligand with respect to amyloid fibrils were considered as additional constrains. In details, the Cartesian coordinates of the $iA\beta5^{inv}$ NMR-structure bound to $A\beta^{1-40}$ were calibrated along the z-axis, based on RDC data (program PALES (*12*)). According the detected parallel orientation of the fibril axis along the magnetic field, the N-H bonds (Cartesian coordinates) of β-sheet of the $A\beta^{1-40}$ were also calibrated along the z-axis using the program VMD (from University of Illinois). For the ligand only translations along x- and y- and rotations around the z-axis were allowed for docking at the amyloid model. All assembling procedures were performed in vacuum.

The three assembled complex models of the peptide inhibitors and the corresponding amyloid peptide oligomers were soaked with water in a periodic boundary box. Initially the

atoms were kept fixed to relax the water during minimization. Later on, the entire system was considered. The resulting models were minimized with an AMBER 7.0 force field and simulated with a 0.5 ns molecular dynamics run at 300 K. The geometric accuracy was analysed by using the PROCHECK programme (*15*).

References

1. Fraser, P., Nguyen, J., Surewicz, W., and Kirschner, D. (1991) *Biophys. J. 60*, 1190-1201.
2. Zagorski, M. G., Yang, J., Shao, H., Ma, K., Zeng, H., and Hong, A. (1999) *Methods Enzymol. 309*, 189-204.
3. Paz, M. L. p. d. l., Goldie, K., Zurdo, J., Lacroix, E., Dobson, C. M., Hoenger, A., and Serrano, L. (2002) *Proc. Natl. Acad. Sci. 99*, 16052–16057.
4. Piotto, M., Saudek, V., and Sklenar, V. (1992) *J.Biomol. NMR 2*, 661–665.
5. Shaka, A. J., Lee, C. J., and Pines, A. (1988) *J. Magn. Reson. 77*, 274-293.
6. Marion, D., Ikura, M., Tschudin, R., and Bax, A. (1989) *J. Magn. Reson. 85*, 393–399.
7. Bodenhausen, G., and Ruben, D. J. (1980) *Chem. Phys. Lett. 69*, 185-189.
8. Gibbs, S. J., and Johnson, C. S. J. (1991) *J. Magn. Reson. 93*, 395-402.
9. Jones, J. A., Wilkins, D. K., Smith, L. J., and Dobson, C. M. (1997) *J. Biomol. NMR 10*, 199-203.
10. Brunger, A. T., Adams, P. D., Clore, G. M., DeLano, W. L., Gros, P., Grosse-Kunstleve, R. W., Jiang, J.-S., Kuszewski, J., Nilges, N., Pannu, N. S., Read, R. J., Rice, L. M., Simonson, T., and Warren, G. L. (1998) *Acta. Cryst. D54*, 905-921.
11. Koradi, R., Billeter, M., and Wuthrich, K. (1996) *J. Mol. Graph. 14*, 51–55.
12. Zweckstetter, M., and Bax, A. (2000) *J. Am. Chem. Soc. 122*, 3791-3792.
13. Tjernberg, L. O., Callaway, D. J. E., Tjernberg, A., Hahne, S., Lilliehöök, C., Terenius, L., Thyberg, J., and Nordstedt, C. (1999) *J. Biol. Chem. 274*, 12619–12625.
14. Petkova, A. T., Ishii, Y., Balbach, J. J., Antzutkin, O. N., Leapman, R. D., Delaglio, F., and Tycko, R. (2002) *Proc. Natl. Acad. Sci. 99*, 16742–16747.
15. Laskowski, R., MacArthur, M., Moss, D., and Thornton, J. (1993) *J. Appl. Cryst. 26*, 283-291.

3 Results and Discussion

3.1 Peptide synthesis and purification

$A\beta^{14-23}$ and its peptide inhibitors iAβ5 (LPFFD) and $iA\beta5^{inv}$ (DPFFL) were prepared manually by solid-phase peptide synthesis using a TCP-resin and Fmoc-chemistry protocols (*1*). The determination of protein structure and dynamics by high resolution NMR requires the incorporation of isotopic labels. $A\beta^{14-23}$ with a ^{19}F label in the para-position of the aromatic ring of Phe19 was successfully synthesized as described in Methods. iAβ5 was synthesized with a ^{19}F label in the para-position of the aromatic ring of Phe3 and uniformly ^{13}C- and ^{15}N-labelled, respectively. Crude peptides were purified by preparatory reverse phase HPLC performed on a C-18 column (YMC-Pack ODS/A) with water and ACN with 0.1 % TFA as eluents. The purity and identity of the peptides were assessed by ESI-MS and RP-HPLC-ESI-MS analyses performed on a Finnigan LCQ-ESI Spectrometer coupled to a Hewlett Packard HP1100 HPLC-System.

It should be noted that the coupling of Phe19 can be a little problematic due to the hydrophobic sequence. Therefore, a longer coupling time or double coupling of this residue are necessary. Purification of these peptides via RP-HPLC was very time-consuming. Only a low concentration of $A\beta^{14-23}$ in the injection solution could be used. A concentration of the injection solute higher than 5 mg/ml peptide in 0.1% TFA/acetronitril solvent caused aggregation of $A\beta^{14-23}$ in the column.

3.2 $A\beta^{14-23}$ forms similar fibrils as $A\beta^{1-40}$ as observed by Electron Microscopy.

Fig. 3-1 shows Electron Microscopy (EM) images of negatively stained $A\beta^{14-23}$ and $A\beta^{1-40}$ samples after incubation at pH 4 at concentration of 0.5 mM and 0.1 mM, respectively. The pH of the buffer has been adjusted to 4.0, 10 mM PO_4^{3-}, in order to allow for optimal formation of fibrils (*2*). At this pH value $A\beta^{14-23}$ formed β-sheet structure immediately after dissolving in buffer as observed by Circular Dichroism spectroscopy (data shown below, Fig. 3-5), which is believed to be related to fibril formation (*3*). Both $A\beta^{14-23}$ and $A\beta^{1-40}$ fibrils display straight, unbranched, ribbon-like morphologies which are 10- to 25-nm in diameter and several micrometers in length. These fibrils appear as twisted pairs of single filaments

with a varying periodicity from 100 nm to 600 nm, as commonly observed for amyloid fibrils (*4*). This is consistent with previous evidences that $A\beta^{14-23}$ forms mature fibrils morphologically identical to $A\beta^{1-40}$ fibrils (*5*). As suggested by Marsh *et al*. (*6*), the length of a β-strand can be calculated as 0.695 nm ×n/2, where n is the number of residues involved in the β-strand. Assuming $A\beta^{14-23}$ forms fibrils with a fully extended β-strand conformation (n = 10), fibrils would be expected to be approximately 3.5 nm in width, which is smaller than the 5-15 nm measured in our EM data as the fibrils' diameter. This discrepancy suggests that fibrils are composed of more than one protofilament. This is in agreement with the previously experimental data for Aβ fibrils observed by EM (*2, 7, 8*) and X-ray diffraction (*9*). For $A\beta^{1-40}$, the width of the fibrils would be expected to be 14 nm (n = 40), provided the molecules were in the extended β conformation. However, the observed maximum widths are only 12.5 nm. This suggests that each $A\beta^{1-40}$ molecule must adopt a hairpin structure or that some regions of the peptide are not involved in the core structure of the fibre. Tycko and co-workers have experimentally shown that $A\beta^{1-40}$ folds into a hairpin structure in the fibrillar state (*10*). Based on EM and solid-state NMR data, they concluded that the first 10 residues of $A\beta^{1-40}$ are structurally disordered in the fibril. Only residues 12-24 and 30-40 adopt β-strand conformations and form in-register parallel β-sheets through intermolecular hydrogen bonds. Residues 25-29 contain a bend of the peptide backbone that brings the two β-sheets in contact through side chain and side chain interactions. Therefore the expected width based on this model would be 4.5 nm (n =13), which is smaller than the 6.5-12.5 nm observed as the $A\beta^{1-40}$ fibrils' diameter. This again suggests that $A\beta^{1-40}$ fibrils consist of several protofibrils.

At pH 4, Aβ forms fibrils with the same morphology, as Aβ peptides in solutions at different pH values (*4*). This finding is not consistent with the previous results obtained by Wood *et al.* (*11*). In their study, the aggregates of $A\beta^{1-40}$ formed at pH 5.8 differed from classical amyloid fibrils. The fibrils appeared in electron micrographs as a mixture of larger particles of different morphologies.

Study of mature amyloid fibrils by EM shows that $A\beta^{14-23}$ forms ordered amyloid fibrils, exhibiting similar morphology to those of full-length Aβ. We have chosen to work with the fibril model $A\beta^{14-23}$ first, rather than the full-length $A\beta^{1-40}$, since this peptide seemed to be - due to its length-an easier model to study ligand-fibril interactions. In addition, this peptide sequence is located in the central region of the full-length Aβ, which is found to be important

for fibril formation (*5*) and may represent the core structure of amyloid fibrils. Also, $A\beta^{14-23}$ was characterized to fold into an anti-parallel β-sheet structure, from which a model (*5*) was available at the time when this project was started. Thus $A\beta^{14-23}$ can serve as a model system for fibril inhibition studies under our working conditions. Furthermore, we extend the same study to full-length Aβ. In addition, comparing the structure of the ligand bound to $A\beta^{14-23}$ and $A\beta^{1-40}$ allows to draw conclusions about possibly different fibril structures.

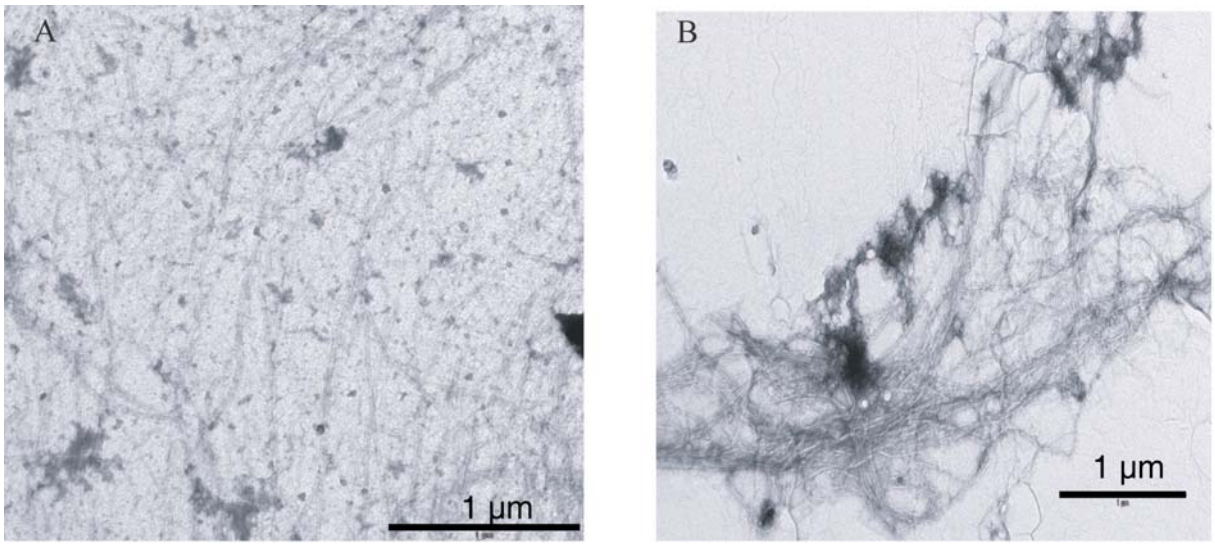

Fig. 3-1. $A\beta^{14-23}$ forms fibrils similar to those formed from full-length Aβ. Aβ peptides were incubated at 0.5mM in buffer at pH 4 as described under "Materials and Methods". After 7 days of incubation, a 5 µl sample was placed on a EM grid and negatively stained with 3% uranyl acetate. A, 0.5 mM $A\beta^{14-23}$; B, 0.1 mM $A\beta^{1-40}$. Scale bars in the EM images are 1 µm.

3.3 Effect of peptide inhibitor iAβ5 and $iA\beta5^{inv}$ on Aβ fibril formation as observed by EM.

The effect of the identified peptide inhibitors on the assembly process of Aβ was investigated by negative staining electron microscopy. iAβ5 was found to be able to inhibit $A\beta^{1-42}$ fibrillogenesis and disassemble preformed fibrils *in vitro* (*12*). Here, we confirm this inhibitory effect of iAβ5 on fibrils formed from synthetic $A\beta^{1-40}$ under our experimental conditions. Fig. 3-2A shows a control sample, in which $A\beta^{1-40}$ was incubated alone in buffer at pH 4, 10 mM PO_4^{3-}. Only mature fibrils are observed. In contrast, a higher percentage of $A\beta^{1-40}$ intermediates, nonfibrillar and polymeric sheet assemblies with only a few detectable mature fibrils are detectable over prolonged incubation of pre-fibrillized $A\beta^{1-40}$ (7 days) with a 100-fold excess of iAβ5 (Fig. 3-2B). The EM experiment was performed 7 days after addition of iAβ5 to the Aβ solution. Generally, while mature fibril formation is decreased, the

occurrence of structural intermediates is increased in the presence of peptide inhibitors. Moreover, we show that this inhibitory effect of iAβ5 is not restricted to $A\beta^{1-40}$, but is also observable for synthetic $A\beta^{14-23}$. Mature fibrils are the predominant structure in the control sample of $A\beta^{14-23}$ (Fig. 3-2D). Under similar incubation conditions, addition of a 10-fold excess of iAβ5 to the 7-day-preformed $A\beta^{14-23}$ fibril solution dramatically changes the morphology of the aggregates as detected 7 days later by EM (Fig. 3-2E). We observed a reduced amount of polymers and mostly short polymeric sheet assemblies that have a length of around 500 nm, instead of elongated fibrils, indicating that fibrils are disassembled into smaller units.

A similar inhibitory effect on Aβ fibrils was observed for another peptide, DPFFL (referred to as $iA\beta5^{inv}$), as shown in Fig. 3-2C and Fig. 3-2F. For $iA\beta5^{inv}$ the inverse hydrophobic and hydrophilic amino acids at the N-terminus and at the C-terminus are exchanged. In Fig. 3-2C, the sample was prepared by addition of a 100-fold excess of $iA\beta5^{inv}$ to a 7-day incubated $A\beta^{1-40}$ solution, and detected 7 days later by EM. Only short fibrils and pseudospherical structures (*13*) are visible. Similarly, $iA\beta5^{inv}$ suppresses the assembly of $A\beta^{14–23}$ peptides into mature fibrils at a molar ratio of 10:1 (Fig. 3-2F). The absence of visible elongated amyloid fibrils is a direct evidence for the fact that the peptide inhibitors iAβ5 and $iA\beta5^{inv}$ can dissolve Aβ peptide aggregates. The inhibitory effect of β-sheet breaker peptides are extensively studied by Soto and co-workers (*12, 14-18*). We wanted to reproduce these findings in order to compare the EM results with our NMR data.

In this study, we present EM data demonstrating that both iAβ5 and $iA\beta5^{inv}$ do interact with $A\beta^{1-40}$ and $A\beta^{14-23}$, which suggests that there is one common binding site for iAβ5 and $iA\beta5^{inv}$ interacting with $A\beta^{1-40}$ or $A\beta^{14-23}$. $A\beta^{14-23}$ has the same hydrophobic core as $A\beta^{1–40}$ (LVFF). Since iAβ5 was designed to recognize this core structure, one could expect that iAβ5 could easily bind to the same core due to its similar hydrophobic pattern. For $iA\beta5^{inv}$, the reversed terminal amino acids do not affect the inhibitory effect of this peptide towards Aβ fibril formation, which shows that the affinity may possibly be driven by the hydrophobic interactions between the two Phe residues on each peptide. However, the neurotoxicity of $A\beta^{14-23}$ in the presence of these two peptide inhibitors remains to be investigated. Also, despite the different sizes Aβ fibrils appear as very similar structures under the conditions examined in this work, with diameters of 5-12 nm and indefinite length in EM images. However, after addition of either of the peptide inhibitors, fibrils are shortened into small

fragments, with a size range of 50 to 80 nm, while the diameter of these short fragments remain at the same scale. Thus, the observed fibril length differences suggest the inhibitory effect of iAβ5 or iAβ5^{inv} to fibrils is taking place along the fibril's axis, not between protofilaments. Very likely, the inhibitors occupy the critical sites which are required for assembly of successive β-sheets, thus disrupting the assembly of Aβ peptides along the fibril axis within one protofilament. In order to answer this question, a structural model for the interaction of inhibitors with Aβ fibrils is required.

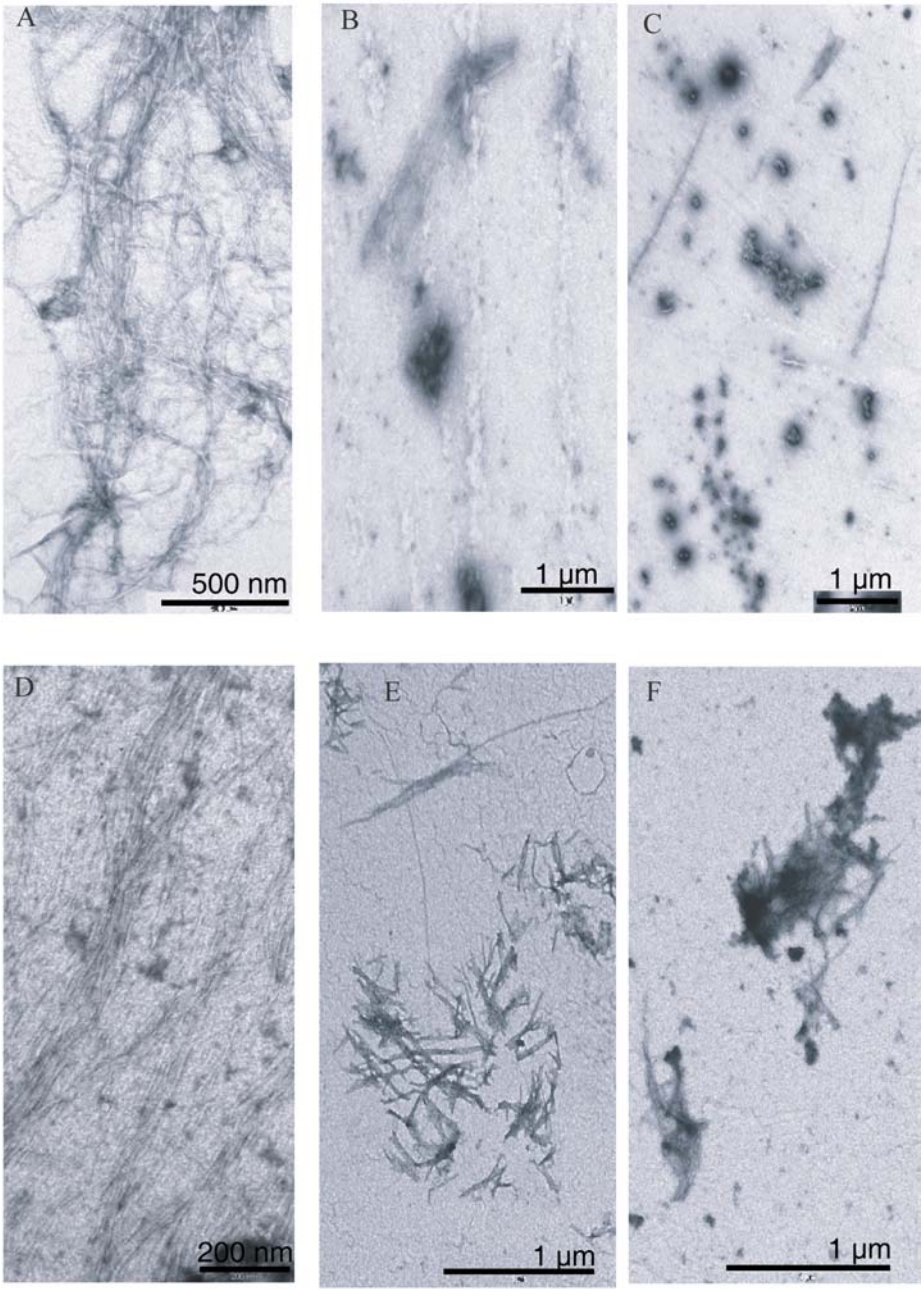

Fig. 3-2. The influence of peptide inhibitors on fibril morphology of Aβ studied by EM. Aβ alone or with peptide inhibitor iAβ5 or iAβ5^{inv} were incubated in buffer at pH 4 as described under "*Materials and Methods*". Measurements were done after 7 days of incubation. A, 0.1 mM Aβ$^{1-40}$ alone; B, 0.1 mM Aβ$^{1-40}$ with 5 mM iAβ5; C, 0.1 mM Aβ$^{1-40}$ with 5 mM iAβ5^{inv}; D, 0.5 mM Aβ$^{14-23}$ alone; E, 0.5 mM Aβ$^{14-23}$ with 5 mM iAβ5; F, 0.5 mM Aβ$^{14-23}$ with 5 mM iAβ5^{inv}.

3.4 Aβ secondary structure studies by CD spectroscopy.

The secondary structure for Aβ in the absence and presence of peptide inhibitors as a function of concentration and pH value was followed by CD, respectively. The CD spectra for $A\beta^{14-23}$ were recorded using five different peptide concentrations, measured at various time intervals up to 72 hours. Fig. 3-3 shows the concentration dependence of the secondary structure of $A\beta^{14-23}$ at pH 4. CD spectra of lower concentration samples (like 50 µM, 100 µM, 200 µM) show a minimum at 195 nm, which is typical of random coil secondary structure in the solution. CD spectra of samples at concentration higher than 300 µM show that there is one minimum at 218 nm, which is a clear indication of a β-sheet structure in solution. Fig. 3-4 shows the time dependence of secondary structures for Aβ. With longer incubation times, the minimum at 218 nm decreases, which indicates that the β-sheet structure in solution is decreasing and more $A\beta^{14-23}$ form fibrils which can not be detected any more. However the indicated β-sheet structure is stable for at least 4 hours in solution as indicated in Fig. 3-4.

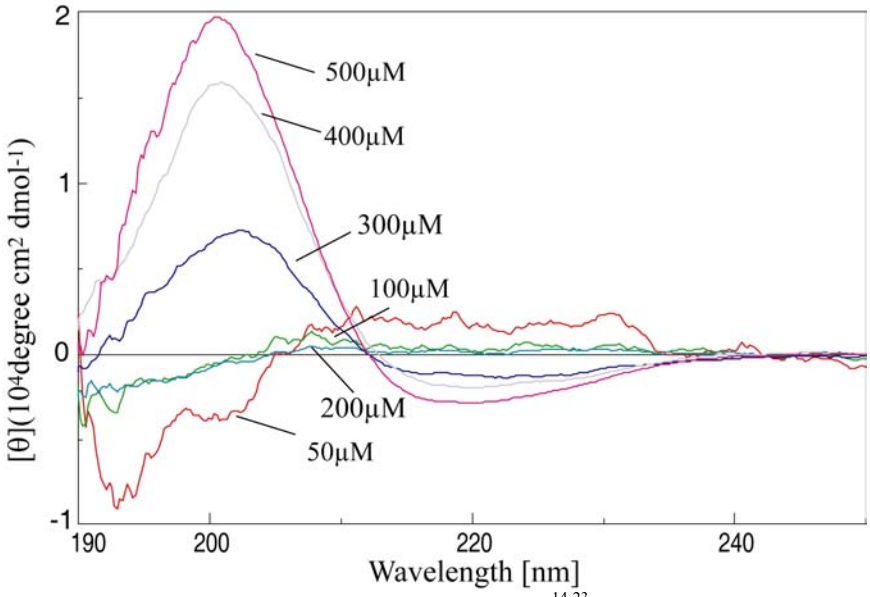

Fig. 3-3. Concentration-dependent secondary structural changes for $A\beta^{14-23}$ analyzed by circular dichroism. Circular dichroism spectra of 100 µM, 200 µM, 300 µM, 400 µM and 500 mM $A\beta^{14-23}$ were recorded in 10 mM phosphate buffer at pH 4, 30°C.

The pH dependence of secondary structure of $A\beta^{14-23}$ at concentration of 300 µM is shown in Fig. 3-5. At higher pH value, like pH 10, or 8, only a random structure is present in the solution. Once the pH value is decreased to pH 5, a spectrum typical of β-sheets with a minimum at 217 nm dominates.

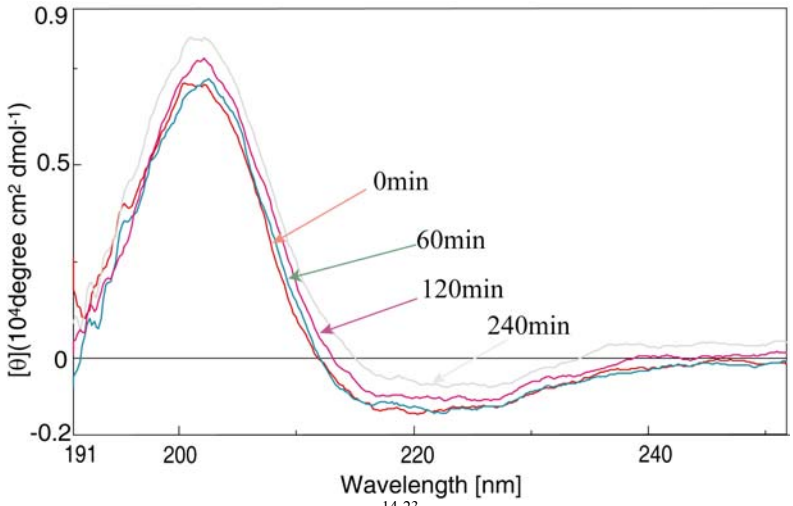

Fig. 3-4. Time-dependent secondary structural changes for $A\beta^{14-23}$ analyzed using circular dichroism. Circular dichroism spectra of 300 µM were recorded in 10 mM phosphate buffer at pH 4 at time zero up to 240 minutes as indicated, 30°C.

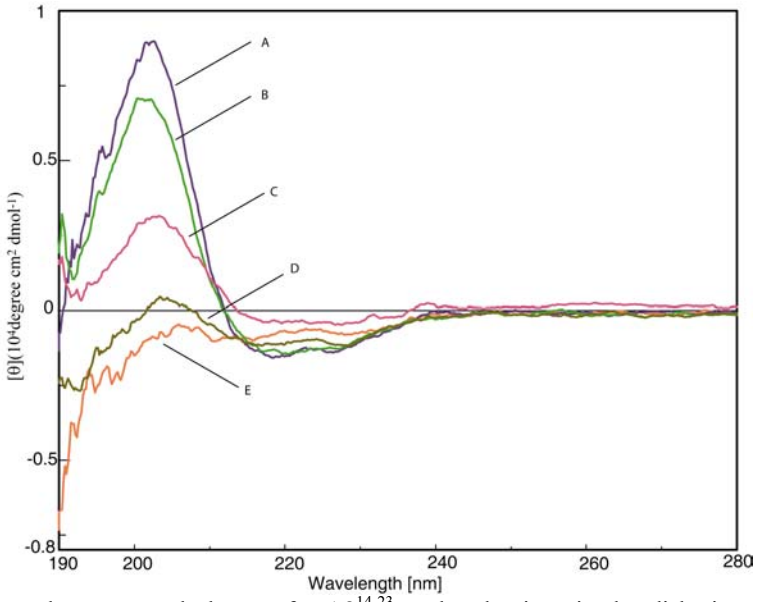

Fig. 3-5. pH-dependent secondary structural changes for $A\beta^{14-23}$ analyzed using circular dichroism. Circular dichroism spectra of pH 3.5 (A), pH 4 (B), pH 7 (C), pH 8 (D) and pH 10 (E) $A\beta^{14-23}$ were recorded in 10 mM phosphate buffer at 300 µM at 30°.

The influence of iAβ5 on the secondary structure of $A\beta^{14-23}$ was also investigated by CD studies (Fig. 3-6). The CD spectra for $A\beta^{14-23}$ in the presence or absence of iAβ5 (Fig. 3-6A) were measured 10 min after dissolution. When 0.5 mM $A\beta^{14-23}$ was incubated alone, the shape of the CD spectrum indicates almost complete β-sheet structures. The CD spectrum of 0.5 mM iAβ5 shows a minimum at 195 nm, typical for random coil secondary structure. If a certain amount of iAβ5 stock solution is added to the Aβ solution to reach a concentration of 0.5 mM for both, the CD spectrum shows a decreased intensity at ~208 nm, but a similar intensity at 218 nm. iAβ5 does not alter CD spectrum of $A\beta^{14-23}$, indicating no disturbance of the secondary structure of $A\beta^{14-23}$ by iAβ5. Studies of $A\beta^{14-23}$ with excess amount of iAβ5 by CD spectroscopy were carried out for 0.1 mM $A\beta^{1-40}$ with 1 mM iAβ5 at pH 4. In Fig. 3-6B,

the CD spectrum of $A\beta^{1-40}$ shows a typical curve of β-sheet structure under the experiment conditions. Addition of 10 fold excess of iAβ5 changed the CD spectrum which is a type of α-helix structure.

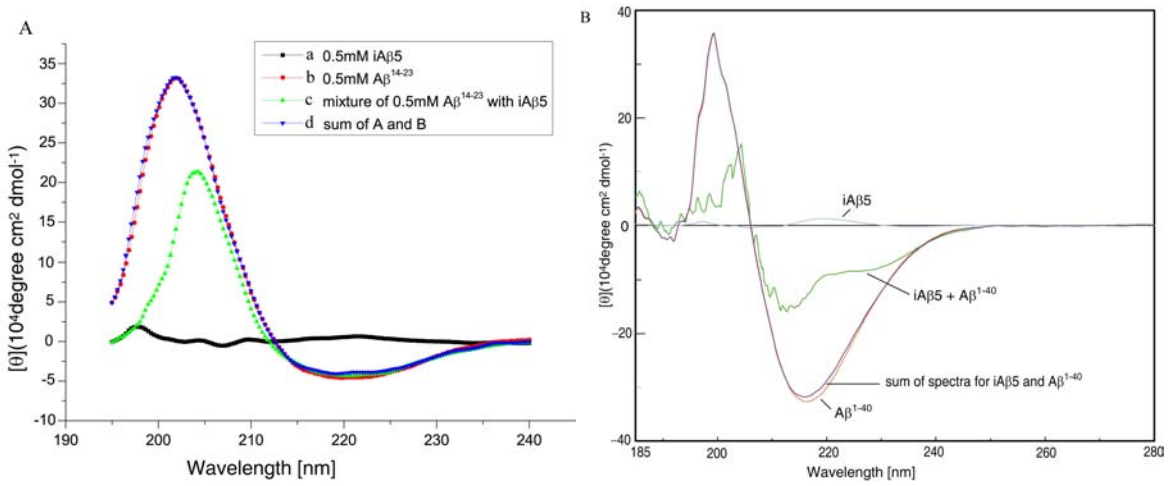

Fig. 3-6. The influence of iAβ5 on the secondary structure transitions in Aβ studied by CD. Figure A: a, 500 μM iAβ5 was also incubated alone and its CD spectrum is included in the figure to illustrate its contribution to the spectrum when mixed with Aβ; b, $A\beta^{14-23}$ was incubated at 500 μM in 10 mM buffer at pH4; c, 500 μM $A\beta^{14-23}$ with 500 μM iAβ5; d, theoretical sum of spectrum A and B. Figure B: the CD spectra for 1 mM iAβ5, 0.1 mM $A\beta^{1-40}$, mixture of 0.1 mM $A\beta^{1-40}$ with 1 mM iAβ5 and theoretical sum of spectrum iAβ5 and $A\beta^{1-40}$.

Aβ aggregation is linked to the conversion of the peptide from a random coil to a β-sheet secondary structure (*19, 20*). Initially we considered the possibility that iAβ5 could prevent Aβ aggregation by binding to Aβ and changing the β-sheet structure of Aβ which is an initial step of fibrillization. Analysis of CD spectra demonstrates that iAβ5 does not change the β-sheet content of Aβ in solution in a ratio of 1:1 (Fig. 3-6A). This means that iAβ5 does not bind to monomeric Aβ. This is consist with the findings obtained by Murphy and co-workers (*21*). In their experiments, $A\beta^{10-35}$ was immobilized on a surface at a low density. iAβ5 and other compounds were used in their assay for determining the relative affinity for Aβ. Unlike the other peptides such as KLVFFKK, iAβ5 showed an insignificant response level in the assay. Murphy and co-workers considered that iAβ5 may only interact with higher-order assemblies of Aβ, which they had attempted to minimize in their experimental conditions. However, at an excess amount, iAβ5 could affect the secondary structure of Aβ peptide (Fig. 3-6B). At the same time, Aβ does not form mature fibrils in the presence of excess amount of inhibitors as detected by EM (Fig. 3-2B, E). These results demonstrate that the inhibition of Aβ fibril formation by iAβ5 is not due to iAβ5 associating with monomeric Aβ and thus changing the Aβ secondary structure, rather its action is more due to a later step in the

aggregation pathway. Moreover, this result demonstrates that the formation of amyloid is a non-necessary end point of β-sheet formation for Aβ.

3.5 The influence of iAβ5 on the ThT binding of $A\beta^{14-23}$.

Fig. 3-7 shows the effect of iAβ5 in preventing the formation of ordered fibrils as investigated by Thioflavine T fluorescence. Thioflavine T (ThT) was reported to associate rapidly with aggregated fibrils formed from native and synthetic Aβ peptides (*22*), which is going along with changes of the excitation (ex) (absorption) and emission (em) wavelength. This change is only related to the aggregated state of Aβ, as monomeric or dimeric peptides do not react with Thioflavine T. Thus, this fluorometric technique should be suitable for testing the effect of the selected peptide inhibitors on the assembly of Aβ peptides. Fluorescence spectra of ThT in the presence of aggregated $A\beta^{14-23}$ exhibits an excitation maximum at 480 nm and an emission at 518 nm. Incubation of $A\beta^{14-23}$ with iAβ5 shows a reduced fluorescence signal at both ex and em wavelengths. Assuming that iAβ5 has no effect on the ThT fluorescence, the decreasing fluorescence signal corresponds to less aggregated material in solution, which indicates that iAβ5 prevented formation of ordered fibril. This result confirms that the inhibitory effect of iAβ5 on the assembly of $A\beta^{14-23}$ resembles that of $A\beta^{1-40}$, as shown by Soto and co-workers (*12*).

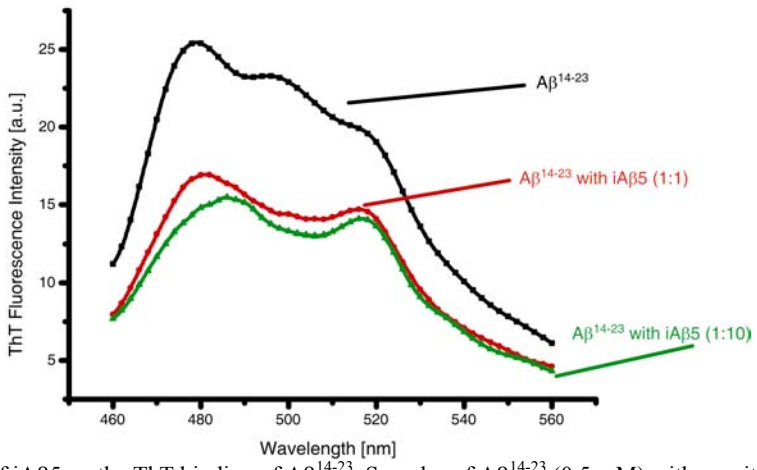

Fig. 3-7. The influence of iAβ5 on the ThT binding of $A\beta^{14-23}$. Samples of $A\beta^{14-23}$ (0.5 mM) with or without iAβ5 (0.5 mM, 5 mM) were incubated for 1 h, and measured by Fluorescence spectroscopy.

In Fig. 3-7, a tenfold excess of iAβ5 prevents the fibril formation only slightly more compared to the effect of an equal amount of iAβ5. Since these experiments were carried out after a short incubation time (1 h), the comparison might not show the inhibitory effects

quantitatively. Time dependent experiments of this effect would be required in order to quantitatively analyse the inhibitory effects for iAβ5 at various ratios with respect to Aβ.

3.6 The assignment of iAβ5 and iAβ5^{inv} in the NMR spectra.

The purity of the synthetic peptides was verified with electrospray mass spectrometery and analytic HPLC to be >98%. However, the proton 1D spectra of iAβ5 and iAβ5^{inv} show two sets of chemical shifts (Fig. 3-8). This is because of the presence of *cis* and *trans* conformers of proline as discussed later.

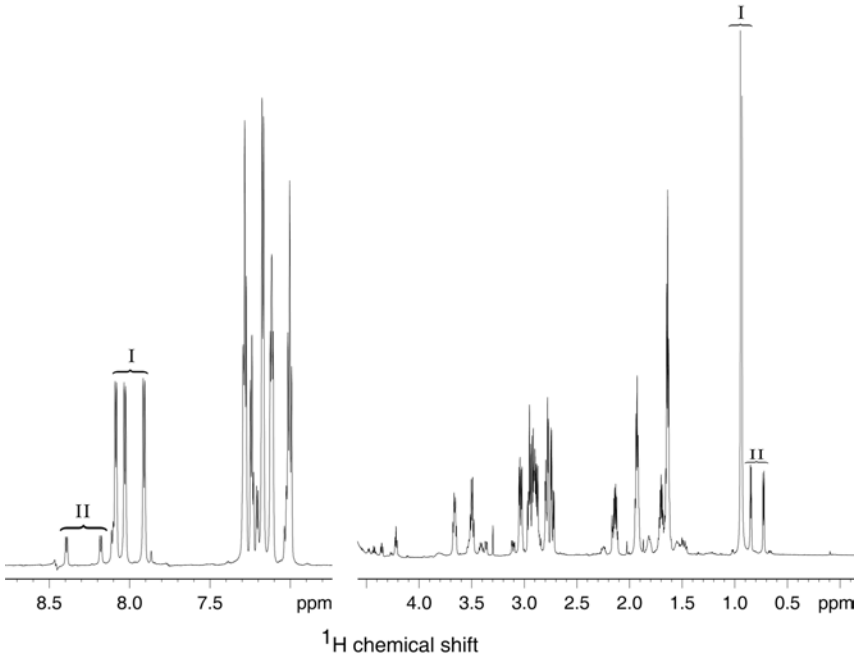

Fig. 3-8. 1D-^{1}H spectrum of iAβ5 at 5 mM in 10 mM PO_4^{3-} at pH 4, 30 °C.

^{1}H chemical shifts of iAβ5 and iAβ5^{inv} were assigned manually using regular TOCSY with a mixing time of 50 ms and NOESY spectra with varying mixing times from 10 ms up to 500 ms. Spectra were recorded on iAβ5 or iAβ5^{inv} with and without Aβ$^{14-23}$ fibrils at 30°C. The identification of most spin systems was achieved unambiguously from proton TOCSY connectivities. Fig. 3-9 shows the residue patterns assigned in the aliphatic region of the TOCSY spectrum. H^N resonances were assigned by connecting H^N with H^α and H^β resonances in a TOCSY spectrum as shown in Fig. 3-10 for ^{19}F-iAβ5. For ^{19}F-iAβ5, due to the overlap of H^N for Phe and Asp residues, the assignments of Phe3 and Phe4 were not available from the sequential H^α_i-H^N_{i+1} connectivities in a NOESY spectrum, but were accomplished by the combined analyses of the H-H connectivities in the aromatic regions of

the NOESY spectra and ascertained by the examination of the H^N-H^β connectivities, as shown in Fig. 3-11. This is done because H^η of Phe3 is substituted by ^{19}F so that the spin pattern of Phe3 in the aromatic region contains two peaks while that of Phe4 contains three. For iAβ5^{inv}, the assignments of Phe3 and Phe4 were easily done by the sequential H^α_i-H^N_{i+1} connectivities in the H^N-H^α region of the NOESY spectrum, as shown in Fig. 3-12. The β and γ protons of Leu and Pro residues were assigned on the basis of their ^{13}C chemical shifts from ^{13}C-HSQC spectra. The complete assignments for the ^1H resonances of all amino acid residues are listed in Table 3-1A. ^{13}C shifts were assigned by correlating them with the assigned proton chemical shifts (Fig. 3-13, Table 3-1B).

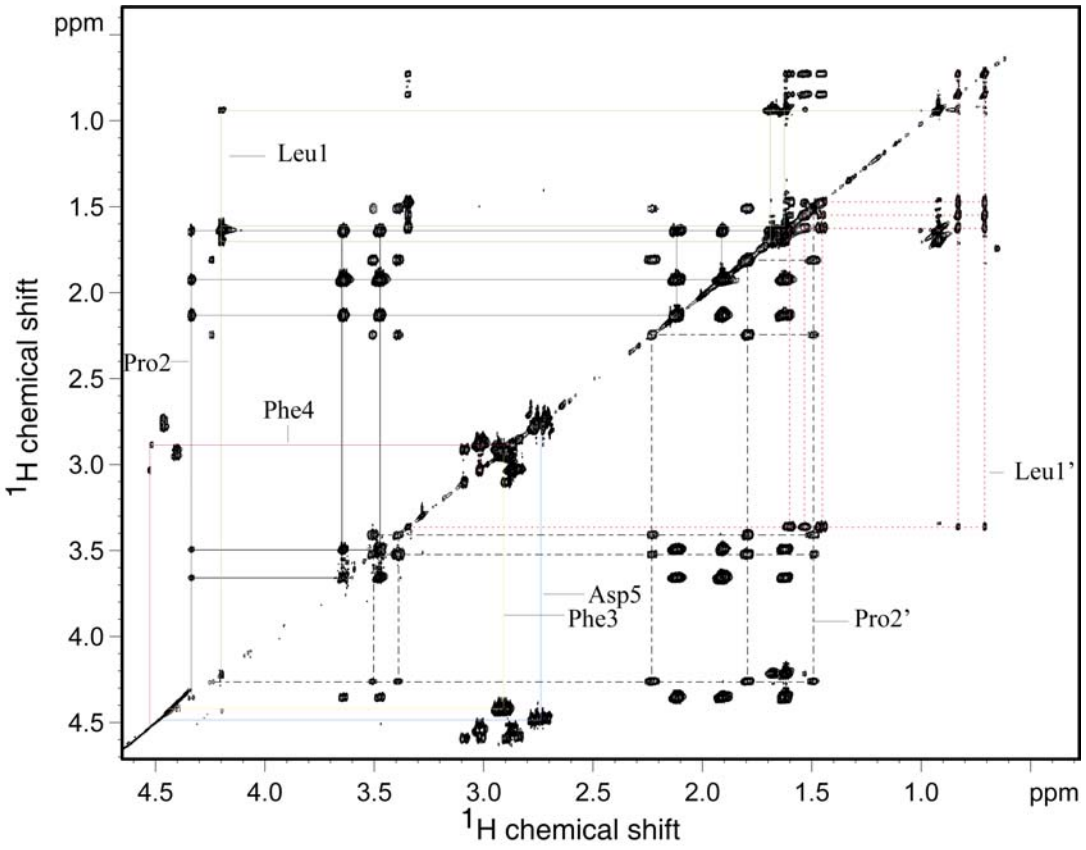

Fig. 3-9. Aliphatic region of a TOCSY spectrum of ^{19}F-iAβ5 (H2O/D2O 9:1, 30 °C, 600 MHz, mixing time 50 ms) with assignments of intraresidue connectivities. Leu1' and Pro2' are the minor conformations of iAβ5.

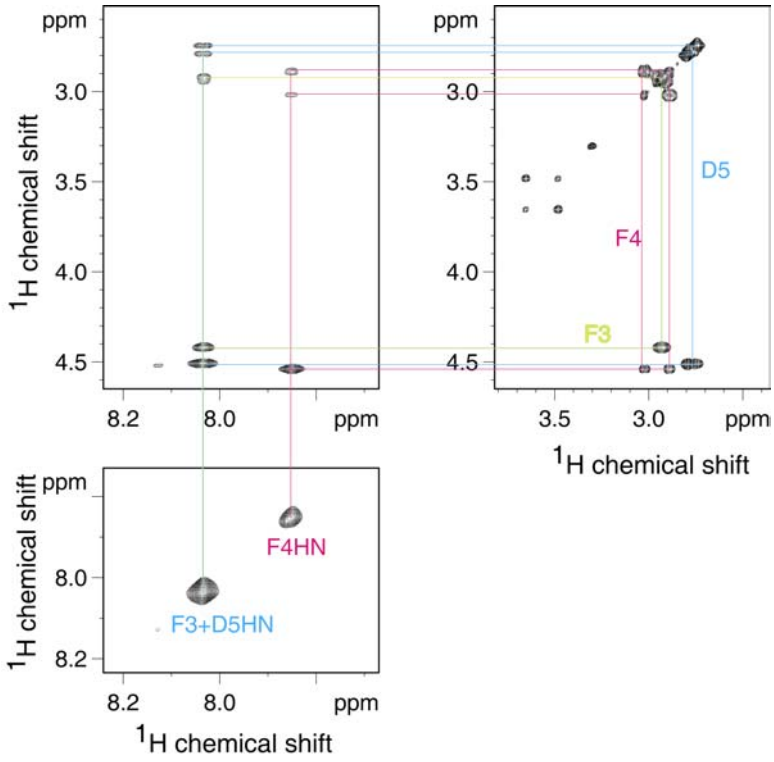

Fig. 3-10. H^N assignment of ^{19}F-iAβ5 in expanded regions of a TOCSY spectrum.

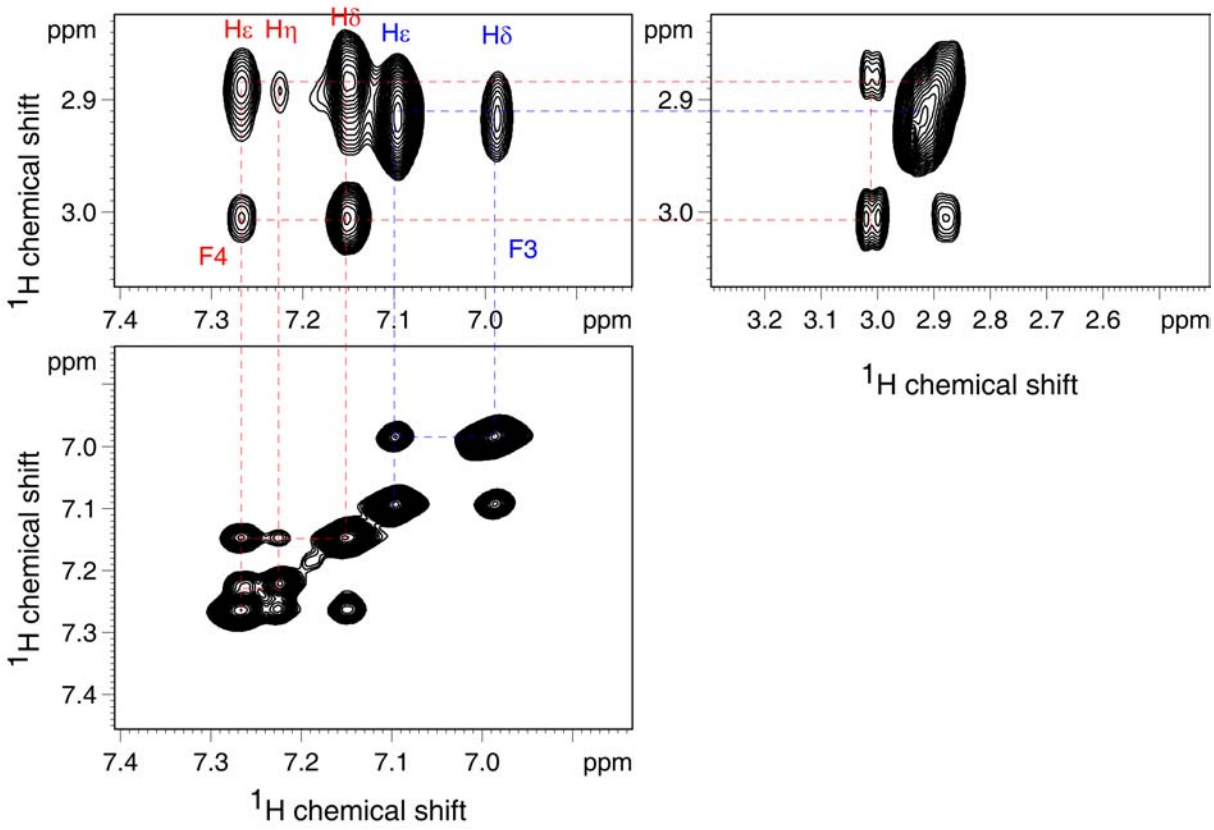

Fig. 3-11. Expanded regions of the NOESY spectrum for the Phe3 and Phe4 assignments of ^{19}F-iAβ5 in the presence of $Aβ^{14-23}$ at pH 4. The spectrum was recorded on a 750 MHz Bruker spectrometer, with a mixing time of 150 ms, at 30 °C.

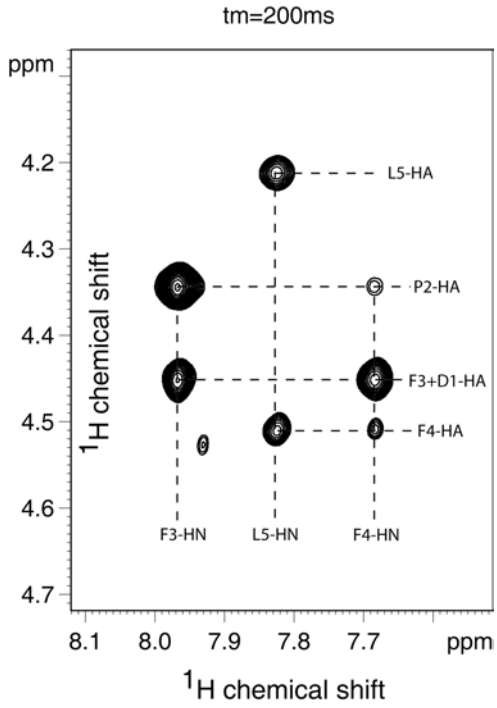

Fig. 3-12. Expanded region of a NOESY spectrum for the Phe3 and Phe4 assignment of iAβ5^{inv} in the presence of Aβ$^{14-23}$ at pH 4. The spectrum was recorded on a 750 MHz Bruker spectrometer, with a mixing time of 200 ms, at 30 °C.

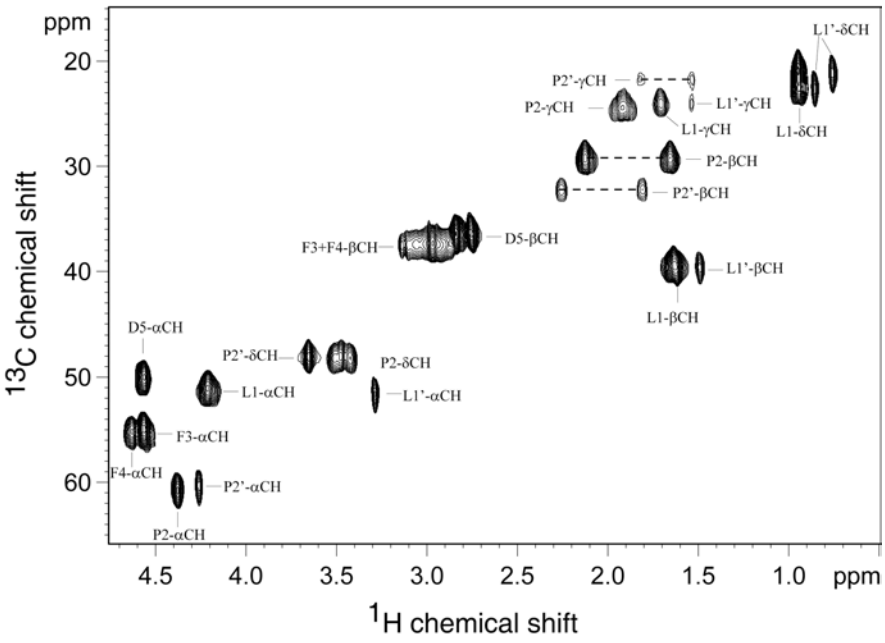

Fig. 3-13. Aliphatic region of the ^{13}C-HSQC spectrum for the ^{13}C assignment of u-^{13}C,^{15}N-iAβ5 at pH 4, 30 °C.

Table 3-1A. ^{1}H chemical shifts of ^{19}F-iAβ5 in the absence of fibrils at pH 4, 303 K.

	NH	αH	βH	γH	δH	εH
Leu1		4.22	1.70	1.64(*)	0.94	
Pro2		4.353	2.133, 1.64 (*)	1.926	3.658, 3.492	
Phe3	8.072	4.424	2.932	2,6H: 7.003	3,5H: 7.115	
Phe4	7.900	4.546	3.034, 2.885	2,6H: 7.170	3,5H: 7.282	4H: 7.239
Asp5	8.023	4.481	2.785, 2.732			

(* indicates the overlap resonances for the protons)

Table 3-1B. ^{13}C chemical shifts of u-^{13}C,^{15}N-iAβ5 in the absence of fibrils at pH 4, 303 K.

	Cα	Cβ	Cγ	Cδ	Cε	Cη
Leu1	51.10	39.52	24.00	20.73, 22.57		
Pro2	60.77	29.24	24.43	48.11		
Phe3	55.14	37.39		130.23	129.7	128.07
Phe4	55.14	37.39		130.23	129.7	128.07
Asp5	50.03	36.38				

(In this sample, Phe3 and Phe4 have the same ^{13}C chemical shifts for all the resonances.)

As can be seen from Fig. 3-9 and Fig. 3-13, two sets of ^{1}H and ^{13}C chemical shifts for Pro and Leu exist, which are due to the *trans* and *cis* conformers of Pro in the peptide. Schubert *et al.* demonstrated that the chemical shift difference of $^{13}C^{\gamma}$ and $^{13}C^{\beta}$ is a reference-independent indicator of the Pro peptide bond conformation (*23*). Thus the two conformations of Pro could be easily distinguished from the assigned $^{13}C^{\gamma}$ and $^{13}C^{\beta}$ chemical shifts using the POP program (Prediction Of Proline conformation) (*23*).

Table 3-2 shows the $^{13}C^{\gamma}$ and $^{13}C^{\beta}$ chemical shifts for two set of Pro residues as assigned in Fig. 3-13, together with the predicted probability of *cis* or *trans* Pro conformations by POP.

Table 3-2A. The probabilities for *cis* or *trans* conformations of Pro in iAβ5 in a 10 mM phosphate buffer at pH 4 derived from $^{13}C^{\gamma}$ and $^{13}C^{\beta}$ chemical shifts using the program POP.

	$^{13}C^{\beta}$ (ppm)	$^{13}C^{\gamma}$ (ppm)	Δ (ppm)	Normalized probability of Pro-*trans*	Normalized probability of Pro-*cis*
Pro2 (major)	29.243	24.432	4.811	99.91%	0.081%
Pro2' (minor)	32.231	21.686	10.545	0%	100%

Table 3-2B. The probabilities for *cis* or *trans* conformations of Pro in iAβ5 in the presence of $A\beta^{14-23}$ in the 10 mM phosphate buffer at pH 4 derived from $^{13}C^{\gamma}$ and $^{13}C^{\beta}$ chemical shifts using the program POP.

	$^{13}C^{\beta}$ (ppm)	$^{13}C^{\gamma}$ (ppm)	Δ (ppm)	Normalized probability of Pro-*trans*	Normalized probability of Pro-*cis*
Pro2 (major)	29.51	24.71	4.80	99.92%	0.076%
Pro2' (minor)	32.17	22.03	10.14	0%	100%

By comparing the intensities of the two sets of resonances in 1D ^{1}H spectra, we find that about 87% iAβ5 has the Pro of *trans* conformer, only 13% has Pro of *cis* conformer. And the population of isomers does not change in the presence of Aβ fibrils (Fig. 3-14). Taken together, the *trans* and *cis* conformers keep the same equilibrium in the absence and presence of Aβ fibrils. Therefore, the inhibitory effect of iAβ5 or $iA\beta5^{inv}$ is not due to the dynamics of *trans* and *cis* conformer of Proline.

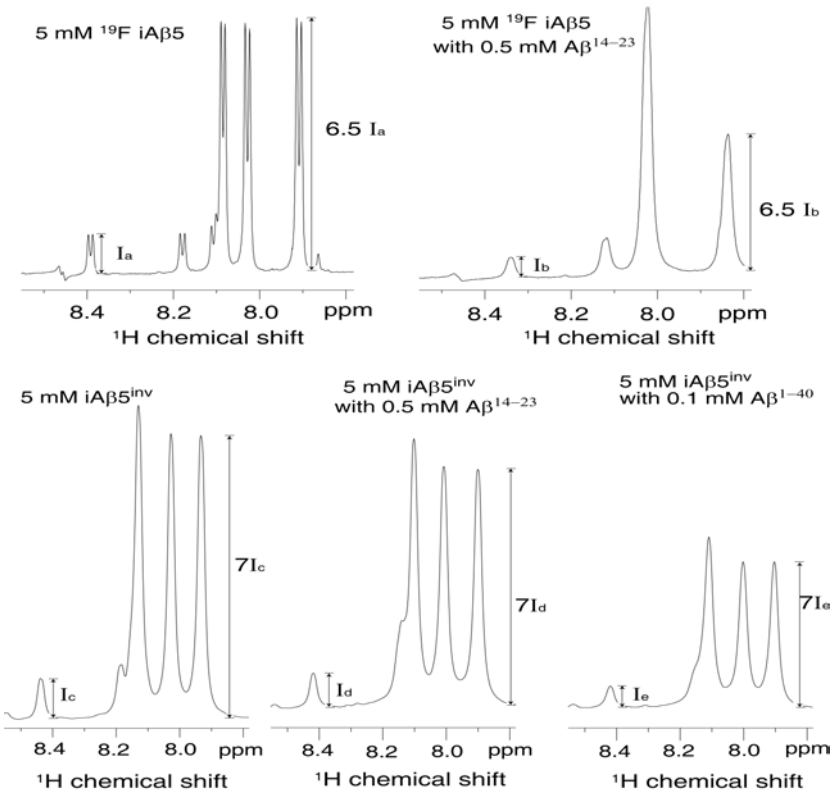

Fig. 3-14. The population of *trans* and *cis* conformer of peptide inhibitors in the absence and presence of Aβ fibrils.

The proton chemical shifts of iAβ5 or iAβ5^{inv} in the presence of fibrils were compared to those in the absence of fibrils as shown in Table 3-3. As we can see, the chemical shift changes induced by Aβ fibrils are moderate and not localized to certain regions within the primary structure. It is therefore very likely that these shifts are due to the residual orientation of inhibitor and not due to modifications of its structure due to interactions with the fibrils. One example shown in Table 3-4 shows the small ^{13}C chemical shift differences observed for peptide inhibitors in the absence and presence of fibrils.

Table 3-3. ^{1}H chemical shifts differences of iAβ5 or iAβ5^{inv} in the absence and presence of fibrils. Sample A is a 5 mM ^{19}F-iAβ5 with and without 0.5 mM Aβ$^{14-23}$ at pH 4, 303 K. Sample B is a 0.5 mM u-^{15}N, 10% ^{13}C- iAβ5^{inv} and 5 mM u-^{15}N, 10% ^{13}C-iAβ5^{inv} with 0.5 mM Aβ$^{14-23}$ at pH 4, 303 K. Sample C is a 0.5 mM ^{19}F-iAβ5 with and without 0.5 mM Aβ$^{14-23}$ at pH 4, 283 K.

		Sample A	Sample B	Sample C
	NH	--	-0.176	--
Leu	αH	-0.008	+0.062	-0.005
	βH	+0.001	+0.001	-0.003
	γh	-0.004	+0.001	-0.004
	δH	0	+0.009, +0.003	0
	αH	+0.008	+0.030	-0.005
Pro	βH	-0.001, -0.006	-0.016, -0.028	-0.006, -0.004
	γh	-0.003	+0.006, -0.023	-0.005
	δH	0, +0.010	-0.025, +0.007	-0.002, -0.001
	NH	-0.034	-0.111	+0.005
Phe3	αH	0	+0.016	-0.003
	βH	0	+0.034	-0.004
	γh	-0.005	+0.008	-0.001

	δH	-0.005	+0.008	-0.005
	εH	--	+0.004	--
	NH	-0.044	-0.238	+0.012
Phe4	αH	-0.002	+0.012	-0.003
	βH	-0.006, +0.006	+0.034	+0.004, -0.007
	γh	-0.008	+0.008	+0.001
	δH	0	+0.008	-0.002
	εH	-0.002	+0.004	-0.005
	NH	+0.015	--	-0.015
Asp	αH	+0.031	+0.015	-0.021
	βH	+0.010, +0.016	+0.078, +0.042	-0.006, -0.007

Table 3-4. ^{13}C chemical shifts differences of iAβ5^{inv} in the absence and presence of Aβ$^{14-23}$ fibrils.

	C^{α}	C^{β}	C^{γ}	C^{δ}	C^{ε}	C^{η}
Asp1	0.06	0.03				
Pro2	0.07	0.025	0.01	0.04		
Phe3	0.084	0.032		-0.008	-0.006	-0.004
Ph4	0.045	0.046		-0.008	-0.003	0.001
Leu5	0.04	0.047	0.015	0, 0.01		

3.7 Binding of iAβ5 or iAβ5^{inv} to Aβ peptides studied by solution NMR.

The interaction of iAβ5 or iAβ5^{inv} with Aβ peptides was further investigated by NMR. 1D ^{1}H spectra of iAβ5 and iAβ5^{inv} in the absence and presence of Aβ fibrils were compared respectively. One representative experiment is shown in Fig. 3-15.

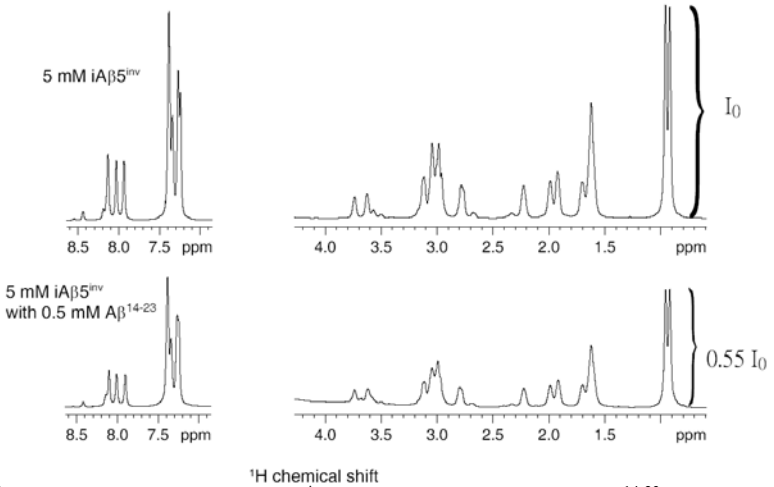

Fig. 3-15. 750 MHz ^{1}H NMR spectra of 5 mM iAβ5^{inv} with and without 0.5 mM Aβ$^{14-23}$, in 10 mM phosphate buffer at pH 4.0, 30 °C.

The 1D proton spectrum for iAβ5^{inv} with Aβ$^{14-23}$ show no signals of Aβ$^{14-23}$ due to its large molecular weight in the fibrillized state. The proton peak intensities of iAβ5 in the mixture sample decrease by 45% compared to those in the pure iAβ5 sample. This indicates that ca.

45% of the iAβ5 is bound to $A\beta^{14-23}$ fibrils and cannot be detected. Care was taken to reproduce the same iAβ5 concentration in both samples (see *Material and Methods*).

Fig. 3-16 represents a column along the aromatic ring resonance H^{δ} of Phe3 in the NOESY spectra recorded on ^{19}F-iAβ5 without (a) and with $A\beta^{14-23}$ fibrils (b-d). Whereas a few negative signals were detected for the free peptide in solution, an extensive set of positive NOE signals of the same sign compared to the diagonal peaks was detected when the peptide was measured after addition of $A\beta^{14-23}$ fibrils. Already at a mixing time of τ_m = 50 msec, cross peaks between almost all ^{1}H resonances are observed (Fig. 3-16b). The detected trNOE signals confirm the binding of the peptide to $A\beta^{14-23}$ fibrils.

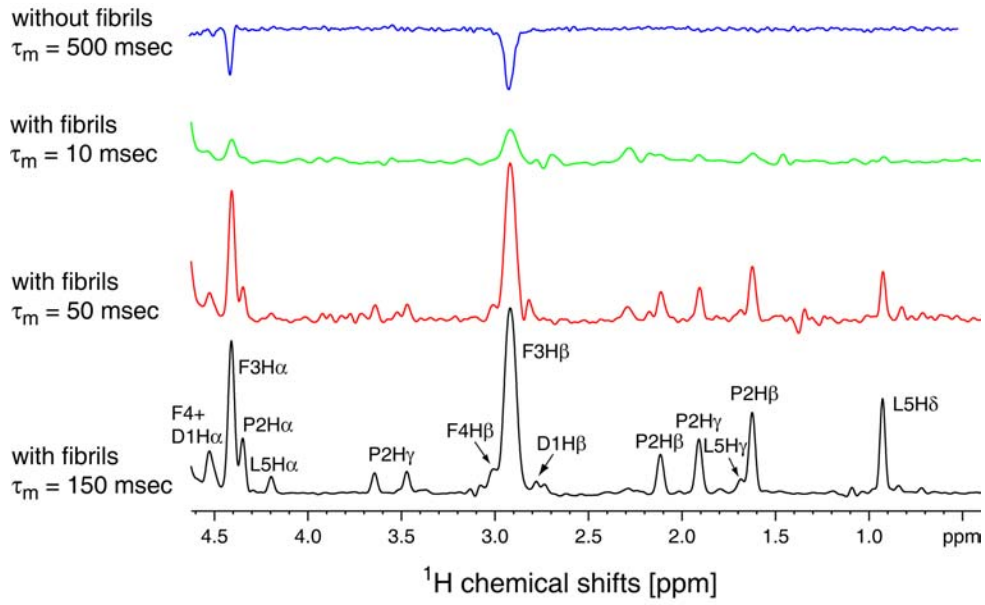

Fig. 3-16. Column along Phe3 H^{δ} of the NOESY spectra recorded on ^{19}F-iAβ5 without (lane 1) and with $A\beta^{14-23}$ fibrils (lanes 2-4) at different mixing times. The reference spectrum of ^{19}F-iAβ5 without $A\beta^{14-23}$ fibrils was recorded at 600 MHz, whereas all other spectra were recorded at 750 MHz field strength.

3.8 Structural studies by trNOE experiments.

As shown before, Aβ forms fibrils in solution and thus gives no signals in the solution NMR spectrum, where their size is far beyond the NMR size limitations of ~50 kDa. However, provided that the *K*d of the ligand-fibril complex is on the oder of μM, regular solution NMR experiments on the excess of free ligand can be used to study the conformation of the bound ligand. The very efficient cross-relaxation processes in the slowly tumbling complex dominate the magnetization transfer processes during the NOE mixing time. The cross-relaxation rate occurring in the free ligand is then negligible. Therefore, NOESY spectra on a

dynamically exchanging system containing an excess of free ligand, in rapid exchange with bound ligand, can be used to determine the structure in the bound form. TrNOE measurements of the type utilized here, when peptide inhibitors transiently bind to a very large particle, require high off-rates, i.e. weak binding constants. Solid-state NMR experiments indicate that the dissociation constant of iAβ5 (with respect to $A\beta^{14-23}$) must be high reflecting a very weak interaction. We subjected a solution NMR preparation to ultracentrifugation. The experimental MAS solid-state NMR 1D ^{13}C spectrum of the pellet does not show significant changes compared to the ^{13}C spectrum of a preparation that only contains fibrillized $A\beta^{14-23}$ (Fig. 3-17). This is in agreement with surface plasmon resonance experiments which were carried out in the past for various inhibitors interacting with Aβ (*21, 24*). The dissociation constants of ligands with respect to Aβ are found to be typically on the order of 100 µM.

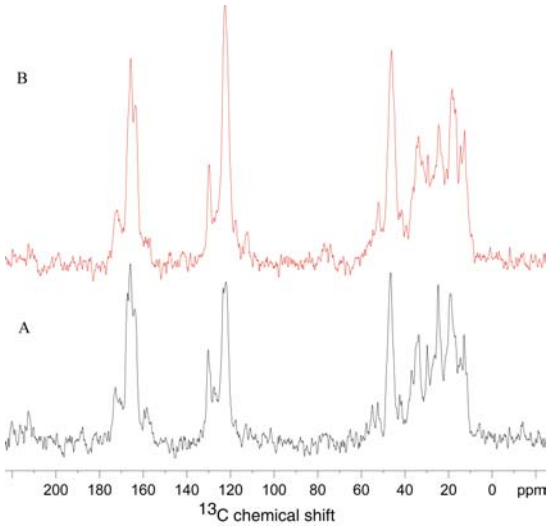

Fig. 3-17. 1D MAS ^{13}C spectrum of fibrillized $A\beta^{14-23}$ incubated alone or with inhibitor iAβ5 at pH 4, room temperature. A, 10 mg lyophilized $A\beta^{14-23}$ was dissolved in 7.5 ml 10 mM phosphate buffer at pH 4 as described in the methods part. The solution was centrifuged after 7 days of incubation and the pellet was filled into a 4-mm MAS rotor. B, 10 mg $A\beta^{14-23}$ together with 5.5 mg u-13C, 15N- iAβ5 (at a molar ratio of 1:1) was prepared as for sample A. Spectra were recorded at 12 °C, ns = 20 K, a MAS frequency of 11 kHz.

*tr*NOE experiments have been recorded in order to characterize the bound structure of iAβ5 with respect to fibrillar Aβ. The NOESY spectrum of the free peptide at 30 °C shows a few cross peaks of opposite sign compared to the diagonal peaks, indicating that the peptide is in the fast tumbling limit (Fig. 3-18A). However, in the NOESY spectrum recorded on iAβ5 in the presence of Aβ fibrils, already at a mixing time of 50 msec, cross peaks between almost all ^{1}H resonances were observed with the same sign as the diagonal peaks, indicating that iAβ5 is in the process of slow tumbling (Fig. 3-18B). Subtraction of the background NOE

peaks corresponding to the free peptide was not used due to the small and weak cross peaks in the spectrum of the free peptide.

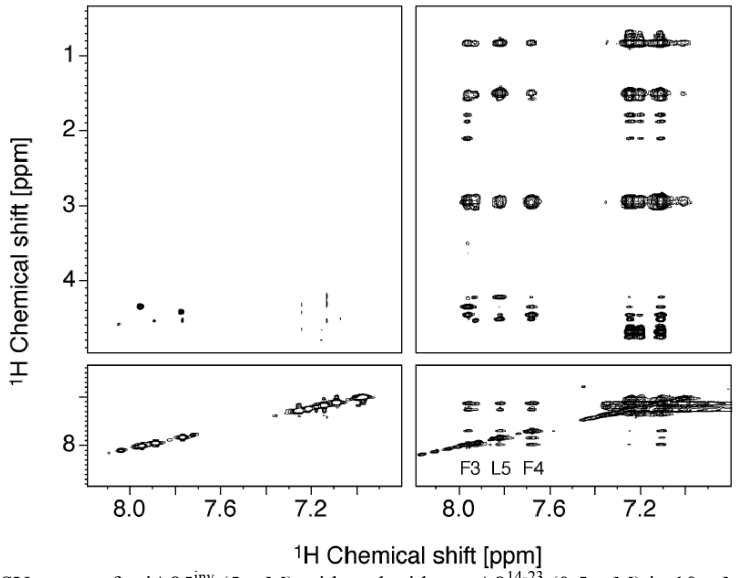

Fig. 3-18. NOESY spectra for iAβ5^{inv} (5 mM) with and without Aβ$^{14-23}$ (0.5 mM) in 10 mM phosphate buffer at pH 4 and 30 °C. A, iAβ5^{inv}, mixing time 500 ms; B, iAβ5^{inv} with Aβ$^{14-23}$, mixing time 50 ms.

At the same time, diffusion experiments were carried out to obtain information about a possible oligomeric arrangement of iAβ5 (in the absence of Aβ fibrils) (Fig. 3-19). We used TMS as a molecular weight reference to estimate the diffusion coefficient and, thus, the molecular weight of u-^{13}C,^{15}N-iAβ5 at different peptide concentrations 0.5 mM and 5 mM, respectively. Assuming a molecular weight of 88 Da for TMS, we can estimate the molecular weight of u-^{13}C, ^{15}N-iAβ5 to be on the order of 690 Da which corresponds quite well with the

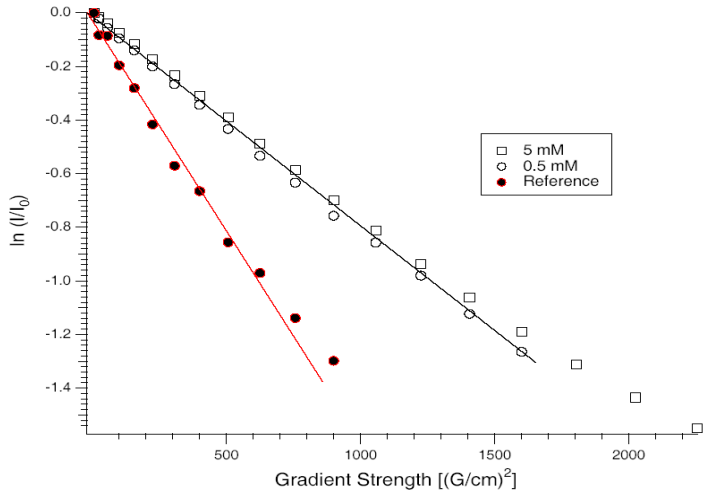

Fig. 3-19. DOSY experiments carried out for iAβ5 at different concentrations (0.5 mM and 5 mM, respectively) in the absence of Aβ$^{14-23}$ fibrils. Trimethylsilane (TMS) was used as a molecular weight standard.

expected value for the monomer (675 Da). This value is rather independent of the employed concentrations, means that the diffusion coefficient for water is comparable for both samples. Therefore, viscosity effects on the correlation time τc which might affect relative intensities of cross peaks in NOESY spectra can be excluded.

Furthermore, a NOESY spectrum was recorded for a 1:2 mixture of u-^{13}C, ^{15}N-iAβ5 and unlabelled iAβ5 in the presence of Aβ fibrils. Theoretically, there are signals originating from unlabelled molecules (Fig. 3-20A, red filled circles) and signals originating from labeled molecules (Fig. 3-20A, blue filled circles). If there exists an intermolecular contact, one would expect the signals at the open circle positions in Fig. 3-20A. However, in Fig. 3-20B, the absence of NOEs originating from protons in the labelled peptide to protons in the unlabelled peptide indicates that there are no intermolecular correlation between peptide inhibitors. However, in some region, shown in Fig. 3-20C, there may exist a very weak cross peak as indicated by an arrow. We therefore conclude that iAβ5 mainly interacts as a monomer and does not form larger oligomeric structures in the bound state.

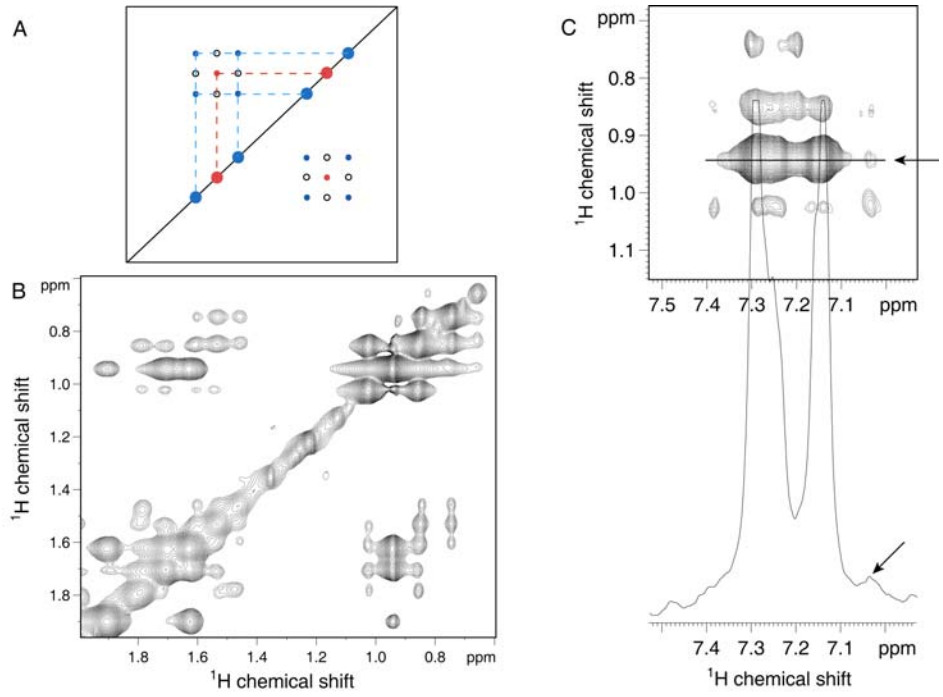

Fig. 3-20. Expanded region of a NOESY spectrum recorded for a 1:2 mixture of u-^{13}C, ^{15}N-iAβ5 and iAβ5 in the presence of Aβ$^{14-23}$ fibrils. A, schematic NOESY spectrum for mixture of labeled and unlabelled two spins. B, expanded aliphatic region of obtained NOESY spectrum. C, expanded region showing aromatic region and alilphatic region correlations. The 1D traces were taken from the positions as indicated.

There are a few key NOEs that should be highlighted in the followings. The Pro2 H$^{\delta}$ protons show NOEs of roughly equal intensities to Leu1 H$^{\alpha}$ (Fig. 3-21). This implies that the ψ angle

is close to 120° and that the peptide bond between Leu1 and Pro2 is *trans*. In an attempt to obtain more accurate distance information from the trNOE experiment, we measured the trNOEs as a function of the mixing time. The significant reduction in some of signal intensity as well as the appearance of new cross peaks that are not present in the data sets with shorter mixing times is assumed to be reflecting spin diffusion effects. The 50-ms, 150-ms and 100-ms data sets were selected for the analysis of trNOE effects for iAβ5^{inv} and iAβ5^{inv} bound to Aβ$^{14–23}$ and iAβ5^{inv} bound to Aβ$^{1-40}$, respectively.

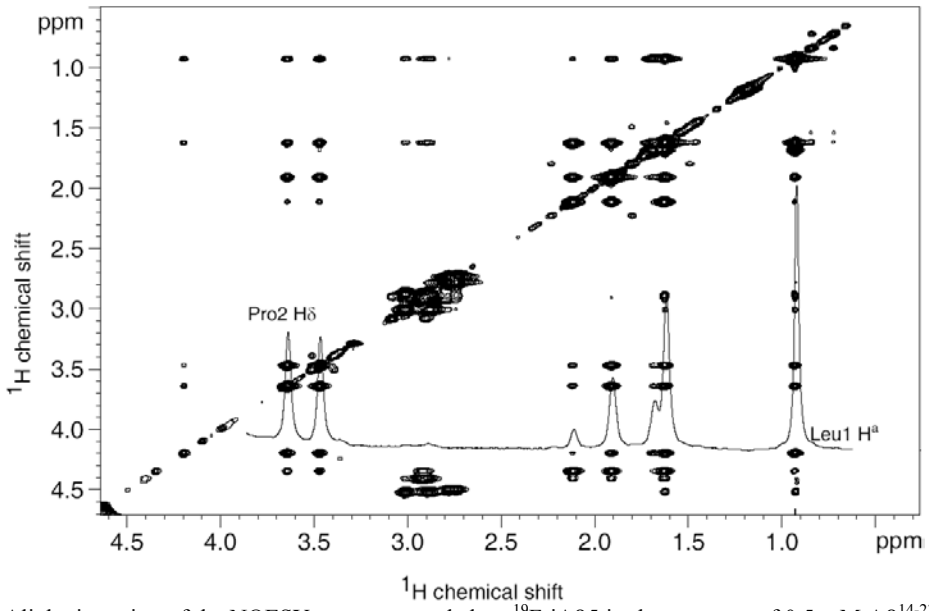

Fig. 3-21. Aliphatic region of the NOESY spectra recorded on ^{19}F-iAβ5 in the presence of 0.5 mM Aβ$^{14-23}$ fibrils (at a molar ration of 10:1) at a mixing time of 150 ms. The inset shows one row along Leu1 H$^{\alpha}$ resonance.

For a NOESY spectrum recorded with a mixing time of 50 ms, only 35 out of 110 observed NOEs were unambigously assigned for ^{19}F-iAβ5 bound to Aβ$^{14-23}$. Ambiguities in the other cross peaks result either from resonance overlap or from the lack of stereospecific assignments. The same experiments were carried out for iAβ5 with Aβ$^{1-40}$, iAβ5^{inv} with Aβ$^{14-23}$ and Aβ$^{1-40}$ respectively. Despite the detected positive NOEs, addition of iAβ5 to Aβ$^{1-40}$ caused strong line broadening in a 1D spectrum, Thus, NOESY spectra were not satisfactory for structural calculation for iAβ5 bound to Aβ$^{1-40}$. NOEs obtained for other combinations of inhibitor and fibril systems were used for structural calculations as shown below.

Transferred NOEs between protons on the peptide inhibitors permit to calculate the geometries in the bound state effectively. However, because no long-range NOEs are available between inhibitors and Aβ peptides, the exact arrangement of the peptide inhibitors on the fibril is not possible using only trNOE data.

3.9 Structural calculation of iAβ5 or iAβ5^{inv} bound to Aβ.

For iAβ5 (iAβ5^{inv}) in solution together with Aβ$^{14–23}$, 35 (40) intraresidue and 75 (38) interresidue NOE contacts were used to calculate the structure. For iAβ5^{inv} bound to Aβ$^{1–40}$, 45 intraresidue and 43 interresidue NOE restrains were employed. All structure calculations, minimizations and simulated annealing procedures were carried out using CNSsolve version 1.0 (*25*). From 200 calculated structures, 20 were selected based on their energy as well as their violations of experimental restraints. These 20 models from each set show a high degree of similarity (Fig. 3-22, Table 3-4). No hydrogen bond restraints were used in the initial rounds of structure calculation. However, analysis of the final calculated structure of ^{19}F-iAβ5 identified a hydrogen bond between Leu1-CO and Asp5-H^{N}.

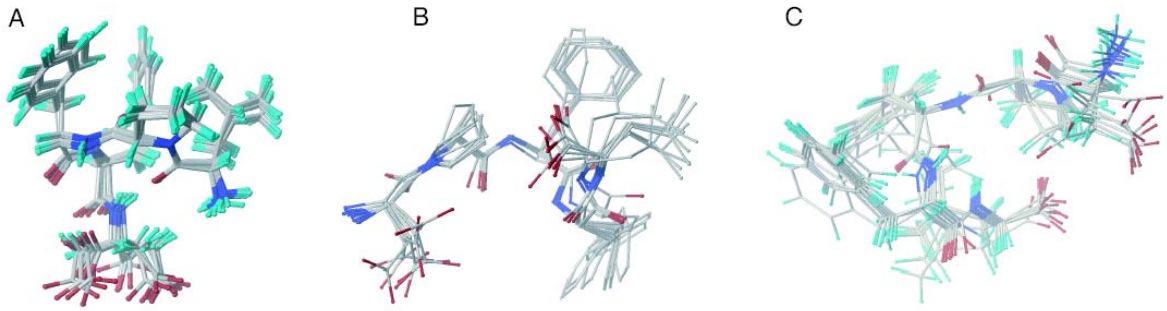

Fig. 3-22. The sets of 20 lowest energy structures of the peptide inhibitors in the bound state. A, ^{19}F-iAβ5 bound to Aβ$^{14-23}$; B, iAβ5^{inv} bound to Aβ$^{14-23}$; C, iAβ5^{inv} bound to Aβ$^{1-40}$.

Table 3-4. Summary of structural statistics.

	^{19}F-iAβ5	iAβ5$^{inv}{}_a$	iAβ5$^{inv}{}_b$
Number of distance restraints	110	78	88
Intraresidue	35	40	45
Interresidue	75	38	43
RMSDs from experimental distance restraints (Å)	0.063	0.001	0.023
RMSDs from idealized covalent geometry			
Bonds (Å)	0.0097	0.0007	0.0032
Angles (°)	0.821	0.606	0.665
Impropers (°)	0.227	0.077	0.195

a iAβ5 was bound to Aβ$^{14-23}$; b iAβ5 was bound to Aβ$^{1-40}$.

The sequences of two peptide inhibitors iAβ5 and iAβ5^{inv} share an equal core sequence (PFF) but posse exchanged N-terminal (L for D) and C-terminal (D for L) residues. The NMR structures of the two peptides iAβ5 and iAβ5^{inv} bound to Aβ$^{14-23}$ fibrils show different backbone structures in the bound state, but identical spatial side chain orientations of equal properties (Fig. 3-23A). Besides the identical side chain orientations for P2, F3 and F4 for both peptides, the superposition reveal that L1 and D5 of iAβ5 can be superimposed with L5

and D1 of iAβ5^{inv}, respectively. This indicates that the spatial binding pattern for the different peptides might be identical and both peptides bind to the same site in Aβ$^{14-23}$.

iAβ5^{inv} binds to fibrils formed by Aβ$^{14-23}$ and Aβ$^{1-40}$, respectively, with different structures showing different backbone and different side chain orientations as shown in Fig. 3-23B. This is an indication for distinct binding geometries at the binding sites of Aβ$^{14-23}$ and Aβ$^{1-40}$ fibrils.

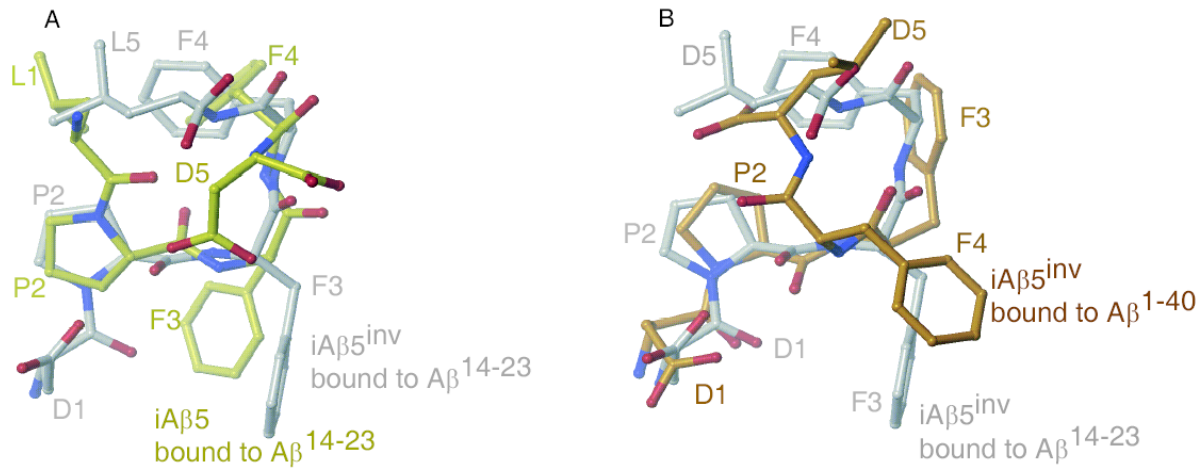

Fig. 3-23. Superposition of the NOE-derived structures for peptide inhibitors. A, superposition of the structures for iAβ5 and iAβ5^{inv} bound to Aβ$^{14-23}$, respectively. B, superposition of the structures for iAβ5^{inv} bound to Aβ$^{14-23}$ and Aβ$^{1-40}$, respectively.

3.10 Measurement of residual dipolar couplings in peptide inhibitors bound to Aβ fibrils.

TrNOE experiments have been successfully used in this work to obtain distance restraints of the bound conformation. However, lacking of the intermolecular NOEs between iAβ5 or iAβ5^{inv} and fibrillized Aβ can not provide any information about the orientation of ligands relative to the fibrils. The determination of the bound geometry of protein ligands is an important issue for improving our understanding of how a structure relates to a certain biological function, and also for building a basis for rational drug design. Recently, residual dipolar couplings (RDCs) have been used successfully to restrain the absolute orientation of dipolar vectors with respect to the magnetic field, and to provide critical structural details of biologically important molecules (*26, 27*). In this work, we suggest to use transferred RDCs (trRDCs) from ^{13}C-^{1}H/^{15}N-^{1}H pairs on peptide inhibitors to validate the structure of peptide inhibitors that bind transiently to oriented amyloid fibrils.

3.10.1 Alignment of amyloid fibrils.

Measurement of dipolar couplings in the peptide inhibitor, which transiently binds to the oriented fibrils requires a significant degree of net orientation of the peptide. Usually, the orientation is introduced through unspecific interactions between the alignment medium and the solute by certain alignment media, like bicelle type lyotropic liquid crystals (*28*), phage particles (*29, 30*), purple membrane fragments (*31, 32*) or strained polyacrylamide gels (*33, 34*). However, similar to transferred NOE (*35*), transferred cross correlated relaxation (*36-38*), and also specific interactions in the limit of weak binding can be exploited to obtain information about transiently bound peptides and proteins (*31, 39, 40*). It has been demonstrated that in favourable cases it is possible to measure dipolar couplings for a ligand which is in rapid exchange between free solution and a bound state (*39*). In this study, we show that the orientation required for measurement of residual dipolar couplings for iAβ5^{inv} could be introduced by transient binding to Aβ fibrils which orient in the magnetic field. Such measurements offer information about the orientation of the bound ligand relative to the oriented fibrils, complement transferred NOE data and result in a more detailed view of the structure of the bound ligand.

In the following paragraph, we show that the diamagnetic anisotropy of β pleated sheets as they are found in the amyloid fibrils can be used to restrain the orientation of small peptides binding to amyloid fibrils. The effect is based on the diamagnetic susceptibility of the peptide bond and can be detected if peptide planes orient synchronously (*41*). The size of the diamagnetic anisotropy for a peptide bond is determined by the angle ϕ between the peptide plane normal and the symmetry axis of the molecular system, and is given by $\Delta\chi = \Delta K (1 - 3\cos^2\phi)/2$ (where ΔK corresponds to the anisotropic diamagnetic susceptibility of the peptide bond, ca. 8.8×10^{-6}). The largest diamagnetic anisotropy is found in α-helices ($\Delta\chi$ = ca. 4.4×10^{-6} N, where N corresponds to the number of peptide bonds; neglecting at this point orienting effects of aromatic rings) and is responsible for the orientation of phages and purple membranes. In β pleated sheets, the planar groups of the peptide bonds are oriented parallel to the sheet and the axis of smallest numerical diamagnetism is parallel to the pleats, so the anisotropy is $\Delta\chi$ = ca. 1.1×10^{-6} N for a pleated sheet (neglecting at this point orienting effects of aromatic rings). Worcester (*41*) has discussed the structural origins of diamagnetic anisotropy in proteins and concluded that for β-sheet structures, an alignment of the hydrogen-bonding direction parallel to the direction of the applied magnetic field is expected.

In the past, the diamagnetic anisotropy and consequent magnetic orientation of amyloid fibres found application in structural analyses of biological material, and especially in the X-ray diffraction analysis of amyloidogenic peptides (*9, 42, 43*). In these experiments, Aβ fibrils were prepared in a 2 Tesla magnetic field, and x-ray diffraction patterns were obtained with the incident beam directed along different directions relative to the direction of the magnetic field, namely, two orthogonal to the magnetic field and one parallel to the magnetic field. The observed x-ray diffraction patterns obtained with the incident beam orthogonal to the applied magnetic field direction show strong meridional diffraction signals appearing at 0.47 nm (Fig. 3-24A, B, labelled as "200") which represents the interchain distance between hydrogen-bonded peptides. Consequently, the hydrogen bond direction (the fibril axis) is aligned with the magnetic field direction. In the diffraction pattern obtained with the incident beam parallel to the magnetic filed axis (Fig. 3-24C), the diffraction signal corresponding to a spacing of 0.47 nm appears to be absent or much weaker confirming the arrangement of β-sheets that Aβ peptides self-assemble and grow in the hydrogen-bonding direction along the magnetic field.

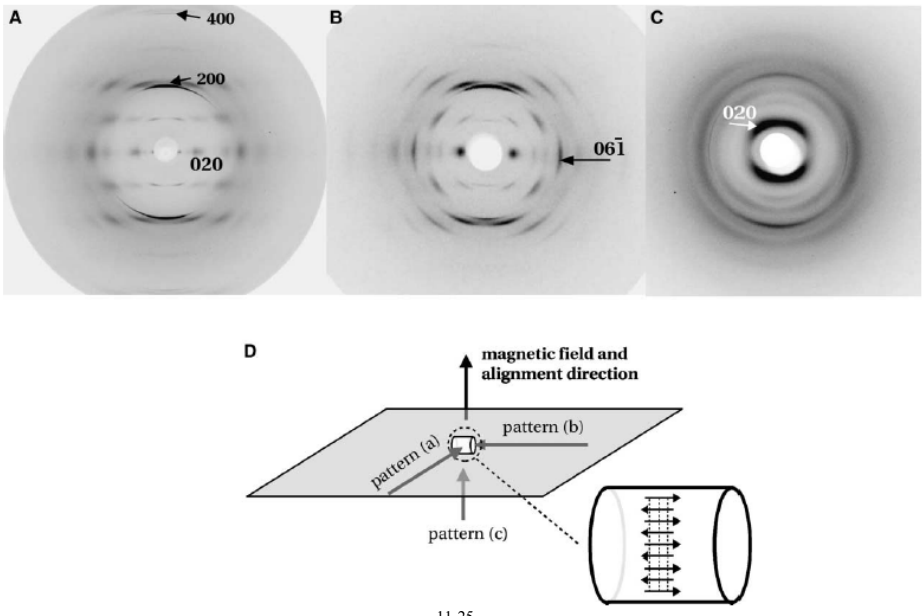

Fig. 3-24. Wide-Angle X-ray diffraction patterns for $A\beta^{11-25}$ fibrils reproduced from Sikorski *et al.*. The fibrils were aligned in a magnetic field. Diffraction pattern (A) and (B) was obtained when the incident X-ray beam is orthogonal to the alignment direction and along the two directions as indicated in (D). In (C), the incident X-ray beam is parallel to the alignment direction (*43*). The diffraction signal indicated as 200 corresponds to a spacing of 0.47 nm.

The extent of the alignment is tunable by changing the fibril concentration. However, at a high concentration of Aβ fibrils, we obtain extensive line broadening. A compromise was found at a concentration of 0.5 mM $A\beta^{14-23}$ in 10 mM phosphate buffer at pH 4. The alignment of macromolecules in the magnetic field is often confirmed by measuring the

residual orientation of water deuterons in H_2O/D_2O mixture (*32*). Fig. 3-25 shows the 1D ^2H spectrum recorded on a sample containing 0.1 mM $A\beta^{1-40}$ with 5 mM $iA\beta5^{inv}$. The spectrum shows that there is no visible splitting of the deuterium resonance in this sample. This is due to the very low concentration of fibrils. As suggested by Sass *et al.* (*32*), splittings larger than 2 Hz are easily observable at high concentration (like 7 mg/ml for purple membrane), however, at the very low concentration required for NMR spectra resolution, the smaller splitting of the deuterium resonance is not easily detected because of the large deuterium line width. However at this low concentration orientation of fibrils can still be determined by the measurement of residual dipolar couplings of $iA\beta5^{inv}$ transiently bound to fibrils.

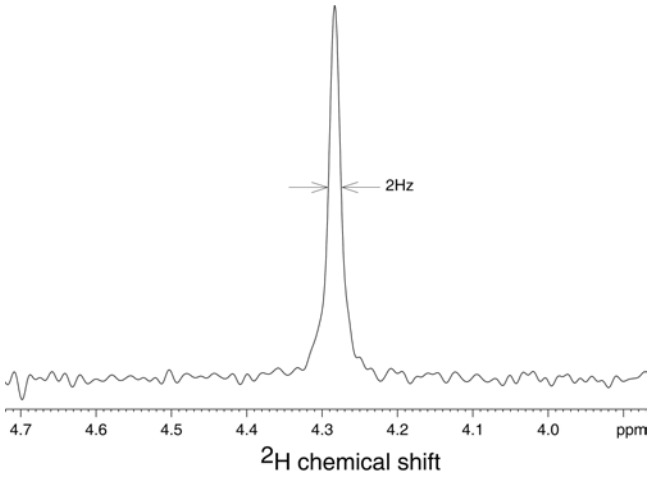

Fig. 3-25. 1D ^2H spectrum of 0.1 mM $A\beta^{1-40}$ with 5 mM $iA\beta5^{inv}$.

3.10.2 Measurement of RDCs for $iA\beta5^{inv}$ bound to Aβ fibrils using amyloid fibrils as orienting medium.

The experiments were carried out using a 5 mM u-^{15}N labelled sample of the 5-residue synthetic peptide $iA\beta5^{inv}$. For preparation of the NMR sample, $iA\beta5^{inv}$ was added to preformed $A\beta^{14-23}$ fibrils (incubation time: 2 days). In the experiments described below, a molar ratio of $[iA\beta5^{inv}]:[A\beta^{14-23}]$ = 10:1 or $[iA\beta5^{inv}]:[A\beta^{1-40}]$ = 100:1 was employed, respectively. The large excess of the peptide inhibitor is in agreement with the reported excess of inhibitor required to prevent neurotoxicity to cultured neuronal cells (*12*). Even larger amounts of fibrils in the NMR tube induced significant line broadening. Approximately two weeks after incubation of fibrillar $A\beta^{14-23}$ and $A\beta^{1-40}$ together with $iA\beta5^{inv}$, neither trNOEs nor trRDCs were observed. This is due to disaggregation of $A\beta^{14-23}$ or $A\beta^{1-40}$ fibrils by $iA\beta5^{inv}$ which is also reflected by the loss of fibrillar material as observed by EM. All spectra were recorded on a Bruker 750 MHz solution state NMR spectrometer, at 30°C.

Successful observation of trRDCs in transiently bound ligands is strongly dependent on the dissociation constant of the complex. In contrast to trNOE, no trRDC might be observable if the life time of the bound state is too long and binding takes place in a slow exchange regime. As pointed out by Koenig *et al*. (*39*), RDCs of transiently bound ligands can be observed if

$$\frac{1}{\tau_f \tau_b} << \left[\rho - \left(\frac{1}{\tau_f} - \frac{1}{\tau_b} \right) \right]^2 , \qquad [3\text{-}2]$$

where τ_f (= $[A\beta_{free}]^{-1}k^{-1}_{on}$) and τ_b (= k^{-1}_{off}) correspond to the lifetime of the free and the bound ligand, and ρ reflects the transverse relaxation rate in the bound state. Since excess molar amounts of inhibitors over the Aβ peptides were used and the inhibitors undergo rapid exchange on and off the fibrils, RDCs are observed as an average between the free and bound states of peptide inhibitors. In our case, in the free state inhibitors have the dipolar coupling averaging to zero, whereas in the bound state the dipolar coupling equals D_b. A quantitative description can be carried out in the framework of chemical exchange (*38*). The size of the observed dipolar coupling is then given as (*39*)

$$D_{obs} = \frac{1}{\tau_f \tau_b} \frac{D_b}{\left[\rho - \left(\frac{1}{\tau_f} - \frac{1}{\tau_b} \right) \right]^2 + D_b^2} , \qquad [3\text{-}3]$$

Theoretically, the size of the observed residual dipolar coupling can be adjusted by variation of the concentrations of peptide with respect to the amount of fibrils within the NMR tube. In practice, however, too high a concentration of $A\beta^{14\text{-}23}$ (1:1 with respect to $iA\beta5^{inv}$) yields extensive line broadening. Using too low concentrations of $A\beta^{14\text{-}23}$ (1:100 with respect to $iA\beta5^{inv}$) prevents the observation of trNOEs. Therefore, we have chosen to use a molar ratio of 1:10 of $A\beta^{14\text{-}23}$ with respect to $iA\beta5^{inv}$ (1:100 of $A\beta^{1\text{-}40}$ with respect to $iA\beta5^{inv}$) as the best compromise in the studies presented below. We speculate that due to different affinities of $iA\beta5^{inv}$ and $iA\beta5^{inv}$ with respect to $A\beta^{14\text{-}23}$, we could not observe significant trRDCs for iAβ5, but only for $iA\beta5^{inv}$.

RDCs for peptide inhibitors $iA\beta5^{inv}$ in the free state and bound to Aβ fibrils were measured from one bond ^1H-^{13}C or ^1H-^{15}N *J*-couplings in the proton dimension of ^1H-^{13}C or ^1H-^{15}N HSQC spectra acquired without proton decoupling. Fig. 3-26 and 3-27 represent 1D traces from ^1H-^{15}N/^1H-^{13}C HSQC spectra that were recorded for $iA\beta5^{inv}$ in the presence and absence

of fibrillized $A\beta^{14-23}$. ^{13}C HSQC spectra were recorded at ^{13}C natural abundance, therefore ^{13}C, ^{13}C homonuclear decoupling is not required in the ^{1}H-^{13}C correlation experiments. More sophisticated approaches using the IPAP pulse scheme (*44*), or a combination of TROSY and semi-TROSY experiments (*45*) to measure residual dipolar couplings yield quantitatively the same results. These experiments are not required, since resolution in the ^{1}H-^{15}N and ^{1}H-^{13}C correlation spectra is not compromised by spectral overlap. Upon addition of $A\beta^{14-23}$ fibrils, only a slight increase in the ^{15}N line width was observed for the ^{15}N resonances of $iA\beta5^{inv}$. At the same time, the N-H^N dipolar/^{15}N-CSA and the C^{α}-H^{α} dipolar/$^{13}C^{\alpha}$ CSA cross relaxation rates are affected. In particular, differential multiplet intensities were observed for Phe3 and Phe4.

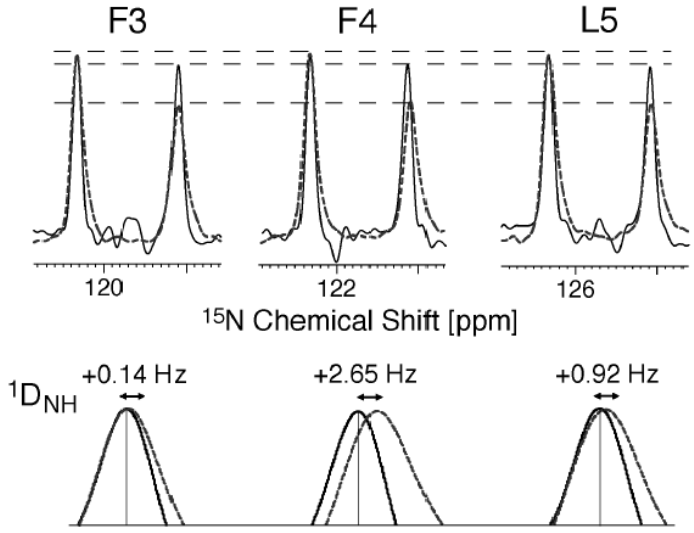

Fig. 3-26. 1D columns of a ^{1}H-^{15}N HSQC spectrum of $iA\beta5^{inv}$ with (dashed line) and without (solid line) fibrillized $A\beta^{14-23}$, recorded without heteronuclear decoupling in the indirect dimension. In the upper figure, intensities were normalized with respect to the low-field multiplet component. On the bottom, only the β multiplet component is represented. The experiment is recorded without phase alternation of the last 90° ^{1}H pulse of the first INEPT.

Similar methods were used to obtain orientational constraints from dipolar coupling for the binding of $iA\beta5^{inv}$ to $A\beta^{1-40}$. $^{1}H^{\alpha}$-$^{13}C^{\alpha}$ couplings were measured at natural abundance for $iA\beta5^{inv}$ using a coupled ^{13}C HSQC spectrum acquired without proton decoupling. ^{1}H-^{13}C couplings for side chains were acquired in the absence of ^{13}C decoupling during acquisition, and the one bond ^{1}H-^{13}C couplings are frequency domain splittings in the proton dimension. Two sets of data were collected for sample corresponding to the free state and bound state (in the presence of $A\beta^{1-40}$). As one would expect for the case of isotropic tumbling, all the couplings obtained for $iA\beta5^{inv}$ in the free state are similar and fall in the range of typical $^{1}J_{CH}$ scalar coupling constants (145 Hz). On the other hand, couplings measured for $iA\beta5^{inv}$ in the presence of fibrils are different because of the presence of a residual dipolar contribution.

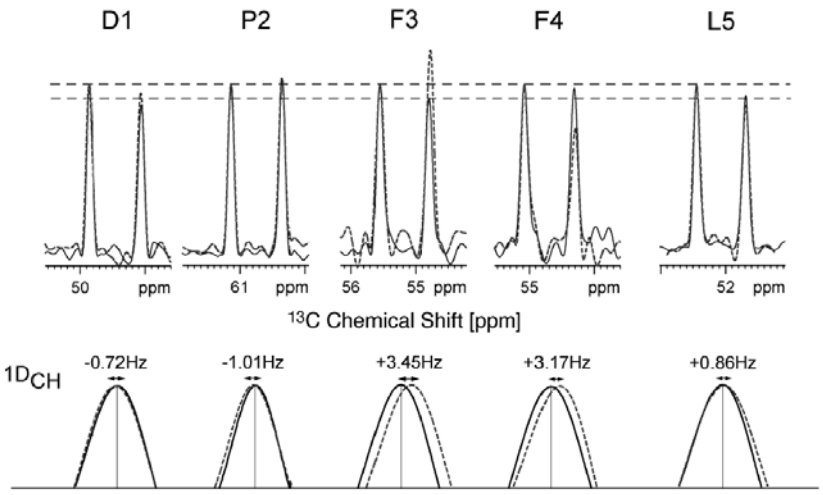

Fig. 3-27. 1D columns of a ^{1}H-^{13}C HSQC correlation spectrum of iAβ5^{inv} with (dashed line) and without (solid line) fibrillized Aβ$^{14-23}$, recorded without heteronuclear scalar decoupling in the indirect dimension. In the lower figure, only the β multiplet component is drawn in order to show residual dipolar coupling effects. For this purpose, signals with and without Aβ$^{14-23}$ are represented with the same intensity. The experiment is recorded with phase alternation of the last 90° ^{1}H pulse of the first INEPT in order to suppress intensity artifacts on the doublet components.

trRDCs were determined as the difference in couplings measured for the isotropic state and the bound state. All experimental values are listed in Table 3-5. A total of 3 backbone ^{15}N-^{1}H and 5 backbone $^{13}C^{\alpha}$-$^{1}H^{\alpha}$ residual dipolar couplings were measured for the 5-residue iAβ5^{inv} in presence of Aβ$^{14-23}$. Amide protons of Asp1 could not be observed due to fast exchange with solvent protons. For iAβ5^{inv} in the presence of Aβ$^{1-40}$, overlap of the ^{13}C-^{1}H correlations of Phe3 and Phe4 prohibited measurement of their $^{1}D_{C^{\alpha}H^{\alpha}}$ dipolar couplings, but an additional seven side-chain ^{13}C-^{1}H couplings were obtained.

In order to estimate the error of the extracted RDC values, experiments have been carried out twice using the same composition of the sample. The indicated values represent the average of the two measurements. Values reported in Table 3-5 correspond to the average trRDC value. The error for C^{α}-H^{α} trRDCs can be estimated to be ± 0.5 Hz, the error for the N-H^{N} trRDCs is found to be ± 0.2 Hz. In all cases, the sign of the residual dipolar coupling could be reproduced. Furthermore, no concentration dependence – measured for iAβ5^{inv} alone – of the read-out coupling constant was observed, indicating that iAβ5^{inv} does not self-orient within the magnetic field.

Table 3-5. Residual dipolar coupling measurements for iAβ5^{inv} bound to Aβ$^{14-23}$/Aβ$^{1-40}$.

	iAβ5^{inv} bound to Aβ$^{14-23}$ (a)	iAβ5^{inv} bound to Aβ$^{1-40}$ (b)
	Observed RDCs (Hz)	Observed RDCs (Hz)
Asp1 C^{α}-H^{α}	–0.7	
Pro2 C^{α}-H^{α}	–1.1	–1.425
Pro2 C^{γ}-H^{γ}		+1.15, +2.6
Pro2 C^{δ}-H^{δ}		+2.175, +1.875

Phe3 N-H^N	+0.14	
Phe3 C^α-H^α	+3.5	
Phe3 C^η-H^η		–0.83
Phe4 N-H^N	+2.65	
Phe4 C^α-H^α	+3.2	
Phe4 C^δ-H^δ		–1.875
Phe4 C^η-H^η		–2.92
Leu5 N-H^N	+0.92	
Leu5 C^α-H^α	+0.9	
Leu5 C^γ-H^γ		–4.725

(a) N-H and C-H trRDCs for iAβ5^{inv} interacting with Aβ$^{14-23}$ employing a molar ratio of 10:1 for [iAβ5^{inv}]:[Aβ$^{14-23}$]
(b) C-H trRDCs for iAβ5^{inv} interacting with Aβ$^{1-40}$ employing a molar ratio of 100:1 for [iAβ5^{inv}]:[Aβ$^{1-40}$]

The sign change in the interpretation of ^{13}C-^{1}H vs. ^{15}N-^{1}H residual dipolar couplings is inferred by the negative sign of the gyromagnetic ratio of ^{15}N (*46-48*). Solid-state NMR studies suggest an antiparallel organization of Aβ$^{16-22}$ (*49*). Contiguous β-sheet polypeptide chains are aligned perpendicular to the long axis of the fibre. Fibrils are stabilized by hydrogen bonding between amide nitrogens and carbonyl atoms in subsequent polypeptides. These hydrogen bonds are directed along the fibril axis. With the exception of Asp1, positive residual dipolar couplings for C^α-H^α are found throughout the backbone of iAβ5^{inv} in the presence of fibrillized Aβ$^{14-23}$. This indicates that these bonds are oriented perpendicular to the direction of the magnetic field. On the other hand, only positive trRDCs can be detected for the case of NH^N, suggesting a parallel arrangement of the N-H^N bond vectors with respect to B_0. We therefore assume that the interaction between iAβ5^{inv} and fibrillized Aβ$^{14-23}$ is driven by side chain interactions. Hydrophobic side chains might intercalate into amyloid fibrils and weaken hydrophobic Aβ·Aβ interactions which stabilize the fibrillar structure. The projection angle between the vectors N-H^N and C^α-H^α within the peptide bond is a function of the backbone torsion angle, and is given as

$$\cos\angle\left(NH^N, C^\alpha H^\alpha\right) = -0.163 - 0.819\cos(120° + \varphi) \qquad [3\text{-}5]$$

This equation can be derived in analogy to the derivation given in (*50*). In a β-sheet structure, the (N-H^N, C^α-H^α) projection angle adopts approximately a value of around 130°–160°. Depending on the exact orientation of the interacting side chains and the planarity of the β-strand, a change of sign for NH^N and $C^\alpha H^\alpha$ trRDC values is plausible, if we assume that the N-H^N vectors are arranged not exactly parallel with the fibril axis. The Pro induces a turn in the structure and places the charged N-terminus appropriate for binding to Aβ$^{14-23}$. This is reflected in the negative sign of the $C^\alpha H^\alpha$ residual dipolar coupling for Asp1 and Pro2. Our experiments do not provide direct information whether iAβ5^{inv} interacts with the long axis or

the tips of an amyloid fibril. A detailed analysis of the mode of interaction requires knowledge of side chain torsion angles.

Large variations for trRDC values were observed along the backbone of iAβ5^{inv}. The largest values were found for Phe3 and Phe4. Alternatively, smaller trRDC values could be due to an increased mobility at the C-terminus of iAβ5^{inv}, and could therefore be due to a faster loss of orientation after being dissociated into the unligated state. The same argument is not directly applicable to the N-terminus, since the N-terminus might be stabilized in a turn-type structure. A quantitative interpretation of trRDC values requires the knowledge of the molecular alignment tensor of iAβ5^{inv}.

The asymmetry of the α/β doublet components induced by binding of iAβ5^{inv} to Aβ$^{14-23}$ is due to $^{13}C^{\alpha}$-$^{1}H^{\alpha}$ dipole, $^{13}C^{\alpha}$ CSA and ^{15}N-$^{1}H^{N}$ dipole, ^{15}N CSA cross correlated relaxation (*51*). These differences are directly related to the binding affinity of the respective sites and chemical groups to the amyloid fibrils. Recently, this effect has been suggested to be employed in drug design (*52*). We also observed differences in the size of the residual dipolar couplings depending on the mode of sample preparation. Almost no changes were observed, if Aβ$^{14-23}$ was solubilized in a solution that already contained iAβ5^{inv}. This is most likely due to the fact that fibril formation is prevented under these conditions, and no preferential orientation of Aβ$^{14-23}$ is possible.

3.10.3 Measurement of RDCs for KLVFFKK peptide bound to Aβ fibrils using amyloid fibrils as orienting medium.

In the **Introduction** part, we have shown that a series of the variants of KLVFF sequence are identified to interact with Aβ and increase its aggregation rate while decreasing its toxicity. The K_d value of KLVFFKK was determined to be around 80 μM (*21*). Therefore, when bound to Aβ fibrils, this peptide is in the fast exchange between free state and bound state and can be used for trRDC measurements.

The experiments were carried out using a 5 mM sample of KLVFFKK in the absence and presence of 0.1 mM Aβ$^{1-40}$ fibrils. ^{1}H resonances were assigned in the TOCSY spectrum recorded for 5 mM sample of KLVFFKK in the absence of Aβ fibrils, shown in Fig. 3-28.

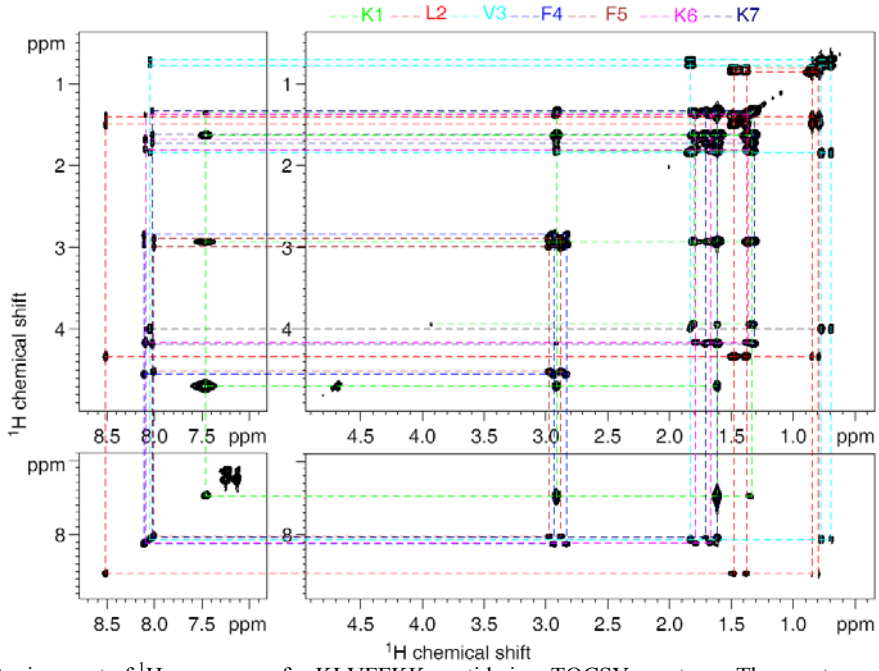

Fig. 3-28. Assignment of ^{1}H resonances for KLVFFKK peptide in a TOCSY spectrum. The spectrum was recorded for 5 mM KLVFFKK in 10 mM PO_4^{3-} buffer, at pH 4, 30 °C.

^{13}C resonance assignment was done by correlating it with the assigned proton chemical shifts. RDCs for KLVFFKK in the free state and bound to Aβ fibrils were measured from one bond ^{1}H-^{13}C *J*-couplings in the proton dimension of ^{1}H-^{13}C HSQC spectra acquired without proton decoupling. Fig. 3-29 shows the obtained spectra for KLVFFKK peptide in the absence and presence of $A\beta^{14-23}$ fibrils. trRDCs were determined as the difference in couplings measured for the isotropic state and the bound state. All experimental values are listed in Table 3-6.

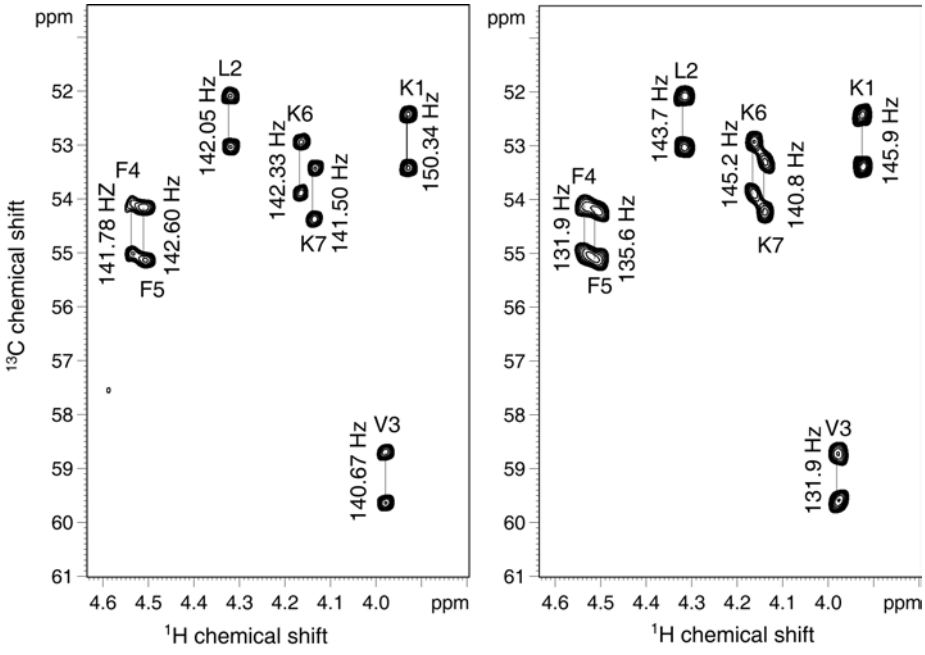

Fig. 3-29. ^{13}C HSQC spectra recorded on 600 MHz Bruker spectrometer for 5 mM KLVFFKK in the absence and presence of 0.5 mM $A\beta^{14-23}$ at 10 mM PO_4^{3-}, pH 4, 30 °C. The spectra were recorded on 750 MHz Bruker spectrometer, without ^{1}H decoupling in the F1 dimention.

Table 3-6. Residual dipolar coupling measurements for KLVFFKK bound to $A\beta^{14-23}$/$A\beta^{1-40}$, respectively.

	KLVFFKK bound to $A\beta^{14-23}$ (a)	KLVFFKK bound to $A\beta^{1-40}$ (b)
	Observed RDCs (Hz)	Observed RDCs (Hz)
Lys1 C^{α}-H^{α}	–4.4	–1.2
Leu2 C^{α}-H^{α}	+1.6	–2.5
Val3 C^{α}-H^{α}	–8.8	–1.8
Phe4 C^{α}-H^{α}	–9.9	–7.1
Phe5 C^{α}-H^{α}	–7.0	–4.8
Lys6 C^{α}-H^{α}	+2.9	0
Lys7 C^{α}-H^{α}	–0.7	0

(a) C-H trRDCs for KLVFFKK interacting with $A\beta^{14-23}$ employing a molar ratio of 10:1 for [KLVFFKK]:[$A\beta^{14-23}$]
(b) C-H trRDCs for KLVFFKK interacting with $A\beta^{1-40}$ employing a molar ratio of 100:1 for [KLVFFKK]:[$A\beta^{1-40}$]

The larger RDCs obtained for KLVFFKK peptide in the presence of Aβ fibrils can be due to a slightly more tight binding of this peptide to Aβ fibrils than $iA\beta5^{inv}$.

Moreover, no or very weak trNOEs are observable for KLVFFKK peptide bound to Aβ fibrils. This could be due to the tight binding of KLVFFKK to Aβ fibrils. For another peptide KLVFF which was reported to have less affinity to Aβ peptide compared to KLVFFKK, stronger trNOEs were obtained for KLVFF in the presence of $A\beta^{14-23}$ fibrils, while no or extremely smaller trRDCs were obtained. This suggested the reasonable *K*d value is required for trNOE, trRDC measurements.

3.11 Order tensor determination for $iA\beta5^{inv}$ bound to Aβ fibrils.

Two directly coupled nuclei A and B, the direct dipolar coupling interaction is quantified by the dipolar coupling constant

$$D^{AB} = \frac{-\mu_0 h \gamma_A \gamma_B}{8\pi^3} \left\langle r_{AB}^{-3} \right\rangle \left\langle \frac{3\cos^2\theta - 1}{2} \right\rangle \quad , \qquad [3\text{-}5]$$

where μ_0 is the permeability of free space, γ_A and γ_B are the magnetogyric ratios of the coupled nuclei, θ is the angle between a unit vector in the internuclear direction and a unit vector parallel to B_0, r_{AB} is the internuclear distance and < > denotes a time average over the motions with time scales short compared to the reciprocal of the splitting.

It is clear from Eq. [3-5] that D^{AB} is a source of dynamic and structural information through their dependence upon θ and upon the motional averaging of these quantities. For a given type of a fixed distance (r_{AB}) A–B interaction, the D^{AB} value measured is angle dependent, which makes it a very important tool for obtaining long-range structural information.

To take advantage of RDCs in the study of biomolecular structures, knowledge of the magnitude and orientation of the alignment tensor, A, with respect to the molecule is advantageous, although optimization of the magnitude and orientation of **A** during the simulated annealing process is also possible (*53, 54*).

In cases where information on the full structure of a molecule is not available prior to beginning of an NMR investigation, but experimentally observed one-bond RDCs are abundant, examination of a histogram of such normalized residual dipolar couplings is a common method for estimating the magnitude and rhombicity of the molecular alignment tensor. The RDCs observed for different types of one-bond interactions are then normalized to the ${}^1D^{NH}$ interaction by removing the dependence of the dipolar couplings on bond length and on the magnetogyric ratios of the coupled nuclei (Eq. 3-5).

The general expression for the residual dipolar coupling D^{AB} between two directly coupled nuclei A and B can be simplified to the form (*53*)

$$D^{AB} = D_a^{AB}\left[\left(3\cos^2\theta - 1\right) + \frac{3}{2}R\sin^2\theta\cos 2\phi\right], \qquad [3\text{-}6]$$

where D_a^{AB} and D_r^{AB} in units of Hertz are the axial and rhombic components of the traceless second rank diagonal tensor **D** given by $\frac{1}{3}\left[D_{zz}^{AB} - \left(D_{xx}^{AB} + D_{yy}^{AB}\right)/2\right]$ and $\frac{1}{3}\left[D_{xx}^{AB} - D_{yy}^{AB}\right]$, respectively, with $\left|D_{zz}^{AB}\right| > \left|D_{yy}^{AB}\right| \geq \left|D_{xx}^{AB}\right|$; R is the rhombicity defined by D_r^{AB}/D_a^{AB} and is always positive; θ is the angle between the A–B interatomic vector and the z axis of the tensor (it should be noted that θ has a different definition as that in Eq. [3-5]); and ϕ is the angle which describes the position of the projection of the A–B interatomic vector on the x–y plane, relative to the x axis. D_a^{AB} subsumes various constants, including the gyromagnetic ratios of the two nuclei γ_A and γ_B.

For a given type of a fixed distance (r_{AB}) A–B interaction, the extreme D^{AB} values measured correspond to orientations of A–B vectors closest to the z (θ = 0°) and y (θ = 90°; ϕ = 90°) principal axes of the alignment tensor. If the A–B vectors are distributed uniformly and isotropically, a histogram describing the probability of finding values of D^{AB} between these two extremes will have the same shape as a chemical shift anisotropy (CSA) powder pattern. The highest probability dipolar coupling value therefore coincides with the magnitude of a

bond vector aligned along the *x* axis of the alignment tensor (θ= 90°, ϕ= 0°). Since D_{xx}^{AB} + D_{yy}^{AB} +D_{zz}^{AB} =0, it follows from Eq. [3-6] that

$$\theta = 0°,\ D_{zz}^{AB} = 2D_a^{AB};$$

$$\theta = 90° \text{ and } \phi = 90°,\ D_{yy}^{AB} = -D_a^{AB}(1 + 1.5\,R)$$

$$\theta = 90° \text{ and } \phi = 0°,\ D_{xx}^{AB} = -D_a^{AB}(1 - 1.5\,R) \qquad [3\text{-}7]$$

Therefore, experimentally, the normalized values of D_{zz} and D_{yy} are obtained by taking the average of the high and low extreme values of the normalized residual dipolar couplings, respectively, such that the standard deviations in the estimated values of D_{zz} and D_{yy} are equal to the measurement error. The value of D_{xx} corresponds to the most populated value in the histogram of the observed normalized residual dipolar couplings. With two unknowns and three observables (D_{xx}, D_{yy}, and D_{zz}), the values of D_a and R are then calculated by nonlinear least squares optimization of Eq. [3-7]. This method is quite useful for macromolecular structure calculation and refinement, while the knowledge of the orientation of the alignment tensor is not required.

For cases where the structure is known, a singular-value decomposition (SVD) approach may be used, which fits the observed RDCs to the known structure (*32, 55*). Eq. [3-5] shows that residual dipolar couplings depend on the average alignment of the molecules. The anisotropic averaging could be represented by an order matrix (*55*)

$$S_{ij} = \left\langle \frac{3\cos\theta_i \cos\theta_j - k_{ij}}{2} \right\rangle, \qquad [3\text{-}8]$$

where θ_i denotes the instantaneous orientation of the *i*th molecular axis with respect to the director (which in the studied case is the direction of the external magnetic field), and k_{ij} is the Kronecker delta. The order matrix is symmetric (S_{ij} = S_{ji}) and traceless (S_{xx} + S_{yy} + S_{zz} = 0), so it has only five independent elements. Therefore, in an arbitrarily chosen molecular frame, the general expression for the residual dipolar coupling D^{AB} could be rewritten as

$$D^{AB} = D_{\max}^{AB} \sum_{ij=\{x,y,z\}} S_{ij} \cos\phi_i^{AB} \cos\phi_j^{AB}, \qquad [3\text{-}9]$$

where $D_{\max}^{AB} = \frac{-\mu_0 h \gamma_A \gamma_B}{8\pi^3} \left\langle r_{AB}^{-3} \right\rangle$ and ϕ_i^{AB} is the angle of the internuclear vector connecting nuclei A and B relative to the *i*th molecular axis. Eq. [3-9] suggests that if the direction cosines of the internuclear vectors in an arbitrary molecular frame are known, it is possible to determine the order parameters, and hence the molecular orientational properties, from just five independent measurements. Knowledge of direction cosines of a sufficient number of internuclear vectors or chemical shift tensors in a particular molecular frame is only available if the local structure of a fragment is known and assumed to be rigid. Therefore for measured RDCs, such a system of linear equations are formed

$$\begin{pmatrix} \cos^2\phi_y^1 - \cos^2\phi_x^1 & \cos^2\phi_z^1 - \cos^2\phi_x^1 & 2\cos\phi_x^1\cos\phi_y^1 & 2\cos\phi_x^1\cos\phi_z^1 & 2\cos\phi_y^1\cos\phi_z^1 \\ \cos^2\phi_y^2 - \cos^2\phi_x^2 & \cos^2\phi_z^2 - \cos^2\phi_x^2 & 2\cos\phi_x^2\cos\phi_y^2 & 2\cos\phi_x^2\cos\phi_z^2 & 2\cos\phi_y^2\cos\phi_z^2 \\ \bullet & \bullet & \bullet & \bullet & \bullet \\ \bullet & \bullet & \bullet & \bullet & \bullet \end{pmatrix} \begin{pmatrix} S_{yy} \\ S_{zz} \\ S_{xy} \\ S_{xz} \\ S_{yz} \end{pmatrix} = \begin{pmatrix} D_{red}^1 \\ D_{red}^2 \\ \bullet \\ \bullet \end{pmatrix}, \qquad [3\text{-}10]$$

where the rows containing the reduced dipolar coupling, D_{red}, are obtained from Eq. [3-9] after division by D_{max}. The number of equations depends on the number of measured angular parameters, but the number of unknowns is always five.

Singular value decomposition (SVD) is a powerful numerical technique for solving systems of linear equations, such as that given in Eq. [3-10], and can be easily implemented for order matrix calculations. If the set of equations has no exact solution, as in an overdetermined linear system ($M > 5$ in this work), the SVD will still produce a solution that will not exactly solve the linear system, but will be the best solution in the least squares sense.

One difficulty encountered in the calculations described above is that experimental uncertainties have to be considered. One way to take this into account is to calculate S_{ij} for several sets of dipole couplings which are sampled from Gaussian distributions centered at the measured values with standard deviations depending on the experimental precisions. The calculated S_{ij} values are then multiplied with the A matrix and are only accepted if the predicted D^{AB} values are within the estimated experimental error. This step is necessary since the SVD method will produce a least squares solution for any set of input data. The width of the resulting distribution of S_{ij} values gives a representation of errors in the derived parameters.

Using NOE-derived structure coordinates for iAβ5^{inv} and observed residual dipolar couplings measured for iAβ5^{inv} in the presence of fibrils is shown in Table 3-5, the five elements of the order matrix were determined using a singular value decomposition approach (*55*), as shown in Table 3-7.

Table 3-7. The calculated order parameters for iAβ5^{inv} bound to Aβ$^{14-23}$/ Aβ$^{1-40}$, respectively.

	iAβ5^{inv} bound to Aβ$^{14-23}$	iAβ5^{inv} bound to Aβ$^{1-40}$
Number of successful steps	475	79
Number of used RDCs	8	10
Order matrix	-1.0949e-04 3.3207e-04 -2.0484e-05	1.3645e-05 1.8146e-04 -9.8683e-05
(Saupe average)	-6.3617e-05 1.7826e-04	-8.9565e-05 3.9474e-05
Principal order matrix	4.7707e-05 2.4279e-04 -2.9049e-04	-4.2724e-05 -1.4087e-04 1.8360e-04
Da (= ½ Szz)	-1.305149e-04	8.920302e-05
Dr (= 1/3(Sxx-Syy)	-7.940946e-05	2.664430e-05
RMS	0.868	1.152
Correlation rate	0.972	0.961

After each set of order parameters was determined and a symmetric tensor formed from them, the tensor was diagonalized to obtain the principal order tensor components, or order parameters, and the transformation matrices that relate the principal order frame to the initial molecular frame are shown in Table 3-8.

Table 3-8. The transformation matrices relating the principal order frame for bound state iAβ5^{inv} to the initial molecular frame.

transformation matrix	iAβ5^{inv} bound to Aβ$^{14-23}$	iAβ5^{inv} bound to Aβ$^{1-40}$
	α β γ	α β γ
1	202.25 44.67 265.07	180.08 119.94 203.72
2	22.25 44.67 265.07	0.08 119.94 203.72
3	337.75 135.33 85.07	359.92 60.06 23.72
4	157.75 135.33 85.07	179.92 60.06 23.72

The orientation of dipolar coupling tensor is described by three Euler angles, defined as follows: alpha, clockwise rotation around z between (0, 360°), leading to a new system x',y',z'; beta, clockwise rotation around y' between (1, 180°), leading to a new system x",y",z"; gamma between (0, 360°), clockwise rotation around z". Four equivalent Euler orientations were reported, due to the sign ambiguity of the eigenvectors.

The set of allowable solutions coming from SVD is plotted as a distribution of points on Sauson-Flamsteed representation, as shown in Fig. 3-30. The blue, green, and red spots depict the direction of the axes (z, y, and x, respectively) of the principal alignment frame relative to the starting structure coordinate frame. The top and bottom tips of the map represent + Z and – Z in the starting structure coordinate frame while + X is in the very centre. The spread of solutions gives an approximate picture of the precision with which the alignment frame can be determined. Two clusters of solutions appear 180° apart for each of axes due to inversion of axes, and four order frames which differ only in the signs of pairs of axes are allowed. The alignment tensor is extremely asymmetric and the directions of all three principal axes of the alignment tensor are well defined, except that inversion of any axis is allowed.

The asymmetry is quantitatively defined by an asymmetry parameter eta (η) that can be written in terms of order parameters S_{ij} ($\eta = (S_{yy} - S_{xx})/S_{zz}$). It is equal to 0.67 and 0.49 for iAβ5^{inv} bound to Aβ$^{14-23}$ and Aβ$^{1-40}$, respectively.

The direction of alignment for the bound ligand is most useful when referenced to the alignment of fibrils. As suggested by Prestegard and co-workers, if fragments of interest experience a common source of order, as they would if they were parts of a rigid ligand-protein complex, the directions and levels of the orienting force should appear the same from the point of view of each fragment when a model for the fragments is assembled with proper fragment orientations (*40, 56, 57*). Therefore, the direction of highest order (S_{zz}) depicted in Fig. 3-30 should coincide with the direction of highest order for the fibril itself. Rotating the molecular frame of iAβ5^{inv} to achieve coincidence then allows determination of the relative orientation of iAβ5^{inv} bound to Aβ fibrils. In the absence of any large conformational flexibility and mobility in the bound state, the order parameters determined from bound iAβ5^{inv} will coincide with the Aβ fibril axis. While amyloid fibrils in the magnetic field are aligned parallel to the magnetic field as determined from x-ray diffraction studies on Aβ fibrils (*43*), the fibril axis for Aβ$^{14–23}$ and Aβ$^{1–40}$ would be identical, namely parallel to the magnetic field. In Table 3-7, the principle order matrices for iAβ5^{inv} bound to Aβ$^{14–23}$ and Aβ$^{1–40}$, respectively, are quite different. This indicates that iAβ5^{inv} adopted different orientations when bound to Aβ$^{14–23}$ and Aβ$^{1–40}$, respectively. This relative orientation is subsequently used as a starting point for the docking studies.

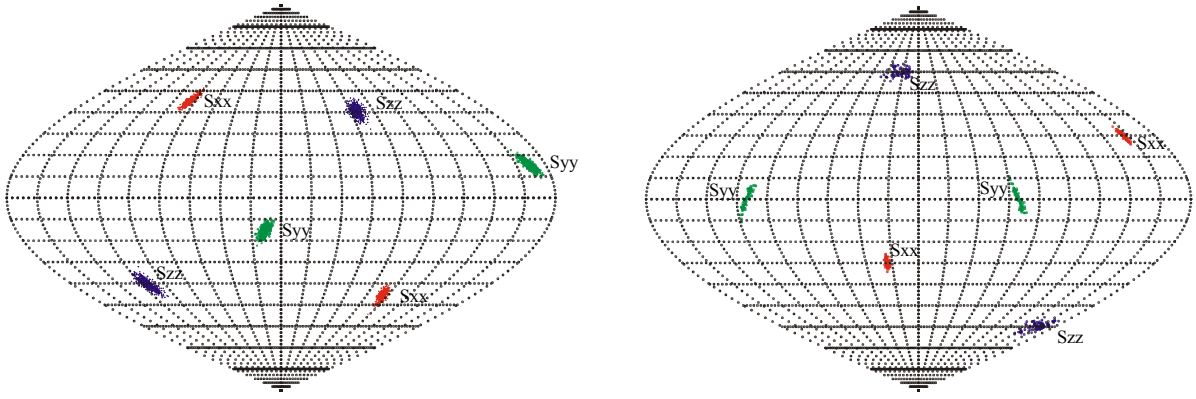

Fig. 3-30. Orientations of the order tensor principal axis systems in the molecular frame as determined via SVD. Panels A and B show the results for iAβ5^{inv} in presence of Aβ$^{14-23}$ and Aβ$^{1-40}$. The Sauson-Flamsteed projection used here maps the surface of a unit sphere into a plane by converting latitude (ϕ) and longitude (λ) to Cartesian coordinates (x, y) via $x = \lambda \cos\phi$, $y = \phi$. The horizontal lines of latitude run from -90° to 90° in 10° increments. Vertical curved lines of longitude run from -180° to 180° in 20° increments. Each point in these plots represents the location, in the molecular frame, of the tip of the x, y, or z unit vector of the order tensor principal axis system.

3.12 Validation of measured trRDCs for iAβ5^{inv} by back fitting to NOE-derived structures.

To validate the measured trRDCs for iAβ5^{inv} in the presence of Aβ fibrils, the measured RDCs were fitted by SVD to NOE-derived structures.

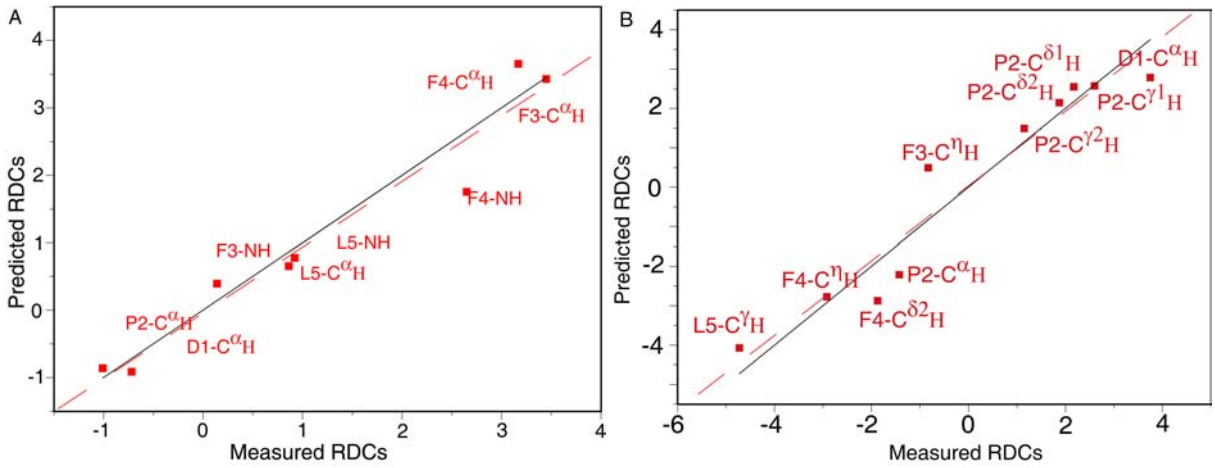

Fig. 3-31. Correlation plot of experimentally measured RDCs versus predicted RDCs from the NOE-derived structures. (A), $^{1}D_{NH}$ and $^{1}D_{CaH}$ RDCs calculated for iAβ5^{inv} bound to Aβ$^{14-23}$, using PDB coordinates DPFFL_Ab1423_SA_5 (see Appendix), are plotted against the RDCs measured in solution. (B), $^{1}D_{CaH}$ RDCs calculated for iAβ5^{inv} bound to Aβ$^{1-40}$, using PDB coordinates DPFFL_Ab40_SA_19 (see Appendix), are plotted against the RDCs measured in solution.

Fig. 3-31 shows the correlation between the experimental RDCs of iAβ5^{inv} with the RDCs calculated from NOE-derived structures. The predicted residual dipolar coupling values in Fig. 3-31 were calculated using an alignment tensor derived from observed RDCs by singular value decomposition (SVD) implemented in Pales (*58*). The slope close to 1 and modest scatter (correlation coefficient of 0.972 and 0.962 for iAβ5^{inv} bound to Aβ$^{14-23}$ and Aβ$^{1-40}$, respectively) confirm that the obtained trRDCs in our studies are real, not due to experimental errors.

In principle, correlation plots of structurally predicted RDCs versus measured RDCs would be expected to have a slope of unity (solid lines in Fig. 3-31A, B). The slopes fitted here are, however, less than 1.0 (dashed lines in Fig. 3-31A, B). This attenuation has been attributed to structural uncertainty that diminishes the apparent degree of alignment. Deviations of measured RDCs from those calculated from a structure can arise from static or dynamic differences. Dynamic structural averaging over time scales ranging from picoseconds to several milliseconds can affect RDCs as well (*59*).

3.13 The docking model of iAβ5/ iAβ5^{inv} bound to Aβ fibrils.

The bound state peptide conformations were docked to the Aβ fibril structures as described in Methods. For selection of suitable structural templates for the Aβ fibrils, we used the structural model of Aβ$^{14-23}$ fibrils provided by Tjernberg *et al.*(*5*) and the structural model of Aβ$^{1-40}$ fibrils provided by Petkova *et al.*(*10*). Aβ$^{1-40}$ fibrils are characterized by parallel in-register β-strand orientation. This model is based on experimental solid state NMR data. The structural model of Aβ$^{14-23}$ fibrils has the antiparallel β-strand orientation based on the molecular modeling, which has a 17 + k ↔ 21 – k registry (i.e. intermolecular hydrogen bonds between residues 17 + k and 21 – k of adjacent peptide chains, for integer k). Subsequently, Tjernberg *et al.* have investigated the registry of hydrogen bonding in antiparallel β-sheets for Aβ$^{14–23}$ fibrils through a combination of predictions based on the statistical analyses by Wouters & Curmi and experimental studies of the aggregation of β-hairpin peptides constrained to favor particular registries (*60*). The results of Tjernberg *et al.* indicate that, in the context of designed β-hairpins, the Aβ$^{14–23}$ sequence can be made to adopt both 17 + k ↔ 20 – k and 17 + k ↔ 21 – k registries in amyloid fibrils at pH 7.4. More recently, Petkova *et al.* reported a pH-dependent antiparrallel β-sheet registry in fibrils formed by Aβ$^{11-25}$ (*4*). In their study, 17 + k ↔ 20 – k and 17 + k ↔ 22 – k registries were determined based on experimental solid-state NMR data for Aβ$^{11-25}$ at pH 7.4 and pH 2.4, respectively. By using the information theory formalism provided by Steward and Thornton, Tycko and co-workers investigated the registry of antiparallel β-sheets formed by Aβ$^{11-25}$. According to their calculation, 17 + k ↔ 20 – k and 17 + k ↔ 21 – k were the two most likely registries, corresponding to the experimental results for Aβ$^{16–22}$ and Aβ$^{11–25}$ fibrils at pH 7.4. The same calculation was performed with substitution of E22 by Q22 and D23 by N23 in the peptide sequence in order to mimic the effects of low pH. The resulting data showed that 17 + k ↔ 21 – k and 17 + k ↔ 22 – k registries have increased likelihood, where 17 + k ↔ 22 – k registry was observed experimentally within Aβ$^{11–25}$ fibrils at pH 2.4 by Petkova *et al.*. Taken together, 17 + k ↔ 21 – k registry in Aβ$^{14-23}$ provided by Tjernberg *et al.* (*5*) is a good model to describe the structure of Aβ$^{14-23}$ fibrils at pH 4 in the absence of solid-state NMR experimental data.

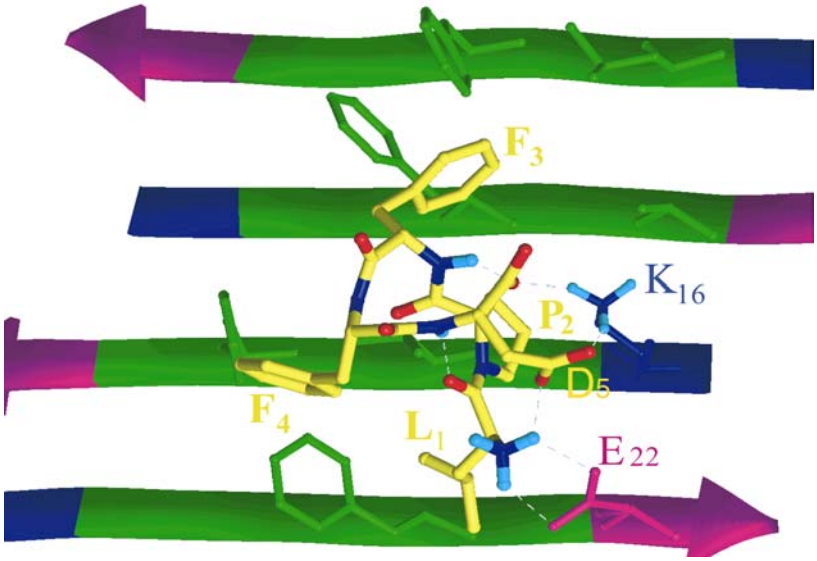

Fig. 3-32A. The docking models of NMR structure of iAβ5 bound to $A\beta^{14-23}$.

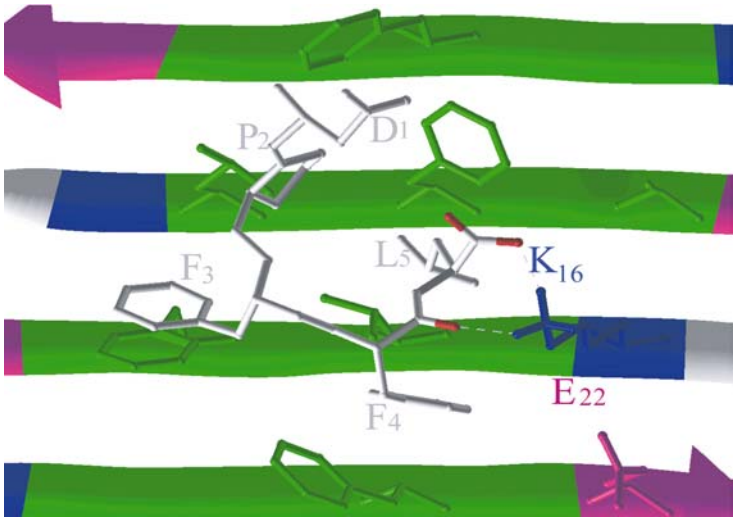

Fig. 3-32. The docking models of NMR structure of $iA\beta5^{inv}$ bound to $A\beta^{14-23}$, with the orientational restraint obtained from trRDC data.

Fig. 3-32 shows the docking model of iAβ5 and $iA\beta5^{inv}$ with $A\beta^{14-23}$, respectively. For iAβ5 (Fig. 3-32A), L1 interacts with $F19_{(I)}$, the carboxylic acid of D5 is interacting with $K16_{(I+1)}$, whereas the N-terminus of iAβ5 is interacting with $E22_{(I)}$ of the amyloid $A\beta^{14-23}$. Here, I or I + 1 is referring to successive β-strands in the fibril structure. For $iA\beta5^{inv}$ (Fig. 3-32B), the C-terminus of D1 is interacting with $K16_{(I+1)}$. There, D_1 is occupying the same binding site as D5 in the case of iAβ5. Moreover, L5 of $iA\beta5^{inv}$ is interacting with $F19_{(I)}$. A similar interaction is found in the case of L1 of iAβ5. Furthermore, the common central residues PFF of both peptides iAβ5 and $iA\beta5^{inv}$ contain similar side chain-side chain contacts. Peptide/fibril interaction sites are $P2/V18_{(I+1)}$, $F3/F19_{(I+2)}$, $F4/V20_{(I+1)}$. We obtain the lowest energies for

docking, if iAβ5 and iAβ5^{inv} are interacting at the same binding sites of Aβ$^{14-23}$. We find that iAβ5 displays more interactions to Aβ$^{14-23}$ than iAβ5^{inv} (one more attractive electrostatic interaction). This is also reflected in the trNOESY cross-relaxation data which contain indirect information on the dissociation of the ligand-fibril complex. Larger cross peaks were observed for iAβ5 bound to Aβ$^{14-23}$ than in the case of iAβ5^{inv}.

From the docking model, one would assume the same interaction strengths for iAβ5 and iAβ5^{inv} bound to Aβ$^{1-40}$. However, the presence of Aβ$^{1-40}$ fibrils induces significant line broadening on the resonances of iAβ5. This could be due to a structural variation of Aβ$^{1-40}$ in the fibrillar state. Different side chain orientations might change the number of hydrophobic and electrostatic interactions and therefore yield a different value for K_D. However, the NMR spectrum of iAβ5 bound to Aβ$^{1-40}$ showed extreme line broadening and was not effectively excited by the radio frequency pulses used in the trNOESY experiment. The magnetization flow from a peptide proton to Aβ fibrils will decrease the intensity of magnetization observed during the detection time. This would explain why we could not obtain a high resolution trNOESY spectrum of iAβ5 bound to Aβ$^{1-40}$.

As mentioned in section 3.9, iAβ5^{inv} shows completely different structures when bound to Aβ$^{14-23}$ and Aβ$^{1-40}$, respectively. One can easily figure out this is due to the different fibril structures adopted by Aβ$^{14-23}$ and Aβ$^{1-40}$. The different interaction patterns could be clearly seen in the docking models. Fig. 3-33A shows the antiparallel organization of the β-strands along the fibril axis for the short amyloid peptide Aβ$^{14-23}$ and it shows that the central residues L^{17}VFFA form a hydrophobic core at a single molecular layer. This hydrophobic block is flanked by alternating patterns of positive and negative charges caused by the charged C-terminal (K16) and N-terminal (E22, D23) residues. These systematic alternations of charges are responsible for interaction of such building blocks along and orthogonal to the fibril axis.

The parallel orientation of the β-strands along the fibril axis for the full-length amyloid peptide Aβ$^{1-40}$ (Fig. 3-33B) shows completely different interaction patterns of the building blocks. The two β-strands of a cross β-motif are separated by a 180° bend and form two in-register parallel β-sheets which interact through mainly hydrophobic side chain contacts. At one surface of a single molecular layer (cross-β unit) the positively charged (K16) and the negatively charged (D22) residues of the first β-strand (9-22) are arranged each in a row along the fibril axis. The two charged rows are separated by a hydrophobic and an aromatic row

(V18, F20). Hydrophobic side chains of the second β-strand (30-40) form a hydrophobic face at the opposite side of the cross-β unit.

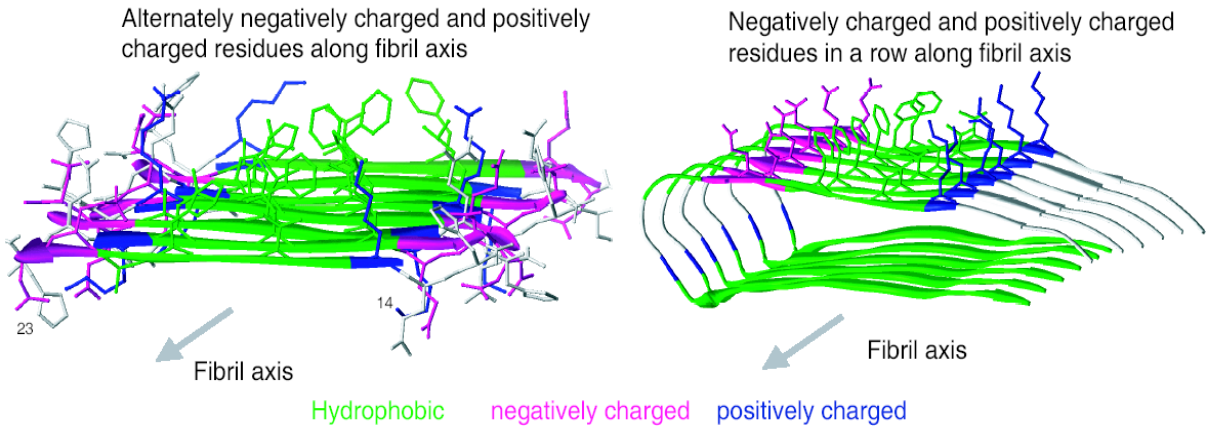

Fig. 3-33. Different interaction patterns of the fibril building block models for $A\beta^{14-23}$ (left) and $A\beta^{1-40}$ (right).

According to the observed RDC data for $iA\beta5^{inv}$, we were able to calculate the alignment tensor of the identified NMR structure. As suggested by Prestegard and co-workers, the direction of axes of the principal order frame for the ligand must coincide with that of the protein (*40, 56, 61*). The orientation of the fibril axis was observed to be parallel to the magnetic field (z-axis) (*43*). Therefore, $iA\beta5^{inv}$, when positioned so that the experimentally determined symmetry axes are aligned as shown in Fig. 3-30 should be oriented along the symmetry axis of the fibrils. This constraint places restrictions on the relative orientations of $iA\beta5^{inv}$ with respect to fibrils and allows two general orientations of $iA\beta5^{inv}$ towards the hydrophilic phase of the amyloid $A\beta^{1-40}$ molecule at a single layer as shown in Fig. 3-34. The orientation where the two negative charges of the ligand are oriented towards the row of positive charged lysines (K16) is energetically preferred to the opposite ligand orientation (allowed rotation around the Z-axis), where the N-terminal positive charge is interacting with the row of negative charges (E22). In detail, the negative charges at D1 and the C-terminus of the ligand $iA\beta5^{inv}$ are interacting with $K16_{(I+2)}$ and $K16_{(I+3)}$ respectively (row of positive charges) of the amyloid. Furthermore, the aromatic residues F4, F3 of the ligand are oriented towards the row of aromatic residues $F20_{(I)}$, $F20_{(I+1)}$), $F20_{(I+2)}$ coming from three successive β-strands (I, I+1, I+2). The hydrophobic residue L5 dives in between the row of hydrophobic ($V18_{(I+2)}$) and the aromatic residues.

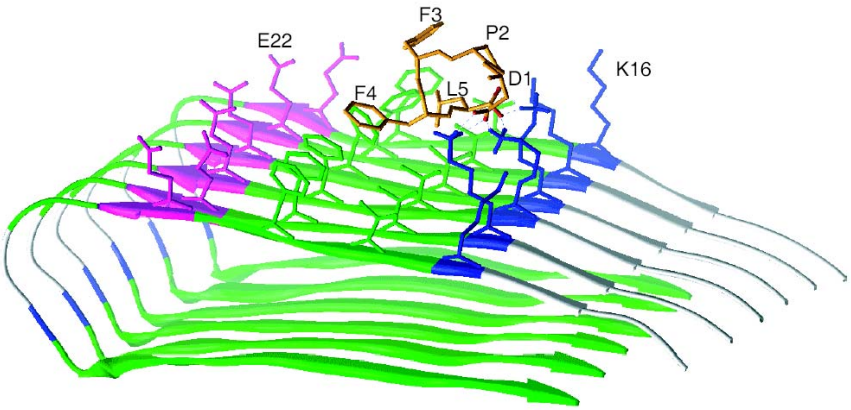

Fig. 3-34. The model of NMR structure of iAβ5^{inv} bound to Aβ$^{1-40}$ fibrils with the orientational restraints from trRDC data.

In general, peptide inhibitors are occupying the amyloid fibrils at the identified binding sites and are therefore disturbing key sites for the oligomerization of the amyloids.

Amyloid fibrillization is generally considered to be driven by hydrophobic and electrostatic interactions (*62, 63*). Residues 17–21 are the hydrophobic segment that is identified to be essential for fibril formation as mentioned above. The in-register parallel alignment of Aβ$^{1–40}$ (*10*) and 17 + k ↔ 21 – k registry of Aβ$^{14-23}$ (*5*) within the β-sheets in the fibrils maximize the hydrophobic contacts of these segments. The only charged side chains in the core of the structure in Aβ$^{1–40}$, D23 and K28, form a salt bridge that may stabilize the structure. All other potentially charged side chains are at positions where they could be solvated as the fibrils grow. This salvation effect overwhelms the electrostatic repulsions between like charges that are implicated in the in-register alignment. In our MD ligand/fibrils docking model, iAβ5^{inv} is located at the hydrophobic core of Aβ. Residue K16 and F20 from Aβ fibrils serve as an anchor for iAβ5^{inv}. We speculate that the hydrophobic and electrostatic interactions between iAβ5 and Aβ fibrils weaken the interactions between Aβ·Aβ strands, therefore destabilize the amyloid structures.

3.14 Structural studies of Aβ$^{14-23}$ by ^{19}F NMR

^{19}F, as a selective marker, has properties that make its use attractive for NMR spectroscopy. First, fluorine is a spin-1/2-nucleus and is present at 100% natural abundance, and, among common nuclei, has a sensitivity to NMR detection that is second only after that of the proton. Second, fluorine NMR is characterized by an extremely wide range of chemical shifts, with the shift being highly responsive not only to changes in chemical bonding within the structure that holds the fluorine nucleus but also to changes in the local environment which would be

the result of protein binding. Third, the **van der Waals** radius of covalent fluorine is about 0.14 nm, only slightly larger than that of hydrogen, so that replacement of single hydrogen by fluorine is not expected to have a major structure-disrupting effect. Fourth, perhaps most important for studies of biological systems is that with in vitro systems there are no fluorine background signals to interfere with the spectroscopy in the way that the water signal intrudes in proton NMR experiments. Moreover, in vivo concentrations of fluorine are sufficiently low that there are no background problems in these systems either.

In our studies, $A\beta^{14-23}$ was ^{19}F labelled in the para-position of the aromatic ring of Phe19. Furthermore, iAβ5 was synthesized with ^{19}F labelled in the para-position of the aromatic ring of Phe3. The 1D solution ^{19}F NMR spectrum of iAβ5 shows two resonances (Fig. 3-35A). The two resonances arise from two conformations of iAβ5 due to the *trans* and *cis* conformation of Pro residue, which is also reflected in the respective ^{1}H spectra as shown in Fig. 3-8. Two signals can be observed in the 1D ^{19}F spectrum of $A\beta^{14-23}$ (Fig. 3-35B). The signal at 119.59 ppm (indicated as an asterisk) is due to an impurity, since it does not show a characteristic splitting of the signal into a triplet in the ^{1}H-coupled experiment. As we can see, ^{19}F resonances from iAβ5 and $A\beta^{14-23}$ are separated and the system can be used for titration experiments.

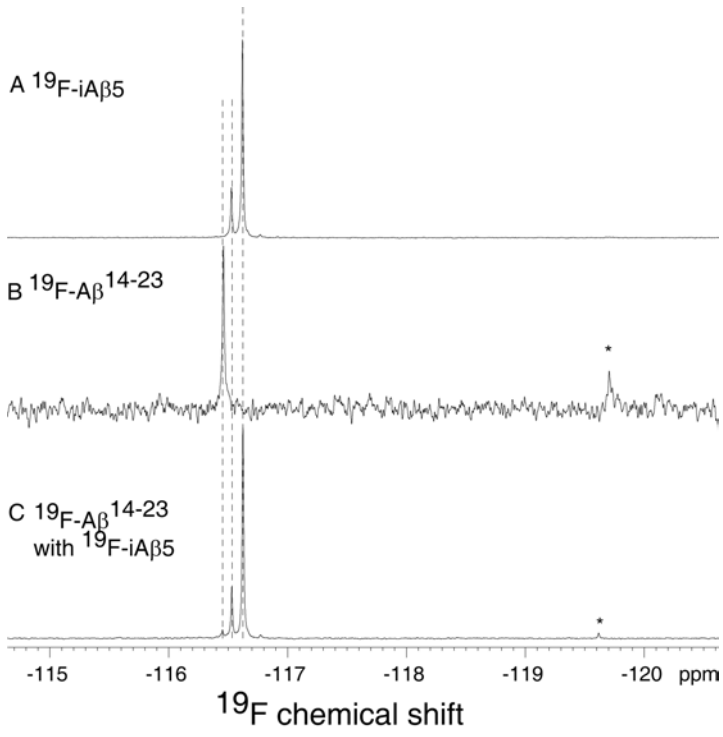

Fig. 3-35. 1D ^{19}F spectrum for ^{19}F-iAβ5 (a), ^{19}F-$A\beta^{14-23}$ without (b) and with (c) ^{19}F-iAβ5 at 1 mM concentration and in 10 mM phosphate buffer at pH 7, 15°C. Spectrum A, B and C were recorded at 12 °C with 3116, 5475 and 3116 scans, respectively.

Titration experiments were carried out by incubation of aqueous ^{19}F-Aβ$^{14-23}$ solutions at concentration of approximately 1mM, at room temperature, using 10 mM phosphate sodium buffer at pH 7. ^{19}F-iAβ5 was dissolved in the same buffer at a concentration of 1 mM. 500 µl of ^{19}F-iAβ5 and fibrillized sample (10% D_2O) were measured by ^{19}F NMR techniques, respectively. Other samples were prepared using 450 µl ^{19}F-iAβ5 (50 µl D2O) and adding 250 µl, 450 µl, 500 µl of a 1 mM ^{19}F-Aβ$^{14-23}$ stock solution, respectively. As can be seen in Fig. 3-36, the resonances originating from ^{19}F-iAβ5 decrease upon addition of ^{19}F-Aβ$^{14-23}$. It is interesting to note that the relative intensity of the two signals of ^{19}F-iAβ5 was constant over the whole titration at the same temperature. Once the temperature was increased to 52 °C, the population of the *cis* conformer increased, while the ratio of *cis*/*trans* returned to the previous value once the temperature was lowered to 12 °C. However, we can not conclude that the reduced population of the *trans* conformer is due to a stronger binding of the *trans* conformer to the fibrils at higher temperature. To do so, a reference spectrum would have to be recorded on ^{19}F-iAβ5 at 52°C.

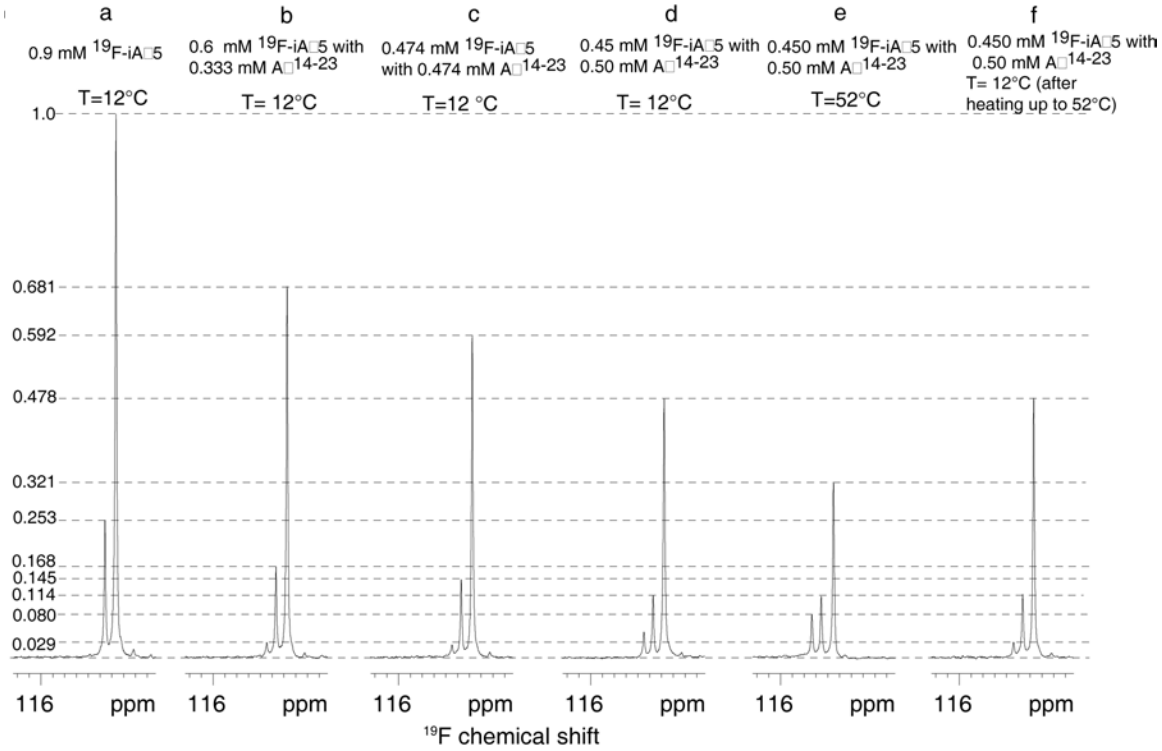

Fig. 3-36. Titration of ^{19}F-iAβ5 with ^{19}F-Aβ$^{14-23}$ as observed by ^{19}F NMR. Peaks at –116.63 ppm and –116.54 ppm came from iAβ5, corresponding to the *trans* and *cis* conforms. Peak at –116.45 ppm came from Aβ$^{14-23}$.

The 1D ^{19}F solid-state spectrum (Fig. 3-37) of fibrillized ^{19}F-Aβ$^{14-23}$ displays a n=0 rotational resonance effect, which is characteristic for two dipolar coupled spins with vanishing

chemical shift difference. The asterisk indicates the isotropic chemical shift of residual TFA in the sample which was used as an internal reference.

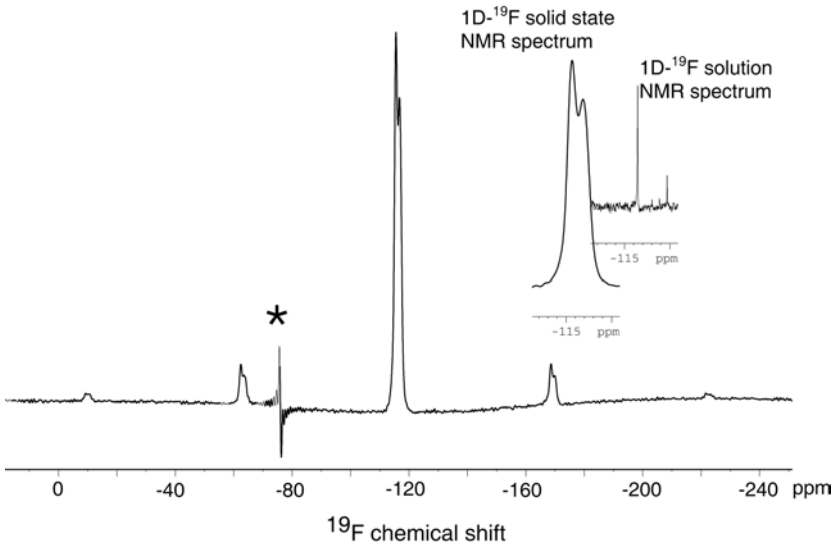

Fig. 3-37. 1D ^{19}F solid-state NMR spectrum of fibrillized ^{19}F-Aβ$^{14-23}$. 46 mg ^{19}F-Aβ$^{14-23}$ was dissolved in 115 ml 10 mM PO_4^{3-} buffer at pH 7, at room temperature. Two weeks later, sample solution was centrifuged and the pellet was packed into 4 mm rotor. The spectrum was recorded on a Bruker 400 MHz solid-state spectrometer in Karlsruhe, Germany.

1D ^{19}F solid-state NMR spectrum shows signs of two dipolar coupled spins in the fibrils. The spinning sideband line shapes in the 1D spectrum contain information about the relative orientation of the Phe-rings.

2D ^{19}F,^{19}F DQF and Post C7 experiments were recorded for a sample of fibrilized ^{19}F-Aβ$^{14-23}$ on a Bruker 600 MHz solid-state spectrometer. 46 mg ^{19}F-Aβ$^{14-23}$ was dissolved in 115 ml 10 mM PO_4^{3-} buffer at pH 7, at room temperature. Two weeks later, the peptide solution was centrifuged and the pellet was packed into a 2.5 mm rotor. The power on the fluorine channel during the Post-C7 mixing was adjusted to 108.7 kHz, corresponding to a MAS frequency of 15 kHz. The decoupling power was set to 41.6 kHz to avoid Hartmann-Hahn matching.

The data were fit using the relation

$$J(t_1) = \int_0^{\pi} d\beta \sin\beta \sin^2\left(k b_{FF} \sin^2 \beta t_1\right) \exp\left(-1/T_2^{eff}\right) \qquad [3\text{-}11]$$

for the dephasing signal. k corresponds to the scaling factor of Post-C7, and b_{FF} to the ^{19}F-^{19}F dipolar coupling: $b_{FF} = \mu_0 \gamma \hbar / 4\pi r_{FF}^3$.

Preliminary data is shown in Fig. 3-38.

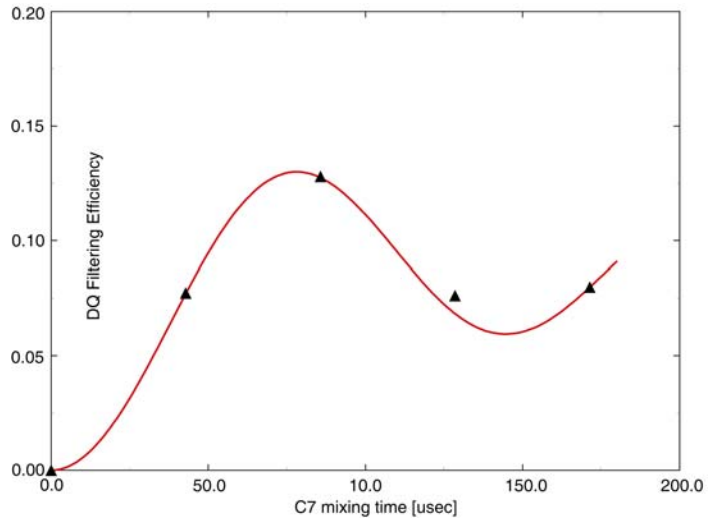

Fig. 3-38. Fit parameters for the least squares fitting in the ^{19}F-^{19}F DQ filtered dephasing signal were b_{FF}=16 kHz (2.0 Å), $1/T2_{eff}$ = 200 Hz and a DQ filtering efficiency of 13%.

From the simulation, we obtain a 2.0 Å for the ^{19}F-^{19}F internuclear distance between two peptides within the fibrils. In the structural models of fibrils formed by this sequence presented by Tjernberg *et al.* (*5*), the shortest ^{19}F-^{19}F distance between two strands within one sheet would be expected to be 5.5 Å. According to these models, the possible shortest ^{19}F-^{19}F distance between two layers is about 2 Å.

3.15 Structural studies of *de novo* designed peptide-based amyloid fibrils by solid-state NMR.

Recently, many efforts directed towards searching a higly simplified system that is able to polymerize into β-sheets. The idea behind it is that the such a simplified system could offer additional insights into the molecular details of amyloid fibril formation which may be common to all fibril formation process of amyloidogenic proteins or peptides.

A series of self-associating hexapeptides with a high propensity to form homopolymeric β-sheets were computer-designed by Paz *et al*. (*64, 65*). Sequences predicted to be highly favorable on this basis were found experimentally to self-associate efficiently into β-sheets. To probe the interactions driving β-sheet aggregation, the effect of specific residues on the propensity of given sequence to form amyloid fibrils was investigated. It is found out that the property to form polymeric β-sheets is not a sufficient requirement for fibril formation because, under the conditions used, preformed β-sheets from these peptides with charged residues form well defined fibrils only if the total net charge of the molecule is ± 1. A detailed

structural model of the fibrils was proposed from their results, in conjunction with x-ray fiber diffraction, electron microscopy, and Fourier transform infrared measurements.

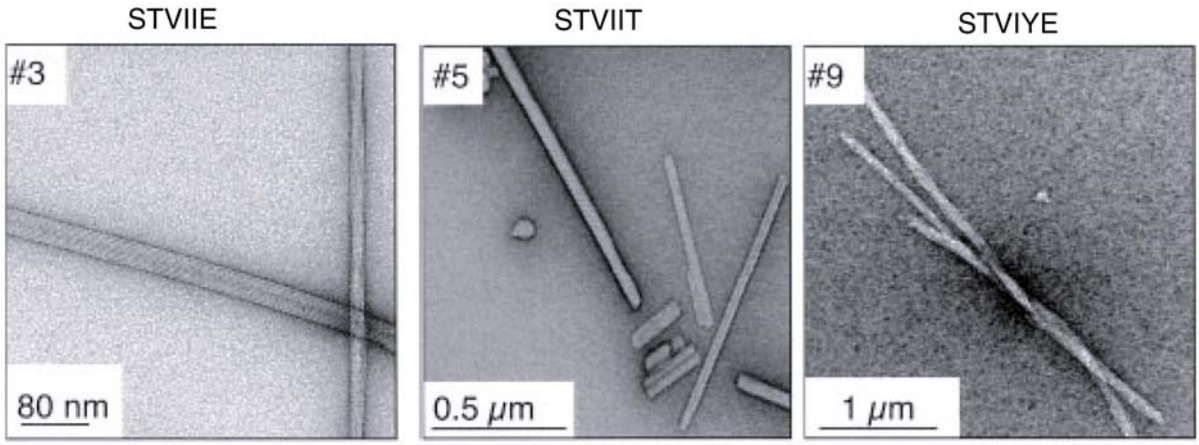

Fig. 3-39. Electron micrographs of negatively stained fibrils from samples where the net charge on the molecules is + 1. (*65*)

Interestingly, in their studies, two hexapeptides which have a single-point mutation form fibrils which have different morphologies under the same polymerization conditions, e.g., the fibrils formed by STVIYE sequence is twisted while fibrils formed by STVIIT is more flatter (Fig. 3-39). Why the β-sheets that make up the protofilaments are twisted or flat could not be answered from the data obtained in their studies. In this work, we suggest to take the advantages of solid state NMR technique to studies the fibrils formed from these hexapeptides, in order to extract more detailed structural information for these systems which would be useful for understanding of the driving forces involved in the formation of these organized assemblies rich in β-sheet structure.

Fig. 3-40 shows 2D ^{13}C-^{13}C correlation spectrum of uniformly ^{13}C-enriched STVIIE peptide, recorded under high-speed magic angle spinning (MAS) and with recoupling of ^{13}C–^{13}C dipolar interactions during a exchange period of 15 ms (see Materials and Methods). Strong cross peaks in these spectra connect isotropic chemical shifts of directly bonded, ^{13}C-labelled carbon sites. Based on the chemical structure and characteristic chemical shift ranges of the amino acid side-chains, site-specific assignments of each resonance are readily obtained. However, for a spectrum recorded using a exchange period of 200 ms, there are some additional cross peaks as shown in Fig. 3-41, which is discussed below.

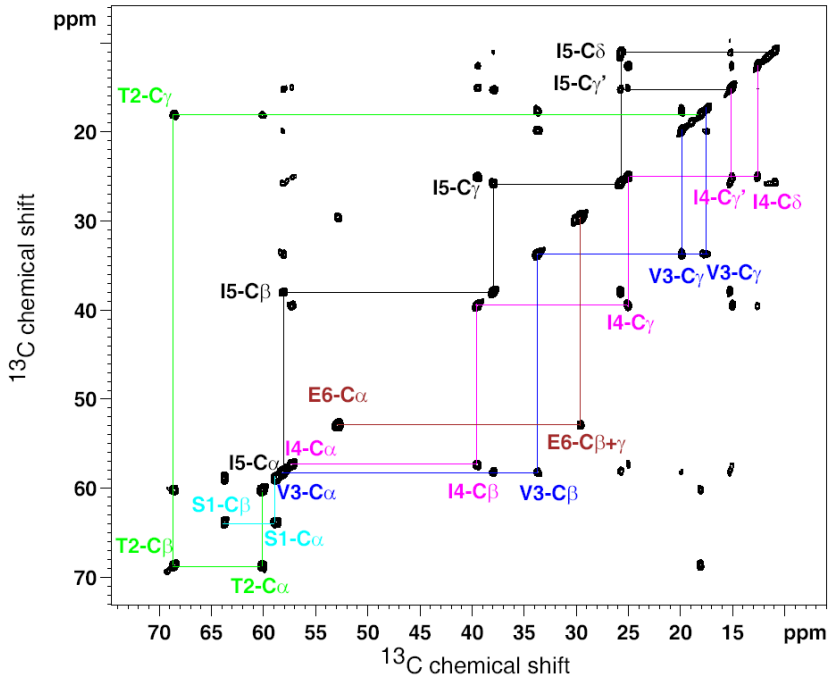

Fig. 3-40. 2D ^{13}C-^{13}C correlation NMR exchange spectrum of 10 mg STVIIE fibrils with uniform ^{13}C and ^{15}N-labelling, prepared at pH 2.6, observed at 14.1 T, with a mixing time of 15 ms, a MAS frequency of 11 kHz and ^{1}H/^{13}C cross-polarization time of 1.8 ms. Chemical shifts assignment pathways that connect strong one-bond, intraresidual cross peaks are shown.

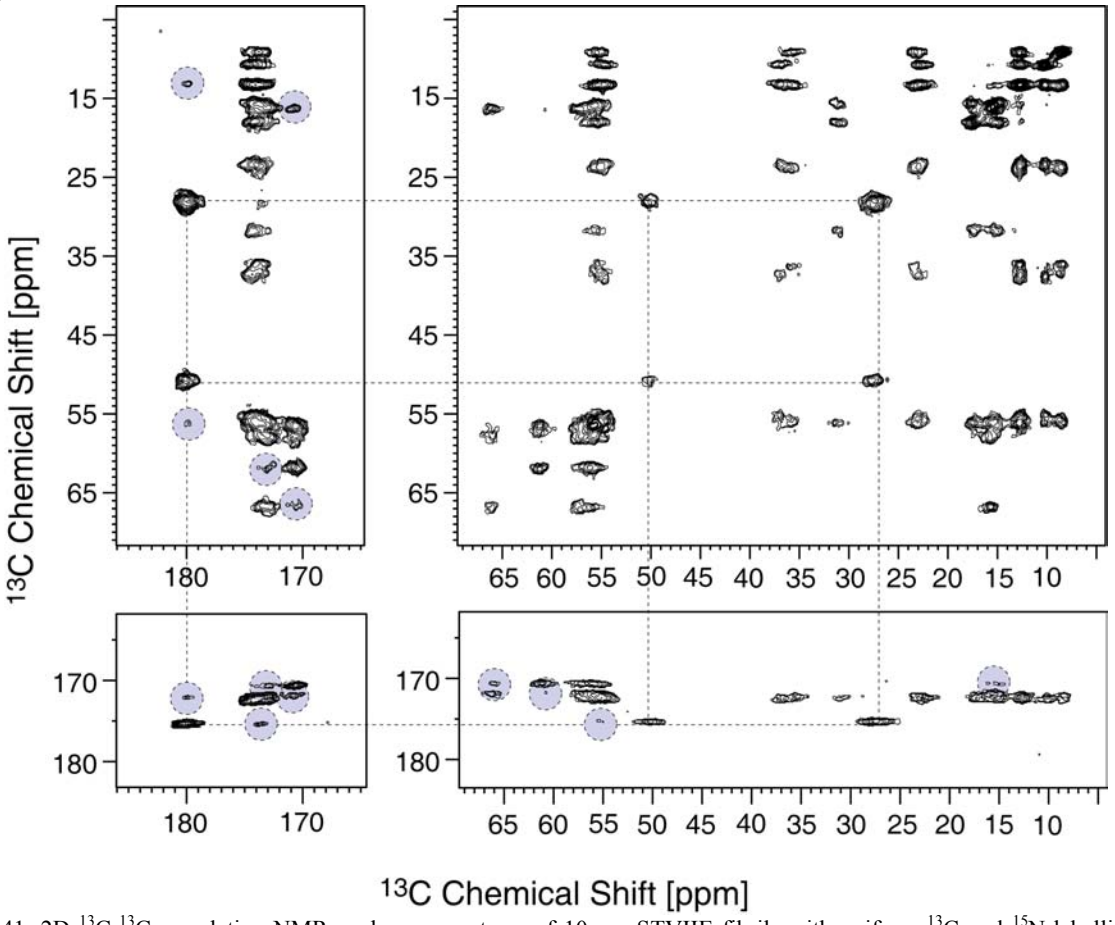

Fig. 3-41. 2D ^{13}C-^{13}C correlation NMR exchange spectrum of 10 mg STVIIE fibrils with uniform ^{13}C and ^{15}N-labelling, prepared at pH 2.6, observed at 14.1 T, with a mixing time of 200 ms, a MAS frequency of 11 kHz and ^{1}H/^{13}C cross-polarization time of 1.8 ms. Marked resonances are unassigned interresidual contacts.

Higher resolution in the C^{α}-C' region was achieved in an experiment using homonuclear decouplings. In Fig. 3-42A, there is no resolution for $C^{aliphatic}$-C' region of the spectrum recorded without homonuclear decouplings. When applying homonuclear decoupling, the resolution of the spectrum (Fig. 3-42B) was enhanced up to a factor of 2-2.5. The enhanced resolution in the spectrum allows unambiguous assignment of all resonances as shown in Fig. 3-43.

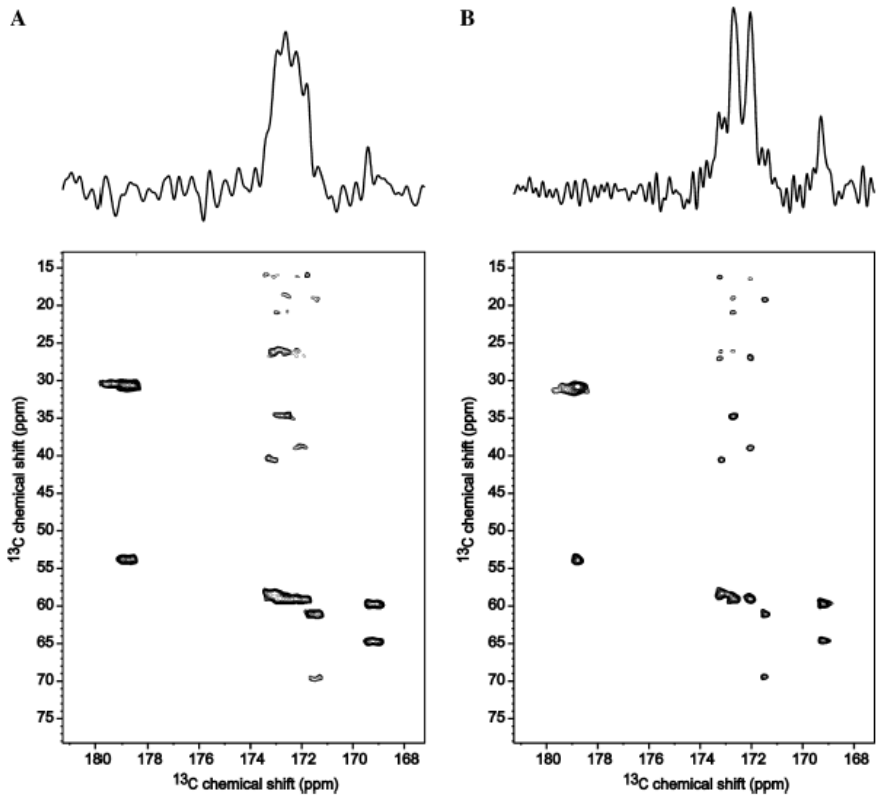

Fig. 3-42. $C^{aliphatic}$-C' regions of two PDSD spectra of fibrillized u-^{13}C,^{15}N-STVIIE using a mixing time of 15 ms. (A) Reference spectrum, recorded without homonuclear *J* decoupling. (B) Spectrum recorded with homonuclear *J* decoupling in both dimensions according the pulse sequence represented in Materials and Methods. The row on top of the spectra represents a trace through the C^{a} spectral region at 59.1 ppm. All spectra were recorded at the same experimental conditions. The MAS frequency was set to 11 kHz, temperature was adjusted to 273 K and TPPM of 90 kHz was used for heteronuclear decoupling in both dimensions.

The pulse sequence used in the experiment allows us to detect the intraresidual cross peaks. However, some interresidual cross peaks were observable as highlighted in Fig. 3-41 and Fig. 3-43. The PDSD experiment using a mixing time of 200 ms allows more such cross peaks observed as listed in Table 3-9. These peaks may be the intermolecular contacts, which may provide information about peptide packing in the fibrils.

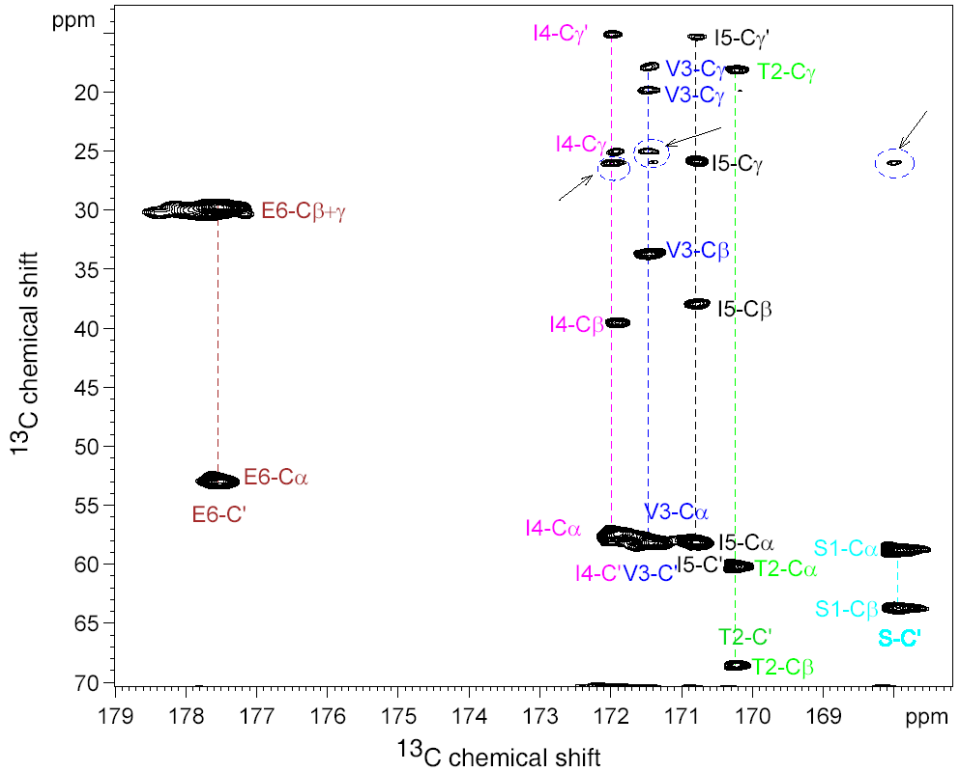

Fig. 3-43. Expanded $C^{aliphatic}$-C' region of 2D ^{13}C-^{13}C NMR exchange spectrum of 10 mg u-^{13}C,^{15}N-STVIIE fibrils recorded with selective homonuclear ^{13}C decoupling. The sample was prepared at pH 2.6. The experiment was carried out at 14.2 T, with a mixing time of 15 ms, a MAS frequency of 11 kHz and $^{1}H/^{13}C$ cross-polarization time of 1.8 ms. Resonance assignment was shown by the $C^{aliphatic}$-C' connectivities. The highlighted cross peaks are due to interresidual contacts.

Table 3-9. Interresidual contacts observed in two PDSD spectra of fibrillized u-^{13}C,^{15}N-STVIIE using a mixing time of 200 ms and 15 ms, respectively.

	T_{mix} = 200 ms	T_{mix} = 15 ms
Ser1-C'	T2-C^{γ}	I5-C^{γ}
Thr2-C'	Ser1-C^{β}, V3-C^{γ}, I4/I5-$C^{\gamma'}$, I4/I5-C^{γ}	
Val3-C'	I4-C^{δ}, I5-C^{δ}, I4/I5-$C^{\gamma'}$, I4/I5-C^{γ}, I4-C^{β}	I4-C^{γ}, I5-C^{γ}
Ile4-C'	I5-C^{δ}, V3-C^{β}	I5- C^{γ}
Glu6-C'	I4/I5-C^{γ}	

Amide ^{15}N chemical shifts can be assigned from 2D ^{15}N–^{13}C correlation spectra as shown in Fig. 3-44. Experimentally determined ^{13}C and ^{15}N isotropic chemical shifts (δ_{ex}) are summarized in Table 3-10, which also lists the random coil chemical shifts (δ_{rc}) reported by Wüthrich *et al* (*66*). Previous solid-state NMR and solution NMR studies have demonstrated that ^{13}C secondary shifts $\Delta\delta = \delta_{ex} - \delta_{rc}$ are reliable indicators of secondary structure in peptides and proteins. For all residues in the peptide, the $\Delta\delta$ values are negative for carbonyl and α-carbon sites and positive for β-carbon sites. These secondary shifts indicate a β-strand conformation for the peptide and are consistent with the CD data reported by Paz *et al*. (*65*).

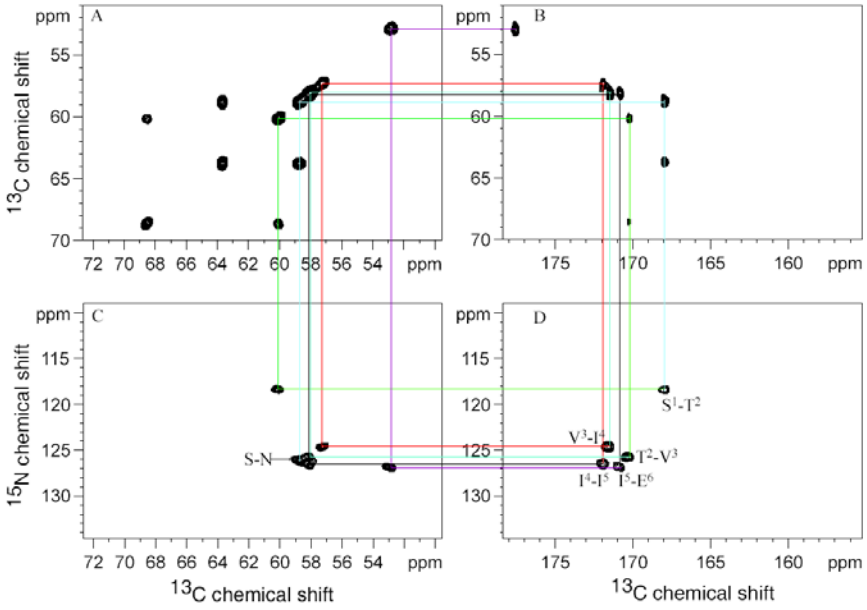

Fig. 3-44. ^{15}N-^{13}C spectrum of STVIIE. A, C^a-C^a region of 2D ^{13}C-^{13}C correlation spectrum without homonuclear decoupling. B, C'-C^a region of 2D ^{13}C-^{13}C correlation spectrum with homonuclear decoupling. C, N-C^a region of ^{15}N-^{13}C correlation spectrum. D, N-C$^{'}$ region of ^{15}N-^{13}C correlation spectrum.

Table 3-10. ^{15}N and ^{13}C NMR chemical shifts in STVIIE fibrils.

Residue	N	CO	αC	βC	γCH$_2$	γCH$_3$	δCH$_x$
Ser1	126.046 (115.62)	167.934 (172.6)	58.696 (56.6)	63.659 (62.3)			
Thr2	118.356 (113.93)	170.316 (172.7)	60.047 (60.2)	68.505 (68.3)	18.024 (20.0)		
Val3	125.657 (119.14)	171.55 (174.9)	58.005 (60.7)	33.664 (30.8)		17.3 (18.5) 19.81 (19.3)	
Ile4	124.541 (119.82)	171.922 (174.3)	57.23 (59.6)	39.420 (36.9)	24.979 (25.4)	15.008 (15.7)	12.536 (11.3)
Ile5	126.44 (119.82)	170.871 (174.3)	58.005 (59.6)	37.874 (36.9)	25.702 (25.4)	15.202 (15.7)	10.861 (11.3)
Glu6	126.874 (119.77)	178.107 (174.3)	52.787 (54.9)	29.530 (28.9)	29.530 (34.6)		

(Values in parentheses are random coil shifts (*66, 67*))

Moreover, *de novo* designed peptides STVIIT and STVIYE have been reported to form amyloid fibrils similar to that formed by STVIIE. Only more flatter morphology has been observed for fibrils formed by STVIIT.

1D ^{13}C MAS spectra were recorded on fibrils formed from STVIIT and STVIYE peptides at natural abundance (Fig. 3-45). Spectral assignment was done with the aid of the assignment of 1D ^{13}C spectrum of STVIIE.

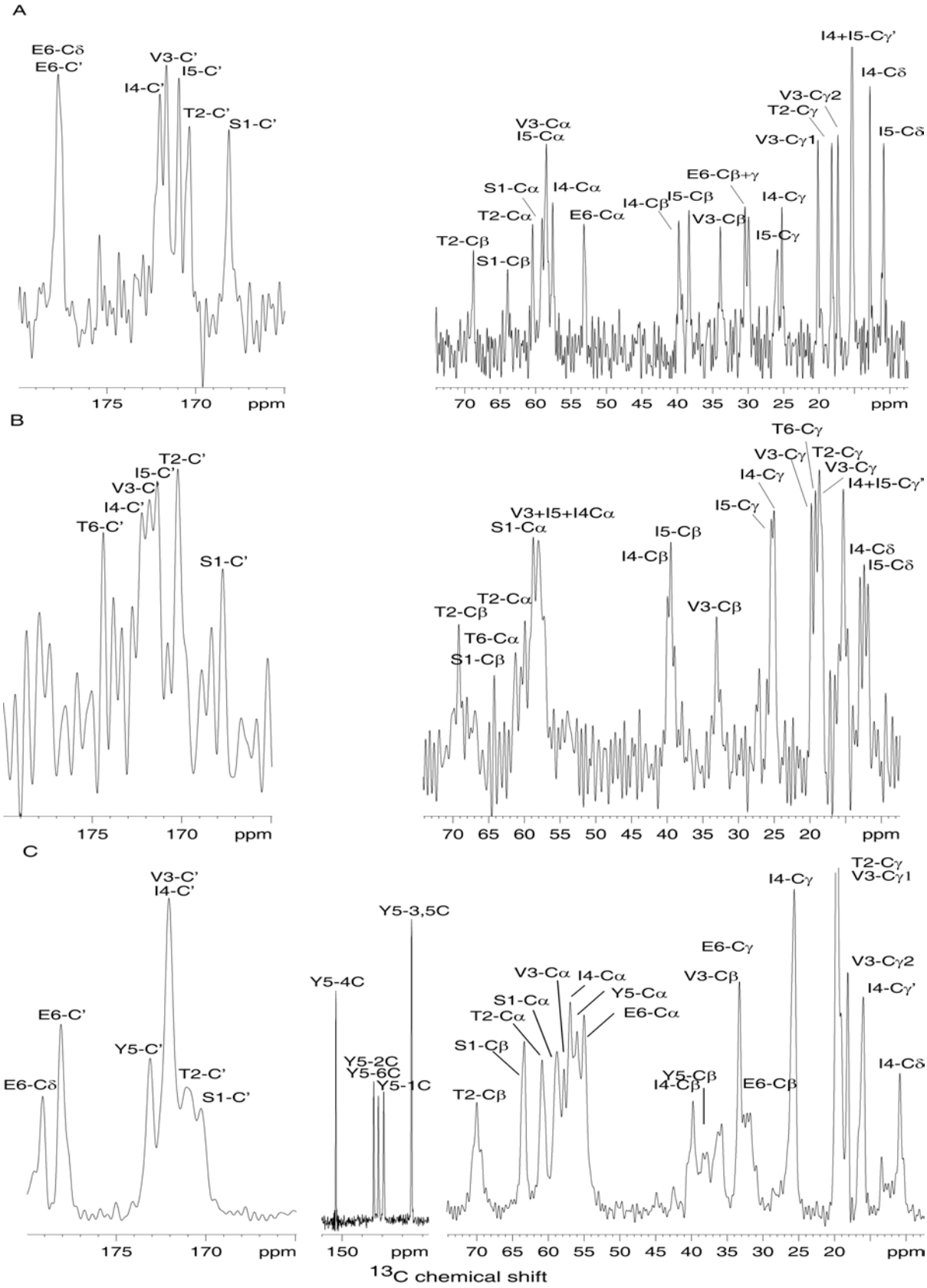

Fig. 3-45. 1D ^{13}C NMR spectra of 10 mg fibrils at natural abundance. A, spectrum for fibrils formed from STVIIE was observed at 11.7 T, with a MAS frequency of 8.3 kHz and $^{1}H/^{13}C$ cross-polarization time of 2 ms; B, spectrum for fibrils formed from STVIIT was observed at 9.47 T, with a MAS frequency of 9 kHz and $^{1}H/^{13}C$ cross-polarization time of 1.3 ms; C, spectrum for fibrils formed from STVIYE was observed at 9.47 T, with a MAS frequency of 9 kHz and $^{1}H/^{13}C$ cross-polarization time of 1.4 ms.

The ^{13}C chemical shift differences for STVIIE and STVIIT, STVIIE and STVIYE are plotted in Fig. 3-46.

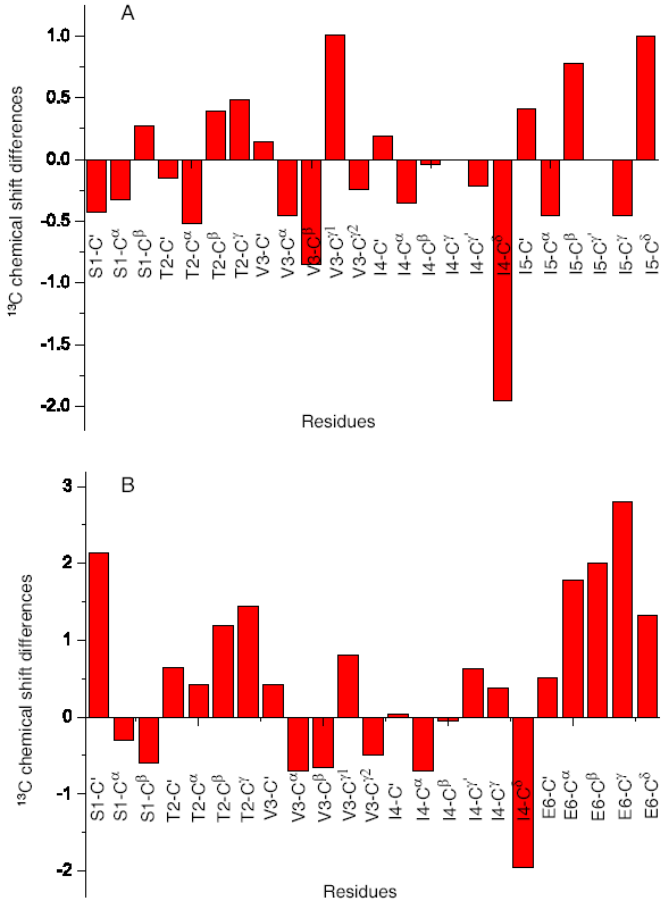

Fig. 3-46. ^{13}C chemical shift differences for fibrils formed by STVIIE and STVIIT (A), and for fibrils formed by STVIIE and STVIYE (B).

The ^{13}C chemical shift comparison for fibrils formed by STVIIE and STVIIT shows that the substitution of residue Glu to Thr induced larger changes of neighboring residue, Ile5 (Fig. 3-46A). In case of STVIIE and STVIYE, a large change are found at residue Glu6, which is also the neighboring residue to the substitution residue, from Ile5 to Tyr5 (Fig. 3-46B). This change could explain the different morphology observed for these fibrils.

To precisely address the structure difference upon peptide sequences, peptides with isotopic labeling would be required for multidimensional solid-state NMR experiments.

References

1. Fields, G. B., and Noble, R. L. (1990) *Int. J. Peptide Protein Res. 35*, 161-214.
2. Fraser, P., Nguyen, J., Surewicz, W., and Kirschner, D. (1991) *Biophys. J. 60*, 1190-1201.

3. Soto, C., Castano, E., Kumar, R., Beavis, R., and Frangione, B. (1995) *Neurosci. Lett. 200*, 105-108.
4. Petkova, A. T., Buntkowsky, G., Dyda, F., Leapman, R. D., Yau, W. M., and Tycko, R. (2004) *J. Mol. Biol. 335*, 247-260.
5. Tjernberg, L. O., Callaway, D. J. E., Tjernberg, A., Hahne, S., Lilliehöök, C., Terenius, L., Thyberg, J., and Nordstedt, C. (1999) *J. Biol. Chem. 274*, 12619–12625.
6. Marsh, R. E., Corey, R. B., and Pauling, L. (1955) *Biochim. Biophys. Acta. 16*, 1-34.
7. Fraser, P., Duffy, L., O'Malley, M., Nguyen, J., Inouye, H., and Kirschner, D. (1991) *J. Neurosci. Res. 28*, 474-485.
8. Kirschner, D., Inouye, H., Duffy, L., Sinclair, A., Lind, M., and Selkoe, D. (1987) *Proc. Natl. Acad. Sci. 84*, 6953-6957.
9. Inouye, H., Fraser, P. E., and Kirschner, D. A. (1993) *Biophys. J. 64*, 502-519.
10. Petkova, A. T., Ishii, Y., Balbach, J. J., Antzutkin, O. N., Leapman, R. D., Delaglio, F., and Tycko, R. (2002) *Proc. Natl. Acad. Sci. 99*, 16742–16747.
11. Wood, S. J., Maleeff, B., Hart, T., and Wetzel, R. (1996) *J. Mol. Biol. 256*, 870-877.
12. Soto, C., Sigurdsson, E., Morelli, L., Kumar, R., Castano, E., and Frangione, B. (1998) *Nat. Med. 4*, 822-826.
13. Goldsbury, C. S., Wirtz, S., Müller, S. A., Sunderji, S., Wicki, P., Aebi, U., and Frey, P. (2000) *J. Struct. Biol. 130*, 217–231.
14. Soto, C., Kindy, M. S., Baumann, M., and Frangione, B. (1996) *Biochemical and Biophysical Research Communications 226*, 672–680.
15. Soto, C. (1999) *J. Mol. Med. 77*, 412-418.
16. Adessi, C., and Soto, C. (2002) *Drug Dev. Res. 56*, 184-193.
17. Permanne, B., Adessi, C. l., Saborio, G. P., Fraga, S., Frossard, M.-J., Dorpe, J. V., Dewachter, I., Banks, W. A., Leuven, F. V., and Soto, C. (2002) *FASEB J. 16*, 860-862.
18. Adessi, C., Frossard, M.-J., Boissard, C., Fraga, S., Bieler, S., Ruckle, T., Vilbois, F., Robinson, S. M., Mutter, M., Banks, W. A., and Soto, C. (2003) *J. Biol. Chem. 278*, 13905-13911.
19. Barrow, C., and Zagorski, M. (1991) *Science 253*, 179-182.
20. Barrow, C., Yasuda, A., Kenny, P., and Zagorski, M. (1992) *J. Mol. Biol. 225*, 1075-1093.
21. Cairo, C. W., Strzelec, A., Murphy, R. M., and Kiessling, L. L. (2002) *Biochemistry 41*, 8620-8629.
22. LEVINE-III, H. (1993) *Protein Sci. 2*, 404-410.
23. Schubert, M., Labudde, D., Oschkinat, H., and Schmieder, P. (2002) *J. Biomol. NMR 24*, 149-154.
24. Tjernberg, L. O., Näslund, J., Lindqvist, F., Johansson, J., Karlström, A. R., Thyberg, J., Terenius, L., and Nordstedt, C. (1996) *J. Biol. Chem. 271*, 8545-8548.
25. Brunger, A. T., Adams, P. D., Clore, G. M., DeLano, W. L., Gros, P., Grosse-Kunstleve, R. W., Jiang, J.-S., Kuszewski, J., Nilges, N., Pannu, N. S., Read, R. J., Rice, L. M., Simonson, T., and Warren, G. L. (1998) *Acta. Cryst. D54*, 905-921.
26. Tolman, J. R., Flanagan, J. M., Kennedy, M. A., and Prestegard, J. H. (1995) *Proc. Natl. Acad. Sci. 92*, 9279-9283.
27. Tjandra, N., and Bax, A. (1997) *Science 278*, 1111-1114.
28. Sanders, C. R., and Schwonek, J. P. (1992) *Biochemistry 31*, 8898-8905.
29. Clore, G. M., Starich, M. R., and Gronenborn, A. M. (1998) *J. Am. Chem. Soc. 120*, 10571-10572.
30. Hansen, M., Mueller, L., and Pardi, A. (1998) *Nat. Struct. Biol. 5*, 1065–1074.
31. Koenig, B. W., Hu, J.-S., Ottiger, M., Bose, S., Hendler, R. W., and Bax, A. (1999) *J. Am. Chem. Soc. 121*, 1385-1386.

32. Sass, J., Cordier, F., Hoffmann, A., Rogowski, M., Cousin, A., Omichinski, J., Löwen, H., and Grzesiek, S. (1999) *J. Am. Chem. Soc. 121*, 2047–2055.
33. Sass, H., Musco, G., Stahl, S., Wingfield, P., and Grzesiek, S. (2000) *J. Biomol. NMR 18*, 303-309.
34. Ishii, Y., Markus, M., and Tycko, R. (2001) *J. Biomol. NMR 21*, 141-151.
35. Ni, F. (1994) *Prog. Nucl. Magn. Reson. Spectrosc. 26*, 517–606.
36. Blommers, M. J. J., Stark, W., Jones, C. E., Head, D., Owen, C. E., and Jahnke, W. (1999) *J. Am. Chem. Soc. 121*, 1949-1953.
37. Carlomagno, T., Felli, I. C., Czech, M., Fischer, R., Sprinzl, M., and Griesinger, C. (1999) *J. Am. Chem. Soc. 121*, 1945-1948.
38. Cavanagh, J., Fairbrother, W. J., Palmer, A. G., and Skelton, N. J. (1996) *Protein NMR Spectroscopy: Principles and Practice*, Academic Press, San Diego.
39. Koenig, B. W., Kontaxis, G., Mitchell, D. C., Louis, J. M., Litman, B. J., and Bax, A. (2002) *J. Mol. Biol. 322*, 441-461.
40. Bolon, P. J., Al-Hashimi, H. M., and Prestegard, J. H. (1999) *J. Mol. Biol. 293*, 107-115.
41. Worcester, D. L. (1978) *Proc. Natl. Acad. Sci. 75*, 5475-5477.
42. Fraser, P., Nguyen, J., Inouye, H., Surewicz, W., Selkoe, D., Podlisny, M., and Kirschner, D. A. (1992) *Biochemistry 31*, 10716-10723.
43. Sikorski, P., Atkins, E., and Serpell, L. (2003) *Structure 11*, 915-926.
44. Ottiger, M., Delaglio, F., Marquardt, J. L., Tjandra, N., and Bax, A. (1998) *J. Magn. Reson. 134*, 365–369.
45. Lerche, M., Meissner, A., Poulsen, F., and Sorensen, O. (1999) *J. Magn. Reson. 140*, 259-263.
46. Clore, G. M., Gronenborn, A. M., and Bax, A. (1998) *J. Magn. Reson. 133*, 216-221.
47. Tian, F., Fowler, C., Zartler, E., Jenney, F. J., Adams, M., and Prestegard, J. (2000) *J. Biomol. NMR 18*, 23-31.
48. Bax, A., Kontaxis, G., and Tjandra, N. (2001) *Meth. Enzymol. 339*, 127-174.
49. Balbach, J. J., Ishii, Y., Antzutkin, O. N., Leapman, R. D., Rizzo, N. W., Dyda, F., Reed, J., and Tycko, R. (2000) *Biochemistry 39*, 13748-13759.
50. Reif, B., Hohwy, M., Jaroniec, C. P., Rienstra, C. M., and Griffin, R. G. (2000) *J. Magn. Reson. 145*, 132–141.
51. Reif, B., Hennig, M., and Griesinger, C. (1997) *Science 276*, 1230-1233.
52. Peng, J. W. (2003) *J. Am. Chem. Soc. 125*, 11116–11130.
53. Clore, G. M., Gronenborn, A. M., and Tjandra, N. (1998) *J. Magn. Reson. 131*, 159-162.
54. Sass, H., Musco, G., Stahl, S., Wingfield, P., and Grzesiek, S. (2001) *J. Biomol. NMR 21*, 275-280.
55. Losonczi, J., Andrec, M., Fischer, M., and Prestegard, J. (1999) *J. Magn. Reson. 138*, 334-342.
56. Jain, N., Noble, S., and Prestegard, J. (2003) *J. Mol. Biol. 328*, 451-462.
57. Fischer, M., Losonczi, J., Weaver, J., and Prestegard, J. (1999) *Biochemistry 38*, 9013-9022.
58. Zweckstetter, M., and Bax, A. (2000) *J. Am. Chem. Soc. 122*, 3791-3792.
59. Tolman, J., Al-Hashimi, H., Kay, L., and Prestegard, J. (2001) *J. Am. Chem. Soc. 123*, 1416-1424.
60. Tjernberg, L. O., Tjernberg, A., Bark, N., Shi, Y., Ruzsicska, B. P., Bu, Z., Thyberg, J., and Callaway, D. J. E. (2002) *Biochem. J. 366*, 343-351.
61. Prestegard, J., Bougault, C., and Kishore, A. (2004) *Chem. Rev. 104*, 3519-3540.
62. Harper, J., Wong, S., Lieber, C., and Lansbury, P. J. (1999) *Biochemistry 38*, 8972-8980.

63. Hilbich, C., Kisters-Woike, B., Reed, J., Masters, C., and Beyreuther, K. (1992) *J. Mol. Biol. 228*, 460-473.
64. Paz, M. L. p. d. l., Lacroix, E., Ramirez-Alvarado, M., and Serrano, L. (2001) *J. Mol. Biol. 312*, 229-246.
65. Paz, M. L. p. d. l., Goldie, K., Zurdo, J., Lacroix, E., Dobson, C. M., Hoenger, A., and Serrano, L. (2002) *Proc. Natl. Acad. Sci. 99*, 16052–16057.
66. Richarz, R., and Wüthrich, K. (1978) *Biopolymers 17*, 2133-2141.
67. Braun, D., Wider, G., and Wuethrich, K. (1994) *J. Am. Chem. Soc. 116*, 8466-8469.

4.0 Summary

β-Amyloid peptide (Aβ) has an important role in the therapy of Alzheimer's Disease. Also it is an excellent example for probing the amyloid structural issues, such as the supermolecular orgination, the participated sequences in the β-sheet, and so on. In this study, the structures of peptide inhibitors to Aβ are studied with the aid of peptide synthesis and NMR spectroscopy, as well as Transmission Electron Microscopy and Circular Dichroism spectroscopy.

Short fragments of the β-amyloid peptide, $A\beta^{14-23}$, and its peptide inhibitors iAβ5 (LPFFD) and $iA\beta5^{inv}$ (DPFFL) were manually synthesized with and without ^{19}F-, ^{13}C- and ^{15}N-labelling using standard Fmoc peptide synthesis protocols. Fibrils formed from synthetic $A\beta^{14-23}$ was characterized by Electron Microscopy. EM images clearly show that $A\beta^{14-23}$ formed fibrils of the same morphology as that of $A\beta^{1-40}$ under our experimental conditions, therefore this β-amyloid peptide could serve as an *in vitro* model of amyloid fibril assembly, structure, and possibly also disruption of such assemblies. The inhibitory effects of iAβ5 and $iA\beta5^{inv}$ to Aβ fibrils were firstly investigated by Electron Microscopy spectroscopy. Small intermediate fibrils in the EM images of Aβ incubated with iAβ5 or $iA\beta5^{inv}$ show that the fibrils formed from Aβ can be disassembled by iAβ5 or $iA\beta5^{inv}$.

The structural information of peptide inhibitors bound to Aβ fibrils was further investigated in solution by using advanced NMR techniques. ^{1}H, ^{13}C and ^{15}N chemical shifts were assigned by combining the information from TOCSY, NOESY and HSQC spectra. A small chemical shift differences were inferred by addition of iAβ5 or $iA\beta5^{inv}$ to Aβ fibrils.

TrNOESY experiments were carried out to structurally define the geometry of iAβ5 and $iA\beta5^{inv}$ in the bound state. Excess of peptide inhibitors was added to preformed Aβ fibrils. Due to the fact that iAβ5 or $iA\beta5^{inv}$ only weakly binds to the fibril (*K*d ~1 nM) and the dependence of the cross peak intensity on τ_c, the structure of iAβ5 or $iA\beta5^{inv}$ can be determined in the bound state. Extensive NOEs were observed among almost all ^{1}H resonances at a mixing time of 50 msec. Viscosity effects and the possibility of oligomer formation of the peptide inhibitors were excluded by performing the diffusion experiments and NOESY experiments on a mixed ^{13}C-labelled and unlabelled iAβ5 sample.

Distance restrains for peptide inhibitors were obtained on the basis of NOE intensities. Structural calculations were performed using the CNSsolve program. When bound to the same type of amyloid fibrils ($A\beta^{14-23}$), iAβ5 and $iA\beta5^{inv}$ show identical spatial side chain

orientations of equal properties with different backbone structures. iAβ5^{inv} binds to fibrils formed from Aβ$^{14-23}$ and Aβ$^{1-40}$, respectively, with different structures showing different backbone and different side chain orientations.

The orientation of peptide inhibitors relative to Aβ was further investigated using transferred RDC techniques developed in the course of this thesis. Aβ fibrils orient in the external magnetic field with the fibrils axis parallel to B_0. The oriented fibrils induce a net orientation to the peptide inhibitor in the bound state. In a favourable case, residual dipolar couplings of the peptide in the bound state are transferred to that in the free state. This trRDCs were detected for iAβ5^{inv}, not for iAβ5 due to their different affinity. The measured trRDCs data were carefully analyzed with the aid of the program PALES, and a best-fit orientation of iAβ5^{inv} was obtained. NOE-derived NMR structure of iAβ5 and iAβ5^{inv} were docked to Aβ$^{14-23}$ and Aβ$^{1-40}$, respectively. The models of iAβ5^{inv} docked to Aβ were refined using the experimental trRDCs data. From the docking models, the binding sites of iAβ5 and iAβ5^{inv} to Aβ could be identified. Taken together, we propose a mechanism how iAβ5 or iAβ5^{inv} disassemble Aβ fibrils.

Our findings provide a basis for further in vitro modeling of amyloid fibril assembly, structure, and possibly also disruption of such assemblies. For example, the model system could be used to examine the effects of other amino acid substitutions in the amyloid protein, or post-translational modifications and various chain lengths of the putative precursor protein on amyloid fibril formation. In the later part of this work, studies on the amyloid fibril structure was presented. ^{19}F-NMR experiments were carried out on ^{19}F-Aβ$^{14-23}$ (with ^{19}F labelled in the para-position of the aromatic ring of Phe19) both in liquid state and solid state.

The *de novo* designed amyloid peptide (STVIIE) was characterized by solid-state NMR. ^{13}C and ^{15}N chemical shifts were unambiguously obtained for STVIIE in the fibrillar state with the aid of ^{13}C- and ^{15}N-labelling. Primary assignments of the 1D ^{13}C spectra for STVIIT and STVIYE fibrils are obtained. The comparison of the chemical shifts shows that the one amino acid substitution causes a large ^{13}C chemical shift change on the neighbouring residues which could explain the different morphology observed for these fibrils.

5 APPENDIX

5.1 NMR experimental details

5.1.1 TOCSY experimental details

Samples	Sfo1 (MHz)	Spectral width (Hz)	Mixing time (msec)	T1 increments	Number scans	T2 data points
5 mM ^{19}F-iAβ5	750.133	10502	49.5	768	32	8192
5 mM ^{19}F-iAβ5 with 0.5 mM $Aβ^{14–23}$	750.133	7501	49.5	512	64	8192
0.5 mM $iAβ5^{inv}$	750.133	10502	49.5	768	32	8192
5 mM $iAβ5^{inv}$ with 0.5 mM $Aβ^{14–23}$	750.133	10502	49.5	512	64	8192

5.1.2 NOESY experimental details

samples	SFO1 (MHz)	Spectral width (Hz)	Mixing time (msec)	T1 increments	Number scans	T2 data points
5 mM ^{19}F-iAβ5	750.133	10502	500	512	128	8192
5 mM ^{19}F-iAβ5 with 0.5 mM $Aβ^{14–23}$	750.133	7501	10, 50, 150, 500	768	64	8192
0.5 mM $iAβ5^{inv}$	750.133	7501	500	512	32	8192
5 mM $iAβ5^{inv}$ with $Aβ^{14–23}$	750.133	7501	100, 200, 500	768	64	8192
5 mM $iAβ5^{inv}$ with $Aβ^{14–23}$	750.013	8250	500	512	8	4096
5 mM $iAβ5^{inv}$ with $Aβ^{1–40}$	750.013	8250	100, 500	768	16	4096
1.5 mM u-^{13}C,^{15}N- iAβ5 and 3.5 mM iAβ5 with $Aβ^{14–23}$	750.013	9001	500	512	80	4096

5.1.3 ^{13}C-HSQC experimental details without decoupling in F1

Samples	SFO1 (MHz)	Spectral width (F1) (Hz)	T2 data points	T1 increments	Number scans	O2 (Hz)
0.5 mM $iAβ5^{inv}$ (10% ^{13}C in rich)	750.133	28294	8192	1024	16	7544
5 mM $iAβ5^{inv}$ (10% ^{13}C in rich) with $Aβ^{14–23}$	750.133	28292	4096	768	16	7544
5 mM $iAβ5^{inv}$	750.013	18750	1318	256	64	10749
5 mM $iAβ5^{inv}$ with $Aβ^{14–23}$	750.013	18750	1318	256	96	10749
5 mM $iAβ5^{inv}$ with $Aβ^{1–40}$	750.013	18750	1318	256	96	10749

5.1.4 ^{13}C-HSQC experimental details Without decoupling in F2

Samples	SFO1 (MHz)	Spectral width (F1) (Hz)	T2 data points	T1 increments	Number scans	O2 (Hz)
5 mM $iAβ5^{inv}$	750.013	30000	4096	256	96	5846

5 mM iAβ5^{inv}	750.013	6000	4096	256	96	24611
5 mM iAβ5^{inv} with Aβ$^{1-40}$	750.013	30000	4096	256	128	24611
5 mM iAβ5^{inv} with Aβ$^{1-40}$	750.013	30000	4096	256	128	5846

5.2 Data appendix

5.2.1 Assignment of ^{19}F-iAβ5 (LPFFD) at 5mM, pH4, 303K

	NH	αH	βH	γH	δH	εH
Leu1		4.22	1.70	1.64(*)	0.94	
Pro2		4.353	2.133, 1.64 (*)	1.926	3.658, 3.492	
Phe3	8.072	4.424	2.932	2,6H: 7.003	3,5H: 7.115	
Phe4	7.900	4.546	3.034, 2.885	2,6H: 7.170	3,5H: 7.282	4H: 7.239
Asp5	8.023	4.481	2.785, 2.732			

(Values indicated with star mean overlapping)

5.2.2 Assignment of ^{19}F-iAβ5 at 5 mM in the presence of 0.5 mM Aβ$^{14-23}$ fibrils, at pH4, 303K

	NH	αH	βH	γH	δH	εH
Leu1		4.212	1.701	1.636(*)	0.94	
Pro2		4.361	2.132, 1.636(*)	1.923	3.658, 3.482	
Phe3	8.038(*)	4.424	2.932	2,6H: 6.998	3,5H: 7.110	
Phe4	7.856	4.544	3.028, 2.891	2,6H: 7.162	3,5H: 7.282	4H: 7.237
Asp5	8.038(*)	4.512	2.795, 2.748			

5.2.3 Assignment of 10% labelling iAβ5^{inv} (DPFFL) at 0.5 mM, pH4, 303 K

	NH	αH	βH	γH	δH	εH
Asp1		4.570	2.754, 2.956			
Pro2		4.437	2.228, 1.696	1.986, 1.922	3.627, 3.735	
Phe3	8.185	4.555	3.038	2,6H: 7.251 (*)	3,5H: 7.375(*)	4H: 7.333(*)
Phe4	7.968	4.616	3.121, 2.985	2,6H: 7.251 (*)	3,5H: 7.375(*)	4H: 7.333(*)
Leu5	8.051	4.282	1.614 (*)	1.614 (*)	0.916, 0.954	

5.2.4 Assignment of 10% labelling iAβ5^{inv} (DPFFL) of 5 mM in the presence of 0.5 mM Aβ$^{14-23}$ at pH4, 303 K

	NH	αH	βH	γH	δH	εH

Asp1		4.585	2.831, 2.998			
Pro2		4.467	2.212, 1.668	1.992 1.899	3.602, 3.742	
Phe3	8.074	4.571	3.072(*)	2,6H: 7.243	3,5H: 7.383(*)	4H: 7.337(*)
Phe4	7.729	4.628	3.062(*)	2,6H: 7.243	3,5H: 7.383(*)	4H: 7.337(*)
Leu5	7.875	4.344	1.615(*)	1.615(*)	0.925, 0.957	

5.2.5 Distance restraints obtained from trNOESY data for ^{19}F-iAβ5 bound to Aβ$^{14–23}$ as an input file for CNSsolve.

```
ASSIgn  atom-selection            atom-selection           dplus dminus dis
assi (resi 1 and name HD* ) ((resi 3 or resi 5) and name HN) 0.00 0.00 4.50
assi ( resi 1 and name HD* ) (  resi 4 and name HN  )        0.00 0.00 5.10
assi ( resi 1 and name HD* ) (  resi 4 and name HE* )        0.00 0.00 4.10
assi ( resi 1 and name HD* ) (  resi 4 and name HZ  )        0.00 0.00 4.60
assi ( resi 1 and name HD* ) (  resi 4 and name HD1 )        0.00 0.00 4.50
assi ( resi 1 and name HD* ) (  resi 4 and name HD2 )        0.00 0.00 4.50
assi ( resi 1 and name HD* ) (  resi 3 and name HE* )        0.00 0.00 4.80
assi ( resi 1 and name HD* ) (  resi 3 and name HD* )        0.00 0.00 4.60
assi ( resi 1 and name HD* ) (  resi 1 and name HA  )        0.00 0.00 4.20
assi ( resi 1 and name HD* ) (  resi 2 and name HD2 )        0.00 0.00 3.90
assi ( resi 1 and name HD* ) (  resi 2 and name HD1 )        0.00 0.00 3.90
assi ( resi 1 and name HD* ) (  resi 4 and name HB1 )        0.00 0.00 4.80
assi ( resi 1 and name HD* ) (  resi 4 and name HB2 )        0.00 0.00 4.80
assi ( resi 1 and name HD* ) (  resi 2 and name HB2 )        0.00 0.00 5.70
assi ( resi 1 and name HD* ) (  resi 2 and name HG* )        0.00 0.00 4.00
assi ( resi 1 and name HD* ) (  resi 1 and name HG  )        0.00 0.00 2.90
assi ( resi 1 and name HD* ) ( (resi 2 and name HB1) or (resi 1 and name HB*))    0.00 0.00 2.80
assi ((resi 2 and name HB1) or (resi 1 and name HB*)) ((resi 3 or resi 5) and name HN) 0.00 0.00 3.90
assi ( ( resi 2 and name HB1 ) or ( resi 1 and name HB* )) (resi 4 and name HN)   0.00 0.00 4.60
assi ( ( resi 2 and name HB1 ) or ( resi 1 and name HB* )) (resi 4 and name HE*)  0.00 0.00 4.90
assi ( ( resi 2 and name HB1 ) or ( resi 1 and name HB* )) (resi 4 and name HZ)   0.00 0.00 5.50
assi ( ( resi 2 and name HB1 ) or ( resi 1 and name HB* )) (resi 4 and name HD1)  0.00 0.00 5.00
assi ( ( resi 2 and name HB1 ) or ( resi 1 and name HB* )) (resi 4 and name HD2)  0.00 0.00 5.10
assi ( ( resi 2 and name HB1 ) or ( resi 1 and name HB* )) (resi 3 and name HE*)  0.00 0.00 4.50
assi ( ( resi 2 and name HB1 ) or ( resi 1 and name HB* )) (resi 3 and name HD*)  0.00 0.00 5.10
assi ( ( resi 2 and name HB1 ) or ( resi 1 and name HB* )) (resi 2 and name HD2)  0.00 0.00 3.80
assi ( ( resi 2 and name HB1 ) or ( resi 1 and name HB* )) (resi 2 and name HD1)  0.00 0.00 3.50
assi ( ( resi 2 and name HB1 ) or ( resi 1 and name HB* )) (resi 4 and name HB2)  0.00 0.00 4.90
assi ( ( resi 2 and name HB1 ) or ( resi 1 and name HB* )) ( resi 4 and name HB1) 0.00 0.00 4.90
assi ( ( resi 2 and name HB1 ) or ( resi 1 and name HB* )) (resi 2 and name HB2)  0.00 0.00 2.90
assi ( ( resi 2 and name HB1 ) or ( resi 1 and name HB* )) (resi 2 and name HG*)  0.00 0.00 3.10
assi ( resi 2 and name HG* ) ( (resi 3 or resi 5 ) and name HN )  0.00 0.00 4.50
assi ( resi 2 and name HG* ) (  resi 4 and name HE* )     0.00 0.00 6.20
```

```
assi ( resi 2 and name HG* ) (  resi 4 and name HZ  )     0.00 0.00 7.70
assi ( resi 2 and name HG* ) (  resi 4 and name HD* )     0.00 0.00 6.50
assi ( resi 2 and name HG* ) (  resi 3 and name HE* )     0.00 0.00 5.10
assi ( resi 2 and name HG* ) (  resi 3 and name HD* )     0.00 0.00 5.90
assi ( resi 2 and name HG* ) (  resi 2 and name HD2 )     0.00 0.00 3.40
assi ( resi 2 and name HG* ) (  resi 2 and name HD1 )     0.00 0.00 3.30
assi ( resi 2 and name HG* ) (  resi 2 and name HB2 )     0.00 0.00 3.10
assi ( resi 2 and name HG* ) (  resi 4 and name HN  )     0.00 0.00 6.60
assi ( resi 2 and name HB2 ) ( (resi 3 or resi 5 ) and name HN )  0.00 0.00 4.20
assi ( resi 2 and name HB2 ) (  resi 4 and name HN  )     0.00 0.00 6.30
assi ( resi 2 and name HB2 ) (  resi 4 and name HE* )     0.00 0.00 4.70
assi ( resi 2 and name HB2 ) (  resi 3 and name HE* )     0.00 0.00 5.40
assi ( resi 2 and name HB2 ) (  resi 3 and name HD* )     0.00 0.00 6.10
assi ( resi 2 and name HB2 ) (  resi 2 and name HD2 )     0.00 0.00 4.70
assi ( resi 2 and name HB2 ) (  resi 2 and name HD1 )     0.00 0.00 4.70
assi ( resi 5 and name HB1 ) ( (resi 3 or resi 5 ) and name HN )  0.00 0.00 4.10
assi ( resi 5 and name HB1 ) (  resi 4 and name HN  )     0.00 0.00 6.40
assi ( resi 5 and name HB2 ) ( (resi 3 or resi 5 ) and name HN )  0.00 0.00 4.20
assi ( resi 5 and name HB2 ) (  resi 4 and name HN  )     0.00 0.00 6.40
assi ( resi 5 and name HB2 ) (  resi 5 and name HB1 )     0.00 0.00 2.30
assi ((resi 3 and name HB*) or (resi 4 and name HB1)) ((resi 3 or resi 5) and name HN) 0.00 0.00 3.30
assi ( ( resi 3 and name HB* ) or (resi 4 and name HB1 )) (  resi 4 and name HN  ) 0.00 0.00 3.30
assi ( resi 3 and name HB* )     (  resi 3 and name HE* ) 0.00 0.00 3.40
assi ( resi 3 and name HB* )     (  resi 3 and name HD* ) 0.00 0.00 4.00
assi ( resi 4 and name HB1 )     (  resi 4 and name HE* ) 0.00 0.00 4.50
assi ( resi 4 and name HB1 )     (  resi 4 and name HD* ) 0.00 0.00 3.50
assi ( resi 4 and name HB1 )     (  resi 4 and name HB2 ) 0.00 0.00 2.70
assi ( resi 4 and name HB2 )  ((resi 3 or resi 5 ) and name HN )  0.00 0.00 4.20
assi ( resi 4 and name HB2 )     (  resi 4 and name HE* )  0.00 0.00 4.90
assi ( resi 4 and name HB2 )     (  resi 4 and name HD* )  0.00 0.00 3.90
assi ( resi 4 and name HB2 )     (  resi 4 and name HN  )  0.00 0.00 4.00
assi ( resi 2 and name HD1 )     (  resi 2 and name HD2 )  0.00 0.00 2.90
assi ( resi 2 and name HD1 )     (  resi 1 and name HG  )  0.00 0.00 4.70
assi ( resi 2 and name HD2 )     (  resi 1 and name HG  )  0.00 0.00 4.90
assi ( resi 1 and name HA  )     (  resi 2 and name HD2 )  0.00 0.00 3.40
assi ( resi 1 and name HA  )     (  resi 2 and name HD1 )  0.00 0.00 3.60
assi ( resi 1 and name HA  )     (  resi 2 and name HB2 )  0.00 0.00 5.50
assi ( resi 1 and name HA  )     (  resi 2 and name HG* )  0.00 0.00 4.20
assi ( resi 1 and name HA ) (( resi 2 and name HB1 ) or ( resi 1 and name HB* ))   0.00 0.00 3.50
assi ( resi 1 and name HA  )     (  resi 1 and name HD* )  0.00 0.00 3.30
assi ( resi 1 and name HA  )     (  resi 1 and name HG  )  0.00 0.00 4.10
assi ( resi 2 and name HA  )     (  resi 1 and name HD* )  0.00 0.00 5.80
assi ( resi 2 and name HA  )     (  resi 3 and name HB* )  0.00 0.00 4.70
assi ( resi 2 and name HA  )     (  resi 2 and name HB2 )  0.00 0.00 3.30
```

```
assi ( resi 2 and name HA  )     (  resi 2 and name HD2 )  0.00 0.00 4.90
assi ( resi 2 and name HA   )    (  resi 2 and name HD1 )  0.00 0.00 5.10
assi ( resi 2 and name HA   )    (  resi 2 and name HG* )  0.00 0.00 3.70
assi ( resi 2 and name HA ) (( resi 2 and name HB1 ) or ( resi 1 and name HB*))   0.00 0.00 3.60
assi ( resi 2 and name HA )     (  resi 3 and name HE* )   0.00 0.00 5.90
assi ( resi 2 and name HA ) ( (resi 3 or resi 5 ) and name HN  )  0.00 0.00 3.20
assi ( resi 2 and name HA )     (  resi 4 and name HN  )   0.00 0.00 5.10
assi ( resi 3 and name HA   )   (  resi 4 and name HN  )   0.00 0.00 3.80
assi ( resi 3 and name HA ) ( (resi 3 or resi 5 ) and name HN )0.00 0.00 3.30
assi ( resi 3 and name HA  )    (  resi 3 and name HE* )       0.00 0.00 3.80
assi ( resi 3 and name HA  )    (  resi 3 and name HD* )       0.00 0.00 5.80
assi ( resi 3 and name HA  )    (  resi 3 and name HB* )       0.00 0.00 3.10
assi ( resi 4 and name HA  )    (  resi 4 and name HB2 )       0.00 0.00 3.40
assi ( resi 4 and name HA  )    (  resi 4 and name HB1 )       0.00 0.00 3.60
assi ( resi 5 and name HA  )    (  resi 5 and name HB2  )      0.00 0.00 3.70
assi ( resi 5 and name HA  )    (  resi 5 and name HB1  )      0.00 0.00 4.10
assi ( (resi 4 or resi 5 ) and name HA )  ( (resi 3 or resi 5 ) and name HN )  0.00 0.00 3.20
assi ( (resi 4 or resi 5 ) and name HA )  ( resi 4 and name HN )  0.00 0.00 3.60
assi ( (resi 4 or resi 5 ) and name HA )  ( resi 4 and name HE*)  0.00 0.00 4.60
assi ( (resi 4 or resi 5 ) and name HA )  ( resi 4 and name HZ )  0.00 0.00 5.90
assi ( (resi 4 or resi 5 ) and name HA )  ( resi 4 and name HD1)  0.00 0.00 4.10
assi ( (resi 4 or resi 5 ) and name HA )  ( resi 4 and name HD2)  0.00 0.00 4.20
assi ( resi 3 and name HE* ) ( (resi 3 or resi 5 ) and name HN )  0.00 0.00 4.40
assi ( resi 3 and name HE* )  (  resi 4 and name HN  )       0.00 0.00 5.40
assi ( resi 4 and name HE* )  (  resi 4 and name HN  )       0.00 0.00 5.10
assi ( resi 4 and name HE* ) ( (resi 3 or resi 5 ) and name HN )  0.00 0.00 5.80
assi ( resi 4 and name HN )  ( (resi 3 or resi 5 ) and name HN )  0.00 0.00 3.30
assi ( resi 4 and name HD* )   (  resi 4 and name HE* )      0.00 0.00 2.50
assi ( resi 4 and name HD* )   (  resi 4 and name HZ  )      0.00 0.00 3.50
assi ( resi 4 and name HD* )   (  resi 4 and name HN  )      0.00 0.00 4.20
assi ( resi 4 and name HD* ) ( (resi 3 or resi 5 ) and name HN )  0.00 0.00 4.90
assi ( resi 3 and name HD* )   (  resi 4 and name HD* )      0.00 0.00 3.70
assi ( resi 3 and name HD* )   (  resi 3 and name HE* )      0.00 0.00 2.60
```

5.2.6 Distance restraints obtained from trNOESY data for iAβ5^{inv} bound to Aβ$^{14–23}$ as an input file for CNSsolve .

```
ASSIgn  atom-selection         atom-selection         dplus dminus dis
assi ( resi 3 and name HN )   ( resi 5 and name HD* )  0.00 0.00 4.74
assi ( resi 3 and name HN ) ( resi 5 and (name HB* or name HG) ) 0.00 0.00 4.69
assi ( resi 3 and name HN )   ( resi 2 and name HB1 )  0.00 0.00 4.74
assi ( resi 3 and name HN )   ( resi 2 and name HG1 )  0.00 0.00 5.01
assi ( resi 3 and name HN )   ( resi 2 and name HG2 )  0.00 0.00 4.83
```

```
assi ( resi 3 and name HN )   ( resi 2 and name HB2 )  0.00 0.00 4.61
assi ( resi 3 and name HN )   ( resi 3 and name HB* )  0.00 0.00 3.96
assi ( resi 3 and name HN )   ( resi 2 and name HA )   0.00 0.00 3.74
assi ( resi 3 and name HN )   ( resi 3 and name HA )   0.00 0.00 3.88
assi ( resi 3 and name HN )   ( resi 3 and name HD* )  0.00 0.00 5.15
assi ( resi 3 and name HN )   ( resi 4 and name HN )   0.00 0.00 5.16
assi ( resi 5 and name HN )   ( resi 5 and name HD* )  0.00 0.00 3.99
assi ( resi 5 and name HN )   ( resi 5 and (name HB* or name HG) ) 0.00 0.00 3.86
assi ( resi 5 and name HN )   ( resi 4 and name HB1 )  0.00 0.00 4.49
assi ( resi 5 and name HN )   ( resi 4 and name HB2 )  0.00 0.00 4.73
assi ( resi 5 and name HN )   ( resi 5 and name HA )   0.00 0.00 4.71
assi ( resi 5 and name HN )   ( resi 4 and name HA )   0.00 0.00 4.07
assi ( resi 5 and name HN )   ( resi 4 and name HN )   0.00 0.00 4.64
assi ( resi 4 and name HN )   ( resi 5 and name HD* )  0.00 0.00 5.15
assi ( resi 4 and name HN )   ( resi 5 and (name HB* or name HG) )  0.00 0.00 4.88
assi ( resi 4 and name HN )   ( resi 2 and name HB1 )  0.00 0.00 5.93
assi ( resi 4 and name HN )   ( (resi 3 and name HB* ) or (resi 4 and name HB1) ) 0.00 0.00 4.15
assi ( resi 4 and name HN )   ( resi 4 and name HB2 )  0.00 0.00 4.49
assi ( resi 4 and name HN )   ( resi 3 and name HA )   0.00 0.00 3.95
assi ( resi 4 and name HN )   ( resi 4 and name HA )   0.00 0.00 4.70
assi ( resi 4 and name HN )   ( resi 4 and name HD* )  0.00 0.00 5.04
assi ( (resi 3 or resi 4 ) and name HE* )    ( resi 5 and name HD*) 0.00 0.00 3.10
assi ( (resi 3 or resi 4 ) and name HE* )   ( resi 5 and (name HB* or name HG) ) 0.00 0.00 3.69
assi ( (resi 3 or resi 4 ) and name HE* )   ( resi 2 and name HB2 )  0.00 0.00 4.61
assi ((resi 3 or resi 4) and name HE*) ((resi 3 and name HB*) or (resi 4 and name HB1)) 0.00 0.00 3.55
assi ( (resi 3 or resi 4 ) and name HE* )  ( resi 4 and name HB2 )  0.00 0.00 5.11
assi ( (resi 3 or resi 4 ) and name HZ )   ( resi 5 and name HD*) 0.00 0.00 3.67
assi ( (resi 3 or resi 4 ) and name HZ )   ( resi 5 and (name HB* or name HG) ) 0.00 0.00 4.36
assi ( (resi 3 or resi 4 ) and name HZ )  ( resi 4 and name HD* )  0.00 0.00 4.04
assi ( (resi 3 or resi 4 ) and name HE* )    ( resi 4 and name HD* ) 0.00 0.00 2.56
assi ( (resi 3 or resi 4 ) and name HE* )    ( resi 3 and name HD* ) 0.00 0.00 2.62
assi ( resi 4 and name HD* )  ( resi 5 and name HD* )  0.00 0.00 3.62
assi ( resi 4 and name HD* )  (resi 5 and (name HB* or name HG) )  0.00 0.00 4.07
assi ( resi 4 and name HD* )  ( resi 2 and name HB2 )  0.00 0.00 4.66
assi ( resi 4 and name HD* )  ( resi 4 and name HB1 )  0.00 0.00 4.13
assi ( resi 4 and name HD* )  ( resi 4 and name HB2 )  0.00 0.00 4.70
assi ( resi 3 and name HD* )  ( resi 5 and name HD* )  0.00 0.00 3.72
assi ( resi 3 and name HD* )  (resi 5 and (name HB* or name HG) )  0.00 0.00 4.03
assi ( resi 3 and name HD* )  ( resi 2 and name HB2 )  0.00 0.00 4.25
assi ( resi 3 and name HD* )  ( resi 3 and name HB* )  0.00 0.00 4.16
assi ( resi 3 and name HD* )  ( resi 3 and name HA )   0.00 0.00 4.51
assi ( resi 3 and name HA )   ( resi 3 and name HB* )  0.00 0.00 3.89
assi ( resi 1 and name HA )   ( resi 2 and name HD2 )  0.00 0.00 4.58
assi ( resi 1 and name HA )   ( resi 2 and name HD1 )  0.00 0.00 4.36
```

```
assi ( resi 1 and name HA )   ( resi 1 and name HB2 )  0.00 0.00 4.00
assi ( resi 1 and name HA )   ( resi 1 and name HB1 )  0.00 0.00 4.23
assi ( resi 1 and name HA )   ( resi 2 and name HG2 )  0.00 0.00 4.63
assi ( resi 1 and name HA )   ( resi 2 and name HG1 )  0.00 0.00 4.50
assi ( resi 4 and name HA )   ( resi 4 and name HB1 )  0.00 0.00 4.81
assi ( resi 4 and name HA )   ( resi 4 and name HB2 )  0.00 0.00 4.24
assi ( resi 2 and name HA )   ( resi 2 and name HB1 )  0.00 0.00 4.11
assi ( resi 2 and name HA )   ( resi 2 and name HG1 )  0.00 0.00 4.67
assi ( resi 2 and name HA )   ( resi 2 and name HG2 )  0.00 0.00 4.75
assi ( resi 2 and name HA )   ( resi 2 and name HB2 )  0.00 0.00 4.14
assi ( resi 5 and name HA )   ( resi 5 and name HD1* )  0.00 0.00 4.13
assi ( resi 5 and name HA )   ( resi 5 and name HD2* )  0.00 0.00 5.00
assi ( resi 5 and name HA )   (resi 5 and (name HB* or name HG) ) 0.00 0.00 3.88
assi ( resi 2 and name HD1 )  ( resi 2 and name HG2 ) 0.00 0.00 4.46
assi ( resi 2 and name HD1 )  ( resi 2 and name HG1 ) 0.00 0.00 4.71
assi ( resi 2 and name HD2 )  ( resi 2 and name HG1 )  0.00 0.00 4.36
assi ( resi 2 and name HD2 )  ( resi 2 and name HG2 )  0.00 0.00 4.69
assi ( resi 2 and name HD1 )  ( resi 2 and name HD2 )  0.00 0.00 4.31
assi ( resi 4 and name HB1 )  ( resi 4 and name HB2 )  0.00 0.00 3.02
assi ( resi 1 and name HB1 )  ( resi 1 and name HB2 )  0.00 0.00 3.11
assi ( resi 2 and name HG2 )  ( resi 2 and name HB2 )  0.00 0.00 4.08
assi ( resi 2 and name HG1 )  ( resi 2 and name HB2 )  0.00 0.00 4.03
assi ( resi 2 and name HB1 )  ( resi 2 and name HB2 )  0.00 0.00 4.84
assi ( resi 2 and name HG1 )  ( resi 2 and name HG2 )  0.00 0.00 3.35
assi ( resi 2 and name HB1 )  ( resi 2 and name HG2 )  0.00 0.00 4.05
assi ( resi 2 and name HB1 )  ( resi 2 and name HG1 )  0.00 0.00 3.71
assi ( resi 2 and name HG1 )  (resi 5 and (name HB* or name HG) ) 0.00 0.00 4.31
assi (resi 5 and (name HB* or name HG) )  ( resi 5 and name HD1* )  0.00 0.00 3.69
assi (resi 5 and (name HB* or name HG) )  ( resi 5 and name HD2* )  0.00 0.00 3.80
```

5.2.7 Distance restraints obtained from trNOESY data for iAβ5^{inv} bound to Aβ$^{1-40}$ as an input file for CNSsolve .

```
ASSIgn  atom-selection         atom-selection       dplus dminus dis
assi ( resi 1 and name HA )  ( resi 2 and name HD1 )  0.00 0.00 3.70
assi ( resi 1 and name HA )  ( resi 2 and name HD2 )  0.00 0.00 3.80
assi ( resi 1 and name HA )  ( resi 1 and name HB1 )  0.00 0.00 3.40
assi ( resi 1 and name HB1 )  ( resi 1 and name HB2 ) 0.00 0.00 2.60
assi ( resi 2 and name HA )  ( resi 2 and name HB1 )  0.00 0.00 3.30
assi ( resi 2 and name HA )  ( resi 2 and name HG1 )  0.00 0.00 4.10
assi ( resi 2 and name HA )  ( resi 2 and name HG2 )  0.00 0.00 4.40
```

```
assi ( resi 2 and name HA )  ( resi 2 and name HB2 )  0.00 0.00 3.60
assi ( resi 2 and name HD1 )  ( resi 2 and name HD2 )  0.00 0.00 3.10
assi ( resi 2 and name HD2 )  ( resi 1 and name HB1 )  0.00 0.00 3.70
assi ( resi 2 and name HD2 )  ( resi 1 and name HB2 )  0.00 0.00 4.30
assi ( resi 2 and name HD2 )  ( resi 2 and name HG1 )  0.00 0.00 3.70
assi ( resi 2 and name HD2 )  ( resi 2 and name HG2 )  0.00 0.00 3.90
assi ( resi 2 and name HD2 )  ( resi 2 and name HB2 )  0.00 0.00 4.30
assi ( resi 2 and name HD1 )  ( resi 1 and name HB1 )  0.00 0.00 4.30
assi ( resi 2 and name HD1 )  ( resi 1 and name HB2 )  0.00 0.00 4.40
assi ( resi 2 and name HD1 )  ( resi 2 and name HB1 )  0.00 0.00 4.60
assi ( resi 2 and name HD1 )  ( resi 2 and name HB2 )  0.00 0.00 4.60
assi ( resi 2 and name HD1 )  ( resi 2 and name HG1 ) 0.00 0.00 3.70
assi ( resi 2 and name HD1 )  ( resi 2 and name HG2 ) 0.00 0.00 3.60
assi ( resi 2 and name HB1 )  ( resi 2 and name HG1 ) 0.00 0.00 3.70
assi ( resi 2 and name HB1 )  ( resi 2 and name HG2 ) 0.00 0.00 3.90
assi ( resi 2 and name HB1 )  ( resi 2 and name HB2 ) 0.00 0.00 2.80
assi ( resi 2 and name HG1 )  ( resi 2 and name HG2 ) 0.00 0.00 3.20
assi ( resi 2 and name HG1 )  ( resi 2 and name HB2 ) 0.00 0.00 3.90
assi ( resi 2 and name HG2 )  ( resi 2 and name HB2 ) 0.00 0.00 3.60
assi ( resi 2 and name HG2 )  (resi 5 and (name HB* or name HG) ) 0.00 0.00 4.10
assi ( resi 3 and name HD* )  ( resi 5 and name HD2* )  0.00 0.00 4.40
assi ( resi 3 and name HD* )  ( resi 5 and name HD1* )  0.00 0.00 4.30
assi ( resi 3 and name HA )  ( resi 3 and name HB* )  0.00 0.00 3.20
assi ( resi 3 and name HN )    (resi 4 and name HN )  0.00 0.00 3.80
assi ( resi 3 and name HN )    (resi 3 and name HD* )  0.00 0.00 4.40
assi ( resi 3 and name HN )    (resi 3 and name HE* )  0.00 0.00 6.30
assi ( resi 3 and name HN )    (resi 2 and name HA )  0.00 0.00 3.20
assi ( resi 3 and name HN )    (resi 3 and name HA )  0.00 0.00 3.50
assi ( resi 3 and name HN )    (resi 3 and name HB* )  0.00 0.00 3.30
assi ( resi 3 and name HN )    (resi 2 and name HB2 )  0.00 0.00 4.30
assi ( resi 3 and name HN )    (resi 2 and name HB1 )  0.00 0.00 4.50
assi ( resi 3 and name HD* )    (resi 3 and name HA )  0.00 0.00 3.60
assi ( resi 3 and name HD* )    (resi 3 and name HB* )  0.00 0.00 3.40
assi ( resi 3 and name HD* )  (resi 5 and (name HB* or name HG) )  0.00 0.00 5.00
assi ( (resi 3 or resi 4 ) and name HE* )    ( resi 3 and name HA ) 0.00 0.00 4.10
assi ( (resi 3 or resi 4 ) and name HE* )    ( resi 4 and name HA ) 0.00 0.00 4.50
assi ( (resi 3 or resi 4 ) and name HE* )  (resi 5 and (name HB* or name HG) ) 0.00 0.00 4.00
assi ( (resi 3 or resi 4 ) and name HE* )   (resi 2 and name HB2 )  0.00 0.00 4.50
assi ( (resi 3 or resi 4 ) and name HE* )   (resi 2 and name HG2 )  0.00 0.00 5.50
assi ( (resi 3 or resi 4 ) and name HE* )   (resi 2 and name HG1 )  0.00 0.00 6.10
assi ( (resi 3 or resi 4 ) and name HE* )   (resi 2 and name HB1 )  0.00 0.00 4.80
assi ( (resi 3 or resi 4 ) and name HZ )   (resi 5 and (name HB* or name HG) )  0.00 0.00 4.80
assi ( (resi 3 or resi 4 ) and name HE* )    ( resi 4 and name HB1 ) 0.00 0.00 4.90
assi ( (resi 3 or resi 4 ) and name HE* )    ( resi 3 and name HB* ) 0.00 0.00 3.80
```

```
assi ( (resi 3 or resi 4 ) and name HE* )    ( resi 4 and name HB2 ) 0.00 0.00 4.10
assi ( (resi 3 or resi 4 ) and name HE* )    ( (resi 3 or resi 4 ) and name HZ ) 0.00 0.00 2.50
assi ( (resi 3 or resi 4 ) and name HE* )    ( resi 4 and name HD* ) 0.00 0.00 2.70
assi ( (resi 3 or resi 4 ) and name HE* )    ( resi 3 and name HD* ) 0.00 0.00 2.60
assi ( (resi 3 or resi 4 ) and name HZ )    ( resi 4 and name HD* ) 0.00 0.00 3.60
assi ( (resi 3 or resi 4 ) and name HE* )    ( resi 5 and name HD1* ) 0.00 0.00 3.50
assi ( (resi 3 or resi 4 ) and name HE* )    ( resi 5 and name HD2* ) 0.00 0.00 3.60
assi ( (resi 3 or resi 4 ) and name HZ )    ( resi 5 and name HD1* ) 0.00 0.00 4.20
assi ( (resi 3 or resi 4 ) and name HZ )    ( resi 5 and name HD2* ) 0.00 0.00 4.20
assi ( resi 4 and name HD* )    (resi 4 and name HA )  0.00 0.00 3.80
assi ( resi 4 and name HD* )  ( resi 5 and name HD2* )  0.00 0.00 4.00
assi ( resi 4 and name HD* )  ( resi 5 and name HD1* )  0.00 0.00 4.10
assi ( resi 4 and name HD* )    (resi 4 and name HB1 )  0.00 0.00 3.60
assi ( resi 4 and name HD* )    (resi 4 and name HB2 )  0.00 0.00 3.50
assi ( resi 4 and name HN )    (resi 4 and name HD* )  0.00 0.00 4.30
assi ( resi 4 and name HN )    (resi 3 and name HA )  0.00 0.00 3.30
assi ( resi 4 and name HN )    (resi 4 and name HA )  0.00 0.00 3.90
assi ( resi 4 and name HN )    (resi 4 and name HB1 )  0.00 0.00 4.20
assi ( resi 4 and name HN )    (resi 3 and name HB* )  0.00 0.00 3.80
assi ( resi 4 and name HN )    (resi 4 and name HB2 )  0.00 0.00 3.80
assi ( resi 4 and name HA )    (resi 4 and name HB1 )  0.00 0.00 3.40
assi ( resi 4 and name HD* )  (resi 5 and (name HB* or name HG) )  0.00 0.00 4.10
assi ( resi 4 and name HB1 )  ( resi 4 and name HB2 ) 0.00 0.00 2.70
assi ( resi 5 and name HA )   (resi 5 and (name HB* or name HG) ) 0.00 0.00 3.20
assi ( resi 5 and name HA )  ( resi 5 and name HD1* )  0.00 0.00 3.90
assi ( resi 5 and name HA )  ( resi 5 and name HD2* )  0.00 0.00 3.30
assi (resi 5 and (name HB* or name HG) )  (resi 5 and name HD1* )  0.00 0.00 3.00
assi (resi 5 and (name HB* or name HG) )  (resi 5 and name HD2* )  0.00 0.00 3.20
assi ( resi 5 and name HN )    (resi 4 and name HN )  0.00 0.00 3.90
assi ( resi 5 and name HN )    (resi 4 and name HA )  0.00 0.00 3.40
assi ( resi 5 and name HN )    (resi 5 and name HA )  0.00 0.00 3.80
assi ( resi 5 and name HN )    (resi 4 and name HD* )  0.00 0.00 4.80
assi ( resi 5 and name HN )    (resi 4 and name HB2 )  0.00 0.00 4.20
assi ( resi 5 and name HN )    (resi 4 and name HB1 )  0.00 0.00 4.50
assi ( resi 5 and name HN )    (resi 5 and (name HB* or name HG) )  0.00 0.00 3.30
assi ( resi 5 and name HN )    (resi 5 and name HD2* )  0.00 0.00 4.50
assi ( resi 5 and name HN )    (resi 5 and name HD1* )  0.00 0.00 4.40
```

5.3 Pulse Programs

Most of the pulse programs used in this project are well known standard programs that were implemented from the literature. Therefore they won't be listed here. Only the pulse programs

that were modified and optimised during the course of this thesis are shown below. All these pulse programs are written for digital AVANCE spectrometers of the BRUKER company controlled by the software XWINNMR 3.0.

5.3.1 HSQC without decoupling in ^{1}H dimension, with phase cycle of the final 90° (^{1}H) pulse of the first INEPT

```
# 1 "/u/exp/stan/nmr/lists/pp/jinginvieags"
;invieags
;avance-version
;2D H-1/X correlation via double inept transfer
;phase sensitive using Echo/Antiecho gradient selection
;with decoupling during acquisition
;using trim pulses in inept transfer
# 1 "/u/exp/stan/nmr/lists/pp/Avance.incl" 1
;Avance.incl
;avance-version (03/02/17)
;$Id: Avance1.incl,v 1.7.2.3 2003/02/25 14:48:47 ber Exp $
# 9 "/u/exp/stan/nmr/lists/pp/jinginvieags" 2
# 1 "/u/exp/stan/nmr/lists/pp/Grad.incl" 1
;Grad.incl  -  include file for Gradient Spectroscopy
;avance-version (02/05/31)
define list<gradient> EA=<EA>
;$Id: Grad1.incl,v 1.7 2002/06/12 09:04:22 ber Exp $
# 10 "/u/exp/stan/nmr/lists/pp/jinginvieags" 2
"p2=p1*2"
"p4=p3*2"
"d0=3u"
"d4=1s/(cnst2*4)"
"d11=30m"
"d13=3u"
"d20=p16+d16+d0*2"
"d21=d4-p16-d13-4u"
"l3=(td1/2)"
"ds=ns*2*cnst0"

1 ze
  d11 pl12:f2
2 d1 do:f2
3 d11 do:f2
4 (p1 ph1)
  d4 pl2:f2
```

```
  (p2 ph0) (p4 ph0):f2
  d4 setnmr2|0 setnmr0|34|32|33
  (p1 ph2) (p3 ph3):f2
  d0
  ;;p2 ph0
  d0
  p16:ngrad:c34
  d16
  (p4 ph0):f2
  d20
  (p1 ph0) (p3 ph4):f2
  d4
  (p2 ph0) (p4 ph0):f2
  d13
  p16:ngrad:c34
  d21 pl12:f2
  4u setnmr2^0 setnmr0^34^32^33
  go=2 ph31 cpd2:f2
  d1 do:f2  wr #0 if #0 zd
  lo to 3 times 2
  d11 id0
  lo to 4 times l3
exit

ph0=0
ph1=0 2
ph2=1 1 3 3
ph3=0 0 0 0 2 2 2 2
ph4=0 0 0 0 0 0 0 0
    2 2 2 2 2 2 2 2
ph31=0 2 2 0 2 0 0 2
     2 0 0 2 0 2 2 0

;pl1 : f1 channel - power level for pulse (default)
;pl2 : f2 channel - power level for pulse (default)
;pl12: f2 channel - power level for CPD/BB decoupling
;p1 : f1 channel -  90 degree high power pulse
;p2 : f1 channel - 180 degree high power pulse
;p3 : f2 channel -  90 degree high power pulse
;p4 : f2 channel - 180 degree high power pulse
;p16: homospoil/gradient pulse
;p28: f1 channel - trim pulse
;d0 : incremented delay (2D)                  [3 usec]
;d1 : relaxation delay; 1-5 * T1
```

```
;d4 : 1/(4J)XH
;d11: delay for disk I/O                                [30 msec]
;d13: short delay                                       [3 usec]
;d16: delay for homospoil/gradient recovery
;d20: =p16+d16+p2+d0*2
;d21: =d4-p16-d13-4u
;cnst0: ds = ns * 2 * cnst0
;cnst2: = J(XH)
;l3: loop for phase sensitive 2D using  E/A method : l3 = td1/2
;in0: 1/(2 * SW(X)) = DW(X)
;nd0: 2
;NS: 1 * n
;DS: >= 16, but 2 * ns * m
;td1: number of experiments
;MC2: echo-antiecho
;cpd2: decoupling according to sequence defined by cpdprg2
;pcpd2: f2 channel - 90 degree pulse for decoupling sequence
;use gradient program (GRDPROG) :    2sineea
;use gradient ratio:  cnst21 : cnst22 : cnst23 : cnst24
;                          80 :     20 :     80 :    -20   for C-13
;                          80 :      8 :     80 :     -8   for N-15
```

5.3.2 HSQC without decoupling of X during detection time, with antiphase.

```
# 1 "/u/exp/stan/nmr/lists/pp/jinginvieags.t3"
;invieags.t3
;avance-version
;2D H-1/X correlation via double inept transfer
;phase sensitive using Echo/Antiecho gradient selection
;with decoupling during acquisition
;using trim pulses in inept transfer
# 1 "/u/exp/stan/nmr/lists/pp/Avance.incl" 1
;Avance.incl
;avance-version (03/02/17)
;$Id: Avance1.incl,v 1.7.2.3 2003/02/25 14:48:47 ber Exp $
# 9 "/u/exp/stan/nmr/lists/pp/jinginvieags.t3" 2
# 1 "/u/exp/stan/nmr/lists/pp/Grad.incl" 1
;Grad.incl  -  include file for Gradient Spectroscopy
;avance-version (02/05/31)
define list<gradient> EA=<EA>
;$Id: Grad1.incl,v 1.7 2002/06/12 09:04:22 ber Exp $
# 10 "/u/exp/stan/nmr/lists/pp/jinginvieags.t3" 2
```

```
"p2=p1*2"
"p4=p3*2"
"d0=3u"
"d4=1s/(cnst2*4)"
"d11=30m"
"d13=3u"
"d20=p16+d16+p2+d0*2"
"d21=d4-p16-d13-4u"
"l3=(td1/2)"
"ds=ns*2*cnst0"

1 ze
  d11 pl12:f2
2 d1 do:f2
3 d11
4 (p1 ph1)
  d4 pl2:f2
  (p2 ph0) (p4 ph0):f2
  d4 setnmr2|0 setnmr0|34|32|33
  (p1 ph2) (p3 ph3):f2
  d0
  p2 ph0
  d0
  p16:ngrad:c34
  d16
  (p4 ph0):f2
  d20
  (p1 ph5) (p3 ph4):f2
  d4
  p2 ph0 ;(p4 ph0):f2
  d13
  p16:ngrad:c34
  d21
  4u setnmr2^0 setnmr0^34^32^33
  go=2 ph31
  d1 wr #0 if #0 zd
  lo to 3 times 2
  d11 id0
  lo to 4 times l3
exit

ph0=0
ph1=0 2
ph2=1 1 3 3
```

```
ph3=0 0 0 0 2 2 2 2
ph4=0 0 0 0 0 0 0 0
    2 2 2 2 2 2 2 2
ph5=0 0 0 0 0 0 0 0
    0 0 0 0 0 0 0 0
    2 2 2 2 2 2 2 2
    2 2 2 2 2 2 2 2
ph31=0 2 2 0 2 0 0 2
     2 0 0 2 0 2 2 0
     2 0 0 2 0 2 2 0
     0 2 2 0 2 0 0 2

;pl1 : f1 channel - power level for pulse (default)
;pl2 : f2 channel - power level for pulse (default)
;pl12: f2 channel - power level for CPD/BB decoupling
;p1 : f1 channel -  90 degree high power pulse
;p2 : f1 channel - 180 degree high power pulse
;p3 : f2 channel -  90 degree high power pulse
;p4 : f2 channel - 180 degree high power pulse
;p16: homospoil/gradient pulse
;p28: f1 channel - trim pulse
;d0 : incremented delay (2D)                  [3 usec]
;d1 : relaxation delay; 1-5 * T1
;d4 : 1/(4J)XH
;d11: delay for disk I/O                             [30 msec]
;d13: short delay                                    [3 usec]
;d16: delay for homospoil/gradient recovery
;d20: =p16+d16+p2+d0*2
;d21: =d4-p16-d13-4u
;cnst0: ds = ns * 2 * cnst0
;cnst2: = J(XH)
;l3: loop for phase sensitive 2D using  E/A method : l3 = td1/2
;in0: 1/(2 * SW(X)) = DW(X)
;nd0: 2
;NS: 1 * n
;DS: >= 16, but 2 * ns * m
;td1: number of experiments
;MC2: echo-antiecho
;cpd2: decoupling according to sequence defined by cpdprg2
;pcpd2: f2 channel - 90 degree pulse for decoupling sequence
;use gradient program (GRDPROG) :    2sineea
;use gradient ratio:  cnst21 : cnst22 : cnst23 : cnst24
;                         80 :     20 :     80 :    -20   for C-13
;                         80 :      8 :     80 :     -8   for N-15
```

5.4 The best calculated structure for iAβ5/iAβ5^{inv} bound to Aβ fibrils derived from trNOE data.

5.4.1 PDB file for ^{19}F-iAβ5 bound to Aβ$^{14-23}$

```
REMARK FILENAME="19F2_anneal_182.pdb"
REMARK The macromolecule has 5 residues
REMARK Accepted structure 126 of 200 structures
REMARK Trial structure 182 of 200 structures
REMARK Molecular dynamics scheme : torsion; torsion; cartesian; minimize
REMARK High temperature dynamics :
REMARK      temp: 50000 steps: 1000 time(ps): 15
REMARK 1st cooling stage         :
REMARK      temp: 50000->0 steps: 1000 time(ps): 15 temp step: 250
REMARK 2nd cooling stage        :
REMARK      temp: 2000->0 steps: 3000 time(ps): 15 temp step: 25
REMARK a total 2000 steps of minimization
REMARK VDW scale factors 0.1; 0.1->1; 1->4; 1
REMARK 110 NOEs in 1 class(es) with scale factors of 150; 150; 150; 75
REMARK      averaging function(s): sum,
REMARK 0 3-bond j-couplings in 0 class(es) with
REMARK      scale factor(s) of NA
REMARK 0 1-bond j-couplings in 0 class(es) with
REMARK      scale factor(s) of NA
REMARK 0 carbon chemical shifts in 0 class(es) with
REMARK      scale factor(s) of NA
REMARK 0 proton chemical shifts in 0 class(es) with
REMARK      scale factor(s) of NA
REMARK 0 diffusion anisotropy restraints in 0 class(es) with
REMARK      scale factor(s) of NA
REMARK 0 susceptability anisotropy restraints in 0 class(es) with
REMARK      scale factor(s) of NA
REMARK 0 dihedral restraints with scale factors of 100; 200; 200; 400
REMARK 0 planarity restraints with a scale factor of NA
REMARK NCS restraints not used.
REMARK ============================================================
REMARK               bond, angles, improp, vdw(<1.6),  dihed
REMARK violations :     1       0       0         0       3
REMARK RMSD       : 0.0097   0.821   0.277            31.575
REMARK ============================================================
REMARK                noe,   cdih,   coup,   oneb, carb-a, carb-b,
REMARK violations :     0       0       0       0       0   -----
REMARK RMSD       :  0.063   0.000   0.000   0.000   0.000   0.000
```

```
REMARK 0.2/2 viol.:     3       0       0
REMARK ============================================================
REMARK               dani,   sani
REMARK violations :     0       0
REMARK RMSD       :  0.000   0.000
REMARK .2/.1 viol.:     0       0
REMARK ============================================================
REMARK Protons       violations, rmsd
REMARK all    :           0       0.000
REMARK class 1:           0       0.000
REMARK class 2:           0       0.000
REMARK class 3:           0       0.000
REMARK class 4:           0       0.000
REMARK ============================================================
REMARK overall = 61.4433
REMARK bon     = 8.4898
REMARK ang     = 16.6295
REMARK imp     = 0.632922
REMARK vdw     = 3.12231
REMARK harm    = 0
REMARK noe     = 32.5688
REMARK coup    = 0
REMARK oneb    = 0
REMARK carb    = 0
REMARK prot    = 0
REMARK dani    = 0
REMARK sani    = 0
REMARK cdih    = 0
REMARK ncs     = 0
REMARK ============================================================
REMARK DATE:31-Mar-04  13:54:20       created by user: chen
REMARK VERSION:1.0
ATOM      1  CA  LEU     1       1.578  -1.795   2.353  1.00  0.00
ATOM      2  HA  LEU     1       2.577  -2.202   2.328  1.00  0.00
ATOM      3  CB  LEU     1       0.616  -2.776   1.679  1.00  0.00
ATOM      4  HB1 LEU     1      -0.125  -2.207   1.137  1.00  0.00
ATOM      5  HB2 LEU     1       0.114  -3.341   2.452  1.00  0.00
ATOM      6  CG  LEU     1       1.268  -3.762   0.706  1.00  0.00
ATOM      7  HG  LEU     1       2.333  -3.784   0.887  1.00  0.00
ATOM      8  CD1 LEU     1       0.727  -5.167   0.925  1.00  0.00
ATOM      9 HD11 LEU     1      -0.322  -5.192   0.666  1.00  0.00
ATOM     10 HD12 LEU     1       0.849  -5.443   1.962  1.00  0.00
ATOM     11 HD13 LEU     1       1.268  -5.862   0.301  1.00  0.00
ATOM     12  CD2 LEU     1       1.041  -3.322  -0.732  1.00  0.00
```

```
ATOM     13 HD21 LEU     1       1.175  -2.252  -0.808  1.00  0.00
ATOM     14 HD22 LEU     1       0.037  -3.581  -1.033  1.00  0.00
ATOM     15 HD23 LEU     1       1.749  -3.820  -1.378  1.00  0.00
ATOM     16  C   LEU     1       1.563  -0.456   1.619  1.00  0.00
ATOM     17  O   LEU     1       0.720   0.399   1.890  1.00  0.00
ATOM     18  N   LEU     1       1.170  -1.633   3.773  1.00  0.00
ATOM     19  HT1 LEU     1       0.321  -1.034   3.793  1.00  0.00
ATOM     20  HT2 LEU     1       1.960  -1.182   4.280  1.00  0.00
ATOM     21  HT3 LEU     1       0.969  -2.579   4.155  1.00  0.00
ATOM     22  N   PRO     2       2.497  -0.256   0.671  1.00  0.00
ATOM     23  CA  PRO     2       2.577   0.986  -0.103  1.00  0.00
ATOM     24  HA  PRO     2       2.887   1.819   0.512  1.00  0.00
ATOM     25  CB  PRO     2       3.651   0.689  -1.153  1.00  0.00
ATOM     26  HB1 PRO     2       4.244   1.575  -1.325  1.00  0.00
ATOM     27  HB2 PRO     2       3.179   0.380  -2.075  1.00  0.00
ATOM     28  CG  PRO     2       4.472  -0.407  -0.568  1.00  0.00
ATOM     29  HG1 PRO     2       5.260   0.009   0.041  1.00  0.00
ATOM     30  HG2 PRO     2       4.887  -1.015  -1.358  1.00  0.00
ATOM     31  CD  PRO     2       3.536  -1.224   0.278  1.00  0.00
ATOM     32  HD1 PRO     2       4.051  -1.608   1.146  1.00  0.00
ATOM     33  HD2 PRO     2       3.113  -2.031  -0.300  1.00  0.00
ATOM     34  C   PRO     2       1.256   1.318  -0.782  1.00  0.00
ATOM     35  O   PRO     2       0.551   0.425  -1.245  1.00  0.00
ATOM     36  N   PHE     3       0.924   2.605  -0.843  1.00  0.00
ATOM     37  HN  PHE     3       1.530   3.272  -0.457  1.00  0.00
ATOM     38  CA  PHE     3      -0.320   3.051  -1.472  1.00  0.00
ATOM     39  HA  PHE     3      -0.234   4.122  -1.637  1.00  0.00
ATOM     40  CB  PHE     3      -0.506   2.375  -2.821  1.00  0.00
ATOM     41  HB1 PHE     3      -1.296   2.858  -3.368  1.00  0.00
ATOM     42  HB2 PHE     3      -0.724   1.330  -2.695  1.00  0.00
ATOM     43  CG  PHE     3       0.703   2.481  -3.605  1.00  0.00
ATOM     44  CD1 PHE     3       1.285   1.373  -4.149  1.00  0.00
ATOM     45  HD1 PHE     3       0.819   0.406  -4.018  1.00  0.00
ATOM     46  CD2 PHE     3       1.275   3.703  -3.758  1.00  0.00
ATOM     47  HD2 PHE     3       0.801   4.569  -3.321  1.00  0.00
ATOM     48  CE1 PHE     3       2.443   1.488  -4.850  1.00  0.00
ATOM     49  HE1 PHE     3       2.885   0.615  -5.262  1.00  0.00
ATOM     50  CE2 PHE     3       2.419   3.844  -4.450  1.00  0.00
ATOM     51  HE2 PHE     3       2.833   4.812  -4.540  1.00  0.00
ATOM     52  CZ  PHE     3       3.029   2.734  -5.011  1.00  0.00
ATOM     53  HZ  PHE     3       3.949   2.838  -5.566  1.00  0.00
ATOM     54  C   PHE     3      -1.510   2.725  -0.592  1.00  0.00
ATOM     55  O   PHE     3      -2.177   3.608  -0.052  1.00  0.00
ATOM     56  N   PHE     4      -1.760   1.426  -0.467  1.00  0.00
```

```
ATOM     57  HN  PHE     4      -1.175   0.789  -0.939  1.00  0.00
ATOM     58  CA  PHE     4      -2.867   0.913   0.336  1.00  0.00
ATOM     59  HA  PHE     4      -3.782   1.106  -0.203  1.00  0.00
ATOM     60  CB  PHE     4      -2.718  -0.597   0.528  1.00  0.00
ATOM     61  HB1 PHE     4      -3.560  -0.966   1.095  1.00  0.00
ATOM     62  HB2 PHE     4      -1.807  -0.797   1.071  1.00  0.00
ATOM     63  CG  PHE     4      -2.663  -1.355  -0.767  1.00  0.00
ATOM     64  CD1 PHE     4      -3.823  -1.799  -1.375  1.00  0.00
ATOM     65  HD1 PHE     4      -4.770  -1.606  -0.913  1.00  0.00
ATOM     66  CD2 PHE     4      -1.451  -1.616  -1.382  1.00  0.00
ATOM     67  HD2 PHE     4      -0.542  -1.282  -0.926  1.00  0.00
ATOM     68  CE1 PHE     4      -3.774  -2.484  -2.564  1.00  0.00
ATOM     69  HE1 PHE     4      -4.687  -2.825  -3.030  1.00  0.00
ATOM     70  CE2 PHE     4      -1.399  -2.301  -2.570  1.00  0.00
ATOM     71  HE2 PHE     4      -0.446  -2.499  -3.040  1.00  0.00
ATOM     72  CZ  PHE     4      -2.561  -2.733  -3.159  1.00  0.00
ATOM     73  HZ  PHE     4      -2.521  -3.262  -4.079  1.00  0.00
ATOM     74  C   PHE     4      -2.936   1.606   1.695  1.00  0.00
ATOM     75  O   PHE     4      -3.984   2.119   2.088  1.00  0.00
ATOM     76  N   ASP     5      -1.814   1.616   2.406  1.00  0.00
ATOM     77  HN  ASP     5      -1.011   1.191   2.038  1.00  0.00
ATOM     78  CA  ASP     5      -1.747   2.245   3.720  1.00  0.00
ATOM     79  HA  ASP     5      -2.759   2.409   4.060  1.00  0.00
ATOM     80  CB  ASP     5      -1.031   1.328   4.712  1.00  0.00
ATOM     81  HB1 ASP     5       0.035   1.412   4.566  1.00  0.00
ATOM     82  HB2 ASP     5      -1.335   0.307   4.533  1.00  0.00
ATOM     83  CG  ASP     5      -1.348   1.675   6.153  1.00  0.00
ATOM     84  OD1 ASP     5      -0.808   2.684   6.653  1.00  0.00
ATOM     85  OD2 ASP     5      -2.138   0.939   6.782  1.00  0.00
ATOM     86  C   ASP     5      -1.030   3.589   3.644  1.00  0.00
ATOM     87  OT1 ASP     5      -0.215   3.773   2.715  1.00  0.00
ATOM     88  OT2 ASP     5      -1.290   4.448   4.513  1.00  0.00
END
```

5.4.2 PDB file for iAβ5^{inv} bound to Aβ$^{14-23}$

```
REMARK FILENAME="DPFFL_10_anneal_69.pdb"
REMARK The macromolecule has 5 residues
REMARK Accepted structure 69 of 200 structures
REMARK Trial structure 69 of 200 structures
REMARK Molecular dynamics scheme : torsion; torsion; cartesian; minimize
REMARK High temperature dynamics :
REMARK      temp: 50000 steps: 1000 time(ps): 15
REMARK 1st cooling stage         :
```

```
REMARK      temp: 50000->0 steps: 1000 time(ps): 15 temp step: 250
REMARK 2nd cooling stage        :
REMARK      temp: 2000->0 steps: 3000 time(ps): 15 temp step: 25
REMARK a total 2000 steps of minimization
REMARK VDW scale factors 0.1; 0.1->1; 1->4; 1
REMARK 78 NOEs in 1 class(es) with scale factors of 150; 150; 150; 75
REMARK      averaging function(s): sum,
REMARK 0 3-bond j-couplings in 0 class(es) with
REMARK      scale factor(s) of NA
REMARK 0 1-bond j-couplings in 0 class(es) with
REMARK      scale factor(s) of NA
REMARK 0 carbon chemical shifts in 0 class(es) with
REMARK      scale factor(s) of NA
REMARK 0 proton chemical shifts in 0 class(es) with
REMARK      scale factor(s) of NA
REMARK 0 diffusion anisotropy restraints in 0 class(es) with
REMARK      scale factor(s) of NA
REMARK 0 susceptability anisotropy restraints in 0 class(es) with
REMARK      scale factor(s) of NA
REMARK 0 dihedral restraints with scale factors of 100; 200; 200; 400
REMARK 0 planarity restraints with a scale factor of NA
REMARK NCS restraints not used.
REMARK ===============================================================
REMARK               bond, angles, improp, vdw(<1.6),  dihed
REMARK violations :     0       0       0         0       2
REMARK RMSD       : 0.0007   0.606   0.077            21.260
REMARK ===============================================================
REMARK                noe,   cdih,   coup,   oneb, carb-a, carb-b,
REMARK violations :     0       0       0       0       0   -----
REMARK RMSD       :  0.001   0.000   0.000   0.000   0.000   0.000
REMARK 0.2/2 viol.:     0       0       0
REMARK ===============================================================
REMARK               dani,   sani
REMARK violations :     0       0
REMARK RMSD       :  0.000   0.000
REMARK .2/.1 viol.:     0       0
REMARK ===============================================================
REMARK Protons       violations, rmsd
REMARK all    :           0       0.000
REMARK class 1:           0       0.000
REMARK class 2:           0       0.000
REMARK class 3:           0       0.000
REMARK class 4:           0       0.000
REMARK ===============================================================
```

```
REMARK overall = 9.64747
REMARK bon     = 4.180711E-02
REMARK ang     = 9.04866
REMARK imp     = 4.884535E-02
REMARK vdw     = 0.505502
REMARK harm    = 0
REMARK noe     = 2.649884E-03
REMARK coup    = 0
REMARK oneb    = 0
REMARK carb    = 0
REMARK prot    = 0
REMARK dani    = 0
REMARK sani    = 0
REMARK cdih    = 0
REMARK ncs     = 0
REMARK ============================================================
REMARK DATE:10-May-04  19:12:31       created by user: chen
REMARK VERSION:1.0
ATOM      1  CA  ASP     1       3.438  -3.494   1.284  1.00  0.00
ATOM      2  HA  ASP     1       3.012  -3.605   2.270  1.00  0.00
ATOM      3  CB  ASP     1       4.101  -2.119   1.173  1.00  0.00
ATOM      4  HB1 ASP     1       3.380  -1.357   1.433  1.00  0.00
ATOM      5  HB2 ASP     1       4.429  -1.966   0.156  1.00  0.00
ATOM      6  CG  ASP     1       5.300  -1.979   2.089  1.00  0.00
ATOM      7  OD1 ASP     1       6.211  -2.831   2.010  1.00  0.00
ATOM      8  OD2 ASP     1       5.330  -1.017   2.885  1.00  0.00
ATOM      9  C   ASP     1       2.330  -3.628   0.242  1.00  0.00
ATOM     10  O   ASP     1       2.573  -4.075  -0.879  1.00  0.00
ATOM     11  N   ASP     1       4.480  -4.538   1.098  1.00  0.00
ATOM     12  HT1 ASP     1       5.098  -4.520   1.934  1.00  0.00
ATOM     13  HT2 ASP     1       5.009  -4.306   0.233  1.00  0.00
ATOM     14  HT3 ASP     1       3.998  -5.454   1.010  1.00  0.00
ATOM     15  N   PRO     2       1.093  -3.241   0.599  1.00  0.00
ATOM     16  CA  PRO     2      -0.052  -3.321  -0.314  1.00  0.00
ATOM     17  HA  PRO     2      -0.328  -4.347  -0.511  1.00  0.00
ATOM     18  CB  PRO     2      -1.178  -2.626   0.457  1.00  0.00
ATOM     19  HB1 PRO     2      -2.114  -3.129   0.264  1.00  0.00
ATOM     20  HB2 PRO     2      -1.248  -1.594   0.145  1.00  0.00
ATOM     21  CG  PRO     2      -0.788  -2.738   1.890  1.00  0.00
ATOM     22  HG1 PRO     2      -1.143  -3.674   2.295  1.00  0.00
ATOM     23  HG2 PRO     2      -1.196  -1.908   2.448  1.00  0.00
ATOM     24  CD  PRO     2       0.714  -2.695   1.916  1.00  0.00
ATOM     25  HD1 PRO     2       1.096  -3.315   2.713  1.00  0.00
ATOM     26  HD2 PRO     2       1.061  -1.679   2.026  1.00  0.00
```

```
ATOM     27  C   PRO     2       0.212  -2.606  -1.635  1.00  0.00
ATOM     28  O   PRO     2       0.255  -3.233  -2.693  1.00  0.00
ATOM     29  N   PHE     3       0.389  -1.290  -1.565  1.00  0.00
ATOM     30  HN  PHE     3       0.345  -0.848  -0.692  1.00  0.00
ATOM     31  CA  PHE     3       0.651  -0.488  -2.755  1.00  0.00
ATOM     32  HA  PHE     3       1.276  -1.070  -3.416  1.00  0.00
ATOM     33  CB  PHE     3      -0.659  -0.155  -3.472  1.00  0.00
ATOM     34  HB1 PHE     3      -0.434   0.253  -4.447  1.00  0.00
ATOM     35  HB2 PHE     3      -1.199   0.582  -2.896  1.00  0.00
ATOM     36  CG  PHE     3      -1.561  -1.341  -3.663  1.00  0.00
ATOM     37  CD1 PHE     3      -1.510  -2.086  -4.830  1.00  0.00
ATOM     38  HD1 PHE     3      -0.814  -1.806  -5.608  1.00  0.00
ATOM     39  CD2 PHE     3      -2.457  -1.711  -2.673  1.00  0.00
ATOM     40  HD2 PHE     3      -2.505  -1.137  -1.759  1.00  0.00
ATOM     41  CE1 PHE     3      -2.338  -3.178  -5.008  1.00  0.00
ATOM     42  HE1 PHE     3      -2.289  -3.750  -5.922  1.00  0.00
ATOM     43  CE2 PHE     3      -3.288  -2.803  -2.845  1.00  0.00
ATOM     44  HE2 PHE     3      -3.982  -3.081  -2.067  1.00  0.00
ATOM     45  CZ  PHE     3      -3.228  -3.537  -4.014  1.00  0.00
ATOM     46  HZ  PHE     3      -3.876  -4.390  -4.150  1.00  0.00
ATOM     47  C   PHE     3       1.383   0.798  -2.390  1.00  0.00
ATOM     48  O   PHE     3       2.537   0.997  -2.768  1.00  0.00
ATOM     49  N   PHE     4       0.702   1.669  -1.652  1.00  0.00
ATOM     50  HN  PHE     4      -0.215   1.452  -1.383  1.00  0.00
ATOM     51  CA  PHE     4       1.285   2.938  -1.233  1.00  0.00
ATOM     52  HA  PHE     4       2.252   3.029  -1.706  1.00  0.00
ATOM     53  CB  PHE     4       0.402   4.103  -1.686  1.00  0.00
ATOM     54  HB1 PHE     4       0.235   4.026  -2.750  1.00  0.00
ATOM     55  HB2 PHE     4       0.908   5.033  -1.474  1.00  0.00
ATOM     56  CG  PHE     4      -0.940   4.145  -1.008  1.00  0.00
ATOM     57  CD1 PHE     4      -1.205   5.085  -0.026  1.00  0.00
ATOM     58  HD1 PHE     4      -0.437   5.792   0.252  1.00  0.00
ATOM     59  CD2 PHE     4      -1.935   3.245  -1.355  1.00  0.00
ATOM     60  HD2 PHE     4      -1.739   2.507  -2.119  1.00  0.00
ATOM     61  CE1 PHE     4      -2.437   5.128   0.597  1.00  0.00
ATOM     62  HE1 PHE     4      -2.631   5.866   1.362  1.00  0.00
ATOM     63  CE2 PHE     4      -3.169   3.282  -0.735  1.00  0.00
ATOM     64  HE2 PHE     4      -3.936   2.575  -1.014  1.00  0.00
ATOM     65  CZ  PHE     4      -3.421   4.225   0.242  1.00  0.00
ATOM     66  HZ  PHE     4      -4.385   4.256   0.728  1.00  0.00
ATOM     67  C   PHE     4       1.475   2.983   0.281  1.00  0.00
ATOM     68  O   PHE     4       2.338   3.701   0.786  1.00  0.00
ATOM     69  N   LEU     5       0.664   2.212   1.002  1.00  0.00
ATOM     70  HN  LEU     5      -0.005   1.662   0.545  1.00  0.00
```

```
ATOM     71  CA  LEU     5       0.746   2.167   2.458  1.00  0.00
ATOM     72  HA  LEU     5       0.523   3.154   2.833  1.00  0.00
ATOM     73  CB  LEU     5      -0.281   1.179   3.017  1.00  0.00
ATOM     74  HB1 LEU     5      -0.252   1.234   4.095  1.00  0.00
ATOM     75  HB2 LEU     5       0.009   0.183   2.716  1.00  0.00
ATOM     76  CG  LEU     5      -1.724   1.416   2.566  1.00  0.00
ATOM     77  HG  LEU     5      -1.748   1.506   1.489  1.00  0.00
ATOM     78  CD1 LEU     5      -2.604   0.241   2.959  1.00  0.00
ATOM     79 HD11 LEU     5      -3.611   0.589   3.137  1.00  0.00
ATOM     80 HD12 LEU     5      -2.216  -0.215   3.858  1.00  0.00
ATOM     81 HD13 LEU     5      -2.611  -0.487   2.161  1.00  0.00
ATOM     82  CD2 LEU     5      -2.261   2.709   3.161  1.00  0.00
ATOM     83 HD21 LEU     5      -2.908   3.193   2.445  1.00  0.00
ATOM     84 HD22 LEU     5      -1.438   3.365   3.402  1.00  0.00
ATOM     85 HD23 LEU     5      -2.820   2.487   4.058  1.00  0.00
ATOM     86  C   LEU     5       2.147   1.771   2.914  1.00  0.00
ATOM     87  OT1 LEU     5       2.972   2.680   3.144  1.00  0.00
ATOM     88  OT2 LEU     5       2.407   0.556   3.038  1.00  0.00
END
```

5.4.3 PDB file for iAβ5^{inv} bound to Aβ$^{1-40}$

```
REMARK FILENAME="DPFFL_40_2_anneal_15.pdb"
REMARK The macromolecule has 5 residues
REMARK Accepted structure 14 of 200 structures
REMARK Trial structure 15 of 200 structures
REMARK Molecular dynamics scheme : torsion; torsion; cartesian; minimize
REMARK High temperature dynamics :
REMARK      temp: 50000 steps: 1000 time(ps): 15
REMARK 1st cooling stage         :
REMARK      temp: 50000->0 steps: 1000 time(ps): 15 temp step: 250
REMARK 2nd cooling stage        :
REMARK      temp: 2000->0 steps: 3000 time(ps): 15 temp step: 25
REMARK a total 2000 steps of minimization
REMARK VDW scale factors 0.1; 0.1->1; 1->4; 1
REMARK 88 NOEs in 1 class(es) with scale factors of 150; 150; 150; 75
REMARK      averaging function(s): sum,
REMARK 0 3-bond j-couplings in 0 class(es) with
REMARK      scale factor(s) of NA
REMARK 0 1-bond j-couplings in 0 class(es) with
REMARK      scale factor(s) of NA
REMARK 0 carbon chemical shifts in 0 class(es) with
REMARK      scale factor(s) of NA
```

```
REMARK 0 proton chemical shifts in 0 class(es) with
REMARK      scale factor(s) of NA
REMARK 0 diffusion anisotropy restraints in 0 class(es) with
REMARK      scale factor(s) of NA
REMARK 0 susceptability anisotropy restraints in 0 class(es) with
REMARK      scale factor(s) of NA
REMARK 0 dihedral restraints with scale factors of 100; 200; 200; 400
REMARK 0 planarity restraints with a scale factor of NA
REMARK NCS restraints not used.
REMARK ===============================================================
REMARK               bond, angles, improp, vdw(<1.6),  dihed
REMARK violations :     0       0       0         0       3
REMARK RMSD       : 0.0032   0.665   0.195            26.430
REMARK ===============================================================
REMARK                noe,   cdih,   coup,   oneb, carb-a, carb-b,
REMARK violations :     0       0       0       0       0   -----
REMARK RMSD       :  0.023   0.000   0.000   0.000   0.000   0.000
REMARK 0.2/2 viol.:     0       0       0
REMARK ===============================================================
REMARK               dani,   sani
REMARK violations :     0       0
REMARK RMSD       :  0.000   0.000
REMARK .2/.1 viol.:     0       0
REMARK ===============================================================
REMARK Protons       violations, rmsd
REMARK all    :           0       0.000
REMARK class 1:           0       0.000
REMARK class 2:           0       0.000
REMARK class 3:           0       0.000
REMARK class 4:           0       0.000
REMARK ===============================================================
REMARK overall = 22.2014
REMARK bon     = 0.950101
REMARK ang     = 10.8984
REMARK imp     = 0.312197
REMARK vdw     = 6.55644
REMARK harm    = 0
REMARK noe     = 3.48423
REMARK coup    = 0
REMARK oneb    = 0
REMARK carb    = 0
REMARK prot    = 0
REMARK dani    = 0
REMARK sani    = 0
```

```
REMARK cdih    = 0
REMARK ncs     = 0
REMARK ============================================================
REMARK DATE:10-May-04  15:23:08       created by user: chen
REMARK VERSION:1.0
ATOM      1  CA  ASP     1      -2.930   3.974  -4.516  1.00  0.00
ATOM      2  HA  ASP     1      -3.978   3.890  -4.270  1.00  0.00
ATOM      3  CB  ASP     1      -2.471   2.689  -5.208  1.00  0.00
ATOM      4  HB1 ASP     1      -1.943   2.072  -4.495  1.00  0.00
ATOM      5  HB2 ASP     1      -1.806   2.943  -6.019  1.00  0.00
ATOM      6  CG  ASP     1      -3.629   1.889  -5.771  1.00  0.00
ATOM      7  OD1 ASP     1      -3.490   0.655  -5.902  1.00  0.00
ATOM      8  OD2 ASP     1      -4.675   2.497  -6.080  1.00  0.00
ATOM      9  C   ASP     1      -2.133   4.198  -3.233  1.00  0.00
ATOM     10  O   ASP     1      -1.313   5.113  -3.153  1.00  0.00
ATOM     11  N   ASP     1      -2.756   5.108  -5.461  1.00  0.00
ATOM     12  HT1 ASP     1      -1.741   5.323  -5.516  1.00  0.00
ATOM     13  HT2 ASP     1      -3.293   5.918  -5.087  1.00  0.00
ATOM     14  HT3 ASP     1      -3.125   4.809  -6.386  1.00  0.00
ATOM     15  N   PRO     2      -2.366   3.361  -2.208  1.00  0.00
ATOM     16  CA  PRO     2      -1.670   3.469  -0.927  1.00  0.00
ATOM     17  HA  PRO     2      -1.574   4.497  -0.612  1.00  0.00
ATOM     18  CB  PRO     2      -2.603   2.722   0.025  1.00  0.00
ATOM     19  HB1 PRO     2      -3.333   3.407   0.429  1.00  0.00
ATOM     20  HB2 PRO     2      -2.031   2.283   0.828  1.00  0.00
ATOM     21  CG  PRO     2      -3.249   1.678  -0.820  1.00  0.00
ATOM     22  HG1 PRO     2      -4.240   1.468  -0.445  1.00  0.00
ATOM     23  HG2 PRO     2      -2.649   0.779  -0.812  1.00  0.00
ATOM     24  CD  PRO     2      -3.329   2.241  -2.218  1.00  0.00
ATOM     25  HD1 PRO     2      -4.328   2.597  -2.424  1.00  0.00
ATOM     26  HD2 PRO     2      -3.039   1.494  -2.941  1.00  0.00
ATOM     27  C   PRO     2      -0.291   2.815  -0.962  1.00  0.00
ATOM     28  O   PRO     2       0.269   2.590  -2.034  1.00  0.00
ATOM     29  N   PHE     3       0.249   2.515   0.217  1.00  0.00
ATOM     30  HN  PHE     3      -0.248   2.723   1.034  1.00  0.00
ATOM     31  CA  PHE     3       1.561   1.886   0.332  1.00  0.00
ATOM     32  HA  PHE     3       2.290   2.580  -0.047  1.00  0.00
ATOM     33  CB  PHE     3       1.879   1.608   1.811  1.00  0.00
ATOM     34  HB1 PHE     3       2.114   2.544   2.297  1.00  0.00
ATOM     35  HB2 PHE     3       2.738   0.958   1.868  1.00  0.00
ATOM     36  CG  PHE     3       0.757   0.955   2.584  1.00  0.00
ATOM     37  CD1 PHE     3       0.817   0.871   3.966  1.00  0.00
ATOM     38  HD1 PHE     3       1.668   1.284   4.485  1.00  0.00
ATOM     39  CD2 PHE     3      -0.346   0.416   1.935  1.00  0.00
```

```
ATOM     40  HD2 PHE     3      -0.408   0.471   0.859  1.00  0.00
ATOM     41  CE1 PHE     3      -0.197   0.265   4.683  1.00  0.00
ATOM     42  HE1 PHE     3      -0.137   0.206   5.760  1.00  0.00
ATOM     43  CE2 PHE     3      -1.362  -0.186   2.646  1.00  0.00
ATOM     44  HE2 PHE     3      -2.212  -0.598   2.125  1.00  0.00
ATOM     45  CZ  PHE     3      -1.288  -0.264   4.022  1.00  0.00
ATOM     46  HZ  PHE     3      -2.080  -0.740   4.579  1.00  0.00
ATOM     47  C   PHE     3       1.645   0.603  -0.510  1.00  0.00
ATOM     48  O   PHE     3       1.649   0.661  -1.739  1.00  0.00
ATOM     49  N   PHE     4       1.727  -0.548   0.149  1.00  0.00
ATOM     50  HN  PHE     4       1.735  -0.539   1.121  1.00  0.00
ATOM     51  CA  PHE     4       1.826  -1.828  -0.547  1.00  0.00
ATOM     52  HA  PHE     4       2.210  -1.637  -1.529  1.00  0.00
ATOM     53  CB  PHE     4       2.789  -2.758   0.195  1.00  0.00
ATOM     54  HB1 PHE     4       3.369  -3.317  -0.524  1.00  0.00
ATOM     55  HB2 PHE     4       2.221  -3.444   0.806  1.00  0.00
ATOM     56  CG  PHE     4       3.740  -2.028   1.092  1.00  0.00
ATOM     57  CD1 PHE     4       4.487  -0.973   0.605  1.00  0.00
ATOM     58  HD1 PHE     4       4.390  -0.687  -0.428  1.00  0.00
ATOM     59  CD2 PHE     4       3.874  -2.385   2.422  1.00  0.00
ATOM     60  HD2 PHE     4       3.294  -3.204   2.815  1.00  0.00
ATOM     61  CE1 PHE     4       5.352  -0.287   1.422  1.00  0.00
ATOM     62  HE1 PHE     4       5.925   0.535   1.026  1.00  0.00
ATOM     63  CE2 PHE     4       4.741  -1.703   3.246  1.00  0.00
ATOM     64  HE2 PHE     4       4.840  -1.991   4.281  1.00  0.00
ATOM     65  CZ  PHE     4       5.481  -0.653   2.745  1.00  0.00
ATOM     66  HZ  PHE     4       6.156  -0.119   3.385  1.00  0.00
ATOM     67  C   PHE     4       0.463  -2.494  -0.666  1.00  0.00
ATOM     68  O   PHE     4       0.141  -3.112  -1.681  1.00  0.00
ATOM     69  N   LEU     5      -0.322  -2.366   0.387  1.00  0.00
ATOM     70  HN  LEU     5       0.008  -1.865   1.157  1.00  0.00
ATOM     71  CA  LEU     5      -1.656  -2.954   0.437  1.00  0.00
ATOM     72  HA  LEU     5      -1.625  -3.887  -0.103  1.00  0.00
ATOM     73  CB  LEU     5      -2.059  -3.237   1.889  1.00  0.00
ATOM     74  HB1 LEU     5      -2.614  -4.162   1.911  1.00  0.00
ATOM     75  HB2 LEU     5      -2.709  -2.440   2.221  1.00  0.00
ATOM     76  CG  LEU     5      -0.895  -3.354   2.880  1.00  0.00
ATOM     77  HG  LEU     5      -0.401  -2.398   2.959  1.00  0.00
ATOM     78  CD1 LEU     5      -1.402  -3.729   4.260  1.00  0.00
ATOM     79 HD11 LEU     5      -2.056  -4.585   4.183  1.00  0.00
ATOM     80 HD12 LEU     5      -1.944  -2.897   4.682  1.00  0.00
ATOM     81 HD13 LEU     5      -0.563  -3.972   4.895  1.00  0.00
ATOM     82  CD2 LEU     5       0.125  -4.371   2.392  1.00  0.00
ATOM     83 HD21 LEU     5      -0.045  -4.582   1.347  1.00  0.00
```

```
ATOM     84 HD22 LEU     5       0.027  -5.282   2.964  1.00  0.00
ATOM     85 HD23 LEU     5       1.120  -3.971   2.521  1.00  0.00
ATOM     86  C   LEU     5      -2.682  -2.038  -0.225  1.00  0.00
ATOM     87  OT1 LEU     5      -3.828  -1.977   0.268  1.00  0.00
ATOM     88  OT2 LEU     5      -2.329  -1.389  -1.232  1.00  0.00
END
```